Maximizing the Therapeutic Window and Elucidating the Toxicity Mechanisms of Intravenous siRNA Polyplex-Based Cancer Nanomedicines

By

Meredith Allyn Jackson

Dissertation

Submitted to the Faculty of the

Graduate School of Vanderbilt University

in partial fulfillment of the requirements

for the degree of

DOCTOR OF PHILOSOPHY

in

Biomedical Engineering

August 9, 2019

Nashville, Tennessee

Approved:

Craig L. Duvall, Ph.D.

Todd D. Giorgio, Ph.D.

John T. Wilson, Ph.D.

Rebecca S. Cook, Ph.D.

Dana M. Brantley-Sieders, Ph.D.

DEDICATION

This work is dedicated to my labmates, who've kept me sane and kept me laughing through graduate school.

ACKNOWLEDGMENTS

There are so many people who have helped me on the road to completing this dissertation. First, I am thankful to my primary advisor, Dr. Craig Duvall, for all that he does for his students and for our science. His dedication to the Advanced Therapeutics Lab has led to the building of a wonderful team of peers and to the funding to pursue all our greatest ideas. I must also thank my secondary advisor, Dr. Todd Giorgio, for his mentorship, his openness, and his infectious positivity. I am grateful to the other members of my committee, Dr. John Wilson, Dr. Rebecca Cook, and Dr. Dana Brantley-Sieders, for mentoring me through the roadblocks and for all their feedback. Each of these scientists is a huge role model to me for maintaining a positive attitude and a sense of humor in the face of challenges.

I am grateful to the many talented members of the Duvall and Giorgio labs who have been an absolute pleasure to spend these last five years with. In particular, I am thankful to Dr. Fang Yu, for her assistance on so many animal studies and for the excellent dinners she shared with us. I am thankful to Dr. Mukesh Gupta, for helping me slog through those first two years in the chemistry lab. I am grateful to Dr. Eric Dailing, for the hilarious game night memories and for keeping us all from blowing up the lab. I am grateful to many lab alumni—particularly Dr. Thomas Werfel, Dr. Samantha Sarett, Dr. Brian Evans, Dr. Kelsey Mayo, Taylor Kavanaugh, Dr. John Martin, and Dr. Kristin O'Grady, who trained me well and who continue to mentor me. I have also enjoyed working with many talented undergraduates—Elizabeth Curvino, Rachel Miles, Mitchell Stokan, Ayisha Jackson, and Allyson King. Most of all, I am grateful to my current lab members—Prarthana Patil, Sean Bedingfield, Isom Kelly, Bryan Dollinger, Ella Hoogenboezem, Kameron Kilchrist, Shrusti Patel, Brock Fletcher, and Carli DeJulius. You guys have filled my life with joy through both the fun times and the struggles. Thanks also to Giorgio

lab members Evan Glass, Chris Haycook, Andrew Cook, Stephanie Dudzinski, Dr. Shirin Masjedi, and Dr. Charleson Bell, for all the support over the years.

I am thankful also to the many friends who have supported me during the last five years. Thank you to Michaela Karis, Joelle Fang, Victoria DeHaven, Sophie Xu, Ira Shrivastava, Agar Woda, Monica Zatarain, and Sanya Mehta for the phone calls, the well of support you provided from afar, and for the fun travels we had together during this time. Thanks also to Shayna Bedingfield, Kate Moyer, Stephanie Pearlman, Booma Narasimhan, Hernan Gonzalez, Evan Kazura, Jeremy Ford, Kristy Walsh, Frances Knight, Tiffany Heaster, and Mohit Ganguly for all the heart-to-hearts, the happy hours, and the bonding. Huge thanks also to Megan Poorman, for being the best roommate ever and a dear friend.

I am incredibly grateful to my boyfriend, Eric Honert, for the constant support, the many laughs, the tao of rock climbing, and for making the final year of graduate school so fun.

Finally, I am so grateful for the love and support of my family. To my parents, Lisa and Paul Jackson, for their unconditional love through all the ups and downs. To my wonderful grandparents—Don and Barbara Jackson and Harold and Sarah Koehn—who have also been there for me throughout my life. Finally, not many people can say their brother is also their best friend, but I get to count myself among the lucky few. Thank you so much to Matt Jackson, who brightens my life with humor and love every day.

I would also like to acknowledge my funding sources: DOD CDMRP OR130302, NIH R01 CA224241, NIH R01 EB019409, NIH R01 DK084246, NSF CAREER BMAT 1349604, NSF GRF 1446197. Thanks also to the Vanderbilt Translational Pathology Shared Resource, the Flow Cytometry Shared Resource, and the Mouse Metabolic Phenotyping Center.

TABLE OF CONTENTS

Page

LIST OF TABLES

Table Page

LIST OF FIGURES

CHAPTER I

Introduction

1.1 Background and Significance

It has been only 20 years since the discovery of the potent gene-silencing effects of RNA interference in 1998, but since then, the potential of siRNA nanomedicines has skyrocketed.[1] The first nanoparticle-formulated siRNA therapeutic received U.S. FDA approval in August 2018, offering new options for patients with a rare, life-threatening disease.[2] siRNAs are short, 15-30 base-pair oligonucleotides that are primarily active in the cell cytoplasm, where they can associate with a group of proteins that make up the RNA-induced silencing complex (RISC).[3] These siRNAs can then bind to complementary mRNA and cause the mRNA to be cleaved, preventing translation to protein and effectively silencing a gene. RNA interference is particularly useful as a therapeutic strategy because it can be used to silence "undruggable" targets—targets for which no effective small molecule inhibitors currently exist.[4]

Despite many promising new cancer therapeutics, from CAR T-cells to PARP inhibitors to immune checkpoint inhibitors, there are commonly over-expressed cancer-associated genes that are considered "undruggable" targets, such as MYC and KRAS.[4, 5] Such targets may lack binding sites amenable to small molecule inhibition or may reside intracellularly and be difficult to reach with standard delivery strategies.[4] Because siRNAs target mRNA before it is translated to an "undruggable" protein, siRNAs can be designed against any target. Furthermore, siRNAs can be used to study the role that certain molecular targets play in cancer progression.

This application is particularly useful in the context of Triple Negative Breast Cancer

(TNBC). Patients with TNBC have tumors that lack expression of estrogen receptors, progesterone receptors, or HER2 amplification. Currently, there are no molecularly targeted therapies available for TNBC treatment, and standard of care is surgical resection with neoadjuvant chemotherapy.[6] Roughly 70% of patients with TNBC still have residual disease after undergoing this treatment regimen and therefore experience high rates of cancer recurrence.[6] There is a significant need for more efficacious, targeted therapeutics with fewer side effects for this patient population. One such potential target is Rictor, a subunit of mTORC2. Our group recently found that increased *RICTOR* gene expression correlated with decreased progression-free survival in patients with basal-like TNBC subtypes.[7] While small molecule inhibitors exist for both mTORC2 and mTORC1 together, there are no potent, specific small molecule inhibitors that target mTORC2 alone. siRNA-based therapeutics hold great potential for silencing molecules like Rictor and evaluating their effectiveness as novel therapeutic targets for TNBC.

Although siRNA could theoretically be used in a variety of disease applications, most clinical programs based on siRNA conjugates or siRNA nanomedicine primarily target liver diseases.[3, 8, 9] This is because GalNAc conjugates actively target the liver and because a major percentage of the injected dose of nanoparticles naturally targets the liver.[10] The liver is the body's default blood filtration system, so intravenously injected therapeutics experience significant liver exposure. The liver is the site of Kupffer cells, a major component of the mononuclear phagocyte system (MPS), which serve as a phagocytic filter for nano-sized materials in the blood.[11] There is therefore a significant need for development of nanocarriers that can delivery siRNAs more efficiently to extra-hepatic targets, such as tumors.

As individual drug components, siRNAs have many properties that make them poorly

amenable to clinical translation. siRNAs are large, hydrophilic biomolecules with a net negative charge. These factors reduce an siRNA's bioavailability due to poor tissue penetration properties. Due to their molecular size being below the cut off for kidney filtration, intravenously-injected, unmodified siRNAs are rapidly excreted in urine.[12] Additionally, un-modified siRNAs are prone to nuclease-mediated degradation in the blood, further preventing them from achieving biological activity. Locally-delivered siRNAs that are able to reach their cellular targets encounter problems associated with poor cell uptake, and an inability to escape the endolysosomal pathway.[13] siRNAs are therefore poorly equipped to reach the cell cytoplasm, where they can actively induce silencing.

Nanoparticle encapsulation has long been hailed as an effective strategy to overcome the many barriers facing siRNAs on their journey to a target cell. Nanoparticles provide siRNAs with protection against nucleases, protection against kidney filtration, increased cell uptake/tissue penetration, and the potential for escape into the cell cytoplasm.[14] While there are many types of nanoparticle-based drug delivery systems, the most common methods of non-viral siRNA nanoparticle encapsulation involve complexation with cationic lipids or cationic polymer-based materials.[15] While viral gene therapies are the subject of extensive research, they have been plagued by safety concerns and therefore inspired the development of non-viral, synthetic alternatives. In this work, we have focused on polymer-based siRNA delivery. While lipids are arguably more "natural" materials, they tend to home to liver and are thus less tunable for non-hepatic targets.[16]

Complexation of siRNAs with polymeric materials results in the formation of polyplex nanoparticles, which are self-assembled and often stabilized by electrostatic interactions between polymeric cationic components and negatively-charged siRNAs.[17] Poly(ethylene imine) is the

classic, gold-standard example of an siRNA-complexing polyplex system, with high cationic charge density on protonated amines that interact with the siRNA and can allow for improved cell uptake and endosomal escape by the "proton sponge" effect.[18] As polyplexes enter the endolysosomal pathway in a cell and the pH of their local environment drops, polymer amines become increasingly protonated, and associated osmotic swelling causes endosomal rupture. Purely cationic polymers can also cause serious cytotoxicity when administered intravenously, and thus many strategies have sought to sterically "shield" polyplexes with hydrophilic, corona-forming polymer blocks such as poly(ethylene glycol) (PEG) that reduce direct exposure of cells to cationic components and improve *in vivo* stability.[19, 20] Additional incorporation of hydrophobic polymer moieties in the core-forming polymer block has been shown to improve stability of polyplex assembly through the additional hydrophobic interactions reinforcing electrostatic association.[21-24] This inclusion of hydrophobicity has also been shown to enhance endosomal escape behavior, allowing for more efficient delivery of the siRNA into the cytoplasm.

However, all polyplex delivery systems still face significant challenges when introduced to the complex milieu that is the *in vivo*, intravenous environment. Due to their electrostatic stabilization, polyplexes are prone to de-complexation when they encounter anionic heparan sulfate proteoglycans in the glomerular basement membrane of the kidney.[25] Despite steric stabilization strategies such as PEGylation, polyplexes remain vulnerable to protein adsorption and associated removal by phagocytic cells of the MPS.[26, 27] Each of these factors contributes to the extremely short circulation half-lives of electrostatically-complexed polyplexes. Polyplex surface chemistry is extremely important in determining *in vivo* fate, as surface properties like charge and hydrophilicity can dictate interactions with serum proteins and kidney proteoglycans.

At the same time, steric shielding such as PEGylation can significantly reduce cell uptake.[28] Optimizing polyplex surface chemistry while overcoming the "PEG dilemma" is therefore imperative for improved polyplex performance.

Nanoparticle drug-delivery systems are known to accumulate at the site of solid tumors based on the enhanced permeability and retention (EPR) effect. The EPR effect describes how vasculature around tumors tends to be tortuous, disordered, and more leaky compared to vasculature in normal tissues.[29, 30] The increased pore sizes between tumor endothelial cells allows for increased "leakage" of ~50-100 nm particles into tissue spaces. While the widespread applicability of the EPR effect has recently been called into question, it has been demonstrated to occur in humans and may differentially impact various subsets of cancer patients.[31-34] Regardless of the magnitude of EPR, it is imperative for nanocarriers to circulate in the bloodstream for extended time periods. Because tumors receive a relatively small portion of cardiac output, sufficient particle accumulation relies upon extended blood persistence.[35]

In order to use si-NPs as a viable platform for cancer *in vivo*, it is of central importance to develop formulations that can be administered repeatedly and efficaciously without systemic toxicity. Despite improvements in stealth nanocarrier materials, many polymer-based siRNA delivery systems consist of cationic polymers with some degree of toxicity.[36] While polyplex dose can be reduced to improve toxicity, it comes at the sacrifice of efficacy. Some of the most advanced systems include cyclodextrin-based carriers, which have made it to early phase clinical testing. In both preclinical and clinical testing, these polymers showed dose-dependent toxicities.[14, 37] In phase 1a and 1b clinical trials, study protocols had to be modified to include earlier low doses to "sensitize" patients to the polymer system and avoid severe immunological toxicities. Even with these modifications, a significant proportion of patients had experienced

immunological dose-limiting toxicities. In preclinical models, these polymeric systems were evaluated for toxicities without the siRNA components, and it was found that the systemic toxicities were primarily associated with polymer, not siRNA.[37]

Many other siRNA delivery systems have known inflammatory and toxic side effects. In lipidic systems, it was found that inflammation associated with cationic lipids is directly dependent on dose and charge ratio. Such lipid vectors can increase activation of interferons and cytokines, including IFN-γ, TNF-α, and IL-12.[38-40] Cationic polymers are known to cause similar immune activation.[41] For example, poly(ethylene imine) (PEI) interacts with negatively charged proteins in the circulation and causes immediate aggregation-related toxicity.[42] While stealth strategies exist to present this type of aggregation, cationic polymer systems continue to experience dose and charge ratio-dependent toxicities.

Given that increasing charge ratio can play an important role in si-NP stability, it is important to find an optimal balance between charge ratio and toxicity.[43] It is also important to develop a better understanding of polymer-based toxicity mechanisms in general to reduce si-NP associated adverse events. A central goal of this work is to develop versatile siRNA carrier systems that are both highly effective at tumor gene silencing *in vivo* and non-toxic. These systems can then be leveraged as an enabling technology for preclinical study of biologically relevant targets in animal models. As a second central goal, this work aims to identify and characterize novel mechanisms of si-NP toxicity. Achieving safe, repeated delivery of siRNA at high doses would significantly improve our ability to interrogate the impact of silencing *in vivo* molecular targets in tumors.

1.2 Innovation

1.2.1 Optimized Zwitterionic Corona Surface Chemistry

Although PEGylation is widely considered the gold standard for circulation-enhancing, steric shielding of nanoparticle drug delivery systems, a promising alternative is "zwitteration." Zwitterionic materials are contain positively-charged and negatively-charged moieties in close proximity and are both net-neutral and highly hydrophilic. Zwitterionic materials are known to interact with water molecules through electrostatic interactions, while PEGylated surfaces interact with water molecules through hydrogen bonding.[44] In the case of PEG, water therefore takes on a less thermodynamically favorable, cage-like structure around the polymer. For zwitterionic materials, water retains its normal molecular conformations, enhancing the overall hydrophilicity of the material.

One example of a zwitterionic polymer is poly(2-methacryloyloxyethyl phosphorylcholine) [PMPC], a polymeric form of phosphorylcholine. It has proven effective as an FDA-approved component of biomedical devices such as contact lenses and drug-eluting stents. [44-46]

Previous si-NPs developed in our lab were PEGylated with 5000 g/mol PEG and contained an optimized core composed of 50% hydrophobic, 50% cationic components.[21] These polyplexes extended the circulatory half-life of siRNA from 2-3 min to 5-8 min. In this work, we study the impact of alternative coronas such as PMPC and brush-like PEGs (POEGMA) on si-NP circulation time, investigating both high and low molecular weight coronas. We further study the impact of lead candidate coronas on tumor uptake and tumor gene knockdown.

We are the first to directly compare PEG to PMPC-based coronas and to demonstrate the significant enhancement in tumor uptake and gene knockdown of the zwitterionic polyplex

corona. We demonstrate that the use of zwitterionic corona can be an effective way to overcome the "PEG dilemma," referring to the reduced cell uptake behavior of PEGylated particles. These non-canonical surface chemistries are generally under-utilized in the field of siRNA delivery. Our work demonstrates that zwitterionic carriers may improve si-NP activity, encouraging their further development for tumor applications.

1.2.2 Dual Hydrophobization of Carrier and Cargo and Charge Ratio Optimization

This work builds on previous work that has shown that dual hydrophobization of both polymer and siRNA cargo (via conjugation of siRNA to polymers), significantly improves si-NP stability and extends si-NP circulation half-lives.[47] This dual hydrophobization strategy is highly unique and under-utilized in the field. Hydrophobization is a strategy that has been more frequently investigated for carrier and cargo separately.[24, 48] Hydrophobization can improve association of cationic polymers with cell membranes and thus improve their uptake properties.[49]

Hydrophobes such as palmitic acid and α-tocopherol have been specifically conjugated to siRNAs to improve their membrane penetration properties and biodistribution.[50-53] Hydrophobic siRNA conjugation can also increase siRNA circulation half-lives.[47, 54]

The Kataoka group in particular has studied hydrophobization of carrier and cargo individually in separate studies.[23, 55] In these works, they found that cholesterol modification of siRNA improved micelle stability and half-lives, but even these optimized carriers only achieved roughly 50% decrease in tumor luminescence after intravenous delivery.[23] When the polymers instead were conjugated with cholesteryl moieties, similar effects were noted in that the polyion complex micelles exhibited increased blood stability and transfection efficiency.[55]

While the benefits of hydrophobic modifications in polyplex systems have been clearly

delineated, some groups have found increased toxicity toward cells with increasing hydrophobicity.[56, 57] These findings were not supported by our own work, and in fact, our data indicate that dual hydrophobization can actually decrease systemic toxicity of cationic polymer systems, a relationship that has not previously been investigated.[47]

1.2.3 N:P Ratio and Pharmacokinetics

This work is also the first to describe the relationship between si-NP charge ratio and pharmacokinetics. Gary and colleagues have previously identified a clear relationship between charge ratio and toxicity, with excessive free polymers causing aggregation-related toxicities *in vivo*.[58] While these authors probed the impact of charge ratio on *in vivo* biodistribution, they did not comprehensively study the pharmacokinetic behavior of polyplexes at varied charge ratios.

Although the risks of increased charge ratio include severe toxicities, this work uniquely leverages a dual hydrophobization strategy to enable safe delivery of si-NPs at high charge ratios, thereby improving si-NP circulation half-lives. This strategy had yet to be thoroughly characterized and will have a significant impact on the field for design of effective and safe siRNA nanocarriers.

1.2.4 The Role of Platelet Activating Factor in Nanocarrier Toxicity

Although reports of *in vivo* nanocarrier toxicities are well-documented, they are poorly-understood.[36, 59] Administration of CALAA-01, a cyclodextrin-based nanopolyplex, in humans resulted in infusion-related immune hypersensitivity reactions that halted further clinical development of the carrier system. Similar types of hypersensitivity reactions have historically been reported for viral-based carriers.[60]

In this work, we are the first to connect a toxicity mechanism affecting adenovirus vectors to synthetic, polymeric nanocarriers. We demonstrate that inhibition of the Platelet Activating Factor Receptor (PAFR), completely abrogates si-NP-associated acute toxicities, indicating a role for PAF in toxicity mechanisms. We further show that nanoparticle-associated Kupffer cell stimulation is a triggering event for the release of PAF in the mouse bloodstream, causing acute shock-like symptoms. Our results fully characterize an anaphylactoid-type response to si-NPs in the absence of prior si-NP exposure. We have identified PAFR inhibitors as potential prophylactic treatments to reduce immunological infusion reactions to si-NPs. This work has significant, broad implications for the field of nanomedicine in general, as other nanoparticle-based therapeutics may trigger the same pathway due to the common Kupffer-cell related clearance of all nanomaterials.

1.3 Specific Aims

The overall goal of this work is to develop long-circulating, non-toxic siRNA nanocarriers that are optimized for intravenous delivery and that enable silencing of targets for which no small molecule inhibitors currently exist. We also seek to understand the biological mechanisms of nanocarrier-associated toxicities to further improve the therapeutic window of siRNA nano-polyplexes (si-NPs) in general. This technology is applied in the context of Triple Negative Breast Cancer (TNBC), an aggressive form of breast cancer for which no clinically-approved, molecularly-targeted therapies currently exist. Patients with TNBC have no other standard of care options apart from surgical resection and chemotherapy. RNAi, enabled by nanotechnology, provides a means to interrogate novel therapeutic targets in a highly specific manner. However, intravenous delivery of siRNA nanocarriers has been plagued by rapid

systemic clearance due to inferior stability and toxicity from cationic carrier components.

This work will optimize si-NP circulation time, tumor uptake, and tumor gene knockdown by implementing novel zwitterionic surface chemistry. The *in vivo* pharmacokinetics and toxicity profile of these si-NPs will be further controlled by screening hydrophobized nucleic acid cargo over a range of charge ratios. Finally, the mechanism of acute toxicities resulting from intravenous si-NP injection will be probed in depth. Understanding the mechanisms of si-NP toxicity will enhance our ability to design future nanocarriers with increased maximum tolerated doses. It is our goal to maximize the therapeutic window in this way—by identifying methods for increased si-NP efficacy and increased tolerability.

Specific Aim 1: Optimize si-NP corona chemistry for improved pharmacokinetics and tumor bioactivity. While previous work has improved si-NP stability and bioactivity through a balanced ratio of cationic and hydrophobic monomers, circulation half-lives remain too short for optimal tumor accumulation. Because tumors receive a relatively low percentage of total blood volume, ideal nanocarriers must circulate for extended times and maximize uptake and retention at the site of the tumor. This work improves si-NP surface chemistry in order to improve siRNA bioavailability, tumor uptake, and silencing activity. A library of polyplexes with different corona blocks including linear poly (ethylene glycol) (PEG), brush-like poly(oligoethylene glycol methacrylate) (POEGMA), and zwitterionic poly(2-methacryloyloxyethyl phosphorylcholine) (PMPC) were synthesized and comprehensively screened for stability, endosomolysis, toxicity, cell uptake, gene silencing, protein adsorption, complement activation, and *in vivo* pharmacokinetics. The lead si-NP candidates were then compared to our previous "gold-standard" si-NP with a 5k PEG corona for *in vivo* tumor gene silencing and cellular uptake.

Specific Aim 2: Reduce si-NP toxicity through charge ratio optimization and dual hydrophobization of carrier and cargo**.** Lead si-NPs with optimized corona chemistry were further improved by varying charge ratio (polymer: siRNA) and by use of hydrophobized, palmitic-acid functionalized siRNAs to reduce toxicity while maintaining improved circulation properties. Si-NPs were formulated at charge ratios of 10, 15, or 20, with or without palmitic acid siRNA functionalization. Si-NPs were screened *in vitro* for stability, endosomolysis, cell viability, uptake, and silencing activity to determine the impact of the charge ratio and hydrophobic modifications on particle performance. *In vivo,* more extensive pharmacokinetic and toxicity screenings were performed. Serum was monitored for ALT, AST, BUN levels, as well as immune markers such as IL-6, IL-12, IFN-γ, and TNF-α. Lead si-NP formulation based on improved half-life and toxicity was screened *in vivo* to confirm luciferase knockdown in a MDA-MB-231 tumor model and compared to Jet-PEI for tumor accumulation.

Specific Aim 3: Determine mechanisms of acute toxicity associated with high-dose intravenous injection of polyplex nanoparticles to inform future nanoparticle design. Based on observed behavioral similarities between si-NP-related toxicities and adenovirus-associated toxicities, the impact of PAFR inhibition was evaluated for reducing si-NP associated toxicities. Acute shock-like symptoms were thoroughly characterized and assessed. The ability of si-NPs to induce PAF release or activate PAFR themselves was explored *in vitro*. Additionally, clodronate liposomes were utilized to assess the importance of the mononuclear phagocyte system (MPS) for si-NP-mediated toxicities. Furthermore, the ability of alternative si-NP types to induce these anaphylactoid-like toxicities was evaluated in both normal BALB/c mice and inflammatory 4T1 tumor-bearing mice.

CHAPTER II

Alternatives to PEGylation: Zwitterionic Nanocarrier Surface Chemistry Improves siRNA Tumor Delivery and Silencing Activity

Text for Chapter II taken from:

Jackson MA, Werfel TA, Curvino EJ, Yu F, Kavanaugh TE, Sarett SM, Dockery MD, Kilchrist KV, Jackson AN, Giorgio TD, Duvall CL. Zwitterionic Nanocarrier Surface Chemistry Improves siRNA Tumor Delivery and Silencing Activity Relative to Polyethylene Glycol. *ACS Nano.* Jun 27, 2017. PMID: 28548843

2.1 Abstract

Although siRNA-based nanomedicines hold promise for cancer treatment, conventional siRNA-polymer complex (polyplex) nanocarrier systems have poor pharmacokinetics following intravenous delivery, hindering tumor accumulation. Here, we determined the impact of surface chemistry on the *in vivo* pharmacokinetics and tumor delivery of siRNA polyplexes. A library of diblock polymers was synthesized, all containing the same pH-responsive, endosomolytic polyplex core-forming block but different corona blocks: 5 kDa (benchmark) and 20 kDa linear PEG, 10 kDa and 20 kDa brush-like poly(oligo ethylene glycol) (POEGMA), and 10 kDa and 20 kDa zwitterionic phosphorylcholine-based polymers (PMPC). *In vitro*, it was found that 20 kDa PEG and 20 kDa PMPC had the highest stability in the presence of salt or heparin and were the most effective at blocking protein adsorption. Following intravenous delivery, 20 kDa PEG and PMPC coronas both extended circulation half-lives five-fold compared to 5 kDa PEG. However, in mouse orthotopic xenograft tumors, zwitterionic PMPC-based polyplexes showed highest *in*

vivo luciferase silencing (>75% knockdown for 10 days with single IV 1 mg/kg dose) and three-fold higher average tumor cell uptake than 5 kDa PEG polyplexes (20 kDa PEG polyplexes were only two-fold higher than 5 kDa PEG). These results show that high molecular weight zwitterionic polyplex coronas significantly enhance siRNA polyplex pharmacokinetics without sacrificing polyplex uptake and bioactivity within tumors when compared to traditional PEG architectures.

2.2 Introduction

There has been great interest in the development of small interfering RNAs (siRNAs) as human therapeutics for a variety of diseases, including cancer, with over 50 clinical trials completed or currently in progress.[61, 62] However, because of the poor pharmacokinetic properties of free siRNA, there remains an unmet need for carriers with optimized systemic bioavailability and delivery to solid tumors.[63] Because tumors are perfused with a relatively small fraction of the body's blood volume, siRNA therapeutics must remain stable and inert in the systemic circulation for extended time in order to maximize the opportunity for passive accumulation within a tumor.[64] The carrier must also be actively internalized and retained within the tumor cells rather than being transported back out of the tumor or being reabsorbed into the systemic circulation.

Upon intravenous administration, polyplexes encounter diverse delivery challenges that cause polyplex destabilization and/or removal by phagocytic cells, resulting in rapid clearance of the majority of the injected dose.[65, 66] Polyplexes can disassemble in circulation when they encounter serum proteins that penetrate polymer coronas or anionic heparan sulfates at the kidney glomerular basement membrane that compete with electrostatic interactions between

polymer and siRNAs; free uncomplexed siRNA is then rapidly filtered for removal in the urine.[25, 26, 66] Moreover, protein adsorption significantly affects biodistribution of polyplexes by marking them for recognition and phagocytosis by macrophages of the mononuclear phagocyte system (MPS) and/or potentially activating the complement pathway.[65, 67, 68]

Polyplex surface chemistry is one of the most influential factors determining pharmacokinetics *in vivo* because physicochemical surface properties like charge and hydrophilicity dictate nature and level of adsorption or penetration by proteins and other molecules such as heparan sulfates.[69] The most common and exhaustively explored surface modification method for increasing particle stability, reducing protein adsorption, and improving pharmacokinetics is the functionalization of particles with a PEG corona (PEGylation). The importance of PEG molecular weight, architecture, and surface density for increasing particle circulation time has been widely studied.[19, 70-73] However, proteins can penetrate PEG layers, resulting in opsonization, destabilization, and RES accumulation.[26, 74] Additionally, many studies have shown that PEG can decrease overall target (*i.e.*, tumor) cell uptake once the carrier reaches the desired tissue.[74, 75]

A promising alternative to PEGylation is "zwitteration" of polyplex coronas. Zwitterionic surfaces are extremely hydrophilic because they are hydrated through strong electrostatic interactions, whereas PEGylated surfaces interact with water molecules through hydrogen bonding.[44] Therefore, molecules that hydrate zwitterionic polymers are structured in the same way as in bulk water. This arrangement makes zwitterionic polymers thermodynamically unfavorable for protein adsorption, because there is no gain in free energy from displacing surface water molecules with protein.[44, 76] In general, zwitterionic coronas have been shown to

improve *in vitro* stability, cell uptake, and pharmacokinetics of some nanocarriers relative to both PEGylated and unmodified carriers.[77, 78]

One type of zwitterion, phosphorylcholine, has found particularly widespread use for anti-fouling applications and is a component of FDA-approved contact lenses and drug-eluting stents.[44-46] Phosphorylcholine-based polymers (*e.g.*, poly-methacryloyloxyethylphosphorylcholine, PMPC) are hemocompatible, easy to synthesize, and can mimic non-thrombogenic surfaces of red blood cells, which contain many phosphorylcholine groups. In the context of nucleic acid delivery, Ukawa and colleagues have used PMPC coatings in GALA-modified lipid nanoparticles to increase their plasmid DNA transfection *in vitro*.[79] PMPC has also been recently applied for tumor delivery of siRNA *in vivo.* Yu and colleagues used PMPC-based cationic polymers to intravenously deliver siRNA against MDM2, reducing NSCLC tumor growth *in vivo* compared to scrambled controls, but there was no analysis of pharmacokinetics, no analysis of per cell particle uptake, and no comparison to PEGylated polyplexes.[80] There remains a need to comprehensively benchmark PMPC against traditional PEG architectures for *in vivo* pharmacokinetics, siRNA delivery, and activity within tumors.

Previous work in our lab focused on optimization of the polyplex core-forming block, resulting in the identification of a leading composition containing a balanced ratio of cationic and hydrophobic monomers (dimethylamino ethyl methacrylate (DMAEMA) and butyl methacrylate (BMA), respectively).[21] This optimization study solely utilized 5kDa linear PEG as the corona-forming block. Here, we preserved the optimal core-forming DMAEMA-*co*-BMA composition and chain extended various corona-forming blocks in order to dissect the impact of corona chemistry on *in vivo* stability, pharmacokinetics, tumor accumulation, and tumor gene knockdown. We and others have sought to improve PEGylated nanocarrier pharmacokinetics

through the use of a brush-like PEG architecture or high molecular weight Y-shaped PEGs, to varying degrees of success.[71, 72, 81-83] In this study we compared PMPC coronas to these PEG architectures in addition to the linear 5kDa PEG. We analyzed these polyplex surface materials using a number of techniques that quantify protein adsorption, polyplex stability, *in vitro* uptake and bioactivity, as well as *in vivo* pharmacokinetics and tumor gene silencing activity.

2.3 Results and Discussion

Six diblock copolymers were synthesized with a pH-responsive block comprising a random copolymer of dimethylaminoethyl methacrylate (DMAEMA) and butyl methacrylate (BMA) at equimolar ratio and a total degree of polymerization of approximately 150. The polyplex corona-forming blocks consisted of 5kDa linear PEG, 20kDa linear Y-shaped PEG, 10kDa poly(oligo(ethylene glycol) methyl ether methacrylate) (POEGMA), 20kDa POEGMA, 10kDa zwitterionic PMPC, or 20kDa zwitterionic PMPC corona (**Figure 2.1**). The 5kDa linear PEG and 20kDa linear Y-shaped PEGs were purchased, conjugated to the RAFT chain transfer agent, and then chain extended with RAFT to form the core-forming DMAEMA-co-BMA block. For the POEGMA and PMPC polymers, the core-forming DMAEMA-*co*-BMA block was first RAFT-polymerized and was subsequently extended using RAFT to polymerize two variants of each hydrophilic block composition near their target molecular weights of 10kDa and 20kDa. All diblock polymers were well-matched in terms of consistent DMAEMA-*co*-BMA block size and composition (approximately 150 degree of polymerization with 50% of each monomer) and all polymers tested had relatively low polydispersity indices (PDI) ranging 1-1.3 (**Table 1, ^{1}H-NMR methods detailed in Supplemental Figures A.S1-S3**). These properties were important to control because small changes in core length or composition could affect the polyplex

performance independent of corona chemistry.[21] The 5k linear PEG, 10k PMPC, and 10k POEGMA corona lengths were chosen because they were the shortest corona lengths that would form relatively monodisperse polyplex structures. The 20k PMPC and 20k POEGMA were chosen as standards to compare to the 20kDa Y-shaped PEG, which has been used in FDA-approved drugs for extending circulation time.[71, 84]

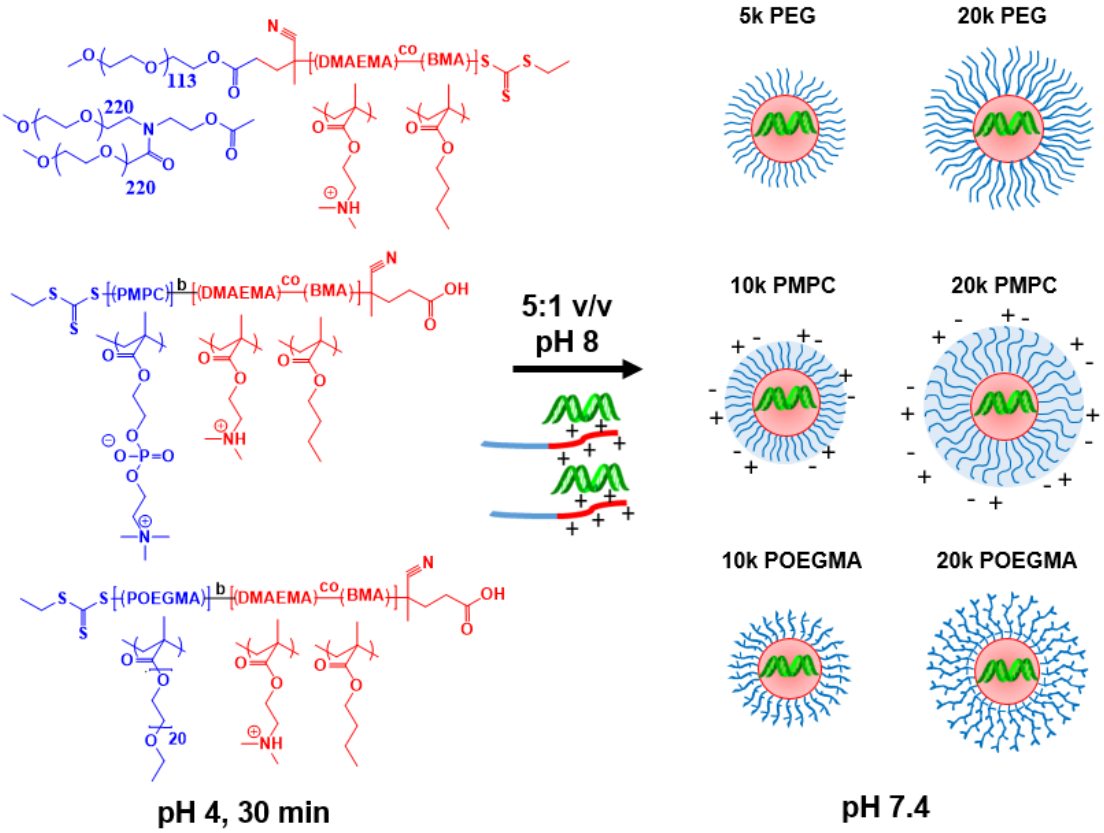

Figure 2.1 siRNA polyplexes containing varied corona architectures. All polymers contain the same polyplex core-forming block consisting of equimolar DMAEMA and BMA. The corona-forming blocks comprise either linear PEG, zwitterionic PMPC, or brush PEG structures (POEGMA), as pictured. Polymer structures are displayed on the left, with core-forming block in red and corona-forming block in blue. Polymers are complexed with siRNA at low pH, triggering spontaneous assembly of polyplexes before the pH is raised to physiological pH.

Table 2.1 Polymer molecular weights (^{1}H NMR), monomer compositions (^{1}H NMR), and polydispersity indices (gel permeation chromatography)**.**

[a] PMPC polymers were not analyzed with GPC due to insolubility in mobile DMF phase.

Polymer	Total MW (g/mol)	Corona MW (g/mol)	% BMA	% DMAEMA	PDI
5k PEG	28636	5000	50	50	1.021
20k PEG	43353	20000	50	50	1.071
10k PMPC	34129	10177	51	49	*a*
20k PMPC	45044	21092	50	50	*a*
10k POEGMA	34171	11716	47	53	1.156
20k POEGMA	42619	18667	49	51	1.296

Polyplexes were formed by first mixing polymer and siRNA at various N^+:P^- ratios (number of protonated polymer amines :number of siRNA backbone phosphates) in pH 4.0 citrate buffer, and then the pH was raised to 7.4 (**Figure 2.1**). Based on a Ribogreen assay, all polyplexes reached an encapsulation efficiency of around 75-80% by N^+:P^- 10, and slightly higher encapsulation efficiencies were achieved at N^+:P^- 20 (**Figure 2.2a**). To determine the best N^+:P^- ratio to use in subsequent testing of this library of polymers, we evaluated the average stability differences between polyplexes at N^+:P^- 10 and N^+:P^- 20 after a brief (30 min) incubation in 30% fetal bovine serum (FBS). By measuring the Förster Resonance Energy Transfer (FRET) signal between co-encapsulated fluorescent siRNAs relative to the signal of polyplexes unchallenged by FBS, we observed a decrease in average stability of all polyplexes at N^+:P^- 10 relative to N^+:P^- 20. Average stability ranged from 75-86% FRET at N^+:P^- 20 and from 42 to 48% FRET at N^+:P^- 10 (**Figure 2.2b**). Because of these results, we selected N^+:P^- 20 ratio for all further studies. At this short serum incubation time, there were no significant differences between polyplexes of different coronas at a given N^+:P^- ratio.

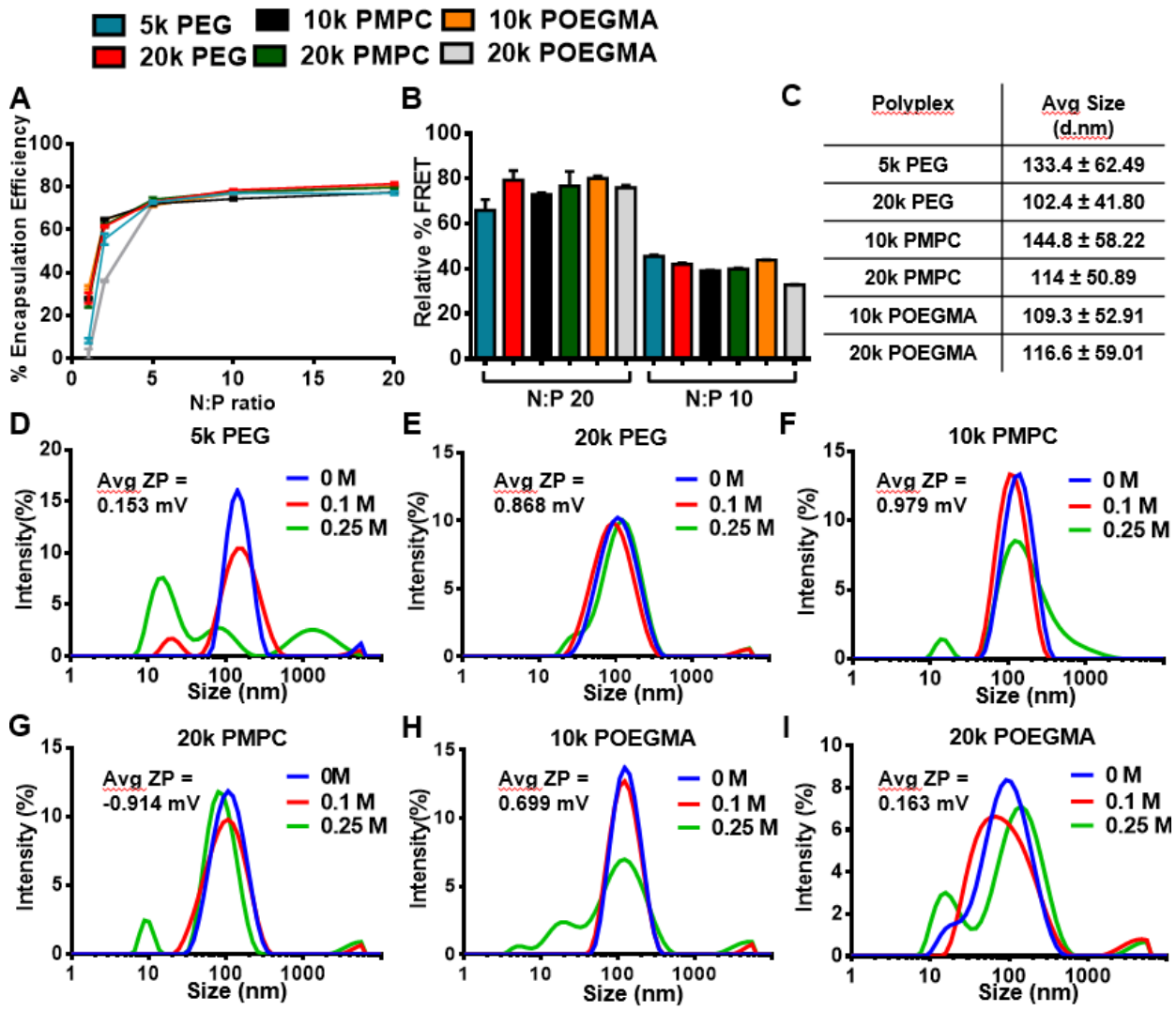

Figure 2.2 Polyplexes with different corona chemistries have similar size, zeta potential, and cargo loading but varied stability against high salt concentrations. (A-B) Polyplex siRNA encapsulation efficiency and stability is highest at N^+:P^- 20. (A) Ribogreen assay reveals polyplex encapsulation plateaus by N^+:P^- ratio of 10. (B) Polyplexes retain higher stability after a 30 minute incubation in 30% FBS at N^+:P^- 20 compared to N^+:P^- 10 ($p<0.01$, n=3). (C) All polyplexes were around 100-145nm in average size. (D-I) Dynamic light scattering traces show that 20k PMPC and 20k PEG populations are more resistant to high salt conditions (N^+:P^- 20).

Importantly, despite their varied corona molecular weights and characteristics, all polyplexes had similar average hydrodynamic diameters of approximately 100 nm and showed no significant differences in surface charge (near neutral zeta potential) (**Figure 2.2c-i,**

Supplemental Figure A.S4). Thus, although size and surface charge are known to affect pharmacokinetics, these factors were constant among each of the polyplexes despite different hydrophilic block chemistries.[68] Polyplex size and stability evaluated under increasing salt concentrations showed that size of most polyplexes was only slightly affected by the addition of 0.1 M salt (**Figure 2.2d-i**). However, at 0.25 M NaCl, the 20k PMPC and 20k PEG polyplexes appeared most resistant to destabilization by increasing salt concentrations, while the 5k PEG and POEGMA corona polyplexes lost their uniform size distribution. This result suggests that larger coronas improved stability for linear PEG and zwitterionic PMPC coronas, but in the case of POEGMA-based polyplexes, increasing corona size did not improve stability. Polyplexes made with the longer 20k POEGMA corona, in addition to being less stable than other polyplexes, were also more polydispersed at baseline in low-salt conditions compared to other polyplexes. This is possibly due to excessive bulkiness, making it more difficult for this polymer to form tightly-packaged micelles through electrostatic interactions in the core.[85] While these POEGMA polymers were selected because the 950 Da side chains form more hydrophilic blocks than 300 Da OEGMAs, high molecular weight monomers are not as well studied as shorter OEGMA monomers, and their extended side chains may cause considerable steric repulsion between corona-forming blocks, a potentially destabilizing factor.[82, 86]

In order to maximize polyplex accumulation at the site of the tumor, polyplexes must resist destabilization in circulation.[64] The main sources of polyplex instability in the blood circulation include serum and anionic heparan sulfates in the kidney glomerular basement membrane, the latter of which can interact with positively charged components of siRNA polyplexes and result in decomplexation.[25, 65, 66] To determine the impact of particle surface chemistry on polyplex stability, we challenged polyplexes containing FRET pair-loaded siRNA

with serum or heparin salts. We found that at higher serum levels (30%), alternative corona chemistries improved stability compared to 5k linear PEG coronas, but there were few stability differences between individual coronas (**Supplemental Figure A.S5**). At 10% serum, all polyplexes at N^+:P^- 20 resisted destabilization regardless of corona block (**Supplemental Figure A.S5**). As shown previously in Figure 2.2b, polyplex N^+:P^- ratio appeared more important for short-term serum stability than corona block differences.

Heparin salt-induced destabilization showed a greater dependency on corona composition. In heparin salts at a range of concentrations (**Figure 2.3a-c**), 20k PEG and zwitterionic 20k PMPC coronas provided the greatest stability over time compared to all other polyplex coronas. In 100 U/mL heparin over 100 minutes, the average FRET signal for 20k PMPC and 20k PEG samples was significantly higher than that of 5k PEG, 20k POEGMA, and 10k PMPC ($p<0.05$), indicating greater resistance to charge-induced destabilization. The 20k PMPC and 20k PEG also performed best with 60 U/mL heparin, only decreasing in average FRET signal by 40 and 36%, respectively, while the FRET signal in all other polyplex samples decreased by 56-63%. At each heparin condition, 10k POEGMA was intermediately stable, and this was most apparent at 20 U/mL heparin, when 10k POEGMA did not diverge from 20k PEG and 20k PMPC until roughly 55 minutes of incubation. The other polyplexes, 5k PEG, 10k PMPC, and 20k POEGMA, were consistently the least heparin-stable. While larger corona molecular weight improved stability for linear PEGylated and zwitterated polyplexes, this advantage did not hold true for POEGMA coronas. This could possibly be due to unfavorable steric properties of the bulky POEGMA side chains, which could potentially reduce core stability at baseline.[85] While some heparin may be binding free, uncomplexed polymer, the results of our Ribogreen assay (**Figure 2.2a**) indicate that the packaging of siRNA is the same for all polyplexes at N^+:P^- 20, so the molar amount of

free polymer is consistent between all polyplexes and unlikely to influence these comparisons. Heparin binding free polymer is also unlikely based on the polyplex DLS traces (**Figure 2.2d-i**) that do not show evidence of free polymer and because any uncomplexed polymer in solution is micellar (due to the presence of hydrophobic BMA in the core-forming block), thus making DMAEMA unavailable for binding.[21]

In order for the polyplexes to enable siRNA bioavailability in the target cell cytoplasm, the polyplexes must exhibit efficient cell uptake, pH-responsive endosomal escape, and target gene knockdown, while also not being cytotoxic to normal (non-cancerous) cells. The core-forming block of each polyplex in our library, consisting of DMAEMA-*co*-BMA, has previously been optimized for pH-responsive endosomolytic behavior, and we hypothesized that the various corona chemistries would not affect this property.[21] We measured pH-dependent membrane disruptive behavior, a surrogate assay for endosome escape capability in which polyplex samples are incubated with red blood cells in buffers of progressively lower pH that mimic extracellular, early/late endosome, and lysosome environments.[87] All of the polyplexes produced membrane disruptive activity at pH values at or below 6.8, corresponding to pHs found in the endolysosomal pathway, but no hemolytic activity occurred at physiological and extracellular pH of 7.4 (**Figure 2.4a**). Because the pH-responsive behavior of these polyplexes is controlled by their core blocks, it was expected that the different coronas would not differentially impact endosomolytic behavior. These trends were independent of polyplex concentration in the range tested (**Supplement Figure A.S6**).

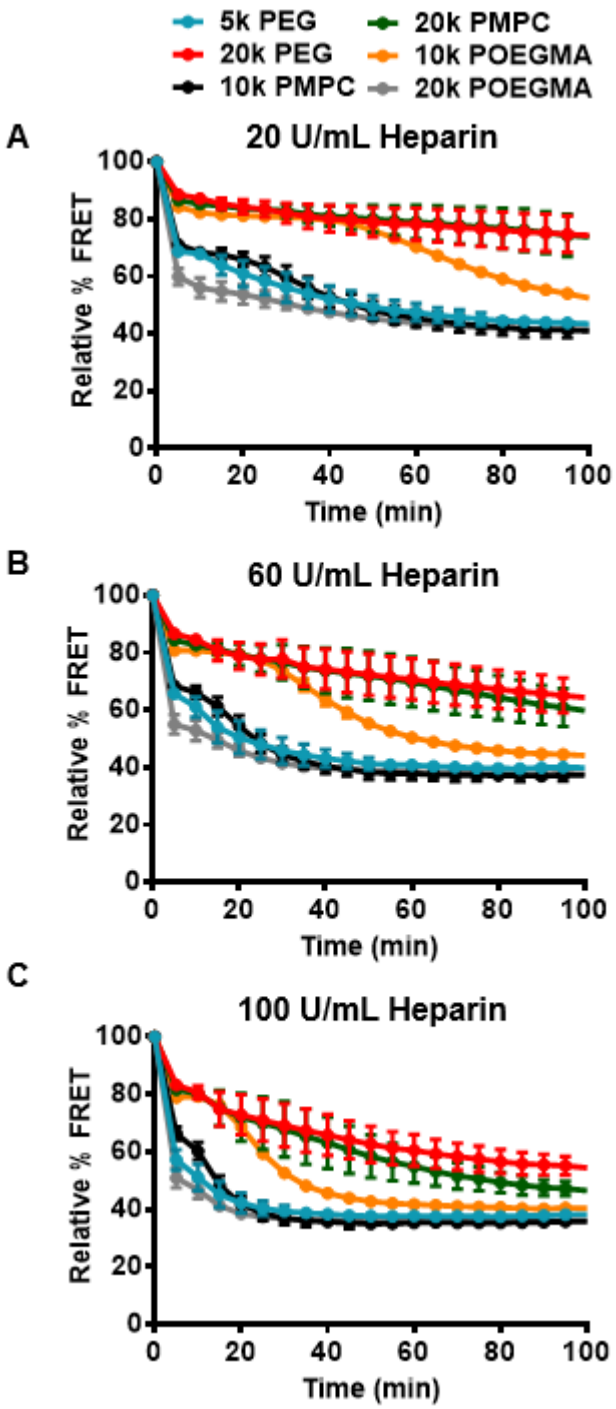

Figure 2.3 20k PEG and 20k PMPC corona-forming blocks increase polyplex stability in heparin salts relative to all other formulations**.** Polyplexes were also incubated for 100 min in 20 U/mL (A), 60 U/mL (B), and 100 U/mL (C) heparin salts. 20k PMPC and 20k PEG maintained greatest stability levels at each heparin condition. All measurements represent average of 3 separate

stability experiments. All polyplexes were formulated at N^+:P^- 20.

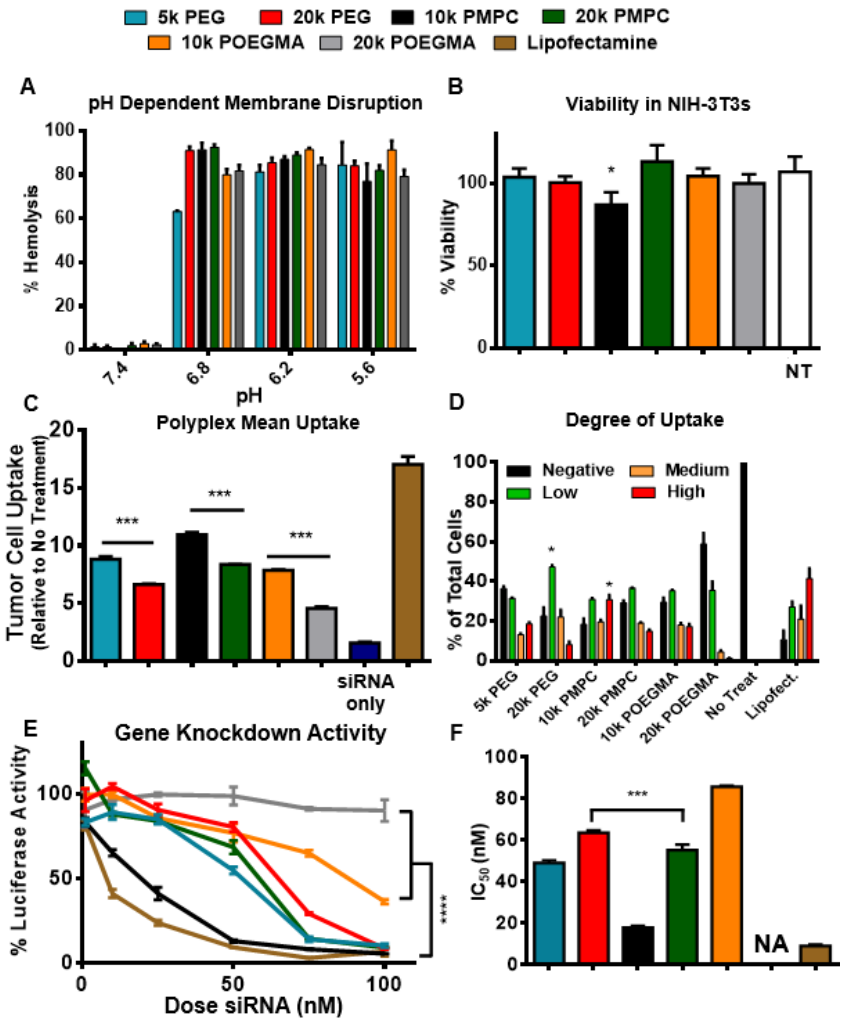

Figure 2.4 *In vitro*, all tested polyplex surface chemistries, except POEGMA, exhibited desirable hemolysis, cytocompatibility, uptake, and target gene knockdown properties. All assays were performed at a dose of 100 nM siRNA and 2.7 µM polymer (N^+:P^- 20) unless otherwise noted. (A) In a red blood cell hemolysis assay, all polyplexes (at 40 µg/mL polymer) displayed similar pH-dependent membrane disruptive behavior well-tuned for endosomal escape due to their consistent core-forming polymer block composition which dictates this behavior. (B) Polyplex viability in NIH 3T3 fibroblasts at 100 nM siRNA 48 h after polyplex addition. (C) All high molecular weight coronas had significantly lower uptake compared to lower molecular weight counterparts, ($p<0.01$, $n=3$). (D) Percent of cells in low, medium, and high gates for each polyplex. 20k PEG polyplexes had the highest percent of cells in the low uptake group compared to any other polyplex ($p<0.001$, $n=3$). (E) Dose-response curve of polyplex inhibition of luciferase activity. Luciferase activity was monitored after 48 hours polyplex treatment. (F) IC_{50}

values for all polyplexes reveal significantly improved efficacy of PMPC-based polyplexes compared to PEGylated polyplexes of similar molecular weight ($p<0.04$, $n=3$).

We next screened for toxicity of all polyplexes in luciferase-expressing NIH3T3 fibroblasts (**Figure 2.4b**), in order to determine whether the polyplexes were harmful to normal and non-cancerous cells. At 48 hours post-treatment, none of the polyplexes significantly affected viability levels relative to untreated cells, with the exception of 10k PMPC. Average viability of 10k PMPC was still quite high, at 87%, indicating it was also relatively non-toxic. We also evaluated cytotoxicity of all polyplexes bearing scrambled siRNA in MDA-MB-231 cancer cells. All cell viability values were still greater than 75% after 48 hour incubation with high polyplex concentrations (**Supplemental Figure A.S7**).

We next evaluated uptake of polyplexes by MDA-MB-231 breast cancer cells (**Figure 2.4c**). Overall, shorter polyplexes made with smaller molecular weight corona blocks had significantly higher mean fluorescence intensities compared to more shielded polyplexes comprising longer corona-forming blocks ($p<0.001$, $n=3$). In comparing different polyplex corona-forming block chemistries, the mean fluorescence intensity of 20k PMPC was greater than 20k PEG polyplexes, and 10k PMPC had the highest uptake levels overall ($p<0.001$, $n=3$). For *in vitro* uptake, lower molecular weight coronas are often associated with increased cell uptake, because the cationic PDMAEMA components are less shielded.[88] However, polyplexes made with shorter corona-forming blocks are generally less stable and therefore likely to produce less favorable *in vivo* pharmacokinetic properties. We also stratified polyplex uptake based on the percent of cells found within low, medium, and high uptake subsets (**Figure 2.4d**, **Supplemental Figure A.S8a**) in order to further interrogate differences in the distribution of polyplex uptake levels within the different treated cell populations. The 20k PEG had the highest

percent of polyplex uptake positive cells in the low uptake group by a significant margin ($p<0.001$), with 47% of cells in this group, while all other polyplex types ranged from 31-36% of cells in the low uptake group. In comparison, 10k PMPC had the highest percent of cells in the "high" group, at 31%. 20k PMPC, while more shielded than both 5k PEG and 10k POEGMA, had a similar percent of cells in the "high" uptake category (14-17%) as the shorter corona polyplexes. In the high uptake category, 20k PEG polyplexes had the lowest percent of cells (8.9%), after 20k POEGMA (1.22%), which was significantly lower than the percent of cells treated with 20k PMPC polyplexes in the high category (8.9% *vs.* 15%, $p<0.04$). These combined data provide support that PMPC-based coronas have higher cell uptake properties compared to their PEGylated counterparts, suggesting that zwitterionic coronas provide polyplexes with stealth properties without limiting polyplex uptake as significantly as incorporation of high molecular weight, stealth PEG coronas. These data suggest that PMPC is less susceptible to the well-described "PEG dilemma" in drug delivery.[26] Histograms of these cell populations can be found in **Supplemental Figure A.S8b**.

After confirming pH-responsiveness, cytocompatibility, and tumor cell uptake behavior of the polyplexes, we evaluated knockdown of the model gene luciferase in luciferase-expressing MDA-MB 231 breast cancer cells (**Figure 2.4e**), across a range of doses. At the highest dose of 100 nM siRNA after 48 hours, cells exposed to 5k PEG, 20k PEG, or either PMPC corona all retained less than 10% luciferase activity (90% knockdown), which was significantly lower than 10k POEGMA, with 50% knockdown, and 20k POEGMA, with no significant knockdown. At 75 nM, differences between linear PEG and PMPC polyplexes emerged. 10k PMPC corona polyplexes had the best bioactivity, with 8% remaining luciferase activity, followed by 20k PMPC and 5k PEG, which were not significantly different from each other at 14% luciferase

activity. 20k PEG coronas at this dose had significantly higher remaining luciferase activity than 20k PMPC and 5k PEG (29%), providing evidence that PMPC-based coronas have increased bioactivity compared to their linear PEG counterparts. These general trends are also evidenced by the IC_{50} values for each polyplex **(Figure 2.4f**). Polyplexes containing 10k PMPC had the lowest IC_{50}, at 18 nM, compared to 5k PEG at 49 nM. 20k PMPC-based polyplexes also had a significantly lower IC_{50} than 20k PEG polyplexes (55 nM *vs.* 64 nM), with values similar to the IC_{50} of less well-shielded 5k PEG. All polyplex IC_{50} averages were significantly different from each other ($p < 0.04$). In general, the POEGMA-based coronas did not produce desirable levels of *in vitro* bioactivity, while all other polyplex formulations produced potent knockdown with negligible cytotoxicity.

Both PEGylation and zwitteration are designed to reduce protein adsorption to nanocarriers because opsonization makes nanocarriers more identifiable to macrophages of the MPS and/or destabilizes polyplexes. If complement protein C3b adsorbs, the complement cascade can be activated, further recruiting immune cells and promoting rapid clearance.[67] We used isothermal titration calorimetry (ITC) and a hemolysis-based complement assay to evaluate how PEGylation and zwitteration differentially affect protein adsorption as a function of block molecular weight.

In ITC, a protein solution is slowly titrated into a solution of polyplexes, and changes in heat resulting from their interaction are recorded (**Figure 2.5a**). These heat changes can be used to calculate entropy, enthalpy, and Gibb's free energy of interaction between the protein and nanocarrier.[89, 90] Albumin was used here as a model for serum proteins, since it comprises the largest percent of human serum compared to other proteins and is known to opsonize PEGylated nanoparticles.[26, 27] Overall, each polyplex, whether PEGylated or zwitterated, had a positive

Gibb's free energy of interaction with albumin (**Figure 2.5b**). This indicates that albumin binding was not spontaneous and therefore not favored. However, the magnitude of average ΔG values was increased for the higher molecular weight coronas as compared to their lower molecular weight counterparts, indicating albumin adsorption was least favorable for these polymers. The 20k linear Y-shaped PEG corona had the largest ΔG values of any polyplex, followed by the 20k PMPC, and both were significantly higher than ΔG of 5k PEG ($p<0.05$, n=3). The significant differences between polyplex coronas of higher and lower molecular weight indicate the importance of corona molecular weight in blocking protein adsorption.

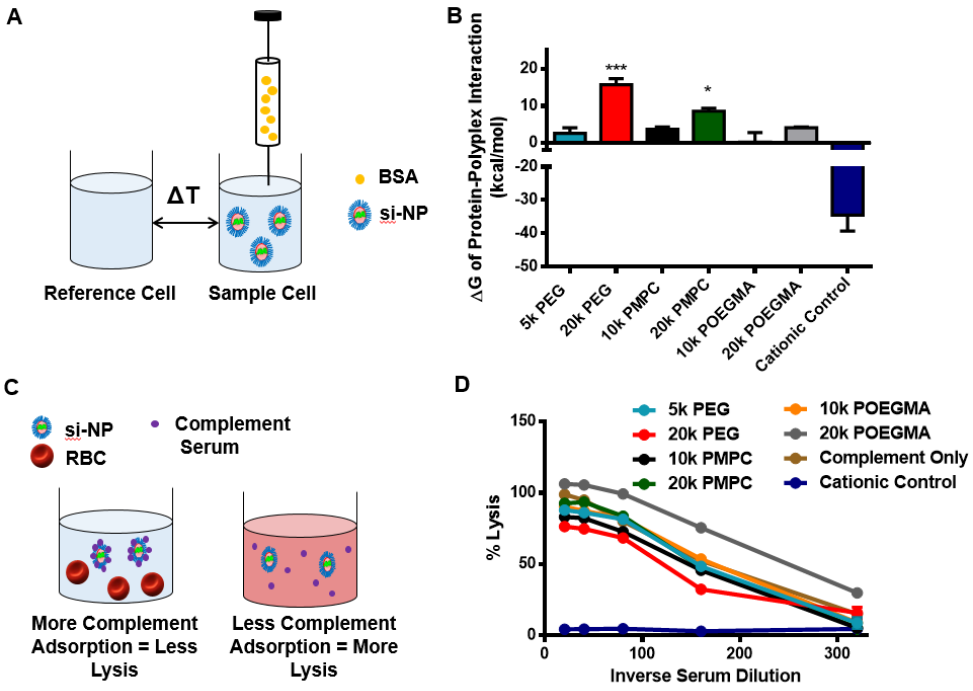

Figure 2.5 Higher molecular weight coronas reduce albumin adsorption while none of the polyplexes significantly adsorb complement proteins. (A) Schematic of isothermal titration calorimetry setup. BSA is slowly titrated into solution of polyplexes, and changes in heat are recorded and used to calculate thermodynamic parameters. (B) ITC of polyplexes (0.5 mg/mL polymer, N^+:P^- 20) indicated significantly less favorable BSA interaction for 20k PEG and 20k PMPC compared to standard 5k PEG (n=3, $p<0.05$). (C) Schematic of complement assay setup. (D) Negligible complement protein adsorption was observed for all polyplex surface chemistries, measured by % lysis compared to complement protein controls at various dilutions. Cationic

control polyplexes (100% PDMAEMA-based particle surface) served as a positive control for protein/complement adsorption in these assays.

All polyplexes with neutrally-charged, hydrophilic coronas were compared to a positive control polyplex containing 100% cationic PDMAEMA in its corona, which is known to significantly adsorb proteins at physiological pH.[71, 91, 92] As expected, this cationic control showed negative ΔG values averaging -35 kcal/mol, indicating a highly favorable interaction with albumin. While all raw ITC data showed endothermic heat changes for all of the shielded polyplexes, the cationic control polyplexes had highly exothermic heat changes (**Supplemental Figure A.S9**). The stark contrast between the cationic control polyplex and the neutral polyplex coronas demonstrates the overall impact of a "stealth" corona in reducing protein adsorption. Because albumin is not the only component of a nanoparticle protein corona, this contrast was also demonstrated for whole FBS, using a qualitative agarose gel binding assay (**Supplemental Figure A.S10**).[27] The cationic PDMAEMA-corona particles retained high FBS signal in the loading well, where polyplexes are known to remain (instead of migrating through the gel), while protein signal from wells containing all other polyplexes was much lower and closely matched the signal from wells containing only FBS.[21] This implies that overall serum adsorption is low for all shielded polyplexes with the various coronas, but high for cationic PDMAEMA particles.

In order to evaluate potential complement protein adsorption by the various corona chemistries, we used a hemolytic assay modified from Bartlett and colleagues.[93] Polyplexes were incubated with various dilutions of human complement sera and then antibody-sensitized sheep erythrocytes were added to each mixture. If complement proteins do not adsorb to polyplexes, then they are available in solution to lyse the erythrocytes. However, if adsorption does occur, red blood cell lysis is reduced as fewer complement proteins are available to cause lysis (**Figure**

2.5c). For all polyplexes, we did not observe significant differences in lysis compared to the complement only protein controls at all concentrations of complement sera, meaning that complement adsorption was negligible (**Figure 2.5d**). The unshielded cationic polyplexes with a PDMAEMA corona, on the other hand, robustly reduced lysis compared to the complement only control, indicating significant adsorption, as expected. The 20k POEGMA corona polyplex exhibited slightly elevated lysis levels compared to the protein only control, probably as a result of its greater instability in serum, but overall, the coronas tested do not react spontaneously with complement proteins to any significant degree, in agreement with the results for albumin adsorption as measured by ITC. These data also indicate that the complement assay may not be as sensitive as the ITC method at detecting small functional differences in protein adsorption.

We next studied the *in vivo* pharmacokinetics of the polyplex library after intravenous administration. Traditional methods of characterizing nanocarrier pharmacokinetics rely on multiple blood draws and extrapolation to determine initial nanocarrier blood concentrations. Intravital confocal laser scanning microscopy (IVM), on the other hand, provides real time, continuous tracking of fluorescence in the mouse ear blood vessels and requires fewer animals.[94] Recently intravital microscopy has been used to monitor polyplexes in blood circulation, particularly to understand the impact of core stabilizing components on circulation time and to characterize the impact of species-specific immune state on nanoparticle clearance.[23, 24, 95] IVM provides a more absolute quantification of particle pharmacokinetic parameters and is therefore a more robust way to discern differences between PEGylated and zwitterionic coronas. For our study, polyplexes were loaded with Cy5-conjugated cargo, and the fluorescence signal tracked for 20 minutes after injection.

Intravital microscopy studies revealed improved pharmacokinetic properties for 20k PMPC and 20k PEG, in agreement with our *in vitro* stability results, as visualized in **Figure 2.6a**. Pharmacokinetic curves of blood circulation (**Figure 2.6b**) were fit to the data, and area under the curve values for 20k PMPC and 20k PEG were 586 and 507 (mg* min)/(L) respectively, roughly three to four times higher than all other polyplexes tested (**Figure 2.6c**). Average circulation half-lives for 20k PMPC and 20k PEG were 26 minutes and 22 minutes, respectively, while circulation half-lives for all other polyplexes ranged from 5-8 minutes (**Table 2.2**). Average circulation half-life for free nucleic acid was less than 2 minutes. Similarly, 20k PMPC and 20k PEG had much lower clearance values than any other polyplexes studied (**Table 2.2**). Organ biodistribution (**Supplemental Figure A.S11**) studies at 20 minutes revealed that for all of the polyplexes, the greatest percentage of the fluorescent siRNA was localized in the kidneys, followed by the MPS organs (liver and spleen). For all polyplexes, less than 50% of the total fluorescence was localized in the kidney, which is an improvement over many other polyplex systems in the literature which are more rapidly disassembled in the kidney and therefore have higher kidney accumulation.[23, 96-99] However, this is likely due in large part to the balance of cationic and hydrophobic monomers in the core-forming block of these polyplexes, which reduces heparan sulfate-based disassembly as our group has shown previously.[21]

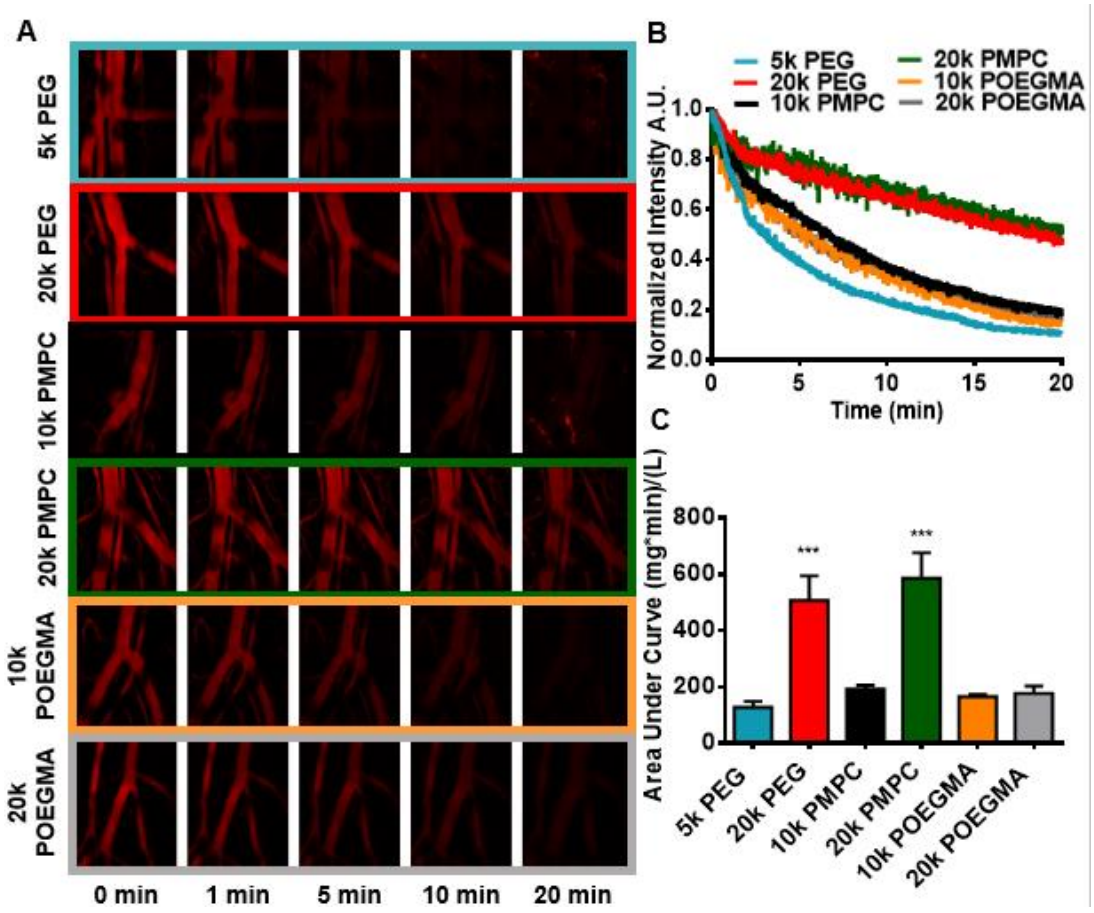

Figure 2.6 High molecular weight zwitterionic and linear PEG coronas significantly improve polyplex pharmacokinetics (1 mg/kg Cy5-siRNA, 1.89 µmol/kg polymer, N^+:P^- 20)**.** (A) Panel of intravital microscopy images for visualization of pharmacokinetic differences between polyplexes shows obvious increase in circulation time for 20k PEG and 20k PMPC compared to gold standard 5k PEG. (B) Average intravascular fluorescence intensity curves from mouse ear vessel imaging quantify this outcome (n=4). (C) Area under the curve shows that 20k PEG and 20k PMPC had roughly three to four-fold higher bioavailability compared to other polyplexes (n=4, $p < 0.001$).

Table 2.2 Pharmacokinetic parameters quantified from intravascular imaging data including half-life (T ½), area under curve (AUC), and clearance (Cl).

Polymer	T ½ (min)	AUC (mg *min)/(L)	Cl (mL/min)
5k PEG	5.2 ± 1.7	127 ± 37	0.22 ± 0.07
20k PEG	22.4 ± 5.8	507 ± 152	0.06 ± 0.02
10k PMPC	8.4 ± 1.0	192 ± 23	0.13 ± 0.02

20k PMPC	26.3 ± 5.5	586 ± 157	0.05 ± 0.01
10k POEGMA	7.6 ± 0.4	165 ± 14	0.15 ± 0.01
20k POEGMA	7.4 ± 2.0	176 ± 45	0.15 ± 0.04
Cy5 Nucleic Acid	1.87±0.20	75 ± 1.4	4.20 ± 0.27

The pharmacokinetic properties of 20k PMPC and 20k PEG tested here are field-leading relative to other published polyplex siRNA delivery systems. For example, the cyclodextrin-based polyplex system, CALAA-01 that was administered to humans in the first ever RNAi clinical trial, cleared from humans, monkeys, mice, and rats below the detection limit only 30 minutes after intravenous injection.[37] Our 20k PEG and 20k PMPC polyplexes, on the other hand, have only just reached their half-life after approximately 30 minutes. Others have sought to improve polyplex circulation stability through the addition of cholesterol-modified siRNA in combination with 20kDa PEG-conjugated cationic polymers, but such modifications only increased half-lives to around 6-10 minutes.[24] An additional approach to increasing circulation time in a similar system is polyplex core crosslinking, but this only increased circulation half-lives to roughly 10 minutes based on intravital microscopy.[96] Our polyplexes effectively combine a highly-stabilized core with highly-stabilizing, protein-stealth coronas, increasing their circulation times beyond the gold standards in the field.

In all, our results indicate that polyplexes of zwitterionic 20k PMPC and 20k PEG were the most blood stable and may also be most resistant to natural clearance mechanisms like renal heparan sulfate-mediated clearance, protein adsorption, and phagocytosis. These properties suggest they are the leading candidates for development for oncological siRNA therapeutics. Similar to our *in vitro* results, the high molecular weight POEGMA coronas did not exhibit the same beneficial properties, most likely due to the poor stability properties of these polyplexes.

When nanoparticles circulate longer in the bloodstream, their systemic bioavailability increases, and they have a greater opportunity to accumulate within tumors. Because our higher molecular weight coronas had such dramatic improvement in circulation half-lives and clearance properties, we hypothesized that they would also improve tumor accumulation and gene silencing. Therefore, we selectively compared the ability of 20k PEG and 20k PMPC to achieve tumor cell delivery and target gene silencing of the model gene luciferase in a mouse orthotopic model of breast cancer. These leading formulations were benchmarked against our previous gold standard 5k PEG polyplexes.[21, 47]

Mice bearing luciferase-expressing MDA-MB 231 mammary fat pad tumors were intravenously injected with 20k PMPC, 20k PEG, or 5k PEG polyplexes bearing 1 mg/kg anti-luciferase or scrambled control siRNAs. Each animal received only one treatment, and tumor luminescence was monitored for a 10-day period post-injection. We compared the relative luminescence of each individual tumor to its luminescence prior to polyplex injection, and the luminescence values for the luciferase siRNA polyplex-treated tumors were compared to average luminescence values for the tumors from scrambled control siRNA polyplex-treated mice. There were no significant differences in relative luminescence between any scrambled polyplex group throughout the study period.

Throughout the 10-day period post-injection, mice treated with zwitterionic 20k PMPC polyplexes containing luciferase siRNA exhibited more potent and long-lasting luciferase silencing than either PEG-based polyplex (**Figure 2.7a**), with significantly increased knockdown on Days 3-7. Throughout the treatment, relative luminescence values for 20k PMPC averaged about 20% that of scrambled controls, indicating 80% knockdown. The differences between 20k PEG and 5k PEG were not significant, but average knockdown potency tended to be slightly

higher for the 20k PEG than 5k PEG polyplexes. Average knockdown of luciferase by 20k PEG ranged from 75% on Day 1 to 36% on Day 10 compared to scrambled polyplex controls, and knockdown of luciferase by 5k PEG ranged from average 56% on Day 1 to 35% on Day 10. This study suggests that, despite their similar pharmacokinetic properties, 20k PMPC has higher *in vivo* bioactivity compared to 20k PEG (representative tumor luminescence images demonstrating these trends are displayed in **Figure 2.7b**). Mouse body weight was recorded each day of the study period as an indicator of toxicity, and there were no significant differences between any polyplex treatment group and untreated tumor-bearing mice (**Supplement Figure A.S12**).

In order to elucidate the mechanism behind the increased tumor gene knockdown of zwitterionic 20k PMPC, we also studied the *in vivo* biodistribution and tumor cell uptake of zwitterated *vs.* PEGylated polyplexes. We injected tumor-bearing mice with 20k PMPC, 20k PEG, and 5k PEG polyplexes bearing Cy5-labeled cargo. After 24 hours, the tumors were removed and dissociated into a single cell suspension to measure polyplex internalization level per tumor cell (tumor cells identified as GFP positive based on reporter transduced prior to tumor cell inoculation into mice). After 24 hours of accumulation time, zwitterionic 20k PMPC showed significantly higher tumor cell uptake levels than either 5k or 20k PEGylated polyplexes (**Figures 2.7c and 2.d**). Mean Cy5 fluorescence intensity in GFP positive (tumor) cells for 20k PMPC was three-fold higher than that of 5k PEG and almost two-fold higher than 20k PEG. Additionally, 20k PMPC had the highest percentage of Cy5-positive tumor cells, with roughly 90% positive, while average percent uptake for 5k PEG and 20k PEG was 40% and 80%, respectively, at 24 hours (**Figure 2.7e**). These data suggest that the longer half-lives of 20k PMPC and 20k PEG played an important role in their tumor uptake, and that 20k PMPC coronas do not sacrifice cell uptake as much as PEG-based coronas. Organ biodistribution data based on

overall fluorescence at this 24-hour time point revealed that average radiance in tumors was 1.2-1.9-fold higher than liver average radiance and 2.4-7.4-fold higher than heart and lung average radiance for all of the polyplexes studied (**Supplemental Figure A.S13**).

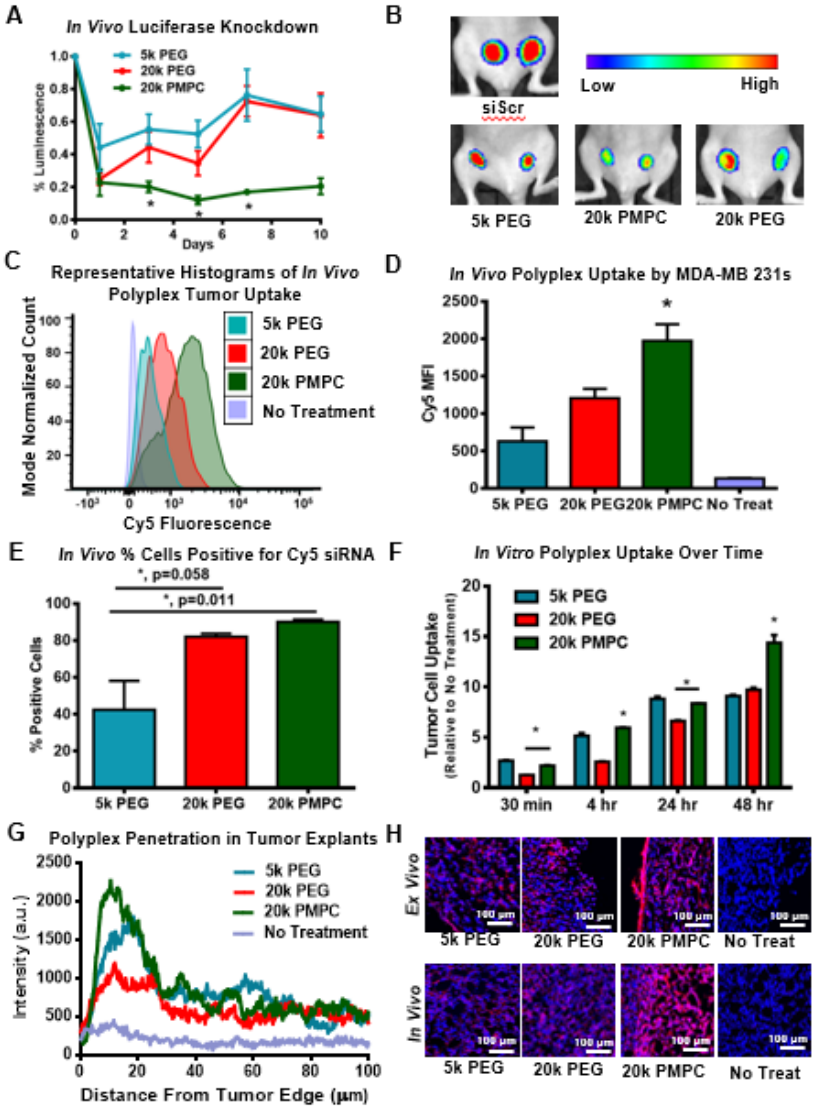

Figure 2.7 Zwitterionic 20k PMPC polyplexes significantly increased luciferase knockdown and siRNA delivery per tumor cell compared to PEGylated polyplexes *in vivo* (1 mg/kg siRNA, 1.89 μmol/kg polymer, N^+:P - 20). (A) 20k PMPC polyplexes decreased tumor luminescence by roughly 80% compared to scrambled control polyplexes over the course of a 10-day study period, with significantly improved knockdown compared to PEGylated polyplexes on days 3-7 (1 mg/kg intravenous siRNA dose on day 0, n=6-10 tumors per group, $p<0.05$). (B) Representative IVIS luminescence images taken on Day 3 post-treatment. (C) Representative

histograms of polyplex uptake for tumor cells analyzed by flow cytometry from tumors harvested at 24 hours post-treatment. Results indicate increased Cy5 fluorescence in GFP positive MDA-MB-231 cells for 20k PMPC polyplex-treated tumors compared to PEGylated polyplexes. (D) At 24 hours, 20k PMPC polyplexes had significant, 63% increased mean Cy5 fluorescence in tumor cells compared to 20k PEG and 213% relative to 5k PEG ($p=0.0005$ *vs*.5k PEG, $p=0.0526$ *vs.* 20k PEG , n=4-6 tumors per group). (E) 20k PMPC had significantly increased % positive cells at 24 hours compared to 5k PEG (n=4-6 tumors per group, $p=0.0114$), while 20k PEG had a strong trend toward increased % positive cells compared to 5k PEG ($p=0.0582$). (F) In an *in vitro* time course, 20k PMPC polyplexes exhibited significantly higher uptake compared to PEGylated polyplexes at 30 minutes, 4 hours, and 48 hours ($p<0.02$, n=3). (G) Histological quantification of polyplex intensity after 24 hrs *ex vivo* incubation with MDA-MB-231 tumors excised from athymic nude mice. Line profiles were drawn starting at the tumor edge (n=27, 3 tumors per polyplex, 9 profiles per tumor). (H) Representative histology images of *ex vivo* and *in vivo* tumor penetration of polyplexes. Overall, polyplexes achieved similar penetration depths both *in vivo* and *ex vivo*, but histology evidence supports differences in uptake between polyplex types.

The increased *in vivo* uptake of 20k PMPC polyplexes compared to 20k PEG polyplexes indicates that the higher levels of gene knockdown of 20k PMPC are driven by a combination of increased circulation time and higher rate of cell uptake of PMPC-based polyplexes. To further elucidate the latter mechanism, we compared the *in vitro* uptake properties of 5k PEG, 20k PEG, and 20k PMPC over a two-day time course (**Figure 2.7f**). Measurements at early time points of 30 minutes and 4 hours showed that 20k PMPC was taken up by MDA-MB-231s more rapidly than 20k PEG, with 2-fold higher uptake at each time point ($p<0.002$, n=3). 20k PMPC uptake was also significantly higher than 20k PEG corona polyplexes at 24 hours. 5k PEG polyplexes had similar uptake levels to 20k PMPC at earlier time points *in vitro*. However, 5k PEG polyplexes lack the same level of corona shielding, resulting in higher uptake levels *in vitro*, but less stability in circulation and therefore reduced *in vivo* tumor biodistribution. Additionally, 20k PMPC more rapidly penetrated the cell population homogenously relative to either PEGylated corona. At 4 hours, 5k PEG showed 60% positive cells compared to 95% for 20k PMPC polyplexes ($p<0.01$, **Supplemental Figure A.S14**). By 48 hours, 20k PMPC polyplexes exhibit significantly increased

uptake compared to both 5k PEG and 20k PEG coronas ($p<0.0003$). Thus, 20k PMPC polyplexes maximize both serum stability and increased cell uptake. While less-shielded 5k PEG polyplexes have higher uptake at early time points, more serum-stable 20k PEG polyplexes catch up to 5k PEG polyplexes over time. 20k PMPC, on the other hand, combines both a high rate of uptake and the increased stabilization properties necessary for continued uptake over longer periods of time in the presence of serum, enabling its improved *in vivo* tumor uptake compared to PEGylated polyplexes.

In order to dissect whether the *in vivo* relative tumor cell uptake differences (**Figure 2.7d**) were driven in part by differences in tumor tissue penetration of the polyplexes, we investigated penetration in an *ex vivo* model, using MDA-MB-231 tumors excised from nude mice. After 24 hours of polyplex incubation with tumors, all polyplexes penetrated to similar depths from the tumor edge (**Figure 2.7g**). Quantification based on line profiles drawn from the tumor edge indicated that, particularly close to the tumor edge (10-20 μm), average intensities of 20k PMPC polyplexes were significantly higher ($p<0.01$) than 5k PEG and 20k PEG polyplexes, at 1.5-fold and 2.1-fold higher, respectively. Overall area under the average intensity curve was also highest for 20k PMPC. However, overall distribution of polyplexes based on depth was similar, as seen in representative histology images (**Figure 2.7h**). While the highest polyplex signal intensities were observed within 40 μm from the tumor edge, average signal from all polyplex-treated tumors was still higher than signal from untreated tumors deeper in the tumor (40-100 um), with no significant differences between individual polyplex types at these deeper tumor regions.

The 5k PEG polyplex intensities near the tumor edge are higher than the 20k PEG intensities in this study, which is different than the tumor delivery levels seen *in vivo*, due to the *ex vivo* nature of the experiment; these polyplexes did not require stability in circulation prior to reaching the

tumors and, with lower molecular weight PEG, are less shielded to begin with, allowing for increased tumor uptake. Given this result, it is noteworthy that the more well-shielded 20k PMPC-based polyplexes displayed higher average intensities at low penetration depths than 5k PEG polyplexes, despite their higher molecular weight coronas, further supporting the improved uptake properties of PMPC-corona polyplexes.

The similar depth penetration profile of each of these polyplexes indicates that the higher bioactivity of 20k PMPC corona polyplexes is driven primarily by higher uptake properties and not by differences in tissue penetration. These penetration profiles were further corroborated with histological evaluation of tumors after *in vivo* tail vein administration of Cy5-bearing polyplexes (**Figure 2.7h**). Here again, Cy5 signal from each polyplex could be found deep within tumor sections and relatively well-penetrated. While all polyplexes appear to have a similar histological distribution in the tumor, the overall amount of uptake is different depending on polyplex type, as we quantified comprehensively through *in vivo* flow cytometry.

Our combined tumor gene knockdown and tumor uptake data indicate that high molecular weight zwitterionic PMPC coronas perform significantly better than their linear PEG counterparts. Our work thoroughly demonstrates the *in vivo* advantages of PMPC compared to PEG in systemically-delivered siRNA polyplexes, and other studies in non-polyplex systems support and corroborate our findings. In gold nanoparticles, for example, multiple studies have shown that zwitterionic coatings increase accumulation at the site of a tumor over PEGylated surface coatings.[100, 101] Similarly, in protein-based nanoparticles, PMPC coatings improve tumor uptake over PEG-based copolymers, and this effect was also primarily observed at later time points (12 h post-injection), implying better tumor accumulation and retention over time as our study reveals.[102]

The observation that PMPC-based polyplexes improve cell uptake while reducing protein adsorption is somewhat counterintuitive and requires further mechanistic investigation, both in normal and cancer cells. One potential explanation is that zwitterionic phosphorylcholine particle surface chemistries improve tumor accumulation because they promote association with cell membranes, given their similarity to membrane phospholipid heads.[102-105] It has also been observed that PMPC surface chemistries are particularly conducive to internalization by cancer cells, even more so than in normal cells.[103, 106] This may be due to the fact that many invasive and rapidly proliferating cancer cells, including the MDA-MB-231 cells in our study, have increased choline transport, due to their higher membrane synthesis and turnover.[107] All of these existing data are consistent with our own results comprehensively demonstrating increased tumor cell uptake of PMPC-based siRNA polyplexes compared to PEGylated polyplexes both *in vitro* and *in vivo*.

In comparing to other siRNA delivery work, our 20k PMPC polyplexes generated higher tumor gene knockdown compared to the few previous examples of *in vivo* PMPC-based siRNA delivery. In one study, siRNA-bearing PMPC-PDPA (poly(diisopropanolamine ethyl methacrylate)) diblock copolymers achieved significant luciferase knockdown (up to 75%), but this level was achieved after 6 repeated injections of low polyplex doses (as opposed to our single 1 mg/kg dose) and these polyplexes were not compared to PEGylated counterparts.[80] Most top-performing polyplex systems are PEGylated and frequently suffer from low tumor uptake without addition of targeting ligands or cholesteryl stabilizing moieties.[24, 108] Our PMPC-based polyplexes, on the other hand, without active targeting, increased average tumor cell uptake three-fold compared to 5k PEG and two-fold compared to 20k PEG, and achieved up to 90% Cy5-positive tumor cells after only a single, relatively low-dose administration. The 20k PMPC

polyplexes preserve the stability advantages of high molecular weight stealth coronas while also producing higher cell uptake than high molecular weight PEGylated polyplexes.

These results are predicated on the assumed presence of the enhanced permeability and retention (EPR) effect in tumors, which enables nanoparticle extravasation through porous tumor vasculature. This effect has been subject to debate in recent literature, with most studies suggesting that this phenomenon is heterogeneous in human cancers.[29, 32] However, a recent clinical trial in human subjects directly confirmed the presence of the EPR effect in all of the patients studied (across multiple solid tumor types), showing micellar accumulation in tumor tissue but not in surrounding tissues.[34] As is the case for clinical, standard of care cancer therapeutics, it is true that some patients may benefit more than others from nanomedicines taking advantage of the EPR effect. Recent work has suggested that magnetic nanoparticles can be used as an imaging agent to predict whether EPR-based nanomedicines will be advantageous in different patients.[32] These opportunities for personalized nanomedicine-based cancer treatment only intensify the need for improved polyplex stability and tumor accumulation in order to maximize the full potential of EPR across a varied patient population. In our study, we have shown that these goals are achievable for siRNA polyplexes using zwitterionic PMPC surface chemistries more so than PEGylated ones.

2.4 Conclusion

Taken together, our data show that while high molecular weight PEG and PMPC coronas generally improve polyplex circulation time, zwitterionic PMPC coronas significantly improve *in vivo* tumor cell uptake and bioactivity compared to canonical PEGs. *In vitro*, larger molecular weight hydrophilic corona-forming blocks performed better in terms of increasing heparin

stability and blocking protein adsorption. In these and other assays, POEGMA was the exception to this trend, and the PEG brush-like architecture as a rule did not perform as well as PMPC and linear PEG corona-forming blocks in the polyplex format used in these studies. These comprehensive *in vitro* data corroborated our *in vivo* pharmacokinetic data, which used intravital microscopy for elucidating the intravenous impact of polyplex corona chemistry. This method quantitatively showed that both high molecular weight corona-forming blocks comprising either 20k Y-shaped PEG or 20k zwitterionic PMPC improve polyplex circulation half-lives over shorter coronas. These results motivated more in-depth studies of the 20k PEG and PMPC formulations in comparison to our 5k PEG benchmark. Our *in vivo* tumor uptake and gene knockdown studies show that high molecular weight zwitterionic coronas significantly improve *in vivo* gene knockdown and tumor cell uptake compared to high molecular weight PEGylated polyplexes. This work has important implications for optimization of siRNA nanocarriers used for systemic cancer therapeutics. PEG has long been regarded as the gold standard, while increasingly well-characterized non-canonical surface chemistries remain under-utilized. We have shown that PMPC, a biocompatible material that is a component of FDA-approved products, is easily and controllably polymerized and significantly improves tumor cell uptake and knockdown activity of siRNA polyplexes over PEG-based structures, encouraging further development of zwitterionic surface chemistries for siRNA oncological therapeutics.

2.5 Materials and Methods

All materials were purchased from Sigma Aldrich unless otherwise described. Inhibitors were removed from dimethylaminoethyl methacrylate (DMAEMA) and butyl methacrylate (BMA) using an activated aluminum oxide column. All DNA or siRNA oligonucleotides were

purchased from Integrated DNA Technologies (Coralville, IA, USA), and sequences can be found in our previous work.[21] In FRET experiments, *in vitro* cell uptake experiments, *in vivo* biodistribution, and pharmacokinetic experiments, DNA oligonucleotides were used as a model for siRNA oligonucleotides of the same length.

Polymer Synthesis: All polymers were synthesized using 4-cyano-4-(ethylsulfanylthiocarbonyl)sulfanylpentanoic acid (ECT) as an initial chain transfer agent. ECT was synthesized in house according to previously published methods.[21] 5k PEG ECT was synthesized as previously described by coupling a 5 kDa hydroxyl-terminated PEG (JenKem, USA) to ECT by DCC DMAP coupling (**Supplemental Figure A.S1**). For the coupling reaction, ECT was added to a reaction vessel at 10:1 molar equivalents of 5kDa or 20kDa PEG (JenKem, USA) and dissolved in dichloromethane at 10% wt/v. Dicyclohexyl carbodiimide (DCC) was then added to activate the carboxylic acids on ECT at a 1:1 molar ratio with ECT. After stirring 5 min, hydroxyl-teminated 5kDa or 20kDa PEG was added to the reaction mixture, followed by 4-dimethylaminopyridine (DMAP). DMAP was added at a 5:1 molar equivalent to PEG. ECT was added to the 5 kDa PEG at a 10:1 molar ratio. Dicyclohexyl carbodiimide (DCC) and 4-dimethylaminopyridine (DMAP) were added at 5 molar equivalents the amount of PEG. The coupling reaction was stirred at room temperature for 48 hours and the final product was purified as previously described.[21] From the 5 kDa or 20kDa PEG macroCTA, DMAEMA and BMA were RAFT polymerized at 50:50 molar ratios using AIBN as an initiator (10:1 CTA:Initiator ratio) in 10% w/v dioxane. Reactions were planned with a degree of polymerization of 240, in order to achieve 75-80 repeating units each of DMAEMA and BMA (at a 65-70% monomer conversion rate). The reaction was nitrogen purged for 30 minutes and then was stirred at 65 ˚C for 24 hours. The final reaction mixture was dialyzed into methanol for two days, then water for

two days, and lyophilized. 20k PEG was synthesized using the same methods as for the 5k PEG polymers, but a 20kDa Y-shaped hydroxyl PEG was conjugated to ECT to create the appropriate macroCTA. Zwitterionic PMPC was synthesized in a two-step process. First, DMAEMA and BMA were RAFT polymerized at the same monomer feed ratios and conversion estimates described above. ^{1}H NMR was used to evaluate conversion rate (**Supplemental Figure A.S2**). This random DMAEMA-BMA copolymer (DB ECT) was then used as a macroCTA to polymerize a homopolymer block of 2-(methacryoyloxyethyl) phosphorylcholine. For a 20 kDa corona or a 10 kDa corona, target degree of polymerizations of 75 and 40 were used, respectively. These polymerizations used AIBN at a 5:1 CTA:initiator ratio and were done at 10% w/v in anhydrous methanol solvent. Reactions were purged with nitrogen for 30 minutes before heating to 65 ˚C for 24 hours. Final reaction products were dialyzed in methanol for two days, then water for two days, and lyophilized. Polymers with POEGMA (poly(ethylene glycol) ethyl ether methacrylate) (Mn = 950) in the corona were synthesized in a similar method using a 10:1 CTA:initiator ratio and dioxane as a reaction solvent (10% wt/v). Prior to polymerization, inhibitors were removed from POEGMA monomers by first dissolving in anhydrous THF, running through an alumna column, and then drying using a rotary evaporator. For 10k POEGMA coronas and 20k POEGMA coronas, aimed degrees of polymerization were 19 and 31, respectively, with conversion rates of 60% and 65%, respectively.

All polymers were characterized using ^{1}H nuclear magnetic resonance spectroscopy (Bruker, 400 MHz). Polymer polydispersity was evaluated with DMF mobile phase gel permeation chromatography (GPC, Agilent Technologies, CA). For this measurement, all PEG or POEGMA polymers were dissolved in DMF containing 0.1M lithium bromide at a concentration of 10 mg/mL. All NMR spectra are shown in **Supplemental Figure A.S3**.

Polyplex Formation and Encapsulation Efficiency: All polyplexes used *in vitro* for this work were first complexed with siRNA in 10 mM citrate buffer at pH 4 for 30 minutes, followed by raising the pH to 7.4 using 10 mM pH 8 phosphate buffer at 5x the volume of the pH 4 solution. Polyplex N^+:P^- ratios were determined as the mole ratio of protonated amines from DMAEMA monomers (50% are assumed protonated at physiological pH) to the number of phosphate groups on the siRNA according to the following equation:[21, 109]

$$nmol\ polymer = \frac{(nmol\ nucleic\ acid)(base\ pairs\ nucleic\ acid)(2)(N{:}P\ ratio)}{(DMAEMA\ repeat\ units)(0.5)}$$

Unless otherwise noted, all *in vitro* polyplex characterization assays were performed at a dose of 100 nM siRNA and 2.7 μM polymer (N^+:P^- 20), which corresponds to 0.074 mg/mL, 0.12 mg/mL, 0.093 mg/mL, 0.12 mg/mL, 0.093 mg/mL, and 0.12 mg/mL, for 5k PEG, 20k PEG, 10k PMPC, 20k PMPC, 10k POEGMA, and 20k POEGMA, respectively.

Polyplex encapsulation efficiency at various N^+:P^- ratios was evaluated using a Quant-iT Ribogreen assay kit (ThermoFisher, USA). Assay solutions were prepared based on manufacturer's instructions, and Ribogreen fluorescence was measured using the high range assay. Polyplex solutions were prepared at 100 nM siRNA, and 50 uL of polyplex solution was diluted by half in 1X TE buffer, followed by addition of 100 uL Ribogreen reagent to each well. Fluorescence was measured at 520 nm and encapsulation efficiency was calculated by normalizing fluorescence of polyplex solutions to fluorescence of siRNA-only control solutions.

Polyplexes were prepared for TEM at 0.5 mg/mL polymer. 5 μL polyplex suspensions were added to pure carbon TEM grids (TED Pella Inc, Redding, CA, USA), and blotted dry after 60 sec. TEM grids were then counterstained with 3% uranyl acetate (5 μL) for 20 seconds and

then dried overnight under vacuum. Images were obtained with a FEI Tecnai Osiris microscope (200 kV).

Polyplex Stability Evaluations: Polyplex diameters and zeta potentials were measured using dynamic light scattering (Zetasizer Nano ZS, Malvern Instruments, Westborough, MA). For these measurements, polyplexes were prepared at final concentrations of 0.167 mg/mL. For stability measurements, each polyplex solution was incubated with 0.1 or 0.25 M NaCl solutions.

Polyplex stability was also measured in FBS and heparan sulfate through a FRET assay described previously.[21, 47, 71] Briefly, polyplexes were co-loaded with nucleic acids conjugated with either Alexa Fluor-488 or Alexa Fluor-546 dyes, forming FRET pairs. Intensity of fluorescence emission after excitation at 488 nm was measured at 514 and 572 nm using a fluorescence plate reader (Tean Infinite F500, Mannedorf, Switzerland). Percent FRET for each polyplex sample was calculated as:

$$\frac{I_{572}}{I_{572} + I_{514}} x100$$

For FBS-based FRET challenge, polyplexes were incubated at concentrations of 100 nM siRNA per well with 10 or 30% FBS. FRET signal of polyplexes incubated with FBS was compared to that of polyplexes in PBS alone. In all cases, black, clear bottom 96 well plates were used for fluorescence measurements. FRET signal was tracked over the course of 100 minutes at 5 minute intervals.

Polyplex stability was also evaluated in response to heparin salts. Again, polyplexes were prepared to have final concentrations of 100 nM siRNA per well. In each well, 90 uL of polyplexes were incubated with 10 uL of various concentrations of heparin salts, ranging from 20 U/mL to 100 U/mL final concentration heparin per well. FRET signal was then evaluated the same as above FBS-based method.

Hemolysis Assay: Red blood cell hemolysis assay was performed using methods described previously.[87] Blood was drawn from consenting human donors according to an IRB-approved protocol. In short, red blood cells (RBCs) were isolated from whole blood and diluted into buffer solutions of pH 5.6, 6.2, 6.8, and 7.4. Polyplexes prepared at 5 and 40 μg/mL polymer concentration were incubated with red blood cells at the various pH values for 1 hour in round-bottom 96 well plates. Negative controls and positive controls of red blood cells in buffer only or Triton-X, respectively, were also used for analysis. The RBCs were then centrifuged and supernatants were analyzed for absorbance at 450 nm using a plate reader. Percent hemolysis was evaluated by subtracting background buffer-only RBC absorbance from the absorbance of polymer-containing wells, and dividing by the difference between Triton-X controls (complete lysis) and buffer-only RBC absorbance (no lysis).

Creation of Luciferase-Expressing MDA-MB-231 Breast Cancer Cells and Luciferase-Expressing NIH3T3 Mouse Fibroblast Cells: Lentivirus was produced by transfecting HEK-293T cells with pGreenFire1-CMV plasmid, along with pMDLg/pRRE, pRSV-Rev, and pMD2.G packaging plasmids with Lipofectamine 2000 as a transfection reagent. Media supernatant containing lentivirus was then collected at 48 and 72 hours. For transfection of MDA-MB-231 and NIH3T3 cell lines, 10 mL lentiviral media was added to the cells containing 6 ug/mL polybrene for 24 hours of incubation. Cells were analyzed post-transduction by detection of GFP using flow cytometry (BD LSR II Flow Cytometer, San Jose, CA, USA). Cells were selected for vector expression by growth in puromycin-containing media.

Cell Culture: All cells used for this manuscript were cultured in Dulbecco's modified Egle's medium (DMEM, Gibco Cell Culture, Carlsbad, CA), containing 4.5 g/L glucose, 10% fetal bovine serum (Gibco), and 0.1% gentamicin (Gibco).

Cell Viability: Luciferase-expressing NIH3T3 cells or MDA-MB-231 cells were seeded in a 96-well plate at 20,000 cells/mL (2000 cells per well). After 24 hours, polyplex solutions were introduced to the wells using an N^+:P^- ratio of 20 with 100 nM scrambled siRNA per well. After 24 hours, polyplex-containing media was removed from the cells and replaced with media containing luciferin substrate (150 µg/mL). After incubating for 5 minutes, cells were imaged using an IVIS Lumina III imaging system (Caliper Life Sciences, Hopkinton, Massachusetts). Luciferin-containing media was then replaced with normal media for 24 hours, followed by IVIS imaging with luciferin media at 48 hours post-treatment. Luminescence signal was compared to untreated controls for analysis.

In Vitro Luciferase Silencing of MDA-MB-231 Cells: Luciferase-expressing MDA-MB-231 cells were seeded in 96-well plates at 2000 cells per well and allowed to adhere for 24 hours. Polyplex solutions containing either luciferase siRNA or scrambled siRNA at 100 nM, 75 nM, 50 nM, 25 nM, 10 nM, and 1 nM were then incubated with MDA-MB-231 cells in quadruplicate. After 24 hours, media was replaced with luciferin-containing media (150 ug/mL) and luminescence was evaluated by IVIS imaging. Luciferin-containing media was then replaced with normal media until 24 or 48 hours, at which point luciferin media was reintroduced, and luminescence again evaluated. For analysis of knockdown, all data were normalized to scrambled control polyplexes to account for any non-specific toxicity effects. IC_{50} values were calculated using nonlinear regression in Graphpad.

Uptake by MDA-MB-231 Cells: Non-luciferase expressing MDA-MB-231 cells were seeded in 12-well plates at 80,000 cells per well. Polyplexes were formed containing 100 nM of Alexa Fluor-488-labeled nucleic acid in media containing 10% serum. Polyplexes were incubated with cells for 30 min, 4 hours, 24 hours, or 48 hours and then removed. Cells were

washed with PBS, trypsinized for 10 minutes in 0.25% trypsin, and centrifuged at 450 x g for 7 min. Cell pellets were then resuspended in PBS containing 0.04% trypan blue (to quench extracellular fluorescence) prior to running through a flow cytometer (3-laser BD LSR II, BD Biosciences, Franklin Lakes, NJ, USA). Cells were monitored for Alexa Fluor-488 fluorescence at excitation and emission wavelengths of 488 and 519 nm, respectively. Quantification of % uptake was performed using FlowJo software (FlowJo, LLC, Ashland, OR). Events were gated for single cells, and then characterized for negative, low, medium, and high uptake levels. Untreated MDA-MB-231 cells were used as negative controls.

Isothermal Titration Calorimetry: Isothermal titration calorimetry experiments were performed using a MicroCal VP-ITC (Malvern, USA) in the Vanderbilt Center for Structural Biology. Polyplexes were prepared at concentrations of 0.5 mg/mL polymer as described above. BSA was dissolved from lyophilized powder at 15 mg/mL in buffer solutions exactly matching the composition of polyplex buffer. Titration experiments were carried out at 37 ºC using a reference power of 10 µcal/ sec, 300 second initial delay, 307 rpm stirring speed. Each injection was 10 µL, with a duration of 20 sec, spacing of 260 seconds, and filter period of 2 seconds. A control consisting of heat of dilution of BSA into buffer only was subtracted from titration data. All data analysis was performed in Origin, using a one set of sites binding model to determine thermodynamic parameters. A cationic control polymer consisting of PDMAEMA only in the corona, as previously described, was used as a positive control for protein adsorption. [71, 109-111]

Gel Shift Protein Adsorption Assay: Polyplexes bearing scrambled siRNA were prepared at 0.5 mg/mL polymer and incubated with 5% FBS. A 2% agarose gel was prepared using 1X TAE buffer. 10 µL of these preparations each was added to wells on an agarose gel with 2 µL loading dye. Agarose gels were run at 90 mV for 30 min. Gels were then stained using SYPRO

Ruby stain according to established commercial protocols (Thermo Fisher), and imaged using a BioRad Chemidoc Imaging System.

Complement Assay: All materials for the hemolysis-based complement assay were purchased from Complement Technologies (Tyler, TX, USA). siRNA polyplexes were prepared at 50 nM siRNA. Complement sera was prepared at five dilutions (1:20, 1:40, 1:80, 1:160, 1:320), and antibody-sensitized sheep red blood cells were prepared separately at 2x 10^8 cells/mL in GVB $^{++}$ buffer. In each test tube, 100 µL of complement sera was added to 100 µL of polyplexes and incubated for 30 minutes. Then 100 µL of antibody-sensitized RBCs were added to each tube, and the mixtures were incubated at 37 ℃ for 1 h with intermittent shaking. All samples were then centrifuged and supernatants were transferred to a 96-well plate. Absorbance at 541 nm was then measured on a plate reader. Absorbance values were used to determine transmittance and absorption (1-transmittance). Percent lysis was calculated as:

$$\frac{(Sample\ Absorption - \ Absorption\ PBS\ only)}{(Absorption\ water\ control\ [complete\ lysis] - Absorption\ PBS\ only)} * 100$$

Percent lysis at each complement dilution was plotted and compared to control samples containing complement proteins only (no polyplexes).

Polyplex pharmacokinetics, biodistribution, and intravital microscopy: For *in vivo* polyplex preparations, polymers were complexed with 1 mg/kg Cy5-labeled oligonucleotides in 100 mM pH4 citrate buffer. Complexing solutions were then loaded into 20 kDa MWCO dialysis tubing (Spectrum Laboratories, Rancho Dominguez, CA) and dialyzed into PBS -/- overnight. Polyplex formation was confirmed by dynamic light scattering (described above) immediately prior to *in vivo* injections.

Male CD-1 mice (Charles River) (n=4 per group) were anesthetized using isoflurane and immobilized on a heated confocal microscope stage. Prior to imaging, mouse ears were cleaned

with a depilatory cream. Microscope immersion fluid was used to immobilize the mouse ear on a glass coverslip. Intravital microscopy was performed using a Nikon Czsi+ system with a Nikon Eclipse Ti-oE inverted microscopy base, Plan ApoVC 20x differential interference contrast N2 objective, 0.75 NA, Galvano scanner, and 543 dichroic mirror. All image analysis and acquisition was done using Nikon NIS-Elements AR version 4.30.01. A laser gain of 98 was used throughout. Ear veins were detected using the light microscope, and images were focused to the plane of greatest vessel width, where flowing red blood cells were clearly visible. Once the ear was in focus, microscope was switched to confocal laser mode and set to image continuously every second. The mouse was then injected with 100 µL polyplex solution *via* tail vein at a 1 mg/kg dose (1.89 µmol/kg polymer, corresponding to 54.0 mg/kg, 81.8 mg/kg, 64.4 mg/kg, 85.0 mg/kg, 64.5 mg/kg, 80.4 mg/kg for 5k PEG, 20k PEG, 10k PMPC, 20k PMPC, 10k POEGMA, and 20k POEGMA, respectively), and Cy5 fluorescence in ear veins was monitored for 20 minutes. For image analysis, initial background fluorescence was subtracted, and circular regions of interest were highlighted within the mouse ear vessels. Fluorescence from these regions of interest was quantified and background fluorescence was subtracted. Intensity values were normalized to initial peak intensity. Fluorescence decay curves were modeled as one-compartment systems using single phase exponential decay. Area under the curve values were calculated by multiplying normalized intensity curves by the dose of siRNA in mg and integrating over time. Pharmacokinetic parameters were calculated using Graphpad Prism analysis software.

After 20 min of monitoring *via* intravital microscopy, animals were sacrificed. Organs were removed and immediately imaged for Cy5 fluorescence using an IVIS system. Fluorescence was quantified using an IVIS Lumina Imaging system (Xenogen Corporation,

Alameda, CA, USA) at excitation and emission wavelengths of 620 and 670 nm, respectively, using Living Image software version 4.4.

In Vivo Tumor Gene Silencing: Athymic female nude mice (4-6 weeks old, Jackson Laboratory) were injected under anesthesia in the mammary fatpad on each side with 1 x 10^6 luciferase expressing MDA-MB-231 cells in a 50:50 mixture of Matrigel:DMEM (serum-free). Tumor growth was followed until they reached approximately 100 mm^3. Polyplexes were prepared loaded with either luciferase or scrambled siRNA at 1 mg/kg as described for pharmacokinetic studies. Animals were injected *i.p.* with luciferin substrate (150mg/kg), imaged for baseline tumor bioluminescence using an IVIS system, and then subsequently injected with polyplexes *via* tail vein. Mice were re-injected with luciferin substrate on Days 1, 3, 5, 7, and 10 post-polyplex treatment. Luminescence signal of each individual tumor was compared to its baseline pre-treatment signal, and each relative luminescence value was normalized to the average relative luminescence of respective scrambled siRNA polyplex groups (n=6-10 tumors per group). Body weight measurements of all mice were recorded every day of the study period to monitor toxicity. Of thirty mice studied, five tumor-bearing mice were removed from the study due to health concerns prior to the end of the study, but there were no statistically significant differences in survival between treatment groups.

Biodistribution of Tumor Bearing Mice: Biodistribution studies for athymic female nude tumor-bearing mice (Jackson Laboratory) were conducted using the same methods as biodistribution studies for the male CD-1 mice. Fluorescence was measured in heart, lungs, kidneys, liver, spleen, and tumors excised at 24 h post-tail vein injection.

In Vivo Polyplex Uptake by MDA-MB-231 breast tumors: Tumors isolated from mice during above-described biodistribution experiments were then used for flow cytometry studies of

polyplex uptake. Tumors were cut into small pieces, washed with HBSS containing Ca^{2+} and Mg^{2+}, and then processed using an enzyme mix containing collagenase (0.5 mg/mL, Roche Life Sciences, Indianapolis, IN, USA) and DNAse (0.19 mg/mL, BioRAD, Hercules, CA, USA) in DMEM. After 1 hour incubation in the enzyme mix, the tumors were centrifuged and re-suspended in HBSS without Ca^{2+} and Mg^{2+}, and then incubated with 5 mM EDTA for 20 minutes. Tumors were then centrifuged and the pellets were re-suspended in HBSS with Ca^{2+} and Mg^{2+} and filtered using a 70 µm Nylon cell strainer. Filtrate was then washed once more with HBSS containing Ca^{2+} and Mg^{2+}, and then incubated in ACK lysis buffer (Thermo Fisher Scientific, USA) for 2 minutes before being diluted in 20 mL of PBS -/-. Cells were then pelleted and re-suspended in 1-2 mL PBS-/- prior to running on a flow cytometer (BD LSRii, BD Biosciences, San Jose, CA, USA). Uptake analysis was performed in FlowJo. Cell populations were isolated using forward and side scatter, then GFP positive tumor cells were gated, and Cy5 fluorescence intensity was measured for the GFP positive tumor cell population.

Tumor Penetration Assays: Ex Vivo *Tumor Penetration.* Athymic nude mice bearing MDA-MB-231 orthotopic mammary tumors were sacrificed when tumors reached 200-300 mm^3. Tumors were then incubated for 24 hours in DMEM containing 10% FBS, 1% gentamicin, and polyplexes bearing 100 nM Cy5-siRNA. After 24 hours, tumors were embedded in OCT compound (Fisher Healthcare) and frozen on dry ice. Tissues were fully-faced and then cryo-sectioned 100 µm deeper in the tissue. Frozen slides were then stained with DAPI and imaged using confocal microscopy (same instrument from intravital microscopy methods). Tissues were analyzed for Cy5 fluorescence by normalizing to untreated tumors to account for background autofluorescence. Line profiles were drawn blinded to Cy5 fluorescence in regions where a clearly

defined tumor edge was visible. Quantitative analysis consisted of 9 line profiles sampled randomly from tumor perimeter, with 3 tumors per polyplex.

In Vivo *Tumor Penetration*: Athymic nude mice bearing MDA-MB-231 orthotopic mammary tumors were injected with 1 mg/kg Cy5-siRNA polyplex solutions (at same polymer concentrations as for tumor uptake and intravital microscopy studies). Animals were sacrificed 24 hours after injections, and tumors were processed by freezing in OCT as described above for *ex vivo* penetration assays. Tumor sections were imaged using confocal microscopy, and images were sampled randomly throughout interior of tumor section, collecting both Cy5 and DAPI signal.

Statistical Methods:Unless otherwise noted, all statistical determinations were made using one-way ANOVA with Tukey multiple comparisons test in Graphpad Prism. All reported data display mean and standard error. Significance was determined using $\alpha=0.05$.

Ethics statement: All animal studies were conducted according to the National Institutes of Health guidelines for care and use of laboratory animals. Each study involving animals in this work was reviewed and approved by the Institutional Animal are and Use Committee (IACUC) at Vanderbilt University.

CHAPTER III

Dual Carrier Cargo Hydrophobization and Charge Ratio Optimization Improve the Systemic Circulation and Safety of Zwitterionic Nano-Polyplexes

Text for Chapter III taken from:

Jackson MA, Bedingfield SK, Yu F, Stokan ME, Miles RE, Curvino EJ, Hoogenboezem EN, Bonami RH, Patel SS, Kendall PL, Giorgio TD, Duvall CL. Dual Carrier-Cargo Hydrophobization and Charge Ratio Optimization Improve the Systemic Circulation and Safety of Zwitterionic Nano-Polyplexes. *Biomaterials.* February 2019. PMID: 30458360.

3.1 Abstract

While polymeric nano-formulations for RNAi therapeutics hold great promise for molecularly-targeted, personalized medicine, they possess significant systemic delivery challenges including rapid clearance from circulation and the potential for carrier-associated toxicity due to cationic polymer or lipid components. Herein, we evaluated the *in vivo* pharmacokinetic and safety impact of often-overlooked formulation parameters, including the ratio of carrier polymer to cargo siRNA and hydrophobic siRNA modification in combination with hydrophobic polymer components (dual hydrophobization). For these studies, we used nano-polyplexes (NPs) with well-shielded, zwitterionic coronas, resulting in various NP formulations of equivalent hydrodynamic size and neutral surface charge regardless of charge ratio. Doubling nano-polyplex charge ratio from 10 to 20 increased circulation half-life five-fold and pharmacokinetic area under the curve four-fold, but was also associated with increased liver

enzymes, a marker of hepatic damage. Dual hydrophobization achieved by formulating NPs with palmitic acid-modified siRNA (siPA-NPs) both reduced the amount of carrier polymer required to achieve optimal pharmacokinetic profiles and abrogated liver toxicities. We also show that optimized zwitterionic siPA-NPs are well-tolerated upon long-term, repeated administration in mice and exhibit greater than two-fold increased uptake in orthotopic MDA-MB-231 xenografts compared to commercial transfection reagent, *in vivo*-jetPEI®. These data suggest that charge ratio optimization has important *in vivo* implications and that dual hydrophobization strategies can be used to maximize both NP circulation time and safety.

3.2 Introduction

In the last twenty years, RNA-based therapeutics have proceeded from discovery, through extensive development, and to the exciting, recent approval of the first siRNA nanomedicine.[112] This progression has been significantly driven by lipid and polymer-based delivery vehicles. However, when administered intravenously, nucleic acids continue to face well-documented barriers including nuclease degradation, poor cell and tissue uptake, and rapid clearance from circulation, especially in the liver and kidney. [14, 113] As a testament to these hurdles, many of the advanced RNA-based therapeutics currently in clinical trials focus on local, carrier-free application or systemic delivery of siRNAs directly conjugated to ligands that drive rapid uptake by hepatocytes in the liver.[114]

There is a significant application space for systemically delivered siRNAs against non-hepatic targets. Oncology is a particularly promising field of application for RNAi therapeutics because they can be designed against tumor drivers that are undruggable by conventional small molecule approaches.[4, 7, 115, 116] However, there is still a significant gap in the technology needed

to make this clinically feasible. Because tumors and target tissues other than the liver receive only a small amount of the total cardiac output, longer nanocarrier circulation times are needed to achieve sufficient biodistribution.[64, 117] In fact, there is a close connection between vascular circulation time and level of tumor delivery of nanomedicines.[43, 47, 118-122] Nonviral polymeric siRNA carriers are often employed to improve cell uptake and provide endosomal escape properties, but these carriers are still prone to instability in circulation from serum proteins or, in the case of electrostatically-assembled formulations, anionic heparan sulfates which are highly concentrated in the kidney, reducing the opportunity for carriers to distribute intact to target sites such as tumors. [25, 65, 66]

Polymeric and lipid carriers often incorporate hydrophilic surface coatings, such as PEG, that shield the electrostatically-packaged/entrapped siRNA cargo in the nano-formulation interior, but such improvements often only marginally improve circulation stability.[123-125] One of the first tested polymeric siRNA carriers, CALAA-01, was shown to be primarily disassembled in the kidney and cleared completely from circulation by 30 minutes after intravenous injection in human patients.[37] It also exhibited signs of liver and kidney toxicity in non-human primates and hypersensitivity immune reactions in human patients that were associated primarily with the polymer components (not siRNA) of the formulation.[37] These experiences point to current major limitations in the field of systemic, polymer-based siRNA delivery—limited circulation stability and the potential for carrier-associated toxicity.

In addition to insufficient circulation stability, siRNA nano-formulations are often plagued by dose-limiting toxicities caused by cationic lipids/polymers that can damage cellular membranes or cause aggregation of serum or cellular blood components.[42, 123] The design of polymer carriers is often a balancing act between increased silencing efficiency and increased

cytotoxicity.[126, 127] These toxicities are dose-dependent, and many have sought to ameliorate them through iterative modification of the polymer structure of nanocarriers to improve stability.[128] The desire to increase the therapeutic window, or the gap between maximum tolerated dose and minimum efficacious dose, has led to a multitude of library-based studies that have examined the relationship between polymer structure and nanocarrier function.[129-131]

With the substantial focus on iterating on polymer structure, the *in vivo* pharmacokinetic and toxicity impact of two important aspects of formulating siRNA nanocarriers are often overlooked—the carrier to cargo ratio ("charge ratio" or "N:P ratio") and stabilizing modifications to siRNA cargo. Few studies have characterized impact of N:P ratio (the ratio of cationic polymer amines to siRNA phosphates) on *in vivo* polyplex pharmacokinetics and toxicity, and those that have are limited exclusively to cationic-only carriers such as polyethylenimine (PEI) and homopolymers of poly(2-(dimethylamino)ethyl methacrylate) (pDMAEMA).[132-134] In these studies, increasing N:P ratios are accompanied by increases in particle zeta potential, which can increase carrier toxicity by inducing aggregation of blood components and shifting biodistribution from the lungs to liver.[133, 135] *In vitro*, increasing N:P ratios can increase both polyplex transfection efficiency and toxicity due to the presence of excess, uncomplexed polymer, but these effects are likely less relevant after systemic administration.[136-138] Little is known about the impact of N:P ratio on *in vivo* circulation half-life and toxicity properties of well-shielded, hydrophobically stabilized polyplexes.

The present study was designed to elucidate the effect of N:P ratio on *in vivo* pharmacokinetics and toxicity profile of siRNA carriers with dual hydrophobic stabilization on both the cationic, siRNA-condensing polymer block and the siRNA cargo. A previously-optimized siRNA-condensing random copolymer block was utilized with balanced (50 mol% of

each) hydrophobic (butyl methacrylate (BMA)) and cationic (DMAEMA) monomer content, referred to as "50B"; this polymer provides pH-responsive, endosomolytic properties along with improved circulation stability and *in vivo* bioactivity relative to traditional nano-polyplexes (NPs) made solely from cationic monomers such as P(DMAEMA).[21] The P(DMAEMA-*co*-BMA) segment was blocked with a super-hydrophilic, zwitterionic phosphorylcholine-based polymer (P(2-methacryloyloxyethyl phosphorylcholine) (P(MPC)) to form the NP corona; we recently showed this composition to achieve superior tumor cell delivery *in vivo* relative to traditional PEG NP surface chemistry[43] Leveraging this optimized polymer structure containing a balance of cationic and hydrophobic content in the siRNA-condensing block, we explored the effect of varying the polymer:siRNA (N:P) ratio with and without hydrophobic modification of the siRNA cargo with palmitic acid (PA, $CH_3(CH_2)_{14}COOH$). Additionally, we studied the long-term toxicologic impacts of repeated administration of candidate formulations. Another contribution from this study is that, despite the growing evidence in favor of zwitterionic polymer NP surface coatings as an alternative to PEG, the toxicology of zwitterionic nanocarrier systems is significantly less studied relative to PEGylated systems.[43, 131, 139, 140]

Several groups, including ours, have shown that the introduction of hydrophobic moieties improves the stability of polymer-based siRNA delivery systems.[21, 47, 48, 118, 128] These strategies have typically involved either modification of the polymer structures or addition of hydrophobic groups such as cholesterol directly onto the siRNA molecules.[23, 48, 50, 53, 141, 142] We previously demonstrated that the use of a "dual hydrophobization" strategy in both the carrier polymers and the cargo siRNA could significantly improve the stability and tumor gene silencing ability of PEGylated polyplexes.[47] Here, we further investigate this strategy utilizing zwitterionic NPs, in the context of various charge ratios, and with a deeper focus on toxicological impacts of

the interplay between N:P ratio and siRNA hydrophobization. These studies provide unique insights into dual hydrophobization as a strategy to reduce N:P ratio and even to reduce toxicity for a specific N:P relative to polymer-only hydrophobization.

3.3 Materials and Methods

Materials: Chemicals and materials for biological assays were purchased from Sigma-Aldrich (St. Louis, MO, USA) or Fisher Scientific (Waltham, MA, USA) unless otherwise noted. All oligonucleotides used in these studies were purchased from Integrated DNA Technologies (Coralville, IA, USA). For all studies involving fluorescently-tagged oligonucleotides, dsDNA of 23 base pairs were used as a model for siRNA. The sequences of all oligonucleotides used in these studies can be found in Supplementary Table 1 and referenced in our previous work.[118]

Polymer Synthesis: Polymers were synthesized using Reversible Addition Fragmentation Chain Transfer (RAFT) techniques. The RAFT chain transfer agent, 4-(ethylsulfanylthiocarbonyl)sulfanylpentanoic acid, was synthesized using previously described methods.[43] A macroCTA consisting of a random co-polymer of poly(dimethylaminoethyl methacrylate-co butyl methacrylate) [P(DMAEMA-*co*-BMA)] was synthesized using a 50:50 monomer feed ratio, targeting 210 repeat units (expecting 70% conversion), with the goal of achieving 75-80 repeating units of each monomer. Prior to polymerization, all monomers were removed of inhibitors by passing through two activated basic alumina columns. The reaction was stirred under nitrogen at 65ºC for 24 h at 20 wt% in dioxane, using a CTA:initiator ratio of 10:1 (AIBN as initiator). The final reaction was precipitated in cold pentane 3 times, then dried under vacuum. Molecular weights and degree of polymerization were confirmed by 400 MHz ^{1}H-NMR in $CDCl_3$ and gel permeation chromatography with DMF mobile phase (0.1 M LiBr; polymer at

10 mg/mL; Agilent Technologies, CA) with Wyatt miniDAWN TREOS light scattering detectors. The dn/dc values for the molecular weight calculation were determined on a refractometer (Abbemat 300, Anton Paar). A corona block of poly(2-methacryloyloxyethyl phosphorylcholine) [P(MPC)] was then RAFT polymerized from the P(DMAEMA-*co*-BMA) macroCTA by targeting a degree of polymerization of 75 (to achieve a 20 kDa block), making the final polymer (referenced as P(MPC-*bl*-(DMAEMA-*co*-BMA))). The reaction was carried out at 20 wt% under nitrogen in methanol (with condenser) at 65ºC for 24 hours, with a 5:1 CTA: Initiator ratio (AIBN initiator). The crude reaction was then dialyzed in methanol for one day, followed by water for one day, and lyophilized. Degree of polymerization was confirmed by ^{1}H-NMR.

Conjugation of Palmitic Acid (PA) to siRNA: Amine-modified siRNA was dissolved in a 50:50 mixture of isopropanol and nuclease-free water to create a 40 nmol/ mL concentration in the final reaction (90% of final volume). NHS-modified PA was dissolved in DMF to create a 4000 nmol/mL concentration in the final reaction (DMF volume was 10% of final reaction volume). The PA was added to the siRNA solution, stirring at room temperature, and diisopropyl ethyl amine (DIPEA) was added at 1 uL per mL of final reaction volume. Further additions of PAin DMF and DIPEA were done at 24 hours and 48 hours. At 72 hours, nuclease-free water was added to dilute the DMF to 10% of the total volume, and the mixture was centrifuged for 10 min at 3000xg to remove precipitated, excess PA. The supernatant was then dialyzed (12 hours, 2 solvent changes) in nuclease free water using 3500 MWCO dialysis tubing. The resulting cloudy mixture was passed through a 0.22 μm filter and then lyophilized. The lyophilized powder was re-dissolved in water and passed through another 0.22 μm filter to further remove residual PA. The mixture was then purified on NAP25 columns, frozen, lyophilized, re-dissolved

in nuclease-free water, and quantified on a Nanoquant plate (Tecan, Mannedof, Switzerland).

The conjugate molecular weight was confirmed using LC-MS, and purity was verified using reverse-phase HPLC. For conjugate molecular weight, siRNA conjugates were run in negative ionization mode using LC-MS-ESI (Waters Synapt). Samples were run using a Kinetix 1.7 μm PFP 100 A LC Column under a linear gradient from 95% water (10 mM triethylammonium acetate), 5% methanol (10mM triethylammonium acetate) to 100% methanol. For additional HPLC confirmation of purity, the conjugate was injected at 5-30 nmol in 200 μL solvent, using water with 100 mM TEAA (triethyl ammonium acetate) and methanol in a linear gradient (95% water, 5% methanol to 100% methanol, back to 95% water/5% methanol) and a Clarity Oligo-RP column (Phenomenex, Torrence, CA). Single-stranded PA conjugates were then annealed to antisense siRNA strands using a C1000 Thermal Cycler (Bio-Rad, Hercules, CA).

Formulation of siRNA NPs: Buffers used for NP formulation were created using the Sigma Buffer Reference Center Online Resource. To form NPs, P(MPC-*bl*-(DMAEMA-*co*-BMA)) polymers were dissolved in 10 mM citric acid buffer (pH=4) and then added to various amounts of siRNA for 30 minutes. The amounts of siRNA or PA-siRNA to add were determined using the N:P ratio (10, 15, or 20), which was calculated using the following equation (50% of DMAEMA monomers are assumed to be protonated at pH 7.4:

$$nmol\ polymer = \frac{(nmol\ nucleic\ acid)(base\ pairs\ nucleic\ acid)(2)(N{:}P\ ratio)}{(\text{DMAEMA repeat units})(0.5)}$$

After complexing at pH 4 for 30 minutes, the pH was raised to 7.4 by adding 10 mM sodium phosphate buffer at pH 8 (5:1 v/v ratio). In all cases, unless otherwise noted, polymer was dissolved at an initial concentration of 3 mg/mL. NP formulations with normal siRNA (si-NPs) at each N:P ratio are referred to as 10, 15, and 20, while NP formulations with PA-siRNA

(siPA-NPs) at each N:P ratio are referred to as 10 PA, 15 PA, 20 PA.

For *in vivo* preparations, NPs formed in dilute solutions at pH 7.4 were then concentrated to desired dosages using 15 mL Amicon spin filters, 50k MWCO, with one additional wash step in PBS -/- (to remove buffer salts and ensure appropriate osmolarity prior to injection). Prior to complexation, polymer and buffer solutions were sterile-filtered.

Formulated si-NPs and siPA-NPs were then evaluated for size and surface charge using a Zetasizer Nano ZS (Malvern Instruments, Worcestershire, UK). For encapsulation efficiency studies, a Quant-iT Ribogreen assay (Thermo Fisher, Waltham, MA) was used according to manufacturers' instructions, with polyplexes formulated at 100 nM siRNA. Unencapsulated siRNA was used for controls. For supplemental size evaluations in heparin and bovine serum albumin (BSA) conditions, polyplexes were formulated in pH4 buffer initially at 1 mg/mL and created as described above. Formulations were then incubated for 10 minutes with 40 U/mL heparin or 50 wt% (of the total polymer amount) BSA, and their size was evaluated using the Zetasizer Nano ZS.

pH-Dependent Hemolysis: To evaluate pH-responsiveness of NPs, a red blood cell hemolysis assay was used; the methods have been thoroughly described in our previous work. [21, 87]

NP Stability: To evaluate polyplex stability, a Förster Resonance Energy Transfer (FRET) method was used. Fluorescently-labeled dsDNAs (5' fluorophores) containing Alexa-546 and Alexa-488 probes on the antisense strands, were co-encapsulated in NPs at equimolar amounts. The NPs were formulated at 100 nM, and challenged with either heparin sulfate (100, 40, 2 U/mL) or FBS (10%, 30%, 50%) in a black, clear bottom 96 well plate. Fluorescence intensity at 514 nm and 572 nm was measured using a plate reader (Tecan Infinite F500,

Mannedorf, Switzerland). Fluorophores were excited at 488 nm. The FRET ratio was calculated as the ratio of emission signal at 572 nm to that at 514 nm.

Endotoxin: P(MPC-*bl*-(DMAEMA-*co*-BMA)) polymers were tested for endotoxin contamination using a Chromogenic LAL Endotoxin Assay Kit (GenScript, Piscataway, NJ). The instructions in the kit protocol were followed exactly with testing done at 3 mg/mL polymer.

In Vitro Knockdown, Uptake, Viability in MDA-MB-231 cells: For *in vitro* luciferase knockdown assays, MDA-MB-231 cells were transduced with the luciferase gene in a manner previously described.[43] Cells were then seeded at 2,000 per well in black, clear-bottom 96-well plates. After allowing cells to adhere for 24 hours, si-NPs and siPA-NPs were introduced into cell media at a concentration of 100 nM siRNA (against luciferase or scrambled control sequences). Treatments were removed after 24 hours of incubation, and cell bioluminescence was then measured on an IVIS Lumina III imaging system (Caliper Life Sciences, Hopkinton, MA) at 24 hours and 48 hours after treatment by addition of 150 μg/mL luciferin. Luminescence was normalized to that of scrambled siRNA NP controls. Cell viability was measured by comparing luminescence of scrambled controls to untreated cells.

Cell uptake was measured after seeding normal, non-luciferase expressing MDA-MB-231 cells at 80,000 per well in 12-well plates (working volume 1 mL). The cells were allowed to adhere for 24 hours, and 100 nM NP treatments were applied (Cy5-labeled). After 24 hours, media was removed, and the cells were trypsinized, pelleted, and resuspended in PBS (-/-). Intracellular NP levels were measured by FACS (BD LSRII, Franklin Lakes, NJ), and data were quantified using FlowJo (Ashland, OR).

Intravital Microscopy, Biodistribution: Anesthetized male CD-1 mice (Charles River) were placed on the stage of a confocal microscope (Nikon Czsi+ with Nikon Eclipse Ti-oE

inverted microscopy base, Plan ApoVC 20X differential interference contrast N2 objective, 0.75 NA, Galvano scanner, 543 dichroic mirror). The ear of the mouse (hair removed) was placed on coverslip glass and immobilized with immersion oil. The microscope was focused onto prominent ear veins until red blood cell flow was clearly visible. Mice were then injected with Cy5-NPs at 1 mg/kg dose via the tail vein; intravital fluorescence was monitored (imaging once per second) immediately prior to injection and for 30 minutes after injection or until the Cy5 signal reached half of its initial intensity (if longer than 30 minutes). Curve-fitting was performed using nonlinear regression in Graphpad Prism. Single phase and two-phase exponential decay models were considered and compared using Akaike's Information Criterion.

Mice (n=5 per group) were sacrificed 24 hours after injection, and organs were imaged for Cy5 (excitation 620, emission 670, auto exposure) fluorescence (total radiant efficiency) using the IVIS imaging system described above. All data were quantified using the Living Image Software (Perkin Elmer).

Toxicity Studies In Vivo: Female BALB/c mice (4-6 weeks, Charles River, Wilmington, MA), were enrolled in either a 6-injection study (n=5 per group) or 3-injection study (n=5-6 per group). For the 3-injection study, mice were injected by tail vein on day 1, 4, and 7 with NPs prepared as described above with 1 mg/kg siRNA. The mice were sacrificed 12 hours after the final day 7 injection by cardiac puncture under isoflurane anesthesia. Blood and organs were harvested for further analysis (detailed below). Mouse body weight was recorded daily throughout the treatment period. For the 6-injection study, mice were injected on day 1, 4, 7, 14, 21, and 28. Mice were sacrificed 12 hours after the day 28 injection. Additional mice (n=5 per group) were injected subcutaneously once with LPS (50 μg) or CCl_4 (1:7 v/v in olive oil, 4

mL/kg) as positive controls for toxicity readouts. These mice were sacrificed 12 hours after injection.

Serum Markers and Complete Blood Counts (CBCs): For serum, CBC, and cytokine measurements, blood was harvested by cardiac puncture and collected in EDTA-coated tubes. Plasma was isolated by centrifuging blood samples at 3000xg for 10 minutes and taking the supernatant. Complete blood counts, as well as plasma alanine aminotransferase (ALT), aspartate aminotransferase (AST), and blood urea nitrogen (BUN) were measured by the Vanderbilt Translational Pathology Shared Resource. Clinical chemistry testing was performed using the Alfa Wasserman ACE Alera system. Cytokines were measured by the Vanderbilt Hormone and Analytical Services Core using Multiplex Luminex technology (https://www.vumc.org/hormone/luminex).

Histology: Upon sacrifice, mouse tissues were collected, preserved in 10% formalin, and submitted to the Vanderbilt Translational Pathology Shared Resource, where they were embedded in paraffin, sectioned into 5 μm sections, and stained with hematoxylin and eosin (H&E). H&E stained slides were processed and scanned by the Vanderbilt Digital Histology Shared Resource (www.mc.vanderbilt.edu/dhsr). Slides were evaluated for toxicity-associated tissue damage by Dr. Kelli Boyd, DVM, PhD, DACVP and Dr. Lauren Himmel, DVM, PhD in the Vanderbilt Translational Pathology Shared Resource.

Liver Immune Cell Analysis: Mice in the 6-injection study were sacrificed 12 hours after final injection, and their livers were removed and stored in media on ice (less than 3 hours). Livers were cut into small pieces and macerated through a 0.45 μm cell filter. Hepatocytes were allowed to settle for 20-30 minutes. Cells remaining in suspension were centrifuged for 5 min at 300 x g. Pelleted cells were resuspended in HBSS, underlayed with ISOLYMPH, and

centrifuged at 300 x g for 30 minutes. The buffy coat was collected, pelleted, and resuspended in FACS buffer (1X PBS + 0.05% FBS + 0.1%NaN_3 + 0.02% EDTA) for staining.

Cells were stained using antibodies reactive against B220 (FITC, RA3-6B2), F4/80 (PE, BM8), CD5 (BV421, 53-7.3), Ly6G (PCPCy5.5, 1A8), CD11b (PECy7, M1/70), and AlexaFluor 700 succinimidyl ester to exclude dead cells. Antibodies were purchased from BD Biosciences, eBioscience, or Tonbo Biosciences. Samples were fixed with1X PBS + 1% paraformaldehyde (in 1X PBS) and run on a BD Biosciences LSRII flow cytometer. Data analysis was performed using FlowJo software (FlowJo LLC, Ashland, OR). Data are represented as percent of immune cells to account for differences in total cell numbers isolated from the buffy coat.

Anti-Phosphocholine Immunogenicity: In order determine whether repeat injection caused carrier-associated immunogenicity, serum of mice treated with 15 PA and 20 PA formulations was assayed for anti-phosphocholine antibodies. We first added 50 μL P(MPC-bl-(DMAEMA-*co*-BMA)) polymer solution (5mg/mL in ethanol) into each well of a Nunc MaxiSorp plate (Thermo Fisher). Plates were allowed to dry completely overnight at room temperature. Blocker BSA (200 μL,Thermo Scientific), diluted to 1X in water, was then added to wells and incubated for 1 hr at room temp. Wells were then washed three times with washing buffer (N503, Thermo Fisher). Plasma from Balb/c mice (n=5) injected with the 6-injection protocol (described above) with siPA-NP formulations of 15 PA or 20 PA was then diluted 1:100 in PBS (-/-), added into the wells (100 μL), and incubated for 1 hour at 37 ºC. Serum positive for anti-phosphocholine and serum negative for anti-phosphocholine from the Mouse Anti-Phosphocholine IgG ELISA kit (Alpha Diagnostic International, San Antonio, TX, USA) were used as positive and negative controls. Wells were then washed five times with washing buffer, and 100 μL of HRP-conjugated antibody (0.2 μg/mL, goat anti-mouse, IgG, IgM H+L) was

added to each well and incubated at room temperature for 1 hour. The plate was then washed five times again with washing buffer. A 1-step slow TMB-ELISA (Thermo Fisher) was then incubated in the wells for 15 minutes in the dark. The colorimetric reaction was stopped using Stop Solution (N600, Thermo Fisher). Absorbance was measured at 450 nm, and absorbance values were normalized to measurements on the negative control serum to determine whether treated animal sera were positive for anti-phosphocholine antibodies.

Tumor Studies: Athymic nude mice (Jackson Laboratories, Bar Harbor, ME, USA), were injected orthotopically in bilateral mammary fatpads with 1e6 luciferase-expressing MDA-MB-231 cells in a 50:50 mixture of Matrigel: serum-free DMEM). Tumor growth was monitored until tumors reached 100 mm^3, at which point mice were injected intravenously with 1 mg/kg siRNA packaged in either siPA-NPs (15 PA formulation, n=19 tumors) or in *in vivo*-JetPEI (n=10 tumors). Each formulation was prepared bearing either luciferase or scrambled siRNA sequences. In vivo Jet PEI was prepared according to optimized manufacturer's protocols (0.16 μL *in vivo*-JetPEI per μg siRNA). Tumor luminescence was measured and quantified using an IVIS Lumina III imaging system prior to injection and 24 hours after treatment following injection of 150 mg/kg luciferin subcutaneously. For analysis, luminescence of each tumor at 24 hours was compared to baseline luminescence for that tumor at 0 hours. Values for tumors receiving luciferase siRNA treatment or PBS were then normalized to the average of tumors receiving scrambled siRNA.

For tumor biodistribution studies, athymic nude mice bearing MDA-MB-231 tumors (prepared as described above) were injected intravenously with either siPA-NPs or *in vivo*-JetPEI formulations (described above), bearing Cy5-labeled oligonucleotides (n=4-6 tumors per group). The tumors were then excised from the mice, minced, and incubated for 1 hour with rotation in

media containing 0.5 mg/mL collagenase, 0.19 mg/mL DNase. Tumors cells were then resuspended in HBSS (-/-), incubated in 5mM EDTA for 20 min, filtered through a 70 μm strainer, washed in HBSS (+/+), immersed in ACK lysis buffer for 2 minutes, washed and resuspended in PBS (-/-), and measured for Cy5 fluorescence using a BD Biosciences LSR II cytometer in the Vanderbilt Flow Cytometry Shared Resource.

Statistical Methods: All statistical tests were performed using either one-way ANOVA with multiple comparisons test (in cases of two or more groups) or two-tailed student's t-test (in comparisons with only 2 groups) with $\alpha = 0.05$. *In vivo* tumor knockdown data was analyzed using a non-parametric Kruskal-Wallis test with Dunn's multiple comparisons test. Data are displayed as mean plus standard error.

Ethics Statement: All animal experiments described herein were carried out according to protocols approved by Vanderbilt University's Institutional Animal Care and Use Committee, and all studies followed the National Institutes of Health's guidelines for the care and use of laboratory animals.

3.4 Results and Discussion

The P(MPC-*bl*-(DMAEMA-*co*-BMA)) diblock co-polymers were successfully synthesized by RAFT polymerization with controlled molecular weight. The core block of these polymers comprised a degree of polymerization (DP) of 156, with a 50:50 monomer composition of DMAEMA:BMA and polydispersity (PDI) of 1.02 as determined by ^{1}H-NMR and gel permeation chromatography (**Supplemental Figure B.S1**). This core block monomer ratio was previously shown to optimally balance cytocompatibility with siRNA packaging, endosomal escape properties, and bioactivity.[21] The P(MPC) hydrophilic block was then polymerized from

the p(DMAEMA-*co*-BMA) macroCTA with a DP of 67 (19.8 kDa) as confirmed by ^{1}H-NMR (**Supplemental Figure B.S1**). NPs with ~20 kDa molecular weight P(MPC)-based coronas were shown previously to extend circulation time compared to shorter PEGs and improve *in vivo* tumor cell uptake compared to high molecular weight PEGs.[43]

The hydrophobized siRNA used in this work was synthesized by conjugating NHS ester-modified PA to amine-modified sense strand of the siRNA. Due to the molar excess of PA used in the reaction, the formation of the PA-conjugated siRNA (PA-siRNA) conjugate was highly efficient, with unmodified siRNA peaks undetectable by HPLC in the final product (data not shown). The molecular weight of the single-stranded, PA-siRNA was confirmed by LC-MS-ESI (m/z=8566 for scrambled-sequence siRNA, expected MW= 8565 g/mol).

We formulated 6 unique NP samples using either normal siRNA (si-NPs) or PA-modified siRNA (siPA-NPs) at N:P ratios of 10, 15, 20 (**Figure 3.1**). These formulations are indicated throughout this work as 10, 15, 20, 10 PA, 15 PA, and 20 PA. For all studies, the dose of siRNA was kept constant, only changing the amount of polymer. Despite the different amounts of polymer utilized, the hydrodynamic diameter of all formulations was similar at approximately 100 nm (**Figure 3.2a**), and all zeta potentials were close to 0 mV (**Figure 3.2b**). Other studies that have explored the impact of N:P ratio on NP performance have mostly done so in the context of PEI or PEG-PEI-based polyplexes, where a change in N:P ratio causes a significant change in surface charge of the polyplex.[125, 132, 133, 136, 143] Because size and surface charge can significantly alter NP biodistribution[65], this polyplex formulation library is advantageous in that it enables exploration of the impact of N:P ratio without confounding changes in size or surface charge. The consistent size and zeta potential of the candidate NPs is likely dictated by the relatively high molecular weight, super-hydrophilic P(MPC) corona-forming polymer that forms

stable, neutrally-charged NPs with high resistance to serum protein or complement adsorption.[43]

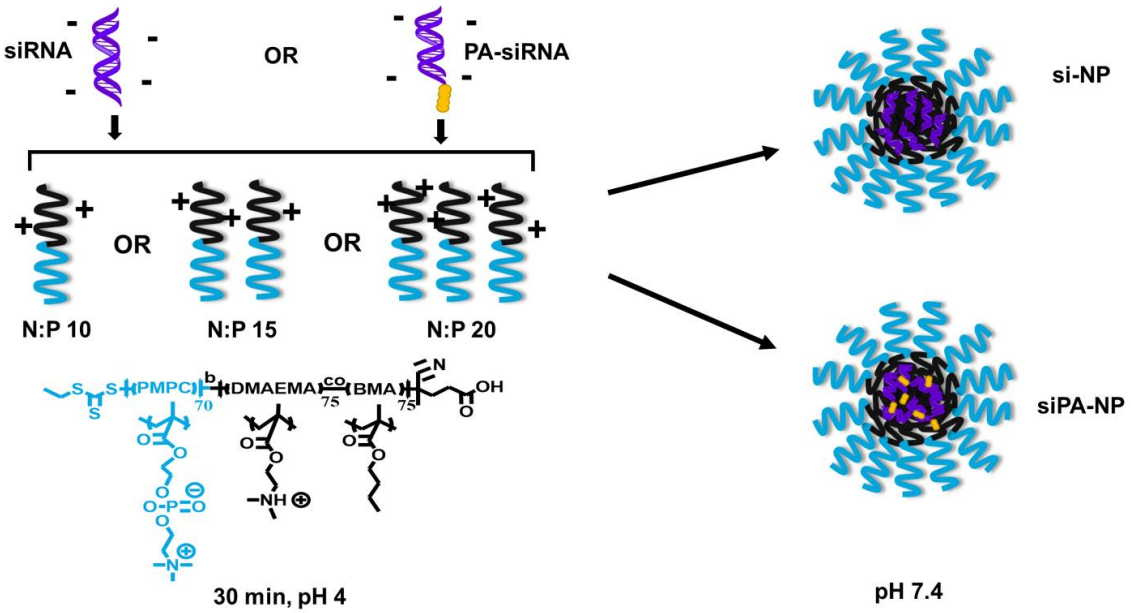

Figure 3.1 Formulation of si-NPs and siPA-NPs. The NPs were made at N:P ratios of 10,15, and 20 with either un-modified siRNA, or hydrophobically-modified PA-siRNA**.** To form NPs, siRNA was complexed with P(MPC-*bl*-(DMAEMA-*co*-BMA)) polymers at pH 4 for 30 minutes, and then pH was raised to 7.4.

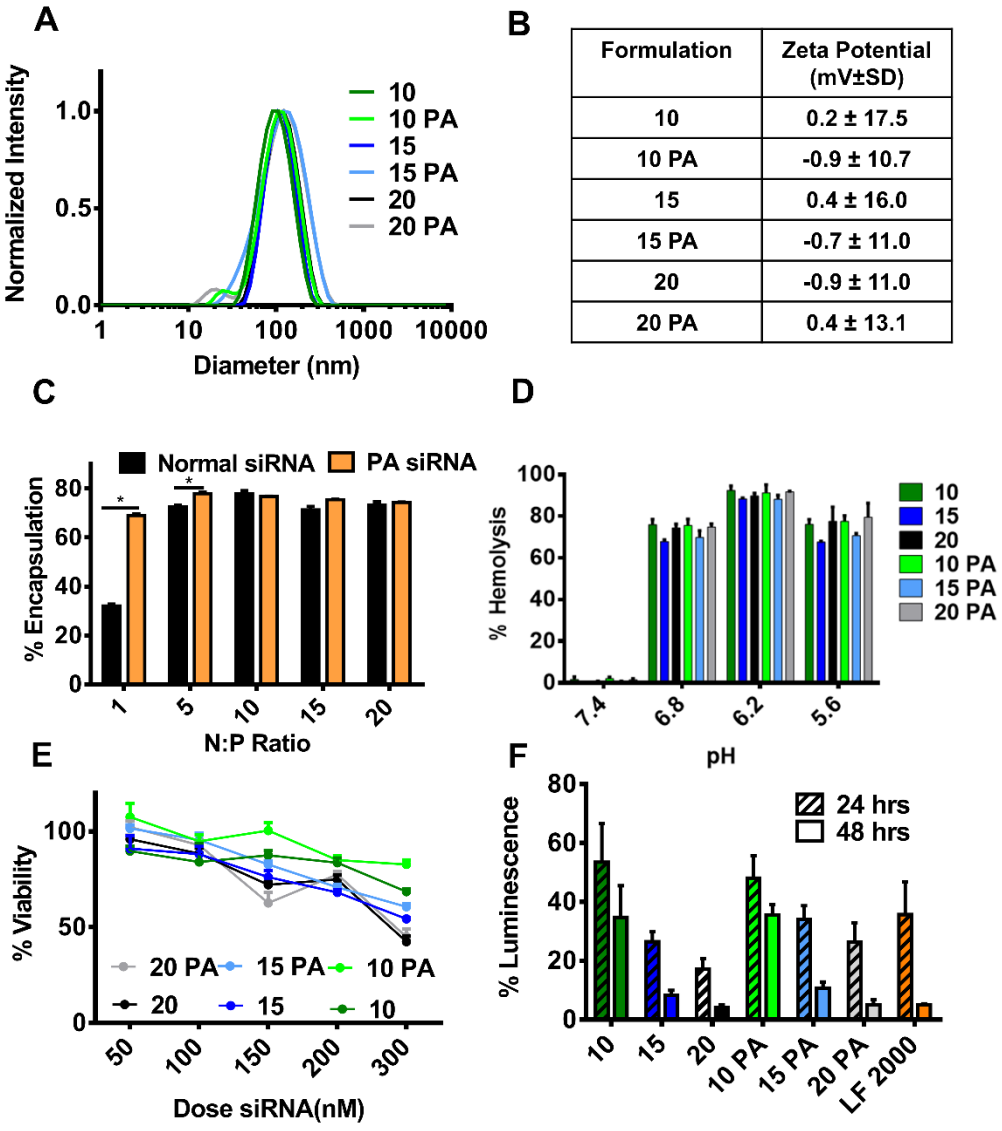

Formulation	Zeta Potential (mV±SD)
10	0.2 ± 17.5
10 PA	-0.9 ± 10.7
15	0.4 ± 16.0
15 PA	-0.7 ± 11.0
20	-0.9 ± 11.0
20 PA	0.4 ± 13.1

Figure 3.2 Characterization of NP size, charge, pH-dependent membrane disruption activity (endosome escape), siRNA encapsulation efficiency, *in vitro* viability, and activity**.** (A) All NP formulations were approximately 100 nm in diameter and (B) had neutral zeta potentials. (C) The siPA-NPs exhibited increased encapsulation efficiency at low N:P ratios relative to si-NPs based on Ribogreen quantification (n=3, $p<0.05$). (D) All NPs display pH-dependent membrane disruption tuned to cause lack of toxicity (no hemolysis at pH 7.4) and endosome disruption (hemolysis at pH 6.8 and below). (E) Viability of MDA-MB-231 cells 48 hours after exposure to NP formulations. (F) *In vitro* knockdown of luciferase in MDA-MB-231 cells 24 and 48 hours after siNP exposure. Increasing N:P ratio increased *in vitro* knockdown, but addition of PA-siRNA had no significant effect.

At N:P ratios of 10, 15, or 20, all formulations maintained 70-80% encapsulation of siRNA (**Figure 3.2c**). However, at lower N:P ratios of 1 or 5, siPA-NPs had significantly higher encapsulation efficiencies than si-NPs. The siPA-NPs with dual hydrophobization on the carrier polymer and cargo siRNA, therefore, more efficiently encapsulate siRNA at lower N:P ratios, likely due to hydrophobic carrier-cargo interactions and/or hydrophobicity-driven clustering of PA-siRNA molecules. However, encapsulation efficiency was consistently high for the 6 formulations used in this work at N:P ratios of 10,15, and 20, regardless of hydrophobization of the siRNA.

The ability to trigger endosomal rupture and escape is a necessary carrier property to ensure siRNA access to the cell cytoplasm where it is active. The pH-dependent membrane disruptive activity of the P(MPC-*bl*-(DMAEMA-*co*-BMA)) polymers was characterized for each formulation using a red blood cell hemolysis assay (**Figure 3.2d**), which simulates endosomolysis.[87] At physiological pH, no formulations exhibited significant hemolytic activity, an indicator of their safety in circulation. However, all formulations exhibited strong hemolytic activity at pH 6.8 or lower, indicating their ability to disrupt endosomal membranes in response to a pH drop on the endolysosomal pathway. Neither the N:P ratio nor the presence of palmitic acid on the siRNA significantly altered the pH-dependent hemolytic behavior, which is driven by the polymer.

Prior to *in vitro* cell assays, the P(MPC-*bl*-(DMAEMA-*co*-BMA)) polymers used for NP formulation were tested for endotoxin. Endotoxin is a potent stimulator of innate immunity and can have significant effects on both *in vitro* and *in vivo* toxicology, independent of the NPs themselves. No endotoxin contamination was found in the P(MPC-*bl*-(DMAEMA-*co*-BMA)) polymers (**Supplemental Figure B.S2a**).

In vitro, all formulations were well-tolerated with low cytotoxicity up to 150 nM siRNA in MDA-MB-231 cells (**Figure 3.2e**). At 100 nM, average viability ranged from 88 to 95%. At higher doses of polymer and siRNA, NP toxicity increased. At these higher doses (200-300 nM siRNA), NP toxicity was positively correlated with N:P ratio, indicating that polymer itself (as opposed to the siRNA) was the source of cytotoxicity since the amount of polymer increased with increasing N:P ratio while siRNA dose was held constant at a given dose level. This trend was present regardless of dual hydrophobization state. At each dose, there were no significant differences between cytotoxicity of si-NPs vs siPA-NPs. After removing NP treatments and waiting 24 hours, cell viability recovered rapidly for all doses up to 300 nM siRNA (**Supplemental Figure B.S2b**). Our data suggest that in an *in vitro* environment, the addition of PA-siRNA did not significantly impact viability. The reduced cell viability at higher N:P ratios highlights the need for reducing polymer dose to achieve non-toxic NP formulations, particularly since DMAEMA, like most cationic polymers involved in nucleic acid delivery, is known to be cytotoxic at high concentrations.[123]

Each si-NP and siPA-NP formulation was next tested for *in vitro* bioactivity by knocking down the model gene luciferase in MDA-MB-231 cells (**Figure 3.2f**). The amount of luciferase knockdown positively correlated with the relative amount of polymer (increasing N:P ratio) in the NP formulation at both 24 and 48 hours after treatment. By 48 hours, NP formulations at 20 or 20 PA achieved 93 to 97% silencing, while formulations at 10 or 10 PA exhibited average silencing of 50% to 70%. Similar to the cell viability results, the presence of PA in the formulations did not significantly alter the silencing efficiency in vitro. Uptake of fluorescently-labeled NPs was also measured for each formulation (**Supplementary Figure B.S2c**). Interestingly, while all formulations exhibited significantly increased uptake compared to

commercial Lipofectamine 2000, there were no significant differences in uptake caused by increasing N:P ratio, which is consistent with the expected result based on these NPs all having similar diameter, zeta potential, and siRNA packaging efficiency. There was a small increase in average mean fluorescence for cells treated with siPA-NPs, but it was only significant at N:P 10. This result agrees with the bioactivity data which shows that addition of PA-siRNA did not significantly change gene knockdown. However, NPs formulated at different N:P ratios had different levels of bioactivity despite achieving similar level of cell internalization, suggesting that increasing N:P ratio may improve bioactivity by mechanisms other than uptake, such as increased endosomolytic properties that are not sensitively measured by *in vitro* hemolysis assays. This result is consistent with earlier work utilizing PA-siRNA in PEGylated si-NP systems.[47] *In vitro,* it was expected that the stability advantages imparted by PA-siRNA would be less apparent, since there is a low percent serum (10% in these studies), a lack of competition by molecules such as proteoglycans, and a hemodynamically static environment with reduced mechanical and dilution concerns. It was anticipated that PA-siRNA may impart stability differences that are more impactful *in vivo* and that could alter the stability (which has impacts on toxicity), systemic circulation, and tissue accumulation/activity of NPs.

Two of the major challenges to NP stability in circulation are serum proteins and anionic heparan sulfate proteoglycans in the kidney glomerular basement membrane.[25, 65] In order to understand the potential impact of N:P ratio and hydrophobized siRNAs on NP stability *in vivo*, we challenged NPs with various concentrations of serum and heparin in a FRET-based assay (**Figure 3.3**). This assay involves co-encapsulation of FRET-paired siRNAs, and an increased FRET ratio indicates better siRNA encapsulation stability.

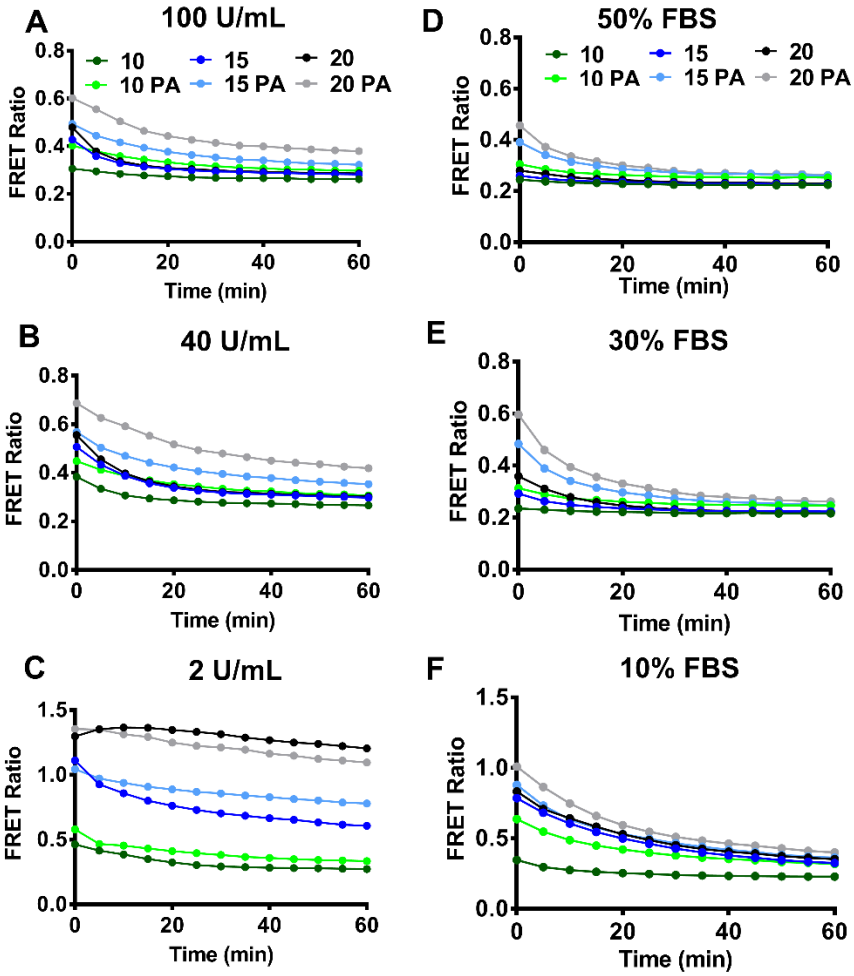

Figure 3.3 Stability of NPs over time in FBS and anionic heparin sulfate is dependent on both N:P and dual hydrophobization. (A-C) NPs at 100 nM siRNA were exposed to 100, 40, or 2 U/mL heparin or (D-F) 10,30, or 50% FBS, and the ratio of fluorescence at 572 nm to 512 nm was measured. In general, NPs at higher N:P ratios or that were made with PA-siRNA displayed increased cargo loading stability.

With both heparin and serum challenge, increasing N:P ratio increased stability, particularly at low challenge concentrations, while siRNA conjugation with PA was increasingly important to stability at high challenge concentrations. In heparin at 100 U/mL and 40 U/mL, 20 PA formulations consistently had the highest average stability, while formulations at N:P 10 with normal siRNA consistently had the lowest average stability, as determined by FRET ratio (**Figure 3.3a and 3.3b**). The 15 PA NPs had the second highest stability, while 15, 20, and 10

PA formulations all displayed similar FRET ratios throughout 60 minutes and were not significantly different from each other. These data suggest that with increased concentration of heparin, siRNA conjugation to PA significantly improves resultant NP stability, particularly at higher N:P ratios. At 2 U/mL of heparin, the effect of N:P ratio on stability was predominant, with polyplexes formulated at 20 significantly more stable than those formed at 15 or 10 (**Figure 3.3c**). Thus, at lower concentrations of heparin, NP stability is significantly increased by increasing N:P ratio, while siRNA conjugation to PA had a relatively negligible effect for each individual N:P ratio.

In 50% or 30% serum, 15 PA and 20 PA once again exhibited the highest FRET ratios, indicating their increased stability (**Figure 3.3d and 3.3e**). Here again, in higher serum conditions, siRNA conjugation to PA increased FRET ratios compared to the si-NPs without dual hydrophobization at equivalent N:P ratios. At 50% serum, all siPA-NPs had higher FRET ratios, while si-NPs at all N:P ratios tested without PA-siRNA exhibited equally low stability, and their FRET traces were not significantly different from each other. At lower serum conditions (10% FBS), the impact of N:P ratio was more apparent, as NPs at 15 and 20 had consistently higher stability than NPs formulated at N:P 10, although 20 PA NPs were still the most stable, with significantly greater FRET ratio than the si-NPs at N:P 10 after one hour of serum exposure (**Figure 3.3f**). Incubation of all NP formulations in 40 U/mL heparin or bovine serum albumin did not significantly impact particle size (**Supplemental Figure B.S3**). Together, these data suggest that formulating NPs at higher N:P ratios can improve their stability against serum or heparin at lower concentrations, but addition of dual hydrophobization (in siPA-NP formulations) is more effective for increasing stability at higher serum or heparin levels representative of the *in vivo* environment.

We next explored the impact of N:P ratio and dual hydrophobization on *in vivo* NP pharmacokinetics using intravital microscopy (IVM) of the mouse ear vasculature. Each formulation bearing fluorescently-labeled siRNA was injected intravenously and tracked via confocal microscopy (representative images in **Figure 3.4a**). Electrostatically-complexed particles historically have more rapid blood clearance than solid nanoparticulate systems. IVM allows for more accurate measurement of NP clearance and early-phase half-lives because it enables continuous sampling of fluorescent signal, starting immediately after injection.

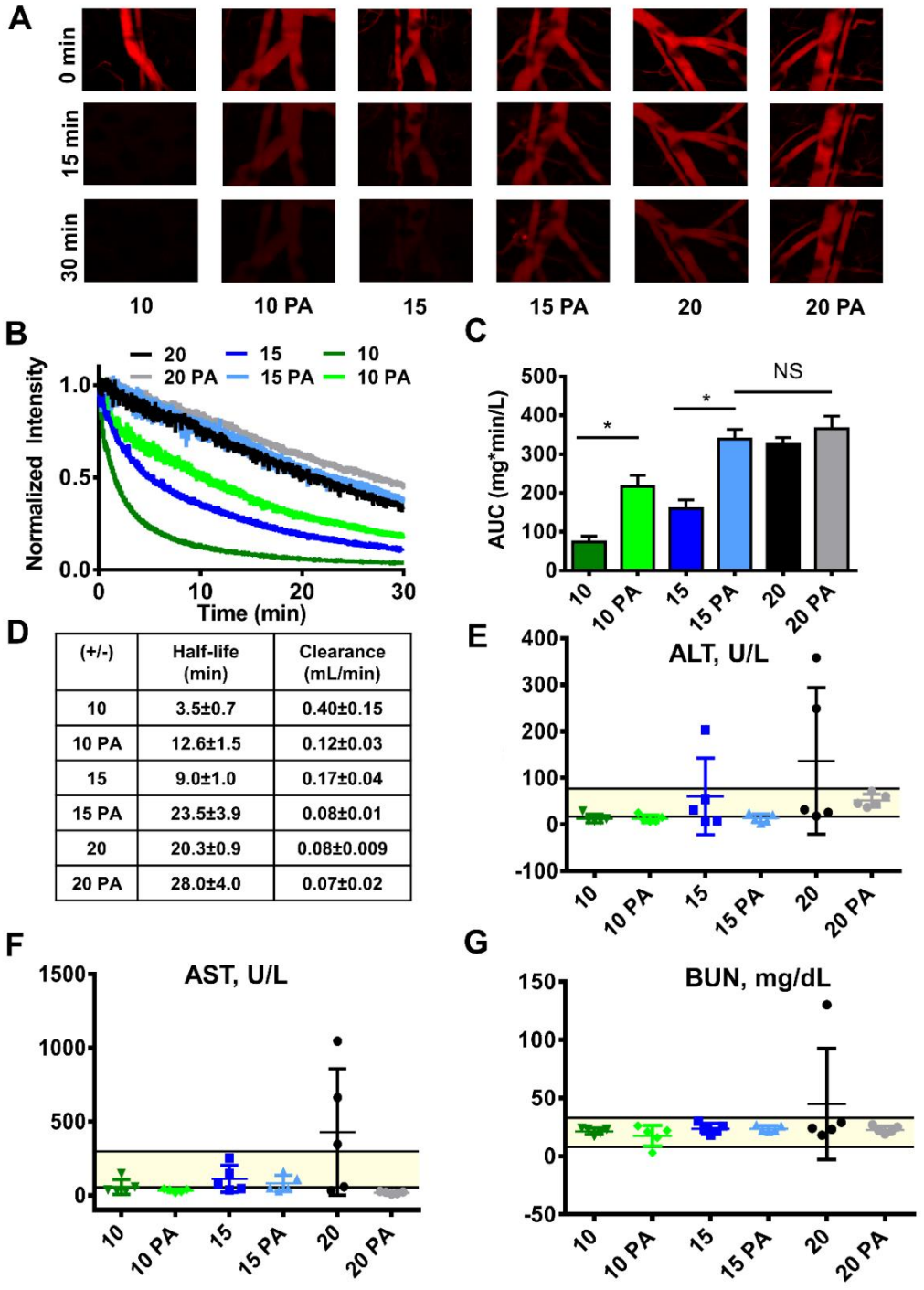

Figure 3.4 Interplay of N:P and dual hydrophobization impacts *in vivo* pharmacokinetics and toxicology**.** (A) Representative intravital microscopy images of Cy5-siNPs in the mouse ear. (B) Average pharmacokinetic curves (first 30 min) for each NP formulation, normalized to initial fluorescence intensity (n=5). (C) Increasing N:P ratios and addition of PA-siRNA at N:P 10 and 15 significantly increased NP area under the curve ($p < 0.05$, n=5). (D) Table of half-lives and clearance values for each NP formulation. Longest half-lives were achieved by siPA-NPs

formulated at 20 PA. (E-G) ALT, AST, and BUN sampled from blood sera collected at 24 hours after a single injection of NPs show toxicities dependent on polymer dose in the N:P 20 and N:P 15 groups (n=5). Toxicities were abrogated in NPs formulated with PA-siRNA. Horizontal y-axis lines indicate normal mouse plasma ranges for ALT, AST, and BUN.

Overall, increasing N:P ratio significantly increased NP area under the curve and circulation half-life (**Figure 3.4b-d**). The si-NPs formulated at 15 and 20 had half-lives increased by 2.5-fold and 5.7-fold respectively compared to si-NPs formulated at N:P 10, ranging from 4 minutes (N:P 10) to 9 minutes (N:P 15) to over 20 minutes (N:P 20). At N:P 20, AUC was significantly increased by over four-fold compared to N:P 10, and two-fold compared to N:P 15. Similarly, average clearance for si-NPs formulated at N:P 20 was significantly greater than either formulations at 10 or 15. Thus, increasing the amount of polymer relative to siRNA significantly improved pharmacokinetic characteristics.

Dual hydrophobized siPA-NPs had enhanced area under the curve and circulation half-lives relative to si-NPs, particularly at the lower N:P ratios. The siPA-NPs at N:P 10 and N:P 15 had a three-fold and two-fold, respectively, increase in area under the curve relative to the corresponding si-NPs at the same N:P ratios. At N:P 10, siRNA conjugation to palmitic acid nearly quadrupled average NP half-life. At N:P 15, dual hydrophobization increased half-life average from 9 minutes to 23.5 minutes. The benefits of dual hydrophobization begin to diminish at N:P 20, at which point addition of PA did not significantly increase half-life or area under the curve. Importantly, siPA-NPs formulated at 15 PA did not have significantly different area under the curves from either 20 or 20 PA NPs. Thus, addition of PA enables delivery of the same doses of siRNA with similar pharmacologic profiles (at 15 PA, 20, and 20 PA), but with a lower dose of polymer for the optimized 15 PA formulation.

Each of the NP formulations was determined to have first order, single-phase elimination

kinetics, based on the best fit nonlinear regression analysis (curves shown in **Supplementary Figure 3.4a**). This fit can also be demonstrated visually by the linearity of each elimination curve when plotted in log scale (**Supplementary Figure 3.4b**). The one exception to this trend is the si-NPs formulated at N:P 10. Because these polyplexes are the least stable, it is likely that some of the Cy5-labeled nucleic acids were not well-complexed, and an early-phase elimination is visible for the free nucleic acid population.

Twenty-four hours after intravenous injection, the organ biodistribution for all NP formulations was similar, with greatest accumulation in the liver and kidneys (**Supplemental Figure 3.4c**). Both 15 PA and 20 PA formulations had significantly lower fluorescence in the kidneys compared to si-NPs at N:P 20 with normal siRNA, which had the highest amount of kidney fluorescence. These data suggest that the dual hydrophobized formulations at higher N:P ratios are less prone to clearance by disassembly in the kidney glomerular basement membrane.

At 24 hours after a single injection, mice treated with NPs formulated at higher N:P ratios (15, 20) with normal siRNAs showed signs of elevations above normal ranges in ALT, AST, and BUN, indicators of liver and kidney toxicity (**Figure 3.4e-g**). In the si-NP N:P 20 group, 3/5 mice had above-normal AST, 2/5 had elevated ALT, and one had increased BUN. In the N:P 15 group, only one mouse showed any sign of abnormally high serum enzymes (ALT). However, addition of PA-siRNA in these formulations completely abrogated signs of toxicity; none of the mice treated with dual hydrophobized siPA-NPs experienced elevation in the serum toxicity markers measured.

The combined pharmacokinetic profiles and liver enzyme data suggest that dual hydrophobization strategies can impart significantly increased stability to electrostatically-complexed polyplexes in circulation while reducing toxicity associated with increased doses of

polymer. We have shown that increasing N:P ratio significantly improves circulation half-life *in vivo*, but comes at a toxicologic cost associated with increased cation-containing polymer in the formulations. This toxicity is likely related to reduced stability and exposure of the cationic core polymer block, as free polycations are known to interact negatively with circulating cells or serum components.[42] PA-modified siRNA increases the hydrophobic interactions between polymer and siRNA relative to unmodified siRNA, increasing NP stability and preventing premature exposure of the cationic moieties in the NP core to the exterior of cells (prior to entry into acidifying endosomes). Addition of PA-siRNA can therefore reduce the toxicity of high-polymer formulations and significantly increase the half-life of low-polymer formulations.

As we and others have demonstrated, increases in pharmacokinetic area under the curve typically correlate with significantly increased tumor biodistribution.[30, 47, 118, 144] Tumor accumulations of nanomedicines is typically driven at least in part by the enhanced permeability and retention effect (EPR), which has been observed in solid tumors in human patients, and is known to positively correlate with intravenous area under the curve.[30, 34, 144] Extended siPA-NP circulation times may indicate reduced polyplex disassembly in the kidney and increased opportunity for passive accumulation of siRNA in target tissues.

It is rare for electrostatically-complexed polymeric NPs to have alpha-phase half-lives as long as those achieved by our high N:P ratio, dual-hydrophobized carriers. PEGylated polycations or emulsion-based cationic nanogels clear from circulation completely by 20 minutes.[66, 133] Though some systems have utilized hydrophobic core monomers to improve stability of PEG-shielded, cationic carriers, first-phase circulation half-life is frequently less than 5 minutes due to a first-pass effect in the liver.[145] Even core disulfide crosslinking, as demonstrated by the Kataoka group, did not improve NP circulation half-life to longer than 5-10

minutes when introduced to polyion complex micelles.[23, 96, 146] When a cholesterol-modified siRNA was added, the half-life was modestly extended to over 20 minutes (single hydrophobization), further supporting the powerful impact of hydrophobization of siRNA on nanocarrier circulation.[23] Similarly, clinically studied CALAA-01 complexes utilizing guest-host cyclodextrin-adamantane stabilization of polymer components were completely cleared from circulation in 30 minutes in humans, probably due to rapid dissociation in the kidney.[25]

To date, few studies have demonstrated the *in vivo* impact of small changes in N:P ratio on polyplex pharmacokinetics or toxicity. N:P ratio is most often explored in the context of encapsulation efficiency *in vitro*, with selection based on the lowest N:P ratio with adequate encapsulation of nucleic acid. However, in our case, NPs formulated at 10, 15, and 20 all had equally high encapsulation efficiencies and identical physicochemical properties (size, surface charge), yet produced markedly different *in vivo* pharmacokinetic properties. Notably, polymer dose has been demonstrated to improve *in vivo* stability in the context of various crosslinking strategies in PEGylated poly(L-lysine)-based NPs; the use of 2-iminothiolane crosslinking increased the ratio of polymer to siRNA and improved polyplex blood circulation compared to 3,3'-dithiobispropionimidate crosslinking, which resulted in lower polymer to siRNA ratios and lower stability.[146] Other groups have primarily studied N:P ratio in the context of how polyplex surface charge impacts organ biodistribution; it has often been observed that increasing N:P correlates with higher accumulation in the lung and rapid clearance from circulation, driven by increasing surface charge.[133, 143] To our knowledge, our data are the first to comprehensively characterize the impact of charge ratio and dual hydrophobization on the pharmacokinetic profiles and toxicity of siRNA-containing NPs and to make the unique observations that dual hydrophobization can reduce the amount of polymer needed to achieve maximal AUC, while

also reducing toxicity *in vivo* for a defined N:P ratio.

Because many applications of siRNA therapeutics, including delivery to solid tumors, require repeated intravenous dosing of NPs, we further explored the impact of charge ratio and PA-siRNAs on more rigorous toxicologic parameters after multiple injections. Additionally, the effects of long-term administration of zwitterionic-corona NPs have thus far not been well-characterized.

We injected two cohorts of healthy BALB/c mice with 1 mg/kg NPs on different treatment schedules. In the first group, we injected NPs i.v. 3 times over the course of a week (3 injection course; day 1,4,7). In the second treatment group, we injected NPs i.v. 6 times over the course of a month (6 injection course; day 1,4,7,14,21,28). In both cases, the animals were sacrificed 12 hours after the final injection. We performed a comprehensive panel of tests to determine the relative safety of the formulations, including assessing serum enzymes, complete blood counts, plasma cytokines, body weight, histology, liver immune cell content, and immunogenicity. Because of the trends toward acute toxicities observed 24 hours after a single injection in the N:P 20 group, we limited our studies to formulations at 10,15, 10PA, 15PA, and 20PA. As a positive control for toxicity, another group of mice was injected with LPS once and sacrificed 12 hours later. For both injection courses, no significant changes in body weight were noted for any of the mice receiving any NP formulation (**Supplementary Figure B.S5**).

After the week-long, 3-injection course, there were no elevations in ALT, AST, or BUN outside of normal ranges, indicating that all formulations were well-tolerated (**Figure 3.5a-c**). However, the ALT levels for N:P 15 group were significantly increased from saline-injected mice and from the 15 PA group ($p < 0.01$, n=5-6), suggesting that addition of PA-siRNA reduced liver toxicity. The 20 PA group also had significantly higher ALT levels than the 15 PA group

($p<0.03$, n=5-6), suggesting some polymer dose-dependent effects in the liver. After the month-long, 6-injection course, all NP formulations remained within normal range except for one mouse in the 20 PA group, which experienced elevations in ALT and AST (**Figure 3.5d-f**). This indicates that in the context of a multi-injection study, even with addition of PA-siRNA, higher N:P ratios may cause liver toxicity. Overall, there were no statistically significant differences between NP formulation groups and saline-treated groups after the 6-injection course. Thus, the relatively small ALT differences observed after the more frequent 3-injection in 1-week schedule are likely temporary elevations that were resolved after the month-long course.

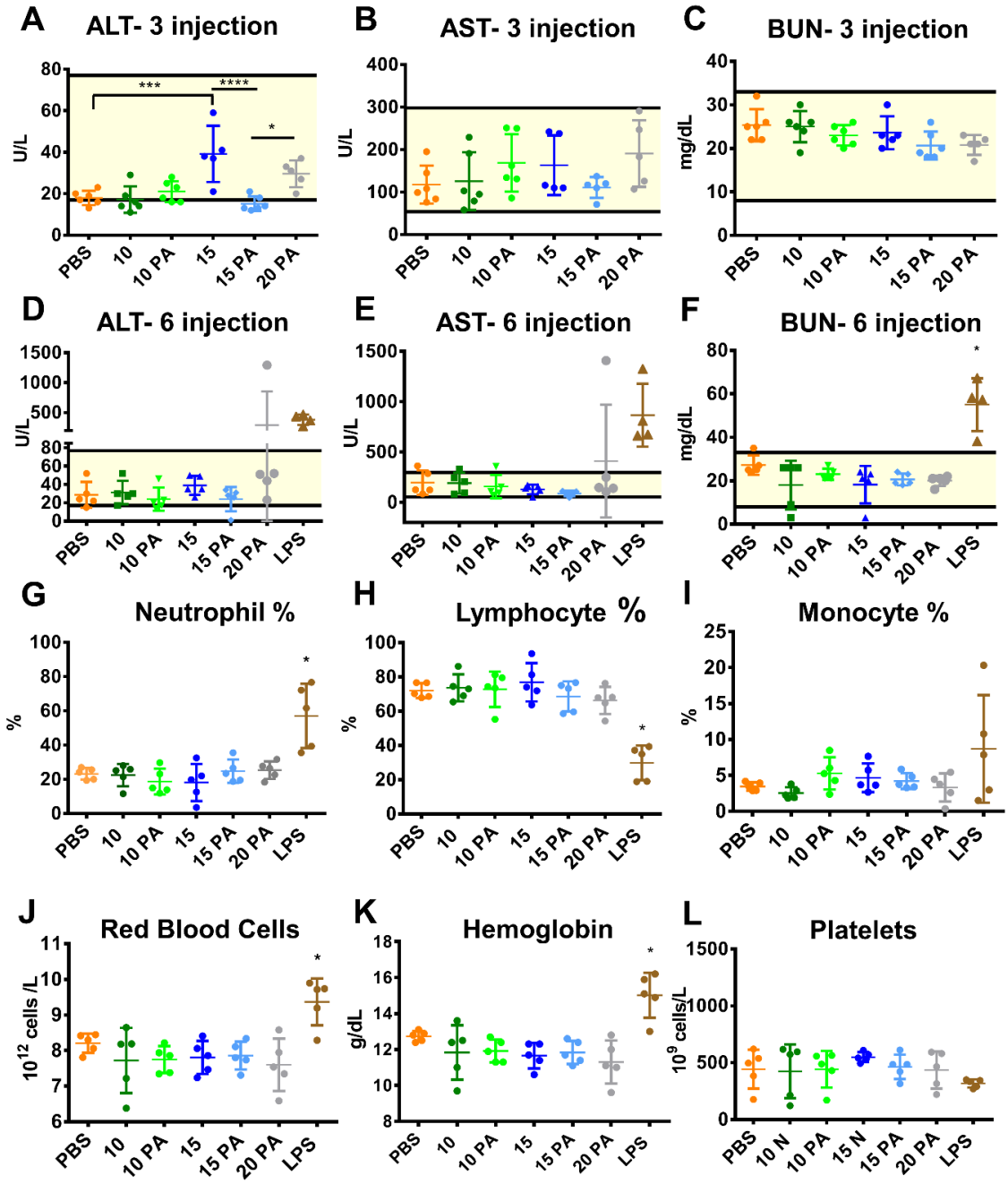

Figure 3.5 All NPs tested had minimal toxicological effects under the multi-injection treatment courses. ALT, AST, and BUN levels in mice sera 12 hours after the final injection of a 3-injection course (A-C) or 6-injection course (D-F) show that NPs were well-tolerated across multiple injections (n=5-6). Yellow boxes indicate normal ranges. The only detectable adverse elevations were in the 20 PA group after 6 doses of 1 mg/kg siPA-NPs over the course of 1 month. Mice treated with LPS were used as a positive control for liver and kidney damage. (G-L) Complete blood counts 12 hours after the final injection of the 6-injection course show no abnormal changes in circulating lymphocytes, erythrocytes, or platelets, for any of the sampled

NP formulations (n=5-6).

The complete blood counts for all formulations were not significantly different from saline-treated mice for either the 3-injection (**Supplemental Figure B.S6a-i**) or 6-injection courses (**Figure 3.6g-l**, **Supplementary Figure B.S6j-l**). Often, a concern with electrostatically-complexed NPs such as the clinically-studied CALAA-01, is that they may cause platelet aggregation in circulation, which reduces overall platelet count.[37] However, no significant changes in platelet counts were recorded for any of the tested NPs, indicating that the NPs in this study did not induce major platelet aggregation, regardless of N:P ratio. LPS treatment, on the other hand, induced significant decreases in % lymphocytes with corresponding increases in % monocytes, % neutrophils, red blood cell count, and hemoglobin. These data provide further support that the si-NPs and siPA-NPs at each N:P ratio tested were well-tolerated upon long-term, repeated administration.

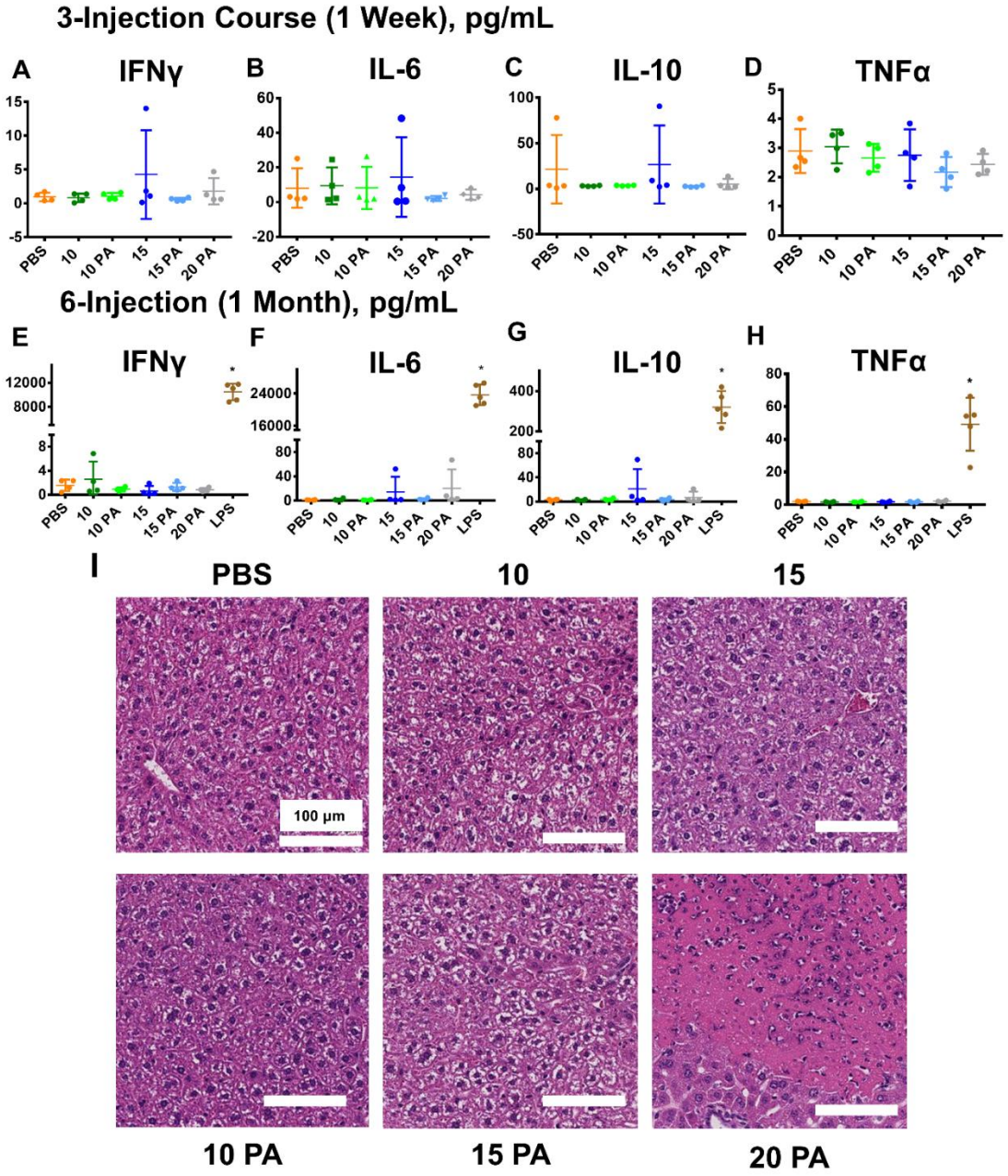

Figure 3.6 Cytokines and liver histology associated with multi-injection courses. IFNγ, IL-6, IL-10, and TNFα sampled from serum of BALB/c mice 12 hours after the final dose of a 3-injection course (A-D) or a 6-injection course (E-H) (n=5). Compared to LPS-injected positive control mice, there were no significant or unsafe elevations in any cytokine levels measured. A few mice experienced cytokine increases after administration of NPs formulated at 15, which were notably the highest polymer dose tested without dual hydrophobization. (I) Representative liver histology after 6-injection course. For NPs formulated at 10, 15, 10 PA, or 15 PA, all livers were similar to saline treated mice or exhibited minimal signs of single cell or focal necrosis. However, at the highest polymer dose of 20 PA, 2/5 mouse livers had visible areas of focal necrosis.

None of the NP formulations tested in this study induced significant increases in cytokines that would indicate immunotoxicity (**Figure 3.6a-h**). At 12 hours after the final injection in the 3-injection course, one mouse in the N:P 15 group showed modest increases in IFNγ (**Figure 3.6a**), and one mouse had increased IL-6 (**Figure 3.6b**) (14- and 6-fold above the saline average, respectively). After the 6-injection course, one mouse in each of the 15 and 20 PA groups had slightly elevated IL-6 (**Figure 3.6f**) (43 and 56-fold above the saline average), and the same mouse from the 15 group and a different mouse in the 20 PA group had elevated IL-10 (**Figure 3.6g**) (26-fold and 8-fold above the saline average, respectively). The increase in IL-10 in these groups after longer-term injections matches evidence from the CALAA-01 studies, in which continuous polyplex dosing increased the serum levels of the anti-inflammatory cytokine IL-10[62], perhaps a compensatory mechanism against carrier-related effects. However, all cytokine increases were modest compared to the LPS-treated mice, which were on the order of hundreds to thousands-fold greater than the saline averages. The siRNAs used in this study contained multiple O-methyl modifications to reduce their potential immunostimulatory effects, so any cytokine increases are likely caused by polymer components of the NP formulations. In our study, only the NP formulation containing either the highest polymer dose (20 PA) or the highest polymer dose without hydrophobized siRNAs (N:P 15), induced slight cytokine responses, further suggesting that any immunostimulation is dependent on overall polymer dose and NP stability. Overall, our data indicate that the zwitterionic NP formulations were well tolerated over long-term, repeated administration.

Liver, spleen, lung, and kidney tissues were evaluated for histological abnormalities by

blinded veterinary pathologists after completion of each injection course. In the 3-injection course, all tissues were determined to be "unremarkable" (data not shown). For the 6-injection course, spleen, lung, and kidney tissues were also determined "unremarkable" (**Supplemental Figure B.S7a-b**). Mouse livers were graded for signs of necrosis, with most NP treated mice showing normal histology (**Figure 3.6i**). However, in the livers of mice in the 20 PA group, there were detectable areas of coagulation necrosis in 2 out of 5 mice. One mouse in the 15 PA group showed evidence of a very small area of coagulation necrosis (**Supplementary Figure 3.7c**). The livers of two mice each in the 15 PA and 15 groups had only 1-2 single necrotic cell foci, while 4/5 mice in the 20 PA group had signs of single cell necrosis (**Supplemental Figure B.S8a**). All cases of cellular necrosis in these mice were therefore very small, with clinically relevant amounts of necrosis occurring in only one of the 20 PA treated mice, which aligns well with serum liver enzyme results **(Figure 3.5d-e**). In the livers of mice treated with a positive control for liver toxicity, carbon tetrachloride (CCl_4), necrosis was more widespread (**Supplemental Figure B.S8b**). The histologic analysis therefore indicates that while all formulations were relatively well-tolerated, repeated injection of many doses at the "high polymer" 20 PA condition could result in some minor but likely manageable liver damage. In sum, we observed a clear polymer dose dependence for liver injury, which highlights the need to reduce overall polymer dose while maintaining optimal pharmacokinetic properties of NP formulations.

Based on our liver histology results, we also characterized the populations of immune cells present in the livers of mice subjected to the 6-injection course to test for an inflammatory response by innate immune cells. While mice treated with the liver-toxic agent, CCl_4, experienced elevations in percentages of liver macrophages and neutrophils, none of the NP

formulations significantly altered macrophage or neutrophil populations compared to saline-treated mice (**Figure 3.7a-b**). However, the percentage of myeloid dendritic cells in the liver was significantly increased in the N:P 15 group (no PA), relative to mice treated with PBS and to all of the siPA-NPs (**Figure 3.7c**). The average percentage of non-myeloid dendritic cells (DCs), which may include lymphoid and plasmacytoid DCs, for the N:P 15 group was also increased compared to saline and other NP formulations, though not significantly (**Figure 3.7d**). Because the 15 group contained the highest N:P ratio for a non-PA-siRNA formulation, our data suggest that less stabilized si-NPs with higher ratios of polymer to siRNA stimulated a DC response in the liver. Liver DCs are known to be antigen-presenting and may be increased in number in response to inflammation or fibrosis.[147] Liver Kupffer cells, a primary phagocyte for intravenously delivered nanoparticles in general, are known to secrete IL-10, which can further recruit DCs to the liver.[148] Because the N:P 15 group also showed some elevations in IL-10 12 hours after the final injection, this effect on DC levels may be due to activation of the Kupffer cells by N:P 15 si-NPs. Previous work has also shown that an i.v. injection of colloidal carbon resulted in increased recruitment of dendritic cells from circulation to the liver, indicating that this could be an underappreciated response to intravenous nanoparticle treatments.[149] Additionally, the presence of PA-siRNA in siPA-NP formulations appears to have a protective effect, since the 15 PA and 20 PA groups did not show signs of increased percentages of dendritic cells. While hepatic DCs can elicit a T cell response, we did not see any increase in liver T cells or B cells in any of the NP formulations (**Supplemental Figure 3.9a-b**).[149, 150] Example gating for all lymphocyte populations can be found in **Supplemental Figure B.S10**.

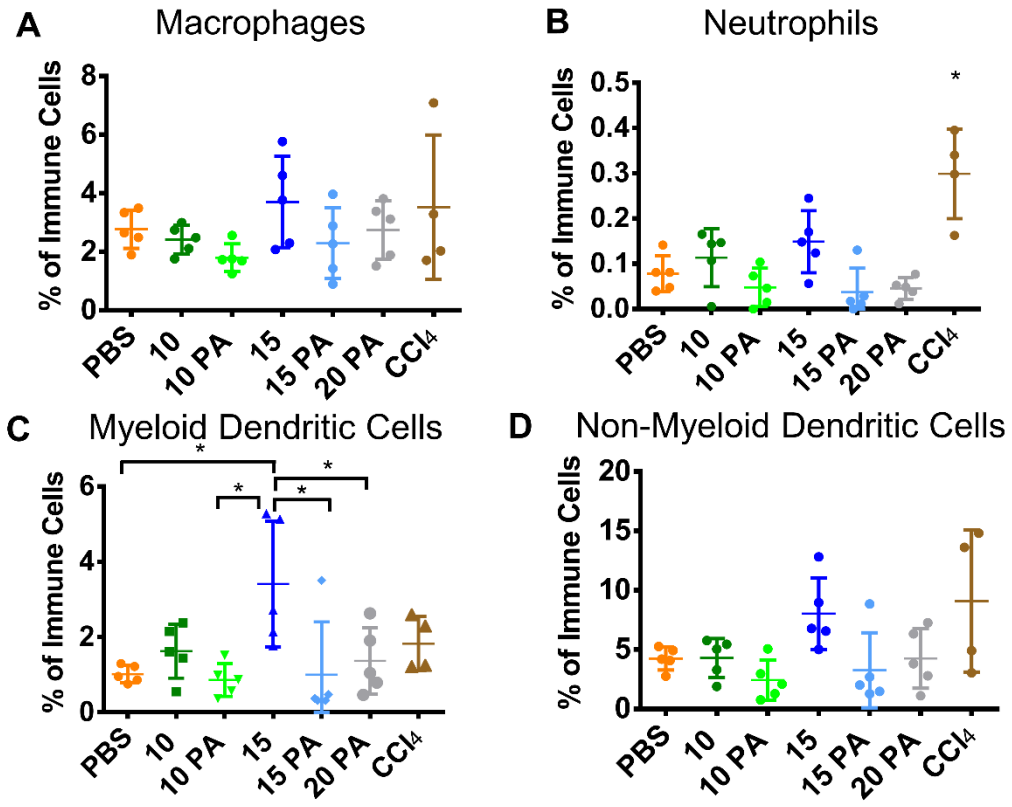

Figure 3.7 Analysis of immune cell types in treated mouse livers**.** None of the NP formulations had significantly increased macrophages or neutrophils (A-B). However, si-NPs formulated at N:P 15 had (C) significantly increased myeloid dendritic cells compared to saline-treated mice and all other NP-treated mice except in the N:P 10 group (n=5, $p<0.05$). (D) Mice treated with si-NPs at N:P 15 also had elevated non-myeloid dendritic cells, though no groups had significantly increased non-myeloid dendritic cells compared to untreated controls.

A common concern with long-term, repeated administration of PEGylated nanocarriers is the development of an immunogenic antibody response against PEG, which can diminish their efficacy as delivery vehicles and lead to clinical adverse events.[151-153] However, the immunogenicity of zwitterionic phosphocholine-nanocarriers has been less extensively measured, particularly after long-term injection courses.[139] We therefore tested the serum of mice injected six times over a month with our longest-circulating zwitterionic siPA-NPs (15 PA and 20 PA), for antibodies against phosphocholine using an ELISA-based assay.[154, 155] There

were no significant increases in ELISA signal for any of the mice sera sampled, indicating the complete absence of anti-phosphocholine in these samples (**Supplemental Figure B.S11**). Notable, positive control mouse sera containing phosphocholine antibodies did react with our polymers adsorbed to the plate, giving a positive ELISA signal. Thus, our long-circulating, dual hydrophobized siPA-NP formulations do not stimulate anti-PC immunogenicity in mice.

Taken together, our data show that zwitterated NPs are well-tolerated upon long-term, repeated administration, evidenced particularly by the normal body weight and complete blood count data. However, we have also demonstrated that the formulation N:P ratio and degree of hydrophobic core stabilization can significantly impact less pronounced markers of nanocarrier toxicology. The siPA-NPs at the highest overall polymer dose (20 PA) tested in the repeat injection studies exhibited mildly upregulated signs of hepatotoxicity based on liver enzymes, histology, and cytokines. Similarly, si-NPs at the highest polymer dose without palmitic acid-siRNA stabilization (15) also exhibited histological, cytokine, and liver dendritic cell responses. Our data indicate that a dual hydrophobization strategy can be used to improve the balance between improved pharmacokinetics and toxicologic factors, as the siPA-NP 15 PA formulation showed negligible signs of toxicity.

The polymer-induced toxicities that we observed are likely a result of destabilization and extracellular exposure of the cationic DMAEMA-containing polymer block. Although they are a driving force for siRNA delivery, cationic polymer components can be associated with aggregation of intracellular and extracellular proteins or unwanted membrane disruption.[156-160] While the positive charge density can be effectively shielded or reduced using hydrophilic NP corona-forming polymers and by copolymerization with other monomers, polyelectrolyte complexes are still prone to destabilization by serum and ionic blood or tissue components. Dual

hydrophobization strategies improve NP stabilization and therefore may ameliorate toxicity concerns.

Based on the favorable long-term toxicity data of the 15 PA siPA-NPs, and their identical pharmacokinetic area under the curves to the long-circulating, high N:P ratio NPs (20 and 20 PA), we compared this optimal formulation to the commercially available *in vivo*-jetPEI® (IVJP) in an orthotopic murine breast cancer model. At 24 hours after intravenous administration, 15 PA siPA-NPs show significantly improved tumor luciferase silencing *in vivo* compared to IVJP formulations relative to matched scrambled controls (**Figure 3.8a,3.8b**). We also performed flow cytometry analysis on extracted tumors after administration of NPs bearing fluorescently-labeled nucleic acids, and we demonstrated a significant, 2.5-fold increased mean fluorescence intensity in tumors for 15 PA siPA-NPs compared to IVJP also at 24 hours after injection (**Figure 3.8c**), indicating better uptake and retention in tumor cells. Our NP optimization process, incorporating *in vivo* charge ratio screening and dual hydrophobization, therefore enables efficient tumor cell delivery and target gene knockdown *in vivo*, outperforming the only (to our knowledge) commercially available intravenously-injectable siRNA delivery reagent.

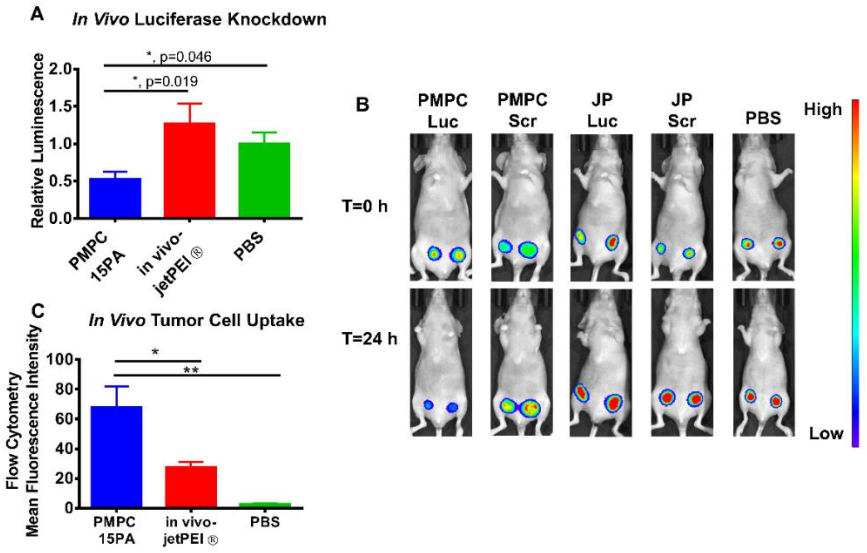

Figure 3.8 NPs formulated at 15 PA (PMPC) display significantly increased knockdown (*p<0.02) (A,B) and tumor uptake (C) *in vivo* compared to equivalent doses of In Vivo Jet-PEI® (JP) in nude mice bearing MDA-MB-231 tumors (*p<0.02, **p<0.01). (A) 1 mg/kg siPA-NPs bearing luciferase siRNA were injected in mice bearing 100 mm^3 tumors, and luminescent signals were monitored immediately before and 24 hours after injection. Luminescence at t=24 h relative to t= 0 h was compared relative to appropriate scrambled control groups. (B) Representative images of tumor luminescence from each treatment group bearing either luciferase (Luc) or scrambled (Scr) siRNA. (C) siPA-NPs bearing Cy5-labeled nucleic acids were injected intravenously in tumor-bearing mice. Tumors were collected 24 hours after intravenous injection and analyzed for uptake by flow cytometry.

3.5 Conclusion

This work comprehensively characterizes the *in vivo* impacts of charge ratio and dual carrier-cargo hydrophobization on NP pharmacokinetics and toxicology. Increasing polymer given equal siRNA doses can significantly improve circulation half-life and area under the curve. These pharmacokinetic benefits may come at a cost of increased toxicity, particularly hepatic toxicities, but these can be overcome through dual hydrophobization—using hydrophobically modified siRNAs with partially hydrophobic polymeric NP cores. Our findings indicate that testing of electrostatically-complexed NPs at different charge ratios should extend to *in vivo*

experiments, as the charge ratio may have a major impact on circulation kinetics, which is not evident *in vitro*. We've shown that dual hydrophobization significantly decreases toxicity while also increasing the circulation half-lives of NPs formulated at lower N:P ratios. Thus, dual hydrophobization allows for equivalent pharmacokinetic profiles at decreased polymer doses, reducing toxicity and increasing the potential for therapeutic efficacy.

This work also uniquely and deeply investigated the long-term impact of repeated administration of zwitterionic polyplexes, encompassing the impact of formulation parameters on their toxicology. We show that overall, zwitterionic polyplexes are well-tolerated upon repeated administration, with minimal histologic or immunologic consequences. Furthermore, optimized zwitterionic siPA-NP formulations are non-immunogenic and achieve improved tumor gene knockdown and biodistribution compared to commercial gold standards *in vivo*. Our work demonstrates that charge ratio optimization is important *in vivo* and that dual hydrophobization strategies improve delivery while overcoming the toxicologic challenges that face all electrostatically-complexed polymeric siRNA carriers.

CHAPTER IV

The Role of Platelet Activating Factor in Acute Toxicities of Intravenously Injected siRNA Nano-Polyplexes

Text for Chapter IV taken from:

Jackson MA, Patel SS, Yu F, Glass EB, Dollinger BD, Hoogenboezem EN, Bedingfield SK, Kelly IB, King AR, Miles RE, Patil P, Giorgio TD, Duvall CL. Inhibition of Platelet Activating Factor Receptor Prevents Acute Toxicities Associated with Intravenous Injection of siRNA-Polymer Nano-Complexes. *In Preparation.*

4.1 Abstract

Nanocarrier-associated toxicity is one of the most significant hurdles to clinical translation of siRNA-bearing nanomedicines. While the many toxicity mechanisms of polymer-based siRNA delivery systems have been thoroughly characterized *in vitro*, *in vivo* reactions are still poorly understood. In this work, we demonstrate that intravenous injection of non-viral siRNA-polymer nano-complexes (si-NPs) can elicit acute, shock-related toxicities similar to those observed upon adenoviral vector administration and cause a three-fold increase in plasma concentrations of Platelet Activating Factor (PAF), a potent lipid mediator of inflammation. Inhibition of the PAF receptor (PAFR) prior to si-NP administration completely prevented these acute toxicities in mice, indicating a role for PAF in non-viral nanocarrier-associated toxicities. We further demonstrate that pre-treatment with clodronate liposomes also abrogates si-NP associated toxicities, suggesting that stimulated Kupffer macrophages are the source of secreted

PAF responsible for cardiovascular effects. This toxicity mechanism was generalizable to other polymer-based siRNA carrier systems, particularly in mice bearing inflammatory tumors. These results are the first to connect PAF with the *in vivo* toxicity mechanisms of a non-viral nanomedicine and suggest PAFR inhibition may be an effective prophylactic strategy to reduce nanocarrier-associated adverse events.

4.2 Introduction

With the recent first-in-class FDA approval of Onpattro in August 2018, nanoparticle-based delivery of siRNA has entered a new era of clinical potential.[1] However, cationic carrier components continue to face toxicologic challenges that hinder their clinical development. As a testament to this fact, Alnylam, the pharmaceutical company behind the landmark RNAi approval, has abandoned Onpattro's cationic MC3 carrier lipids for future clinical development programs due to the carrier-associated immune toxicities that necessitate immunosuppressive steroid pretreatment in patients.[1, 161]

For polymeric nanoparticle-based siRNA delivery, there is a well-known positive correlation between transfection efficiency and toxicity.[127, 162] This poses a significant challenge for maximizing the therapeutic window of polyplex (polymer-siRNA complex) nanomedicines, since often the carriers most effective at gene silencing are also the most toxic. Many strategies have been employed to reduce the cytotoxicity of these carriers while maintaining their efficacy, including reducible cross-linking and increased hydrophobic stabilization of polymeric components.[11, 22, 23, 127, 162] Countless studies have also investigated the *in vitro* cytotoxicity mechanisms of common polymeric carriers such as poly(ethylene imine) (PEI).[59, 162, 163] Cationic, siRNA-condensing polymers can cause nanoscale breakages in cellular membranes and

mitochondrial membranes, disrupting cellular homeostasis, releasing reactive oxygen species (ROS), and inducing apoptosis pathways. [162, 163]

However, *in vivo* mechanisms of polyplex toxicity are less well-understood.[59] After intravenous injection, nanosized materials such as polyplexes are known to be rapidly cleared by the cells of the mononuclear phagocyte system (MPS).[11] Complement adsorption to nano-polyplex surfaces can increase MPS clearance while also inducing cardiopulmonary distress and inflammatory innate immune reactions.[162, 164] The ability of most polyplexes to trigger endosomolysis for cytoplasmic cargo delivery also increases the potential for activation of toll-like receptors and the triggering of further systemic immune responses.[162] Finally, aggregation of cationic polyplexes in the lungs is thought to induce severe clotting and asphyxiation resulting in acute, fatal toxicity in mice. [162, 165-167]

Steric shielding of polyplexes with materials such as poly(ethylene glycol) is often recommended as a panacea to these *in vitro* and *in vivo* toxicities.[162, 164, 167] Hydrophilic shielding reduces protein adsorption and can help reduce damage to plasma membranes from cationic polymer components. However, PEGylated nanomaterials can still be toxic at high doses. [11, 168] CALAA-01, a PEGylated cyclodextrin polymer-based siRNA carrier, was discontinued from clinical development in part due to infusion-related innate immune responses, including grade 3 hypersensitivity reactions.[1, 169] These and other clinically-optimized nanomedicine formulations have been reported in humans to cause poorly-understood allergic-type adverse reactions even in the absence of prior nanomaterial exposure (no IgE antibodies).[168]

We have previously developed novel siRNA-complexing polymers containing a high molecular weight zwitterionic corona composed of a homopolymer of poly(2-methacryloyloxyethyl phosphorylcholine) (PMPC) with a core block composed of a random

copolymer of poly(dimethylaminoethyl methacrylate-co-butyl methacrylate) (DB).[43] The core polymer block contains a 50:50 ratio of cationic to hydrophobic monomers, which provides optimal endosomolytic behavior while reducing cytotoxicity.[21] These PMPC-DB-based polyplexes (siNPs) were shown to have improved intravenous half-lives compared to counterparts with smaller hydrophilic coronas. They also exhibited enhanced uptake in murine breast tumors compared to their high molecular weight PEGylated comparator particles. [43]

Despite their strong hydrophilic shielding, these siNPs exhibited signs of acute toxicities in mice when delivered as formulations containing high polymer:siRNA ratios (N:P 20). While we were able to prevent these toxicities through increased hydrophobic stabilization of both polymer and siRNA components, we were puzzled by the unusual pathologies noted in the more toxic formulations.[22] Mice receiving these formulations intravenously often exhibited marked lethargy, inactivity, and prostrated body positions within the first 5-15 minutes of injection. At lower doses, these mice would recover and resume normal activity after roughly one hour. At higher doses, these mice would succumb within 1 hour of injection without signs of respiratory distress. Gross pathology indicated dark, congested livers, reddish intestines, and general signs of vasodilation.

Similar pathologies have been reported in an entirely different type of nucleic-acid carrying nanomaterial—adenoviruses.[170, 171] High doses of intravenously injected adenoviruses have been reported to induce behavior changes such as lethargy, prostration, as well as GI pathologies and shock in both mice and rats.[170, 171] These symptoms were similar to anaphylactic shock, but the animals had received no prior exposure to adenovirus antigens. Xu et al. reported that these systemic shock-related pathologies were associated with a molecule called platelet-activating factor (PAF).[170] PAF is a potent phospholipid signaling molecule that can trigger a

variety of biological responses, including vasodilation, vascular permeability, and neutrophil degranulation. [172-175] PAF is involved in many inflammatory diseases including allergic rhinitis, sepsis, asthma, and inflammatory bowel disease and is both secreted and received by numerous innate immune cells including macrophages, neutrophils, and platelets.[172, 173, 176, 177] In the case of adenovirus administration, it was found that adenovirus phagocytosis triggered Kupffer cells to secrete PAF, causing vasoactive changes in rats.[170, 178] A major percentage of the dose of intravenously administered nanoparticles is also phagocytosed and cleared by liver Kupffer cells.[11]

We therefore hypothesized that PAF could play a role in non-viral polyplex-induced *in vivo* toxicities. In this work, we explore the impact of PAF receptor inhibition on acute toxicities associated with siNP administration. We also investigate the role of Kupffer cell uptake in these effects, as well as the ability of other particle systems to induce PAF-associated toxicities. This work is the first, to our knowledge, to connect PAF to the toxicities of intravenously-injected, non-viral nanomedicines of any kind.

4.3 Materials and Methods

All materials were purchased from Sigma-Aldrich (St. Louis, MO, USA) or Fisher Scientific (Waltham, MA, USA) unless indicated otherwise. siRNAs used in these studies were purchased from Integrated DNA Technologies (Coralville, IA, USA) and consisted of a sense strand (5'-CAAUUGCACUGAUAAUGAACUCC[dT][dC]-3') and antisense strand (5'-GAGGAGUUCA[mU]U[mA]A[mU]U[mG][mU][mU]-3') [Note: m=2'O-methyl modification; d=chimeric DNA base].

Polymer Synthesis and Characterization (NMR, GPC, DLS): Polymers were made using

Reversible Addition Fragmentation Chain Transfer (RAFT) polymerization using a chain transfer agent (CTA)of 4-(ethylsulfanylthiocarbonyl)sulfanylpentanoic acid (ECT). Prior to polymerization, all monomers except 2-methacryloyloxyethyl phosphorylcholine were passed twice through activated alumina columns to remove inhibitors. PMPC-DB polymers (poly(2-methacryloyloxyethyl phosphorylcholine (PMPC))-*b*-(dimethylaminoethyl methacrylate (DMAEMA)-*co*-butyl methacrylate (BMA))) was synthesized by first creating a random copolymer of 50% DMAEMA and 50% BMA polymerized from ECT in dioxane under nitrogen (30 min purge) for 24 h at 65°C using azobisisobutyronitrile (AIBN) as an initiator (1:10 CTA:AIBN ratio). Equivalent molar amounts of DMAEMA and BMA were added to target 210 repeating units overall (anticipating ~ 70% conversion and final repeating units of 150-160). The crude reaction was precipitated in cold pentane three times to remove monomers and dried under vacuum overnight. Degree of polymerization was confirmed using ^{1}H-NMR. From this purified first block (DB-ECT), the PMPC corona block was polymerized in methanol for 24 hours at 65°C (utilized condenser since near methanol boiling point) under nitrogen (30 minute purge) with a 1:5 CTA:AIBN ratio. A degree of polymerization of 75 was targeted to achieve a 20,000 g/mol corona block. Crude reaction mixture was then dialyzed overnight in fresh methanol and then in dI water for one day. The polymer was lyophilized, and it's degree of polymerization was confirmed with ^{1}H-NMR. PMPC-BMA polymers were synthesized in a similar manner, starting from a butyl methacrylate homopolymer. The PMPC block was polymerized in pure ethanol with all other conditions the same to improve solubility of the PBMA homopolymer CTA. The 20kPEG DB polymer was synthesized and characterized as described previously.[43] All NMR spectra are featured in **Supplemental Figures C.S1-S3**. Polymers were evaluated for endotoxin using a Chromogenic LAL Endotoxin Assay Kit (GenScript, Nanjing, China).

Polyplex and Micelle Formulations: PMPC-DB and 20k PEGDB polyplexes were formulated as described previously.[43] Briefly, polymers were complexed with siRNA at a 20:1 N:P ratio (protonated nitrogens on polymer: anionic phosphates on siRNA) in 10 mM citrate buffer at pH4. Complexing proceeded for 30 minutes and was followed by addition of a 5x volume excess of 10 mM phosphate buffer at pH8 to achieve a final pH of 7.4. Buffers were created using the Sigma Buffer Reference Center website (https://www.sigmaaldrich.com/life-science/core-bioreagents/biological-buffers/learning-center/buffer-reference-center.html). Note that polymers were initially dissolved at 30 mg/mL in pure ethanol and then diluted to 3 mg/mL in the pH 4 citrate buffer. PMPC-BMA micelles were dissolved in ethanol (5% of the final volume), and added dropwise to PBS for a final concentration equivalent to the polymer concentration of PMPC-DB for delivering 1.2 mg/kg siRNA (roughly 18 mg/mL). For *in vivo* preparations, polyplexes and micelles were sterile filtered (0.45 μm filters) and were then concentrated to the appropriate volume (1.2 mg/kg dose in 100 uL injections) in Amicon spin filters (MWCO 50,000 kDa). In Vivo-Jet PEI (IVJP) (Polyplus, NY, USA) was prepared according to manufacturer instructions, at a dose of 2 mg/kg siRNA.

PAFR Inhibition Studies: Mice (BALB/c, C57BL/6) were purchased from Jackson Laboratories (Bar Harbor, ME) or Charles River Laboratories (Wilmington, MA). For survival study and PAFR inhibition studies, mice were pre-injected with either 50 μL saline or 50 μL of ABT-491 (0.05 mg/mL in PBS -/-). Ten minutes after the first injection, mice were then injected with 1.2 mg/kg si-NPs (PMPC-DB polyplexes). A separate cohort was injected with saline only. For hematology and pathology studies, mice were sacrificed 30 minutes following si-NP injection by cardiac puncture using EDTA as an anti-coagulant. Blood samples were analyzed for complete blood count (including hematocrit, hemoglobin, and red blood cell measures) by the

Vanderbilt Translational Pathology Shared Resource using a Forcyte Analyzer (Oxford Science, CT, USA). Mouse organs were removed, saving the pancreas and duodenum for further analysis and fixing other organs in 10% formalin for histologic analysis. The pancreas was weighed after removal, frozen, lyophilized, and weighed again for pancreas wet/dry weight analysis. The duodenum was washed with a saline solution containing 0.16 mg/mL heparin to remove excess blood. The tissue was then weighed and homogenized in 1 mL of saline/heparin solution. The tissue was centrifuged at 10,000x for 15 minutes at 4°C. Supernatants were removed and assayed for hemoglobin content using a Hemoglobin Colorimetric Assay Kit (Cayman Chemical No 700540) according to manufacturers' instructions. Fixed tissues were embedded in paraffin and stained with hematoxylin and eosin by the Vanderbilt Translational Pathology Shared Resource. For Evans Blue measurements, 2 minutes after si-NP (or saline) injection, mice were injected with 50 µL of a 0.5% (wt/v%) Evans Blue solution in saline that had been sterile-filtered through a 0.45 µm filter. After sacrificing mice at 30 minutes post-injection, livers were removed, weighed, and then incubated in 1 mL formamide for 24 hours at room temperature. A 50 uL aliquot of formamide for each sample was then transferred to a 96-well plate, and Evans Blue absorbance was measured at 610 nm using a plate reader (Tecan, Mannedorf, Switzerland).

Clodronate Liposome Studies: For animal studies involving clodronate pre-treatment, ½ of the mice were injected both i.v. and i.p. with 100 µL of Clodronate Liposomes (Cedarlane, Burlington, Canada) 24 hours prior to si-NP treatments. Both normal mice and clodronate-treated mice were then either injected with si-NPs or saline 24 hours later and sacrificed 30 minutes after si-NP injection. Organs and blood were collected and processed as described above.

PAF ELISA: Mouse EDTA-treated blood samples were centrifuged at 3,000xg for 10 min at 4°C and plasma was removed for ELISA analysis. Mouse PAF ELISA kits were

purchased from LifeSpan Biosciences (Seattle, WA, USA). Plasma samples were assayed in duplicate according to kit manual using 50 µL sample per well. For *in vitro* PAF release assays, mouse bone marrow-derived macrophages (BMDMs) were extracted from the femurs and tibias of healthy female FVB mice sacrificed at 4-8 weeks of age. Bone marrow was flushed out with DMEM using a 5 mL syringe and collected in DMEM on ice. The cell suspension was centrifuged at 1000xg for 5 min and the pellet was resuspended in 2 mL ACK Lysis buffer and incubated for 2 minutes. The lysis solution was then diluted in 20 mL warm DMEM (37°C) and centrifuged again at 1000xg for 5 minutes. BMDMs were then re-suspended in 10 mL of BMDM media (DMEM, 10% FBS, 1% PenStrep, 1% L-glutamine, 14% (1:1 v/v) L929 media week 1 and week 2 media (created by culturing L929 murine fibroblast cells in complete DMEM and collecting media after 7 days of incubation [week 1] and again 7 days later [week 2]). The cells were then seeded in a 96 well plate at $1x10^5$ cells per well. BMDMs were polarized to M1 by incubation with M1-inducing cytokines.[179] Briefly, 7 days after seeding (after replenishing media on day 2 and day 4), M1 BMDMs received media supplemented with 0.1 µg/mL IFN-γ and 0.1 ng/mL LPS. 24 hours later, media was removed, cells were washed, and 100 nM si-NPs were introduced to cells. Cell supernatants were sampled at 30 minutes and 24 hours post-treatment and assayed using mouse PAF ELISA kits.

PAFR Activation Studies: Ready-to-Assay Platelet Activating Factor Receptor Cells (Millipore Sigma, Burlington, MA), were thawed and seeded at 14,000 cells per well in a 384-well plate according to manufacturer instructions. Cells were then washed with HBSS (20 mM HEPES) and loaded with FLIPR Calcium 6 dye (dissolved in HBSS [20mM HEPES, 2.5 mM probenecid] and incubated for 2 hours according to FLIPR Calcium 6 kit instructions. Si-NPs were prepared at 100, 50, 25, and 12.5 nM siRNA (final in-well concentrations) in a separate

384-well plate; and ABT-491 was prepared at 125 nM in an additional plate. Fluorescence from calcium influx was assayed using the Vanderbilt High Throughput Screening Facility, on a Panoptic instrument. Five µL ABT-491 or saline were first added to the cells, incubated for 5 minutes, and then 12.5 µL of si-NP preparations, saline, or PAF positive control were added to the cells, and fluorescence was recorded once per second for 30 minutes following particle addition.

Tumor Mice: Seven-week-old female BALB/c mice were implanted with $1x10^5$ 4T1 cells per tumor (in 50:50 mixture of serum-free DMEM and Matrigel) in the mammary fatpad (2 tumors per mouse). Polyplex and micelle treatments were initiated once tumors had reached 150-300 mm^3. All tissue processing/endpoint timing occurred as stated above for the PAFR inhibition studies.

Liver Uptake: Relative uptake of 20k-PEG-DB and PMPC-DB particles bearing Cy5-labeled dsDNAs was originally investigated as part of broader biodistribution studies in tumor-bearing mice.[43] Briefly, the polyplexes were prepared as described above and injected in nude mice (Jackson Laboratories, Bar Harbor, ME, USA) bearing MDA-MB-231 tumors in the mammary fatpad. Mice were sacrificed at 2 hours after polyplex injections, and organs were analyzed for Cy5 fluorescence using an IVIS imaging system (Perkin-Elmer, Waltham, MA, USA).

Ethics Statement: All animal studies were approved by Vanderbilt's Institutional Animal Care and Use Committee. All studies were performed in accordance with the National Institute of Health's guidelines for the care and use of laboratory animals.

Statistical Methods: Unless otherwise noted, all statistical analyses involved either one-way ANOVA with multiple comparisons test (>2 groups) or a student's t-test, two-tailed (2

groups only). Data are mean with standard error.

4.4 Results and Discussion

The polymers used for this study (PMPC-DB) were synthesized as previously reported by Reversible Addition-Fragmentation Chain-Transfer polymerizations such that the corona block contained a roughly 20,000 g/mol hydrophilic, zwitterionic corona, and a core block composed of a random copolymer of 78 repeating units each of dimethyl amino ethyl methacrylate and butyl methacrylate.[43] These results were confirmed by ^{1}H-NMR and gel permeation chromatography analysis as previously reported.[43] The polymers were tested and found to be free of endotoxin contamination prior to initiation of all studies (**Supplemental Figure C.S2**). Polyplex nanoparticles (si-NPs) were prepared by complexing siRNA with polymer at a 20:1 N:P ratio (cationic amines in polymer: anionic phosphates in siRNA), yielding monodisperse nanoparticles with an average diameter close to 100 nm (**Figure 4.1a**). This si-NP formulation was previously reported to have an extended circulation half-life up to 22-26 minutes, but also more toxicities compared to si-NPs prepared at lower N:P ratios or si-NPs prepared with hydrophobically-modified siRNAs, with notable liver necroses and elevations in ALT/AST/BUN markers 24 hours after injections.[22, 43]

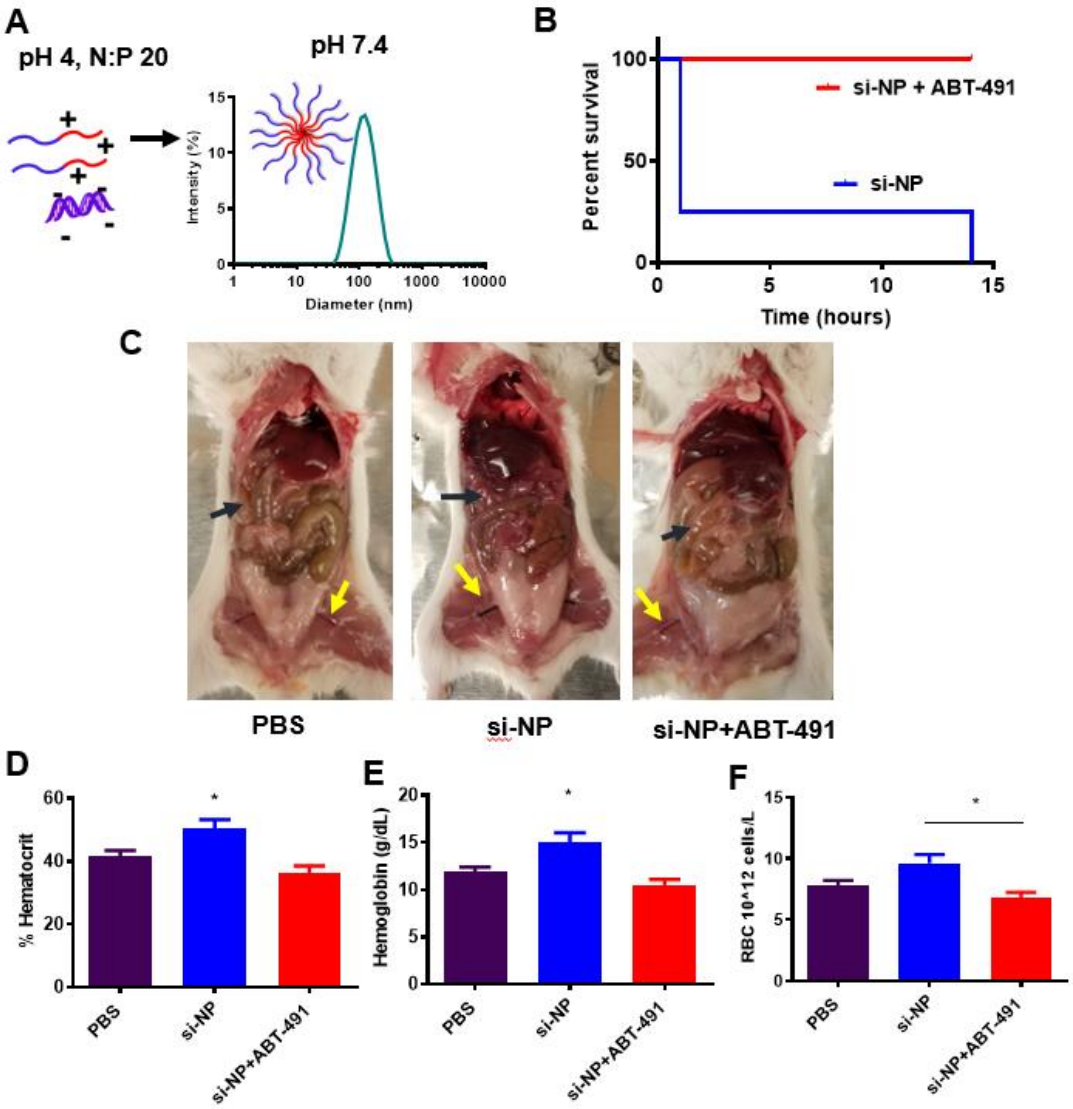

Figure 4.1 PAFR inhibitor ABT-491 rescues acute toxicities associated with high-dose si-NP injection. A) si-NPs are formulated at N:P 20 by complexing with siRNA at a reduced pH. Raising pH to 7.4 produces si-NPs of roughly 100 nm in diameter. B) Upon intravenous injection of si-NPs at high N:P ratio (high polymer dose) and 1.2 mg/kg siRNA, 4 out of 5 mice experienced fatal toxicities within 1 hour, but all deaths were prevented by pre-injection of ABT-491 10 minutes prior to si-NP injection. C) Gross pathology demonstrates obvious vasodilatory pathology in major blood vessels (yellow arrows) and reddening of intestines (black arrows) in mice treated with si-NPs, but not for those treated with saline or ABT-491. D-F) Mice injected with high-dose si-NPs experienced significant increases in blood hematocrit (D), hemoglobin (E), and red blood cell concentration (F) 30 minutes after injection, all of which were abrogated by ABT-491 pretreatment.

As described above, we had previously noted behavioral changes in mice injected with

these potent but more toxic si-NP formulations characterized by lethargy and prostration within the first hour after injection. These changes bore striking similarities to the behaviors noted in adenovirus-treated rats by Xu et al.[170] We therefore sought to interrogate whether the mechanisms of si-NP toxicity were also mediated by platelet activating factor, as described for adenovirus-treated rats.

We pre-treated BALB/c mice with either saline or ABT-491 10 minutes intravenously prior to injecting mice via tail vein with a relatively high dose (1.2 mg/kg) of siNPs. ABT-491 is a potent and highly specific small-molecule inhibitor of the platelet activating factor receptor (PAFR).[176, 180] Of five mice pre-treated with saline, four mice experienced acute, fatal toxicity within 1 hour of injection, while the fifth mouse perished several hours later (**Figure 4.1b**). Mice pre-treated with ABT-491 experienced no fatalities and no outward behavioral changes indicative of toxicities. Thirty minutes after si-NP injection, mice treated with si-NPs but no PAFR inhibitor exhibited gross pathology changes characteristic of shock and hypotension, including reddened intestines, dark, congested livers, and dilated veins (**Figure 4.1c**). Mice pre-treated with ABT-491 did not experience these changes and appeared similar to mice treated with saline only.

Mice treated with si-NPs and no PAFR inhibitor experienced significant increases in blood hematocrit percentage, hemoglobin concentration, and red blood cell concentration at 30 minutes post-injection compared to saline-treated or ABT-491-pre-treated mice (**Figure 4.1d-f**). For some mice in the si-NP treatment group, blood was so concentrated that it was notably more difficult to withdraw by cardiac puncture compared to saline-treated or inhibitor pre-treated mice. We observed hematocrit percentages of up to 60% in the si-NP treatment group, which matched the peak hematocrit levels previously observed in adenovirus-treated rats. [170]These

blood hemoconcentration symptoms were indicative of shock. Shock is known to cause increased vascular permeability, which leads to leakage of plasma fluid in tissues and resulting hemoconcentration. Hemoconcentration is also one of the hallmark side effects of administration of PAF intravenously.[181]

Increased permeability resulting from shock can lead to edema in organs, and GI tract effects including increased duodenal hemoglobin.[170] We noted increases (though not statistically significant) in the pancreas wet/dry weight ratio for siNP-treated mice compared to inhibitor-pre-treated mice (**Figure 4.2a**). We further confirmed these symptoms of tissue edema by pre-injecting mice in each treatment group with Evans Blue dye five minutes after si-NP treatment and measuring the absorbance of the dye in liver homogenates 30 minutes after si-NP treatment. Evans Blue is an albumin-binding dye that can be used to assess vascular permeability and plasma leakage into tissues. [182] Mice treated with siNPs had significantly increased Evans Blue dye absorbance per g liver tissue compared to saline-treated mice, while ABT-491 pre-treated mice did not have increased dye absorbance (**Figure 4.2b**). These results indicate that ABT-491 pre-treatment rescued mice from siNP-induced vascular permeability. siNP-treated mice also had nearly four times higher hemoglobin concentrations in their duodenums than mice in the saline-only treatment or PAFR inhibitor pre-treatment groups (**Figure 4.2c**).

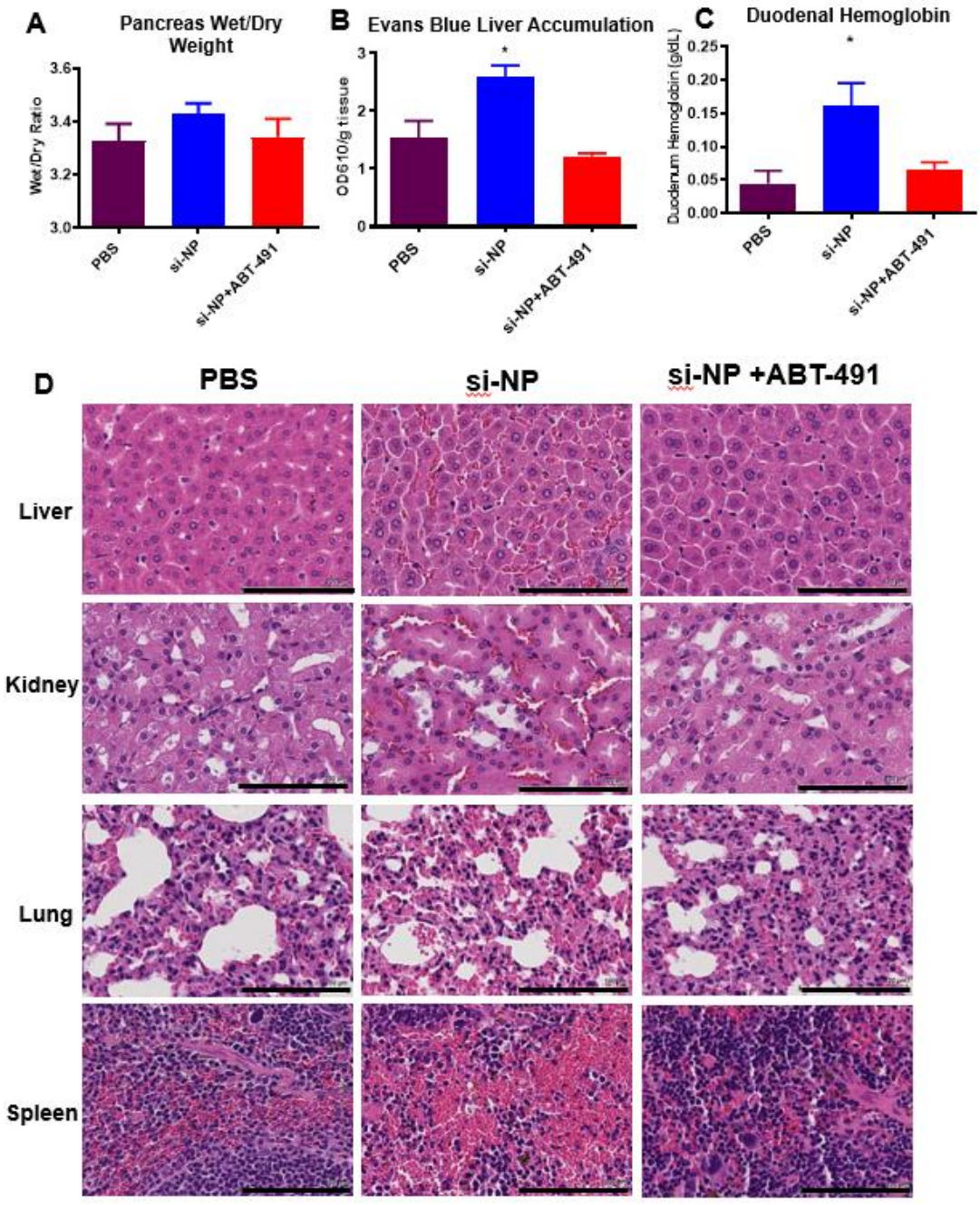

Figure 4.2 Mice injected with high-dose si-NPs exhibit signs of organ vasocongestion, vasodilation, and edema, all potential effects of vasoactive actions of PAF. A) Mice injected with si-NPs exhibit signs of tissue edema, demonstrated by a slight increase in average pancreas wet/dry ratio (B) and significant increase in duodenum hemoglobin concentration, each of which were normalized by ABT-491 pre-injection. C) Accumulation of Evan's Blue dye in the livers of mice 30 minutes after treatment with si-NPs, saline, or pre-treated with ABT-491 10 min prior to si-NP injection. D) H&E staining demonstrated increased red blood cell presence and congestion in liver, kidney, lung, and spleen tissues of mice treated with si-NPs compared to saline-treated

or ABT-491 pre-treated mice 30 minutes after si-NP injection.

Histologically, these results were confirmed by evidence of significant congestion in multiple organs of mice receiving siNPs only (**Figure 4.2d**). Notably increased amounts of red blood cells were visible by H&E staining in the liver, kidney, lungs, and spleen of these mice. Once again, mice pre-treated with ABT-491 did not experience histologic changes compared to mice receiving saline only.

Taken together, these data suggest that PAF plays a significant role in the acute toxicities caused by high-dose si-NP injection. Inhibition of PAFR completely rescued mice from polyplex-associated toxicities such that there were no phenotypical or pathological differences observed between ABT-491/si-NP-treated mice and saline-treated mice. Additionally, we have demonstrated that the acute toxicities resulting from si-NP treatment are symptomatic of shock-like conditions including vasodilation, hemoconcentration, and vascular edema. These symptoms virtually match the symptoms observed in mice and rats treated with high doses of adenovirus vectors. Just like the symptoms observed in the adenovirus case, the shock was apparent upon first exposure to siNP treatments and thus not the same as anaphylactic, IgE-mediated shock.To our knowledge, this work is the first to demonstrate PAF involvement in nonviral nanoparticle-related toxicities.

The PAF receptor is found on variety of immune cells, including neutrophils, eosinophils, macrophages, and platelets.[171, 176]. Activation of PAFR by its ligand can induce neutrophil degranulation and/or inflammatory release of vasoactive agents such as leukotrienes or nitric oxide.[183] However, the exact mechanism of PAF-induced vasodilation is variable and poorly characterized.[184] We measured blood samples for increases in the vasoactive agents including nitric oxide and histamine, but did not find significant increases in any of these mediators

(**Supplemental Figure C.S5A-B**). We did observe an increase in myeloperoxidase activity in si-NP-treated mice, indicating possible neutrophil degranulation, but the increase was not significant (**Supplemental Figure C.S5C**). We did not observe toxicity-associated changes in white blood cell counts at 30 minutes post siNP injection (**Supplemental Figure C.S6A-D**). In rabbits, PAFR activation can induce platelet aggregation or degranulation, but because rodent platelets lack the PAFR, we did not observe changes in platelet counts (**Supplemental Figure C.S6E**).

Because of the presence of PAFR on multiple types of immune cells, we hypothesized that the acute toxicities we observed upon si-NP administration might be dependent on mouse strain. Others have shown, for example, that mice strains that have Th-1 biased macrophages clear nanoparticles from circulation more slowly than Th2-biased mice, leading to starkly different pharmacokinetic and biodistribution profiles for the same nanoparticles in different mouse strains. [95] We therefore injected C57BL/6 mice with the same si-NP formulations and measured the effects of PAFR inhibition on blood hemoconcentration, pancreas edema, and duodenal hemoglobin (**Figure 4.3**). While Balb/C mice are generally more prone to Th-2 -type responses, C57/Bl6 are Th-1 biased.[95] Overall, we found that the shock-like toxicities associated with si-NP administration were consistent with data presented in **Figure 4.1** and therefore not strain-dependent. Mice treated with si-NPs experienced significantly increased hematocrit, hemoglobin, and red blood cell concentrations (**Figure 4.3a-c**), while ABT-491 pre-treatment completely abrogated these vasoactive effects. Similarly, there was significantly increased pancreas edema for siNP-treated mice and slightly increased duodenal hemoglobin for the same group (**Figure 4.3d-e**). Thus, the PAFR-mediated effects of si-NP administration are consistent across disparate mouse strains.

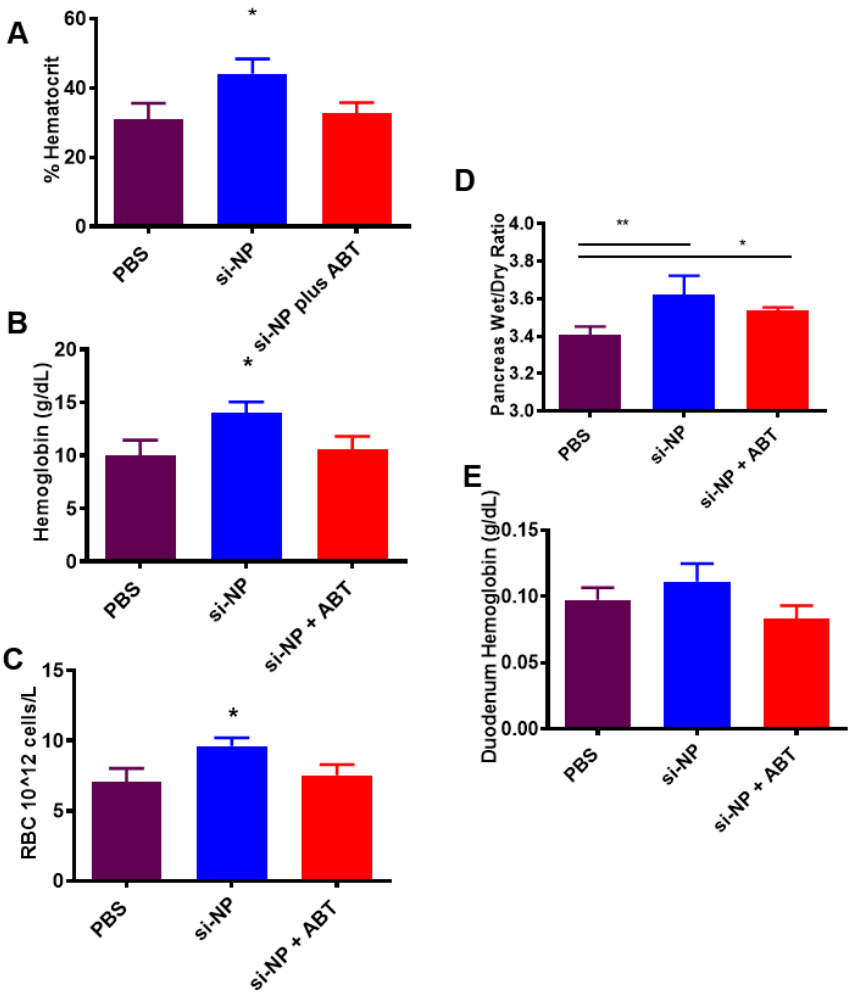

Figure 4.3 Vasodilatory and edema-related toxicities and impact of PAFR inhibition are not limited to the Balb/c strain. A-C) Injection of si-NPs in C57/Bl6 mice resulted in significant increases in hematocrit, hemoglobin, and red blood cell concentration 30 minutes after injection. These effects were abrogated by inhibition of PAFR. D-E) C57/Bl6 mice injected with si-NPs also exhibited significant increases in pancrease wet/dry ratio (D) and slight increases in duodenum hemoglobin (E), which were reduced by PAFR inhibition.

To further understand the involvement of PAFR in si-NP-induced toxicities, we measured levels of PAF in the blood of si-NP-treated mice compared to saline-treated mice. Thirty minutes post-si-NP treatment, mice experienced significant increases in blood PAF levels, in the range of 6-8 ng/mL (**Figure 4.4a**). Because of the severe hemoconcentration caused by si-NP treatment, obtaining sufficient blood for PAF ELISAs was challenging. Therefore, blood from the most

severely affected mice was not able to be sampled, so the blood concentration in PAF may have increased even higher for those mice. PAF can be lethal at doses as low as 0.36 μmol/kg, so it is reasonable that this PAF concentration would cause increased systemic toxicities.[181] This data suggests that systemic administration of si-NPs induces systemic release of PAF.

Because macrophages are one of the cell types known to release PAF, we stimulated mouse bone marrow-derived macrophages (BMDMs) with si-NPs for 24 hours and measured PAF release into cell media (**Figure 4.4b**). We found a significant increase in PAF in the media of si-NP-treated cells compared to saline-treated cells, suggesting that macrophages may be one source of PAF released *in vivo* in mice.

We also hypothesized that our si-NPs themselves might be capable of agonizing the PAF receptor. The polymer corona of these si-NPs is made up of zwitterionic, phosphorylcholine moieties, and the chemical structure of platelet activating factor itself contains a prominent phosphorylcholine. Additionally, there have been examples in nature of bacteria using PAF-mimicry to engage the PAF receptor. For example, *Streptococcus Pneumoniae* uses phosphorylcholine moieties in its cell wall to bind PAFR, block PAF signaling, and prevent inflammatory neutrophil reactions.[174, 185] Additionally, other phosphorylcholine derivatives have been shown to induce some PAF-like activities such as neutrophil activation.[186] We therefore treated Chem-1 cells overexpressing recombinant PAFR with increasing doses of si-NPs and used an intracellular calcium dye to measure fluorescence from calcium influx (indicative of receptor activation). None of the si-NP concentrations increased fluorescence area under the curves compared to saline-treated mice (**Figure 4.4c**).

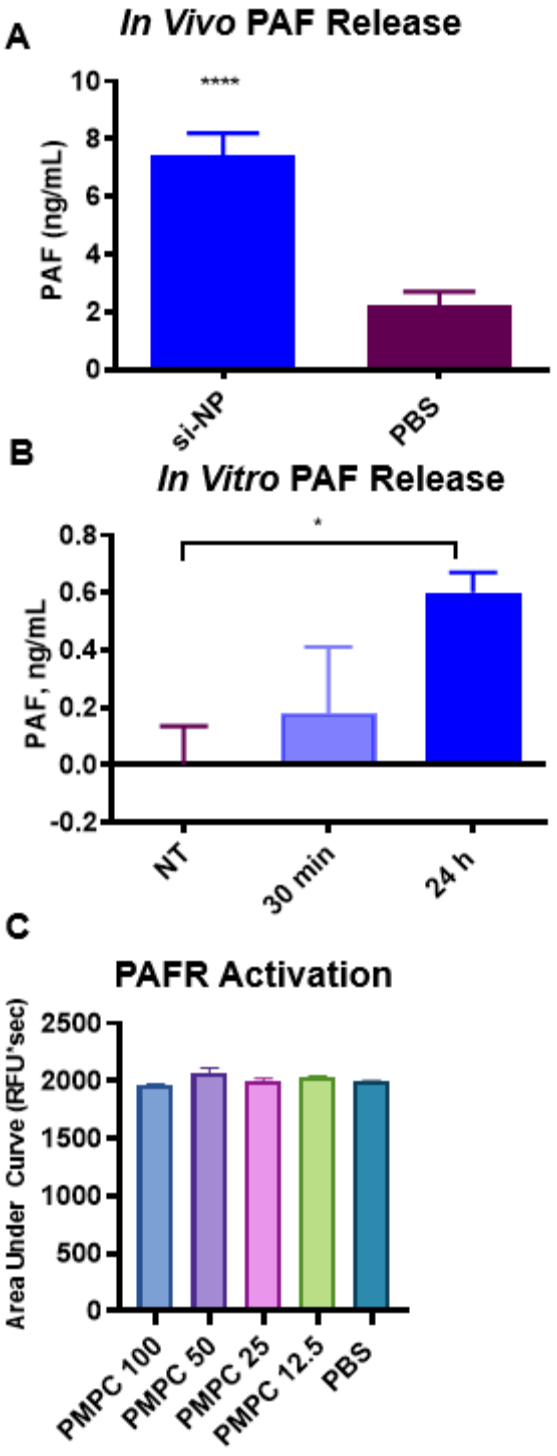

Figure 4.4 si-NPs stimulate PAF release and do not directly agonize the PAF receptor. A) Balb/c mice injected with si-NPs display increased PAF concentration in blood samples 30 minutes after injection. B) *In vitro,* mouse BMDMs stimulated with 100 nM siNPs exhibited increased PAF release into culture media after 24 hours of polyplex treatment. C) Introduction of 100, 50, 25, and 12.5 nM si-NPs to Chem-1 cells overexpressing PAFR did not cause calcium efflux,

resulting in no change in the fluorescence area under the curve compared to saline-treated cells.

These data suggest that si-NPs do not directly act on the PAF receptor but instead stimulate systemic release of PAF, which then acts on its receptor to mediate vasoactive changes leading to si-NP toxicities. Release of PAF has been shown to cause dose-dependent increases in vascular permeability and hemoconcentration.[175, 181]

PAF can also be released when cells of the mononuclear phagocyte system (MPS) are activated by phagocytosing material.[175] Nanoparticles in the 100 nm size range are well-known to be cleared from circulation by the MPS, particularly by Kupffer cells of the liver.[11] Kupffer cells reside intravascularly in liver tissue and serve as a filter for the blood. [11] In the case of adenovirus-mediated shock, Kupffer cells were found to be responsible for PAF release.[170] We hypothesized that the same cells evolutionarily primed to fight virus invaders might also respond similarly to siRNA nanoparticle engulfment.

We therefore used clodronate liposomes to selectively inhibit Kupffer cells. Clodronate liposome treatment can cause specific depletion of liver macrophages because liposomal encapsulation allows for an otherwise hydrophilic drug (clodronate) to pass through the cell membrane upon phagocytosis.[187] Clodronate liposomes are not toxic to other cell types as they do not extravasate into tissues and are only taken up by intravascular-residing phagocytic macrophages in the lung, spleen, and liver.[187]

We found that pre-treatment of mice with clodronate liposomes (Clod) prevented shock toxicities associated with intravenous si-NP injections (**Figure 4.5**). Clod-pretreated mice receiving intravenous si-NPs did not experience significant elevations in hematocrit (**Figure 4.5a**), duodenal hemoglobin (**4.5b**), or blood PAF levels (**4.5c**), with respective to Clod-treated

mice receiving saline only. These data suggest that the macrophages of the MPS are primary mediators of the PAF-related shock toxicities associated with siNP injection. The Kupffer cells of the mouse liver, upon stimulation with intravenous siNPs, release PAF into the blood, resulting in release of PAF-associated vasoactive signaling and resulting symptoms of hypotension, edema, and tissue congestion (**Figure 4.5D**).

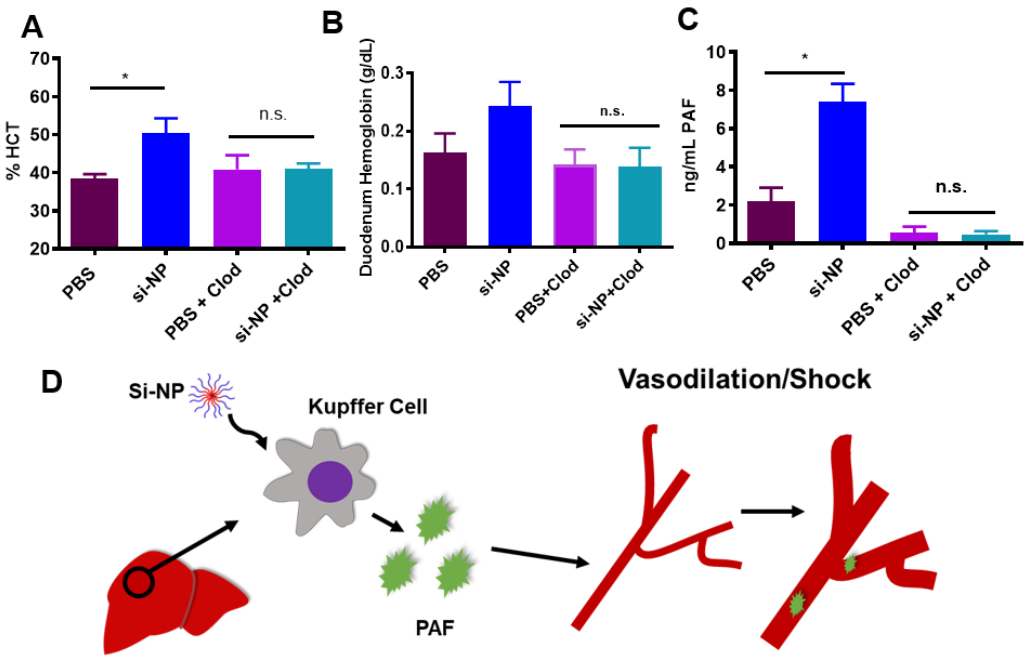

Figure 4.5 Pre-treatment with clodronate liposomes abrogates si-NP-related toxicities. A) Mice pre-treated with Clod liposomes 24 hours prior to injection do not experience significant elevations in blood hematocrit 30 mi after intravenous si-NP injection. B) Mice pre-treated with Clod liposomes do not experience significant increases in duodenal hemoglobin after intravenous si-NP injection. C) Clod pre-treatment prevents increase in blood PAF levels after si-NP injection. Note that PBS and si-NP group data are also featured in Figure 4.4a. D) Schematic of proposed mechanism for PAF-mediated effects upon si-NP injection.

Kupffer cells are a natural defense system for pathogenic, immunoreactive, nano-sized invaders, which are similar in many ways to nanoparticle drug delivery systems. [11, 178] In addition to adenovirus-triggered release, PAF has also been shown to be released from rat Kupffer cells in

response to zymosan particles, antibody-coated erythrocytes, immune complexes, and *Bordella pertussis*, so it follows that other nanomaterials could also be a trigger for PAF release.[188] Particle endocytosis may not be directly causing PAF release, however. One study found that antibody-coated erythrocytes stimulated PAF release from Kupffer cells even when phagocytosis was blocked by cytochalasin B, indicating that membrane signaling but not phagocytosis itself, may trigger PAF release.[188]

In the case of adenoviruses, Kupffer cell uptake of viral vectors was also associated with Kupffer cell death. [171]While we did not explore Kupffer cell viability in this study due to short, 30 minute post-injection evaluations, our previous work indicated elevated AST/ALT levels and histologically-evident liver damage in mice treated with multiple rounds of less stable, high-polymer dose siNP formulations.[22] Kupffer cell death may be further associated with increased PAF signaling—Kupffer cells are known to release PAF in response to CCl_4-induced inflammation.[189] It is possible that a combination of membrane signaling, phagocytosis, and Kupffer cell death may result in nanomaterial-stimulated PAF release.

As this work is the first documentation of the role of PAF in nanoparticle-related toxicities, the exact mechanisms of downstream PAF signaling are ripe for further investigations. PAF has been shown to stimulate release of leukotrienes from rat Kupffer cells, and prostaglandin E2 in neutrophils, both of which can stimulate vascular permeability and hypersensitivity reactions.[190] PAF release may also be regulated by positive feedback loops—the same macrophages with PAF receptors may also secrete PAF in response to PAFR stimulation.[191] These studies point to potential mechanisms involved in nanoparticle-related toxicities.

While our data reveals a new connection between PAF and siNP-initiated acute toxicities

in mice, we wanted to determine whether these PAF-related mechanisms were generalizable to other polymeric nanoparticles and to determine the dependency of the shock symptoms on polyplex structure. If the PAF-related symptoms were primarily initiated by Kupffer cell interactions, we hypothesized that other polymeric nanoparticles should also stimulate PAF-related symptoms. As stated previously, the siNPs used in this work were composed of a unique, phosphorylcholine-based corona surface with a pH-responsive, endosomolytic polymer core (PMPC-DB). We therefore investigated alternative polymers containing either the same endosomolytic core component with a 20 kDa poly(ethylene glycol) (PEG) corona component (20k PEG-DB), or polymers containing the same phosphocholine-based corona with a hydrophobic, non-endosomolytic core component (PMPC-BMA) (**Figure 4.6a**). We additionally included in our assessment a commercial polymeric *in vivo* transfection reagent, *In Vivo* Jet-PEI (IVJP), which contains poly(ethylene imine), though the actual structure is proprietary (**Figure 4.6a**). PEI is considered a gold standard siRNA transfection reagent and is capable of triggering endosomolysis via the proton-sponge effect with its cationic polymer components. Both 20k PEG-DB and PMPC-BMA were synthesized by RAFT polymerization to contain 20 kDa coronas and core components of roughly 20-23 kDa. These results were confirmed by ^{1}H-NMR, and a table of polymer characteristics is provided in **Supplemental Figure C.S7a**. The 20k PEG-DB polyplexes were formulated similarly to PMPC-DB at the same siRNA dose. PMPC-BMA, which had a hydrophobic core and no siRNA-complexing ability, was prepared in PBS and matched to PMPB-DB formulations/dose based on polymer mass. 20k PEG DB and PMPC BMA particles also matched PMPC DB based on particle size, with diameters of roughly 100 nm (**Supplemental Figure C.S7b**). IVJP was injected at 2 mg/kg, deliberately above the manufacturer's dose recommendations, due to our group's previous observations of toxicities

associated with this IVJP dose.[47]

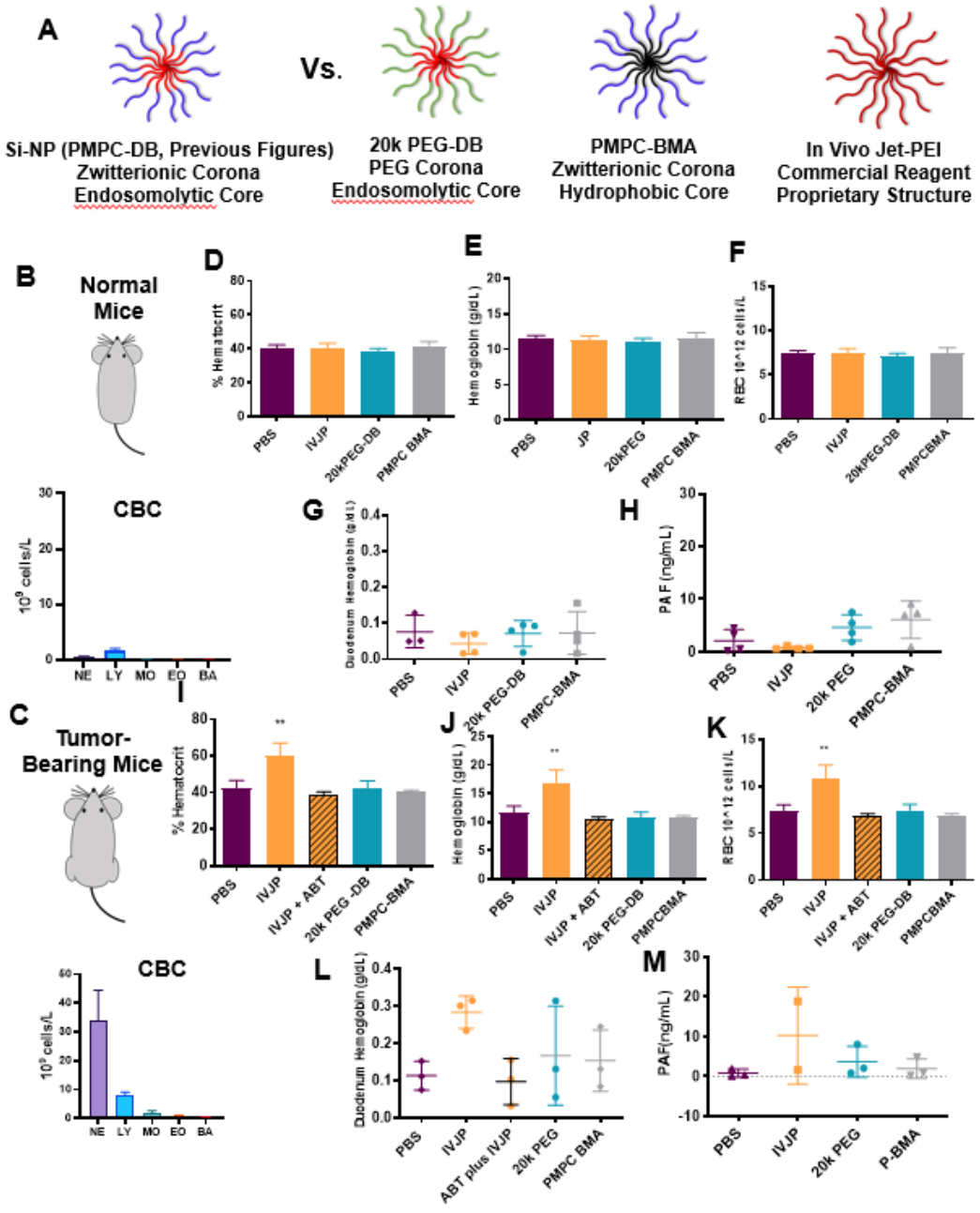

Figure 4.6 PAF-related effects are generalizable to other polyplex structures, particularly in inflammatory breast tumor models. A) si-NPs from previous figures containing an endosomolytic core and zwitterionic corona were compared to nanoparticles containing either the same endosomolytic core and a PEGylated corona, or the same zwitterionic core and a hydrophobic-only, non-endosomolytic core. Commercial transfection reagent *in vivo*-JetPEI was also investigated due to the known toxicities of cationic siRNA carriers. B-C) Nanoparticles were compared in both normal mice and 4T1 tumor-bearing mice. 4T1 tumor-bearing mice had

significantly elevated levels of white blood cells, particularly neutrophils. D-G) In normal mice, alternative nanoparticles did not exhibit significant changes in hematocrit, hemoglobin, red blood cell concentration, or duodenum hemoglobin concentration. H) In some normal Balb/C mice, slight increases in blood PAF concentration were detected relative to saline-treated mice. I-K) In tumor-bearing mice, *In Vivo*-Jet PEI injection stimulated significant increases in hematocrit, hemoglobin, and red blood cell concentration compared to saline-treated mice, effects which were abrogated by pre-treatment with ABT-491. L) Mice treated with *In Vivo*-Jet PEI had significantly elevated duodenum hemoglobin, but not those pre-treated with ABT-491. Individual mice in groups treated with 20k PEG DB and PMPC-BMA nanoparticles also exhibited elevated duodenum hemoglobin and M) elevated PAF blood concentrations.

We investigated PAF-related symptoms in both normal, non-tumor-bearing BALB/c mice and in BALB/c mice bearing 4T1 mammary tumors (**Figure 4.6b-c**). Relative to normal mice, 4T1-tumor bearing mice have significantly elevated white blood cell counts, particularly for circulating neutrophils, leukocytes, monocytes, and eosinophils, all of which have PAF receptors. We had previously observed enhanced toxicities from si-NP injection in 4T1 tumor-bearing mice and therefore hypothesized that the abundance of inflammatory cells in tumor-bearing mice may prime them to increased PAF-related toxicities.

In normal BALB/c mice, none of the alternative polymeric nanoparticles caused changes in hematocrit, hemoglobin, or red blood cell concentration (**Figure 4.6d-f**). Similarly, there were no changes in duodenum hemoglobin concentration or organ congestion (**Figure 4.6g, Supplemental Figure C.S8**) and no statistically significant increases in blood PAF levels relative to saline-treated mice (**Figure 4.6h**). However, one mouse in the 20k PEG DB group and three mice in the PMPC-BMA group did experience PAF levels around 7-9 ng/mL in the blood, which matches levels observed in PMPC-DB (siNP)-treated mice. These data suggest that other polyplexes may be capable of initiating PAF release into the blood, but not to the extent required for significant blood concentration and shock. These data also suggest that the combination of a phosphorylcholine-based corona and an endosomolytic core may somehow increase PAF-

mediated shock, since the endosomolytic core (20k PEG DB) and phosphorylcholine corona (PMPC-BMA) individually did not induce the same level of symptoms in mice as both elements together.

In 4T1 tumor-bearing mice, on the other hand, treatment with high doses of commercial transfection reagent IVJP resulted in significant increases in blood hematocrit, hemoglobin, and red blood cell concentration (**Figure 4.6i-k**), indicating shock in these mice. Pre-treatment with ABT-491 completely abrogated these blood changes in IVJP-treated mice, indicating involvement of the PAFR in IVJP-related toxicity. We also noted similar behavioral changes in the mice treated with IVJP compared to mice treated with PMPC-DB (si-NPs), including lethargy, inactivity, and prostrated body positioning. Mice treated with IVJP also had significantly increased duodenum hemoglobin concentration, which was prevented by ABT-491 pre-treatment (**Figure 4.6l**). There were slightly increased signs of blood congestion in the livers and kidneys of IVJP-treated mice, but not tumors (**Supplemental Figure C.S9**). Finally, for the IVJP-treated mice, sufficient blood for PAF ELISAs was difficult to procure due to blood concentration and was therefore only assessed for 2 mice. However, in one of the IVJP-treated mice, blood PAF levels were increased up to 18 ng/mL, higher than any measured values for PMPC-DB (siNP)-treated mice (**Figure 4.6m**). Notably, one tumor-bearing mouse in each of the 20k PEG-DB and PMPC-BMA groups experienced elevations in both duodenal hemoglobin and PAF blood levels, suggesting that these mice may also have experienced PAF-mediated responses to nanoparticle-Kupffer cell interactions.

Our data indicate that the role PAF plays in nanoparticle-mediated toxicity is generalizable to other types of polymeric nanoparticles, particularly in mice bearing inflammatory tumors. Tumor-bearing mice that were injected intravenously with IVJP exhibited

strong evidence of PAF-related shock symptoms, and these symptoms were completely prevented by pre-treatment with ABT-491. Additional tumor-bearing mice in the PMPC-BMA and 20k PEG DB groups exhibited symptoms of increased duodenal hemoglobin and had elevated PAF blood levels. Although non tumor bearing mice did not significantly react to nanoparticle treatments, there was some evidence of slight PAF blood concentration increases for mice in the 20k PEG DB and PMPC-BMA group.

The reasons for the increased sensitivity of non-tumor-bearing mice to PMPC-DB particles compared to PEGylated or non-endosomolytic counterparts are unclear. We have previously shown that PMPC-DB particles exhibit much higher tumor uptake compared to PEGylated particles with equivalent pharmacokinetics.[43] When these same particles were loaded with fluorescent DNA, the livers of mice receiving PMPC-DB exhibited significantly higher fluorescence than the livers of mice receiving 20k PEG DB (**Supplemental Figure C.S10**). This increased Kupffer cell-mediated uptake may be the cause of the increased PAF-related toxicities observed after PMPC-DB siNP injection in this study. The increased uptake is thought to be a result of differences in the physicochemical properties and molecular structures between PEG and PMPC. While both are hydrophilic surface coronas, water tends to organize in cage-like structures around PEG, but maintains its normal molecular organization around PMPC.[44] Additionally, the presence of phosphorylcholine moieties in PMPC may increase interactions with cell membranes, which contain phospholipids with phosphocholine moieties themselves and the liver is known to actively engage in choline recycling.[192]

However, non-endosomolytic PMPC-BMA particles also did not activate PAF-related toxicities to the extent of PMPC-DB particle despite the presence of the zwitterionic PMPC corona. This could indicate that pH-responsive, endosomolytic capabilities of nanoparticles can

increase the Kupffer cell PAF response. Others have shown that the innate immune-stimulatory effects of adenovirus administration in mice were prevented by impairing the viral vectors' ability to achieve endosomal escape. [193] Endosomal or lysosomal rupture caused by nanoparticles can result in mitochondrial disruption and activation of inflammatory pathways such as the NLPR3 inflammasome.[11, 194] Any of these inflammatory effects may further provoke PAF-related cardiovascular changes in mice.

While no studies have yet connected nanoparticle toxicities to PAF, there have been multiple reports of nanocarriers inducing toxicities that may hint at PAF involvement. For example, multiple studies have reported rapid fatalities within the first hour of injection of PEI polyplexes, although this lethality is often blamed on pulmonary clotting due to cationic polymer components. [166, 167] However, other in-depth studies of *in vivo* PEI-mediated toxicities have shown evidence of liver necrosis, shock, and smaller aggregates of CD11b+ cells and platelets, without major lung obstruction.[165] Cationic additives like cetyl trimethyl ammonium bromide and soyaethyl morpholinium ethosulfate in nanoparticle systems have been shown to provoke neutrophil inflammatory responses *in vitro*.[163] Other types of non-cationic nanocarriers have also been shown to induce poorly-understood cardiovascular changes in mice, including carbon nanotubes, acrylic polymers, and mesoporous silicon.[195, 196] Our work suggests that the role of PAF in the response to intravenous nanocarriers should be further explored for other types of nanomaterials.

One mechanism of intravenous nanoparticle-related toxicity we have yet to discuss is complement activation-related pseudoallergy(CARPA), which can induce cardiovascular changes and leukopenia, particularly in pigs, which have large amounts of pulmonary intravascular macrophages (PIMs).[125] While we did not specifically explore CARPA for the si-

NPs in this study, we have previously shown that our si-NPs do not adsorb complement proteins.[43] The si-NPs in this study notably also did not cause changes in white blood cell counts (**Supplemental Figure 4.S6**), indicating that PAF-related toxicities may be independent of CARPA phenomena. The role of complement in nanoparticle-mediated hypersensitivities has recently been called into question, as non-adsorptive PEGylated polymers and liposomes can still induce the release of inflammatory thromboxanes and leuokotrienes from PIMs in pigs.[168] While humans, like rodents, have Kupffer cells instead of PIMs, there have also been many similarities between liposome-induced hypersensitivity reactions in both humans and pigs. Like the reactions explored in our work, these hypersensitivity reactions bear some resemblance to anaphylactic shock, but with no prior exposure to injected agents.[168] Our results suggest that involvement of PAF, the PAF receptor, and Kupffer macrophages should be investigated further in hypersensitivity reactions to these nanomedicines.

The increased PAF-related sensitivity of tumor-bearing mice to IVJP is likely a result of the expansion of PAFR-bearing cells in these mice. 4T1 tumors are particularly malignant and can stimulate expansion of CD11b+ cell populations.[197] These tumors are also known to sensitize mice to anaphylactoid-type reactions in response to adenovirus treatment.[197] This increased sensitivity may also carry over to human cancer patients. In human cancer patients, there are often elevated platelet counts and an increased risk of clotting due to the secretion of pro-clotting factors by tumor macrophages.[198] Unlike rodent platelets, human platelets do possess PAFR and this hyper-coagulative state in human cancer patients could therefore increase nanoparticle and PAF-mediated toxic effects. Indeed, adverse events reported in the Phase 1a/1b clinical trial for cancer patients receiving cyclodextrin-based siRNA carrier CALAA-01 included hypersensitivity and GI effects such as ischemic colitis and diarrhea.[37] There are additional

reports of hypotension-related adverse effects in cancer patients injected with adenovirus vectors.[170] Additionally, the impact of PAF and vasodilation-related nanocarrier toxicities on cancer cell intravasation/extravasation may be an important future topic of study, as the other metal-based nanoparticles have already been shown to promote breast cancer metastasis *in vivo* by disrupting cadherin interactions.[199] The inflammatory, vasoactive responses induced by PAF could pose another means by which nanoparticles might promote cancer metastasis.

Our results suggest that inhibition of PAFR may help prevent intravenous nanomedicine-associated toxicities. Prophylactic treatment protocols are already the norm in the clinical translation of nanomedicine---Onpattro, the only FDA-approved siRNA nanomedicine, requires pre-treatment of patients with corticosteroids to dampen immune activation.[1] While no PAFR antagonists have yet been clinically approved in the U.S. rupatadine is a combination anti-histamine and PAFR inhibitor approved for use in other countries.[170, 173] Our results suggest that PAFR inhibitors such as ABT-491 or rupatadine may find new clinical benefit in the field of nanomedicine.

4.5 Conclusion

Overall, this work provides compelling evidence for the role of PAF in siRNA nanopolyplex-induced toxicity. To our knowledge, PAF has never been connected to synthetic, non-viral nanocarrier toxicities associated with intravenous injection. We have shown that PAF release is dependent on nanocarrier interaction with Kupffer cells and that the presence of malignant tumors can predispose mice to PAF-mediated toxicities. We have also shown that PAF-related toxicities are generalizable to other types of polymeric nanocarriers, indicating that this may be an unrealized or under-studied toxicity mechanism for other types of particles.

Inhibition of PAFR prior to nano-polyplex administration can completely prevent acute shock-associated toxicities in mice, suggesting a potential novel strategy for clinical management of adverse events related to siRNA nanomedicines.

CHAPTER V

Conclusion

5.1 Chapter Summaries and Impact

In the first aim of this dissertation (Chapter II), we hypothesized that alternative hydrophilic coronas to conventional 5 kDa PEG could significantly improve polyplex pharmacokinetics, tumor uptake, and tumor bioactivity. Electrostatically-complexed polymer-siRNA complexes face general delivery challenges related to poor intravenous stability and reduced tumor uptake. Polyplexes are frequently destabilized by serum proteins or by anionic proteoglycans.[25] Circulation half-lives of polyplexes are further shortened due to clearance by the mononuclear phagocyte system (MPS), which can be assisted by general protein adsorption or complement activation.[200] Hydrophilic surface coatings like PEG can also decrease tumor uptake due to reduced interactions with cell membranes.[19, 75]

In this chapter, we present non-fouling, zwitterionic, phosphorylcholine-based coronas as a viable alternative to PEGylation. This work is the first comprehensive benchmark of zwitterated, PMPC-based polyplexes against PEGylated polyplexes for *in vivo* pharmacokinetics and tumor bioactivity. We demonstrated that both high molecular weight PMPC and high molecular weight PEG coronas could impart circulation half-lives five times as long as conventional 5000 Da PEG coronas. In mice containing human triple negative breast tumors, PMPC-corona polyplexes achieved greater than 75% luciferase knock down sustained for over a week with only one intravenous injection. The PMPC-based polyplexes out-performed both high and low molecular weight PEG polyplexes in terms of both tumor knockdown and tumor cell uptake. Our data demonstrate that PMPC coronas can be used to both extend circulation half-

lives and overcome the "PEG dilemma" of reduced tumor cell uptake. This work is the first to demonstrate the advantages of PMPC polyplex coronas over PEG polyplex coronas of equal molecular weight. These polyplexes take advantage of the EPR effect in tumors for improved tumor biodistribution, since they lack active targeting. While the EPR effect has been shown to be heterogenous across cancer types, studies have demonstrated its existence in humans.[29, 34] The heterogeneity of the EPR effect across patients highlights the need for improved polyplex circulation time and enhanced cell uptake properties, because polyplexes that circulate longer are more likely to accumulate at the site of a tumor. Our work presents PMPC, a component of other FDA-approved biomaterials, as a promising alternative to PEGylation for cancer nanomedicines.

The second central hypothesis of this work was that polyplex circulation and toxicity could be optimally balanced by adjusting polymer: siRNA ratios and by "dual hydrophobization" of both siRNA and polymer components. Our work on the previous hypothesis yielded polyplexes with undesirable toxicities which we associated with the high N:P ratios utilized throughout. We hypothesized that the relatively high doses of polymer containing cationic components in siRNA polyplex (si-NP) formulations contributed significantly to their toxic effects in mice and therefore sought to find less toxic formulation alternatives that preserved si-NP activity. Problems associated with toxicity and pharmacokinetics are not unique to our polyplex systems. Cationic formulation components are known to cause membrane damage, serum aggregation, and acute, inflammatory *in vivo* toxicities.[42, 123] Indeed, CALAA-01, one of the few polymeric siRNA nanocarriers to undergo clinical testing, circulated intravenously for less than 30 minutes and was terminated from clinical development due to significant toxicity hurdles.[37] While most efforts to improve these aspects of polyplex performance have traditionally relied on the testing of large alternative polymer libraries, we have focused on the

large impact of small changes to existing components of polyplex formulations.[129-131]

This work built on a foundation of previous work demonstrating that conjugation of hydrophobic palmitic acid moieties to siRNA and inclusion of hydrophobized siRNAs in already hydrophobic polyplex cores (dual hydrophobization) could significantly improve the circulation time and tumor gene knockdown of polyplex systems.[47] Our work, however, is the first to study the impact of "dual hydrophobization" on the toxicity of siRNA nanocarriers in the context of varied N:P ratios. We demonstrated that for electrostatically and hydrophobically complexed si-NPs, increasing N:P ratio from 10 to 20 significantly increases si-NP circulation half-life, despite these formulations having equivalent size, charge, and encapsulation efficiencies. We have also demonstrated that addition of a "dual hydrophobization" approach significantly enhances the pharmacokinetic area under the curve (AUC), particularly for polyplexes at lower N:P ratios of 10 or 15. These data indicated that "dual hydrophobization" allows si-NPs at N:P 15 with palmitic acid-siRNAs to achieve the same AUCs as si-NPs at N:P 20, while reducing the total amount of polymer in the formulation. This polymer reduction also manifested as a reduction in hepatic toxicities. This work is also the first to demonstrate long-term toxicity impacts of repeated administration of zwitterionic, phosphorylcholine corona-containing si-NPs. Dual hydrophobized si-NPs at an N:P of 15 were well-tolerated over the course of six intravenous administrations in one month. These optimized formulations had two-fold higher tumor uptake in MDA-MB-231 xenografts than *In Vivo*-JetPEI® carriers, a commercially available polymeric siRNA delivery system. This chapter was a thorough analysis of the impact of formulation parameters on nanocarrier pharmacokinetics and toxicity and further developed dual hydrophobization as a strategy for future polyplex systems to limit toxic polymer side effects.

The third major part of this work (Chapter IV) further investigated the mechanisms of

toxicity caused by si-NPs at high N:P ratios. While the work featured in Chapter III highlighted methods for overcoming si-NP toxicity based on dual hydrophobization, the luciferase gene knockdown achieved in this work was much lower than that of the more toxic formulations utilized in Chapter II. Therefore, in the hopes of further improving the overall therapeutic window of si-NPs, we sought to further understand the mechanism of si-NP induced toxicities. Based on observed symptomatic similarities between mice treated with high dose si-NPs and mice treated with high dose adenoviruses, we hypothesized that platelet activating factor (PAF) plays a mechanistic role in si-NP toxicity. PAF has been shown to be released by Kupffer macrophages in response to systemic adenovirus vector injection and is a potent lipid mediator of vasodilation and shock response in both rodents and mice.

The work described in Chapter IV is the first to connect PAF to the toxicity mechanisms of non-viral nanomedicines of any kind. We have extensively characterized the rapid, acute toxicities present upon high-dose si-NP injection, including vasodilation, hemoconcentration, edema, and organ congestion. We have shown that inhibition of the PAF receptor (PAFR) with ABT-491 completely prevented nanocarrier-associated toxicities. We have additionally demonstrated that PAF is secreted into systemic circulation by Kupffer macrophages upon stimulation by si-NPs, and that the si-NPs do not activate PAFR directly. We have shown that this phenomenon is generalizable in inflammatory tumor-bearing mice to other nanocarrier materials, such as commercially available *in vivo*-JetPEI.

This work has broad implications for the field of nanomedicine. We have highlighted and characterized a novel mechanism of si-NP toxicity, providing a foundation for future nanocarrier designs to reduce this toxicity. We have also demonstrated that prophylactic treatment with a PAFR inhibitor can prevent si-NP -associated toxicities. As prophylactic steroid treatments are

already in use for clinically-approved siRNA nanomedicines, our work outlines a potential clinical strategy for increasing the therapeutic window of siRNA nanocarriers.[161]

5.2 Shortcomings

Overall, this work has developed a novel polyplex surface corona and a more stable and safe formulation of this polyplex, while also characterizing the mechanisms of polyplex-induced toxicities. While it is a significant addition to the field of polyplex-based drug delivery, the work also contains several shortcomings that merit discussion.

First, the polymers themselves utilized in this study possess a number of characteristics that would impede their clinical translation. Although RAFT polymerization is highly regarded as a controlled polymerization technique that yields monodisperse polymer populations, we and others have experienced significant batch-to-batch variability among polymer preparations.[201, 202] Industrial production of polymers would have to significantly control for this variability to obtain reproducible polyplex nanocarriers. To overcome this challenge, we have extensively and carefully characterized our polymer preparations by ^{1}H-NMR and gel permeation chromatography (GPC). However, for the polymers containing PMPC blocks, we were unable to characterize corona molecular weight with our GPC system due to insolubility of these polymers in the dimethyl formamide (DMF) mobile phase. Thus, for more thorough molecular weight characterization of PMPC-containing polymers, we would have to use a system containing an even more hydrophilic mobile phase and adequate, controlled standards.

Additionally, all the polymers used in these studies are not biodegradable. The long-term effects of accumulation of non-biodegradable polymers in cells and tissues is poorly understood.[203] Future work could also incorporate biodegradable moieties in the polymer

backbone to improve their tolerability and long-term safety in living organisms. Future studies could incorporate fluorescent rhodamine acrylate monomers to further understand the long-term fate of polymers in the body. Another significant limitation of this work that would benefit from fluorescent polymer labeling, is that all biodistribution studies were completed using Cy5-labeled DNAs. Thus, all biodistribution and tumor uptake studies have tracked nucleic acid cargo, but not polymer carrier. Future work should also track polymer components. Additionally, because Cy5 is a relatively bulky, hydrophobic fluorophore, it may significantly alter polyplex stability and uptake, particularly *in vitro*. Future studies should identify fluorophore alternatives that are less likely to exert hydrophobic forces on the polyplex preparations.

The polyplex formulations used in this study also have batch-to-batch variability and can range in average size, varying by as much as 50-100 nm between batches. We have overcome this problem by thoroughly characterizing each polyplex batch using dynamic light scattering prior to use. However, this may be prevented in the future by use of microfluidic mixing systems, such as the NanoAssemblr, to ensure more uniformity of mixing and assembly of polyplex components.[204] Additionally, the polyplexes used in these studies must be made fresh for each experiment and are not yet conducive to long-term storage. This shortcoming may be overcome in the future by extensive lyophilization studies to identify appropriate excipients that will preserve polyplex size, charge, and encapsulation efficiency upon long-term storage and re-constitution in diluent.[205]

While the overall average size of the polyplex formulations used in these studies was consistently around 100 nm, ideal tumor accumulation and uptake by the EPR effect may require development of slightly smaller formulations closer to the 50-70 nm range.[206] Smaller polyplex formulations are more amenable to extravasation in the leaky tumor endothelium, while particles

greater than ~40 nm are too large to be filtered through the kidneys. This shortcoming may also be solved by future usage of a microfluidic NanoAssemblr system, which has been shown to improving packaging of siRNA in particles and may also reduce overall particle size.[204]

A final notable shortcoming with this work is associated with the conjugation of palmitic acid to siRNA. While we have demonstrated that hydrophobized siRNAs significantly enhance polyplex formulations, the preparation of these siRNAs comes at a high expense with significant loss of siRNA in the purification steps. Because efficient conjugation requires high molar amounts of palmitic acid-NHS, there remains significant un-reacted palmitic acid left in the crude reaction mixture. This palmitic acid can be effectively removed through multiple rounds of filtration and column purification, but each purification step results in a significant loss of the final product, giving total yields of around 50%. Future work must optimize the purification steps to reduce the high cost of production of palmitic acid-siRNA conjugates. This may be achievable through the use of modified bases in custom oligonucleotide synthesis reactions.

5.3 Future Work and Potential Applications

Future work associated with the research described in this work will further optimize si-NPs for intravenous tumor delivery through a variety of strategies, including core-crosslinking (covalent or hydrophobic), alternative zwitterionic corona chemistries, strategies for Kupffer cell avoidance, and albumin-binding coronas. Additional work may improve the EPR effect through the use of focused ultrasound on the tumor microvasculature. Further work is needed to understand the impact of PAFR inhibition on gene knockdown efficacy of si-NPs, with potential for significantly increasing the maximum tolerated intravenous dose. Finally, future studies will apply si-NPs for *in vivo* knockdown of Rictor in mouse models of Triple Negative Breast

Cancer, with the goal of better understanding the therapeutic potential of selective mTORC2 silencing.

Because our polyplex drug delivery systems are formed by non-covalent, electrostatic and hydrophobic complexing between polymer and siRNA, they remain on the lower end of the spectrum for nanoparticle circulation times.[207] While we were able to extend si-NP half-lives to 25-30 minutes, many common micellar systems or solid nanoparticle systems circulate with half-lives on the order of hours or days. One potential solution to this problem that is the subject of ongoing work is to develop cross-linking strategies in the polyplex core that will provide greater circulation stability. A range of options exist toward this strategy including thermo-responsive poly (N-isopropylacrylamide) [pNIPAAm], cyclodextrin-based guest-host chemistry, and the use of reducible crosslinking by addition of pyridyl disulfide monomers to the polyplex core.[208-210] An additional strategy that we have explored as part of ongoing work is the use of a third, 100% hydrophobic polymer block such as poly(propylene sulfide) to further increase the core stability through stronger hydrophobic interactions. The use of these strategies may also improve the silencing efficiency of polyplexes and thereby allow for a reduction in the amount of cationic monomer needed for gene knockdown. The reduction in the cationic components would also potentially further improve polyplex toxicity. The pyridyl disulfide strategy was recently incorporated in polymersome systems with similar polymer components to those of the si-NPs used for this study, resulting in nanocarriers that could be repeatedly delivered with minimal toxicity.[210]

A second strategy for further optimization of si-NPs may be to incorporate alternative types of zwitterionic surface chemistries—namely sulfobetaines and carboxybetaines. Sulfobetaines pose challenges related to their limited solubility in solvents other than water.

Sulfobetaines have been incorporated as steric shielding for solid silica nanoparticles, as well as in DMAEMA-based polyplexes.[211, 212] Carboxybetaines have found wider applications in the realm of nucleic acid delivery.[77, 213, 214] These polymeric materials could be investigated as alternative coronas for reduced activation of PAF-related toxicity mechanisms. While we have hypothesized in this work that the PAF-releasing effects are associated with increased Kupffer cell uptake of PMPC-corona polyplexes, alternative zwitterionic coronas may have lower affinities to Kupffer cells and therefore be less inflammatory.

Another strategy for reducing polyplex association with Kupffer cells is to incorporate a "don't eat me" signal such as CD47, which has been proven to reduce phagocytosis of nanomaterials.[215, 216] *In vivo*, CD47 "self" peptide significantly reduced clearance of nanoparticles and improved both their circulation half-lives and delivery to tumors.[216] These "self" peptides bind phagocytes and inhibit particle clearance. Based on our data presented in Chapter IV, incorporation of CD47 or other phagocytosis-reducing agents may significantly reduce si-NP-associated toxicities and increase the amount of polyplexes that can be safely injected. Incorporation of other types of peptides to the polyplex corona, such as albumin-binding peptides, may also significantly enhance the circulation half-life of polyplexes.

Another strategy we have begun to explore for improving polyplex tumor uptake is the use of focused ultrasound to enhance vascular leakiness. Focused ultrasound (FUS) has already been used to improve drug delivery across the blood brain barrier.[217] However, the use of FUS for solid tumors outside of the brain remains under-studied. Given the heterogeneity of the EPR effect, clinically translatable strategies to improve nanomedicine accumulation at the site of a tumor are needed.

The work on toxicity mechanisms outlined in Chapter IV also suggests that an important

subject for future work is the impact of PAFR inhibition on si-NP efficacy. In other words, does use of ABT-491 as a prophylactic treatment for si-NP toxicity impact the si-NP silencing efficiency in tumors? Additional studies could explore whether pre-treatment with ABT-491 allows for significant increases in the si-NP dose of administration. Significantly increasing the si-NP dose could enhance tumor gene silencing beyond currently achievable levels.

The development of safe, efficacious si-NPs is a work in progress. However, this work has demonstrated that usage of "dual hydrophobization" strategies at lower N:P ratios or pre-treatment of mice with a PAFR inhibitor could significantly improve si-NP tolerability. Additionally, it is worth noting that si-NPs containing 20 kDa PEG coronas did not significantly cause release of PAF and still achieved significantly improved tumor uptake and gene knockdown compared to 5 kDa PEG coronas. Thus, the use of 20 kDa PEG-containing polyplexes as a less toxic alternative to PMPC-corona polyplexes is worth further exploration.

The development of improved siRNA nanocarriers is critical for interrogation of the therapeutic impact of inhibiting specific molecular targets. One such target, as mentioned in Chapter I, is Rictor, a subunit of mTORC 2. While small molecule inhibitors of mTORC1 (rapalogs), and mTORC1/2 (dual kinase inhibitors), currently exist, there are no small molecule inhibitors specific for mTORC2. Thus, the impact of specific mTORC2 inhibition in TNBC is unknown. Dual inhibition of mTORC1/2 has shown more clinical promise than mTORC1 singular inhibition, which failed to improve clinical outcomes over chemotherapy alone.[218] mTORC1 inhibition is also associated with relief of feedback inhibition on Akt and development of resistance. However, mTORC1/2 dual inhibition has been shown to leave a drug-resistant, cancer stem cell-like population, primarily due to mTORC1 inhibition.[219] Our previous work has shown that selective inhibition of Rictor in combination with lapatinib treatment, significantly

slowed the growth of HER2-amplified breast cancers. We have also demonstrated preliminary data that selective Rictor inhibition effectively reduced tumor growth in at least one model of triple negative breast cancer (TNBC).[7] Our optimized si-NP delivery technology will be uniquely capable of the first investigations of the therapeutic impact of individual mTORC2 silencing across multiple sub-types of TNBC.

5.4 Conclusion

In 2019, just 21 years since the discovery of RNA interference and a mere 16 years since the publication of the full sequence of the human genome, we now live in a truly remarkable age of "genomic medicine." Gene therapy holds great promise for a wide variety of diseases, from rare disorders to "undruggable" cancer targets. The development of RNAi-based therapeutics has seen a rocky road from idea to reality, but our understanding of the delivery challenges and toxicity mechanisms is constantly advancing and improving.

The work described in this dissertation has focused on strategies to improve the circulation, tumor gene knockdown, and tolerability of siRNA nanocarriers. We have demonstrated the benefits of zwitterionic polyplex coronas for achieving greater efficacy in solid tumors compared to PEGylated counterparts. However, we have also extensively characterized the toxicity of these advanced nanomaterials. We have highlighted "dual hydrophobization" and charge ratio optimization as strategies to significantly improve the stability and safety of polymeric nanocarriers while preserving their efficacy. We have also characterized a novel PAF-related mechanism of nanoparticle-based toxicity previously only known to occur in response to adenoviral vectors. Each component of this work enhances our understanding of how to increase the gap between minimum efficacious dose and maximum tolerated dose of siRNA nanocarriers.

Maximizing the therapeutic window of siRNA nanocarriers will enhance our ability to interrogate novel genetic targets across many disease states and will pave the way for a revolution in versatile, molecularly-targeted RNAi therapeutics.

APPENDIX A

SUPPLEMENTARY MATERIAL FOR CHAPTER II

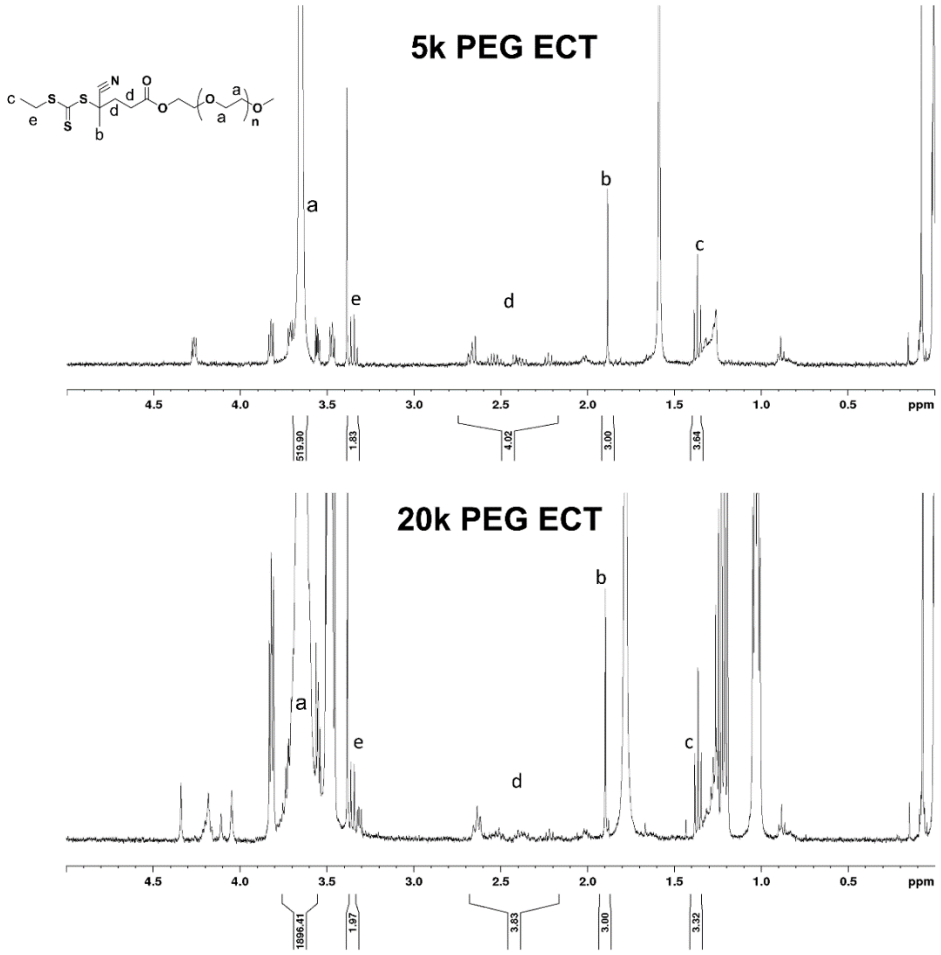

Supplemental Figure A.S1 ^{1}H-NMR data in CDCl3 for 5k PEG ECT and 20k PEG ECT. Conjugation efficiency of PEG to ECT was quantified by integrating PEG peak relative to the (CCNCH3) ECT peak (δ 1.88 s), and dividing the expected number of protons for that given PEG peak (454 for 5k PEG, 1818 for 20k PEG) by the integral of the PEG (δ3.65 s). Efficiencies were 87% for 5k PEG ECT and 96% for 20k PEG ECT.

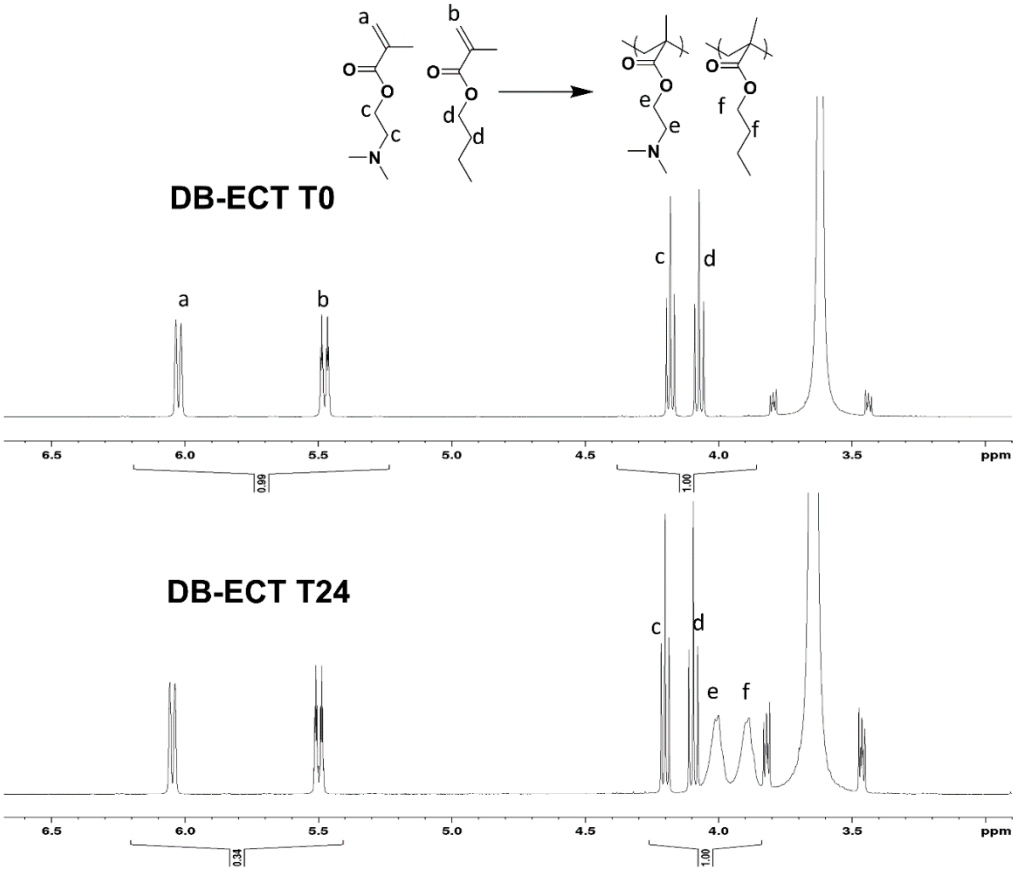

Supplemental Figure A.S2 Polymerization of core poly(DMAEMA-co-BMA) block. Polymerization conversion was calculated by integrating monomer peaks at δ6.05s and δ5.5s, while setting integrals of polymer/monomer peaks in the range of δ3.8-4.2s to 1 at 0 hrs and 24 hrs. Conversion was calculated by [1-(integral at T24/integral at T0)]. CDCl3 solvent.

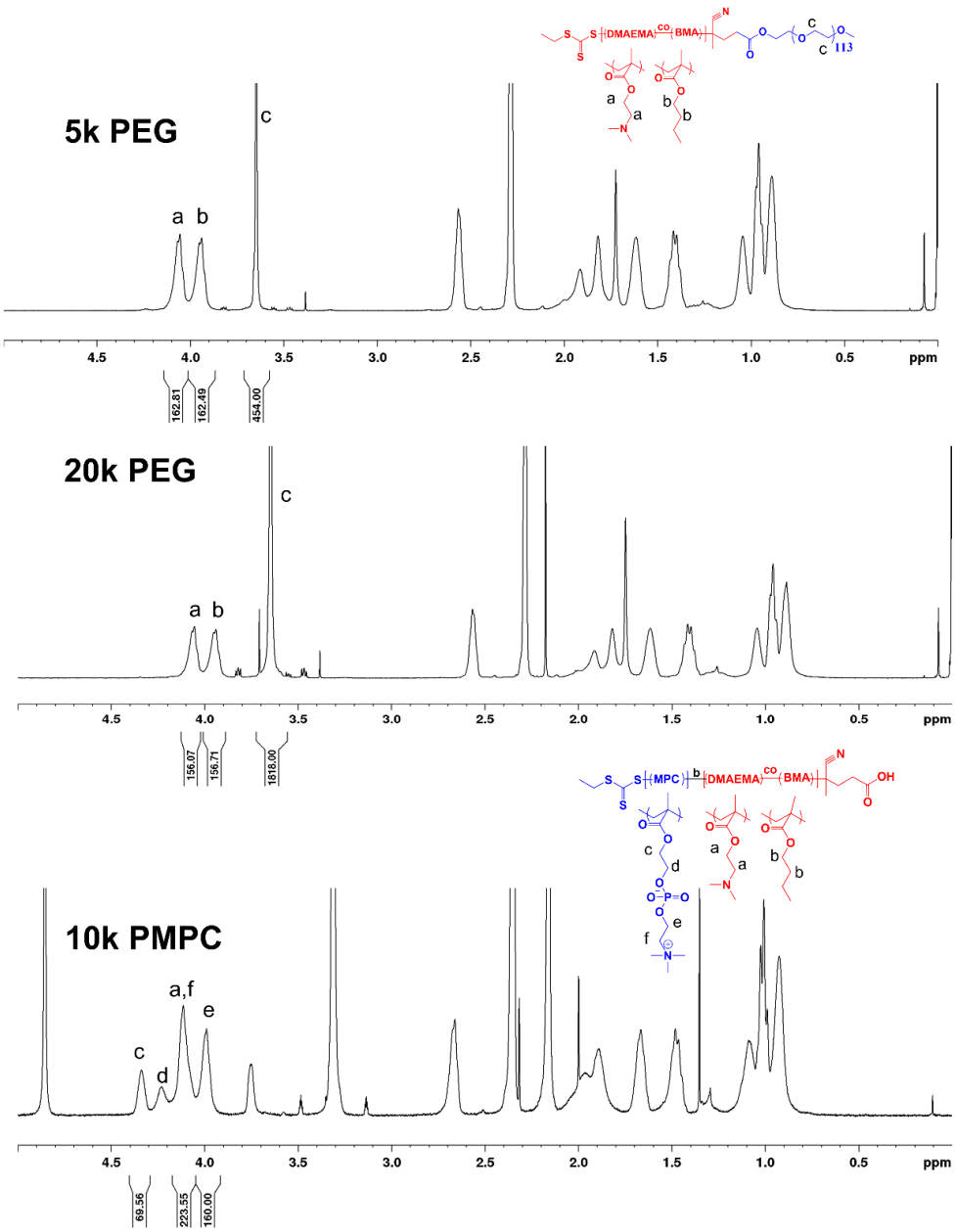

Supplemental Figure A.S 3- ^{1}H-NMR of polymer panel-continued on next page

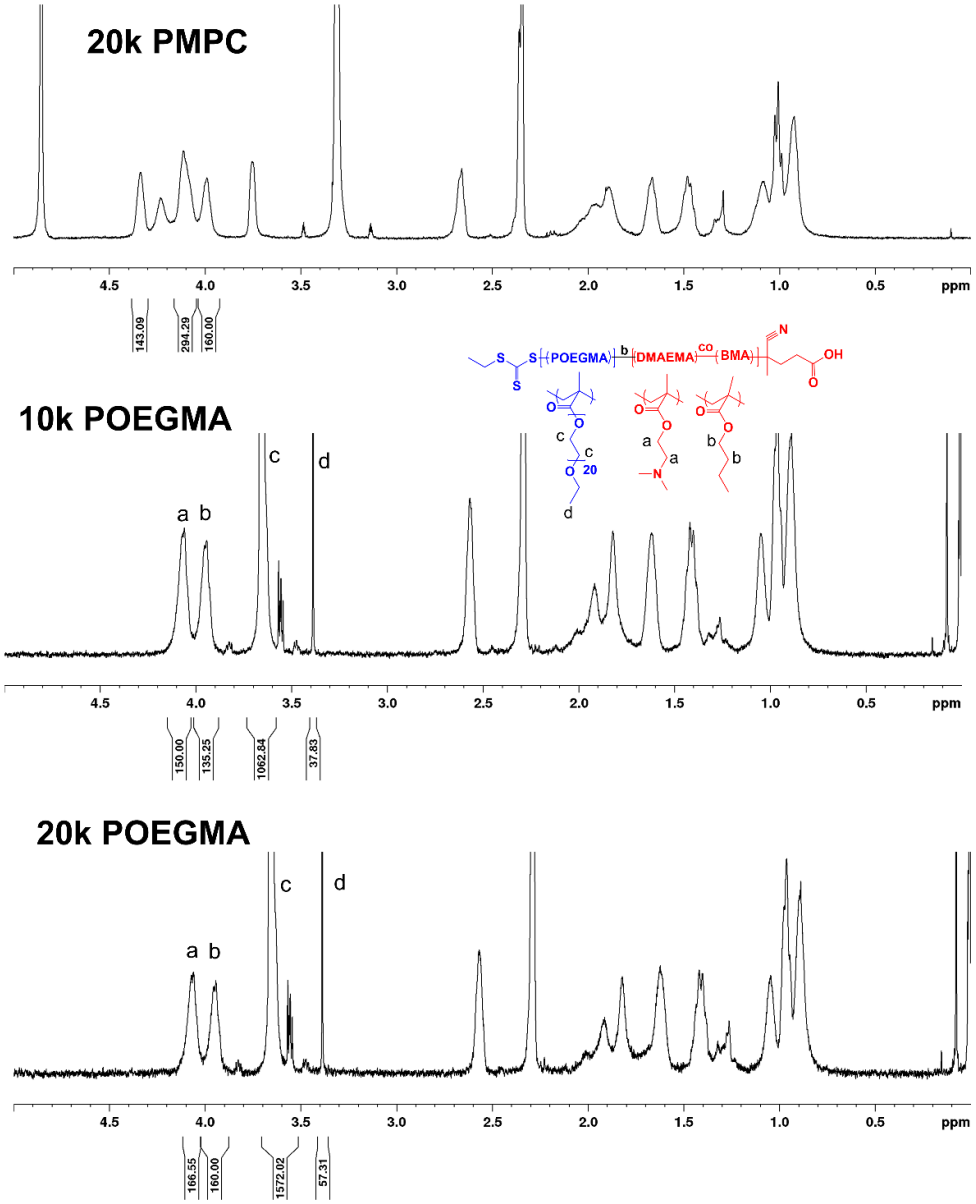

Supplemental Figure A.S 3 ^{1}H-NMR of polymer panel. Polymer repeating units for 5k PEG and 20k PEG were calculated by comparing DMAEMA (δ4.05 s) and BMA (δ3.95 s) peak integrals to PEG integrals (δ3.65s) (in CDCl3). For PMPC (MeOD) and POEGMA polymers (CDCl3), PMPC and POEGMA peaks (labeled) were integrated relative to known DMAEMA and BMA lengths (from DB ECT NMR). DMAEMA:BMA ratios of ~50:50 were confirmed using this method.

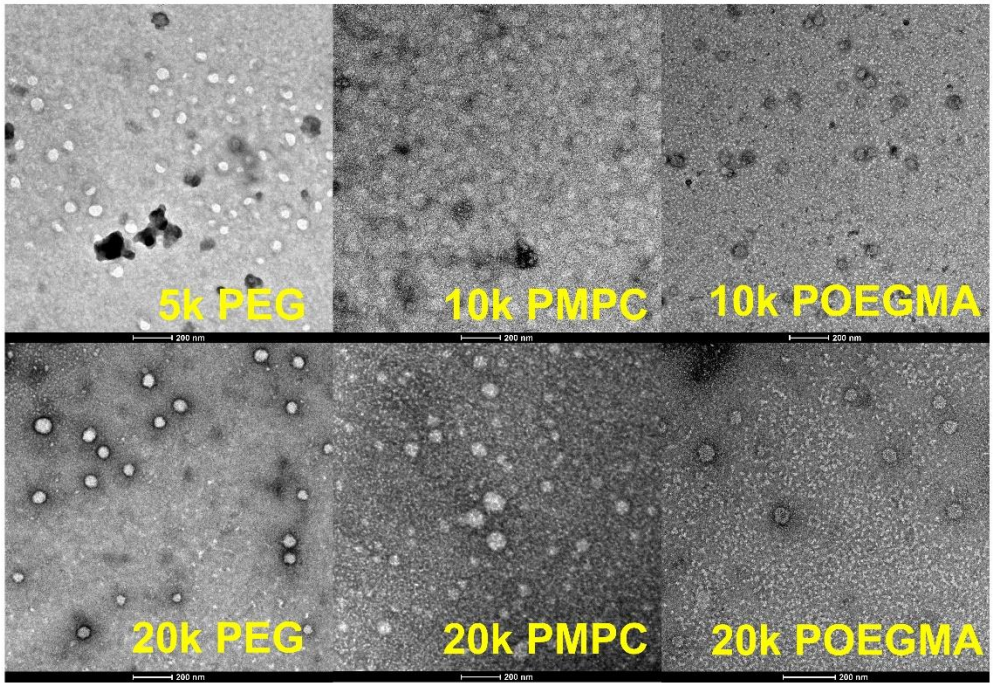

Supplemental Figure A.S4 TEM images of polyplex suspensions at N^+:P^- 20, 0.5 mg/mL polymer, counterstained with 3 % uranyl acetate. All scale bars represent 200 nm. TEM confirms DLS data that particle sizes are in 100-150nm range. Note that dried particles are typically smaller in appearance on TEM than hydrated particles measured by DLS.

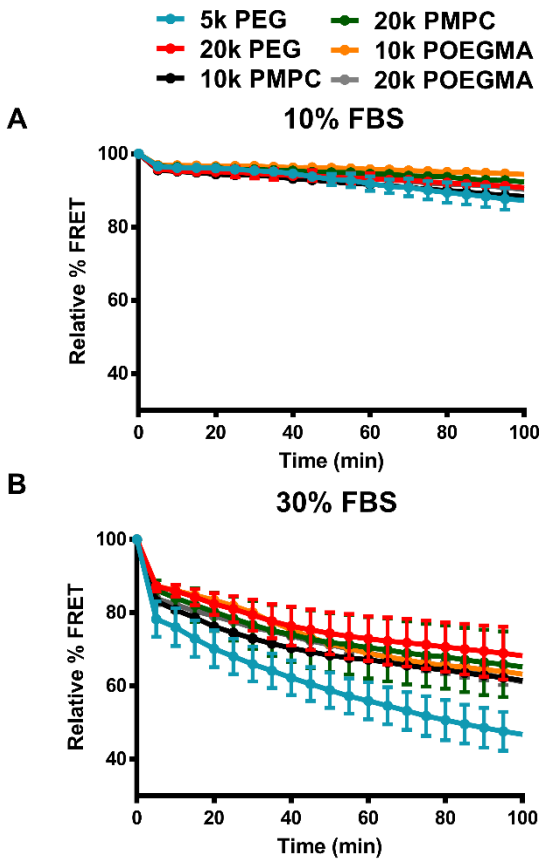

Supplemental Figure A.S5 Alternative polyplex coronas (N^+:P^- 20) improve stability in FBS compared to traditional 5k PEG coronas. (A) Over 100 minutes, polyplexes remain stable in 10% serum. In 30% serum (B), polyplexes are partially destabilized over longer time periods, with no significant differences between PMPC, POEGMA, and 20k PEG coronas.

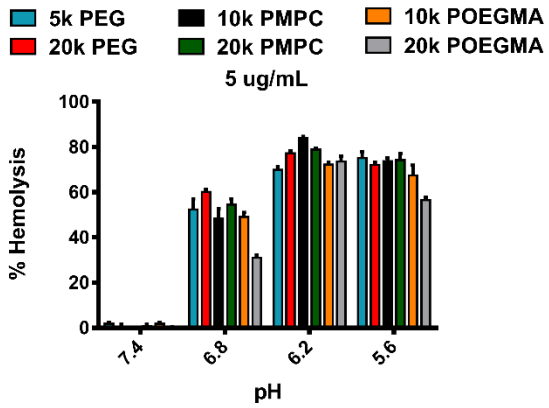

Supplemental Figure A.S6 Hemolysis panel of polymer library at lower concentration of polymer. Polyplexes were formulated at N^+:P^- ratios of 20:1. Polyplexes at 5 µg/mL polymer showed similar hemolytic properties to 40 µg/mL samples. Results represent average of n=3 experiments.

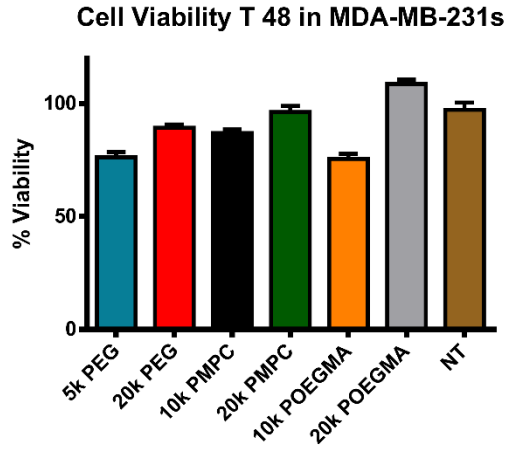

Supplemental Figure A.S7 Cell viability in MDA-MB-231s 48 hours post polyplex introduction**.** All polyplexes maintained greater than 75% cell viability. Polyplexes were delivered with 100 nM scrambled siRNA at N^+:P^- 20.

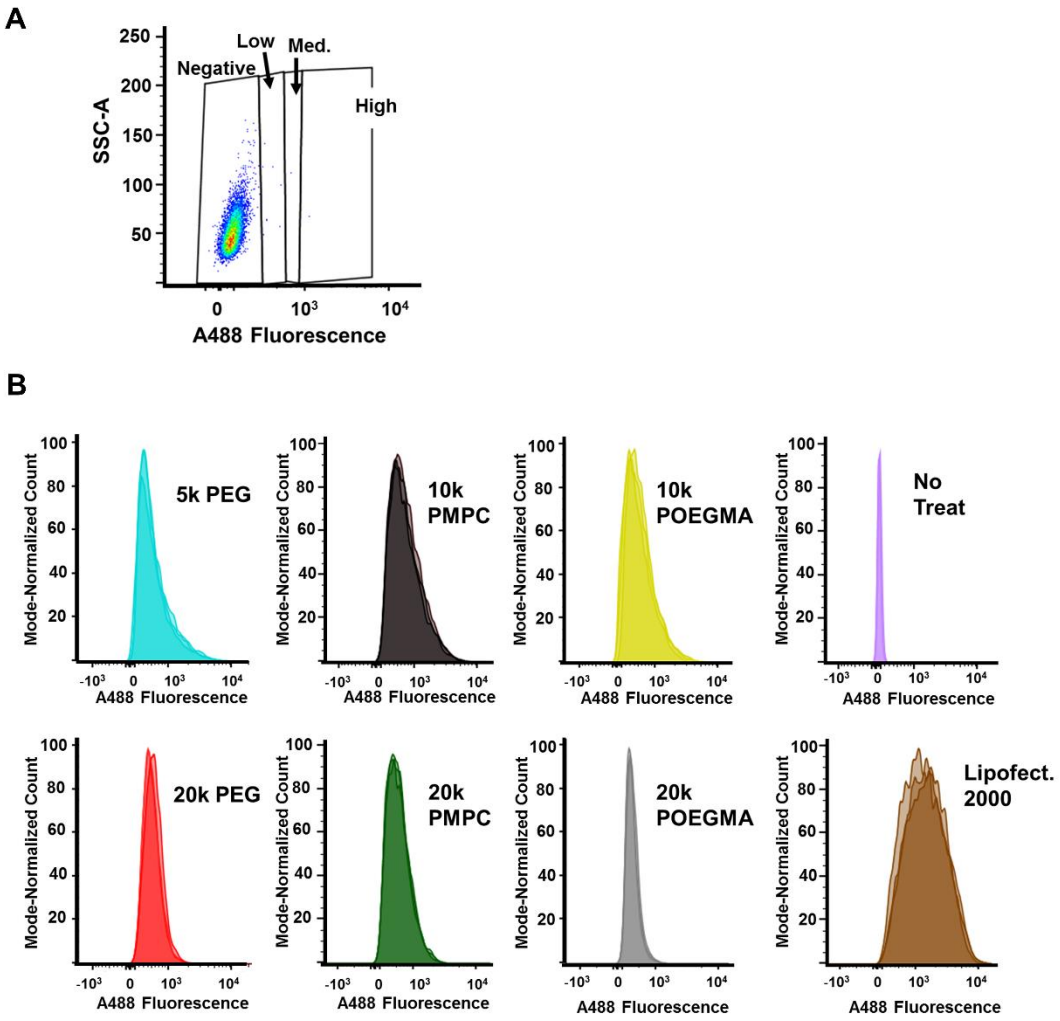

Supplemental Figure A.S8 Flow Gating (A) Example of low-medium-high gating on Alexa488 fluorescence. (B) Histograms for all flow samples. MDA-MB-231 cells were treated with polyplexes bearing 100 nM A488-siRNA for 24 hours (N^+:P^- 20).

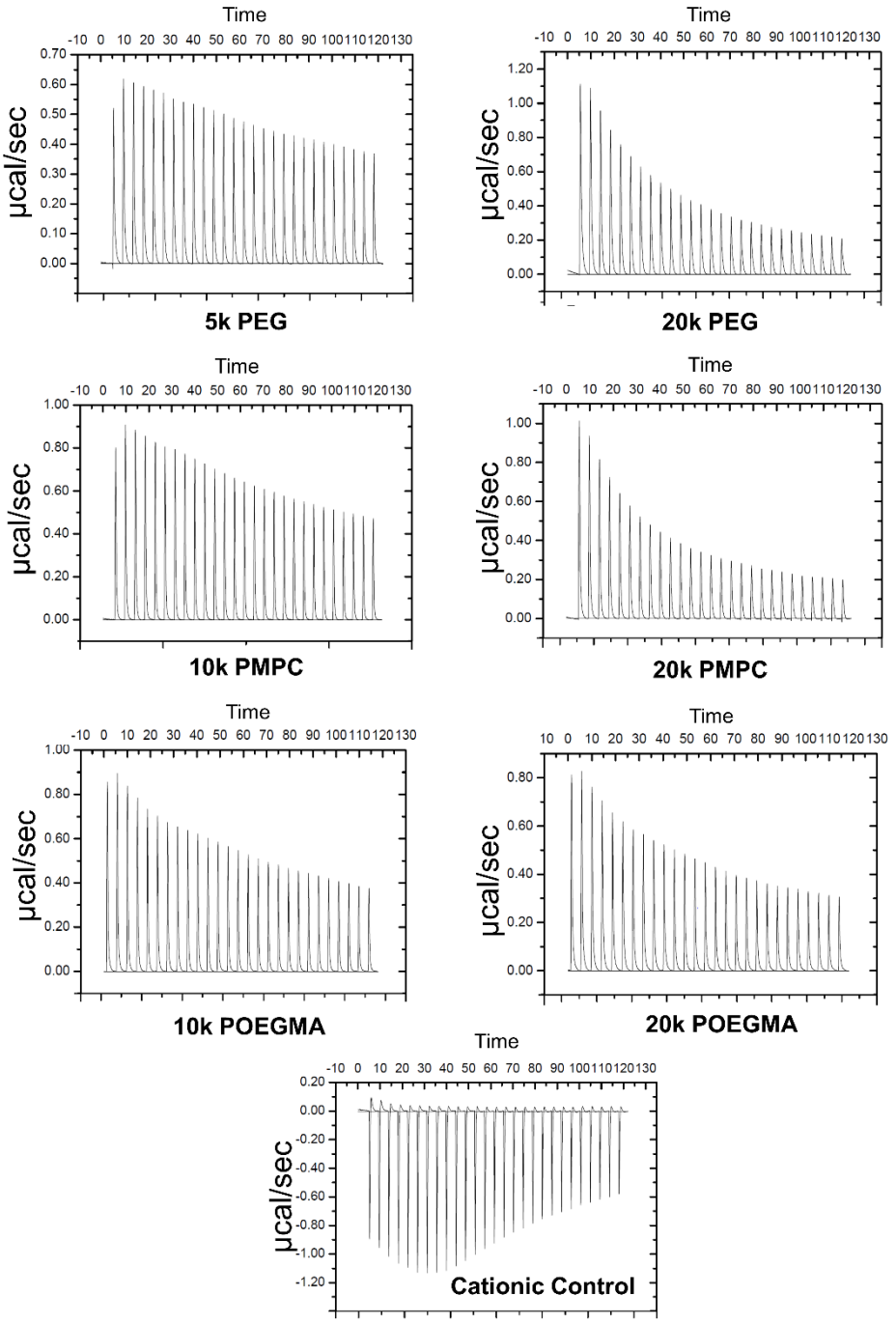

Supplemental Figure A.S9 Raw ITC panel**.** Panels display raw thermodynamic ITC data, with µcal/sec on the y axis and time on the x axis. Each peak represents heat change associated with a 10 µL injection of 15 mg/mL BSA (exothermic is negative).

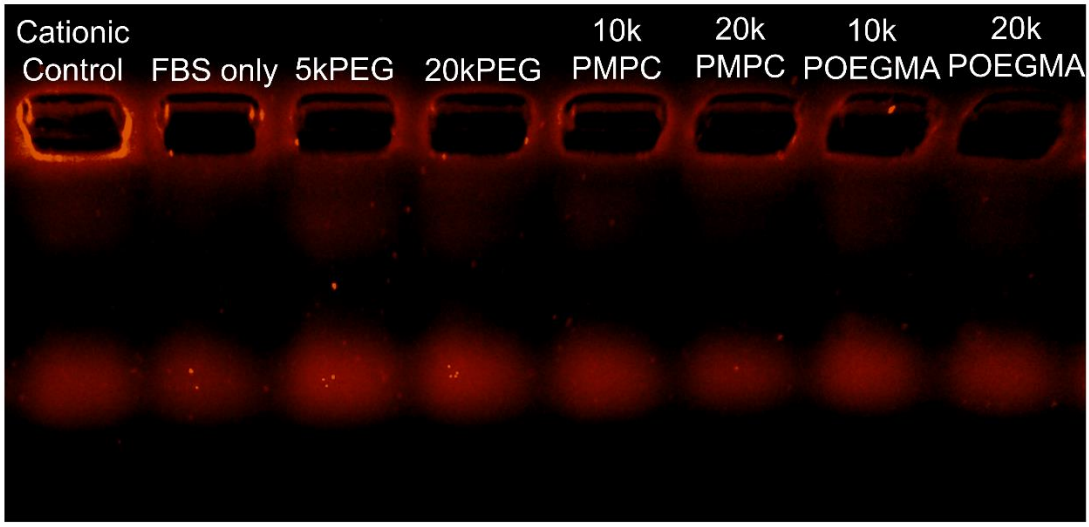

Supplemental Figure A.S10 Gel retention assay of FBS-incubated polyplexes. Polyplexes (100nM siRNA, N^+:P^- 20) were incubated with 5% FBS and run on an agarose gel, which was then stained for protein using SYPRO Ruby. The cationic control exhibits intense protein staining within the loading well, while the appearance of binding to all other polyplexes was negligible and appeared similar to the FBS only control.

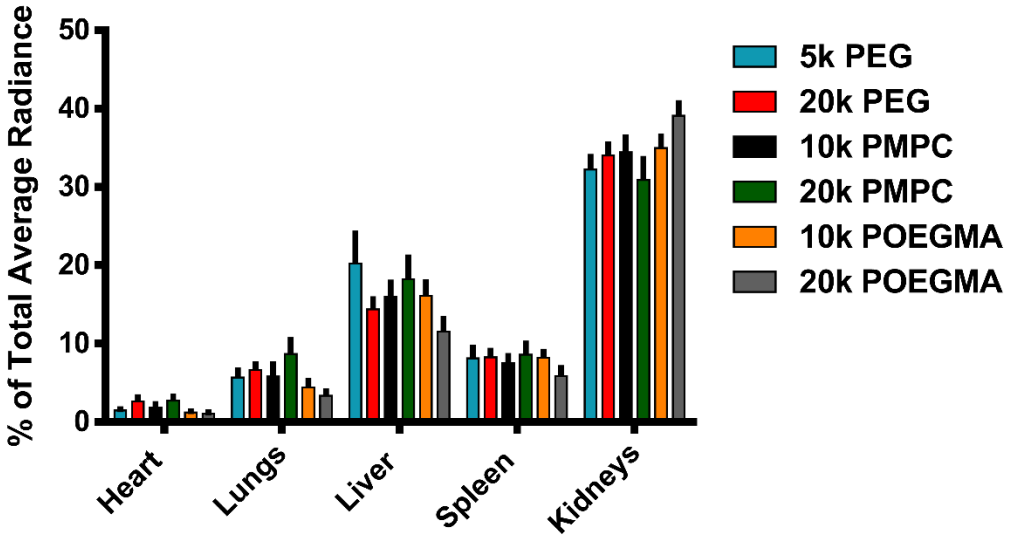

Supplemental Figure A.S11 Tissue biodistribution of Cy5-siRNA 20 min post-injection. Data represent average of n=5 animals. Polyplexes were administered at a dose of 1 mg/kg siRNA, N^+:P^- 20.

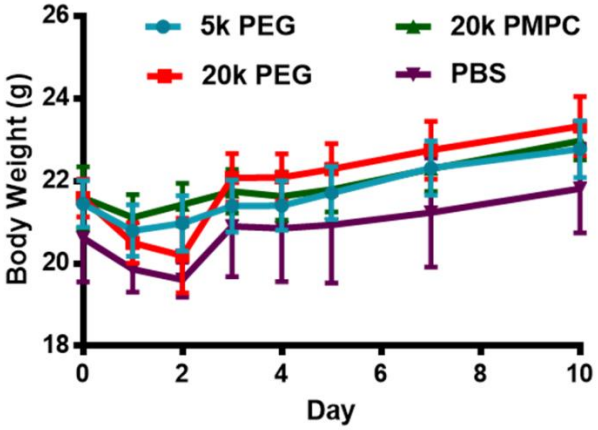

Supplemental Figure A.S12 Body weight measurements of tumor bearing mice throughout 10-day study period show that there were no significant differences in body weight between mice receiving different polyplex treatments.

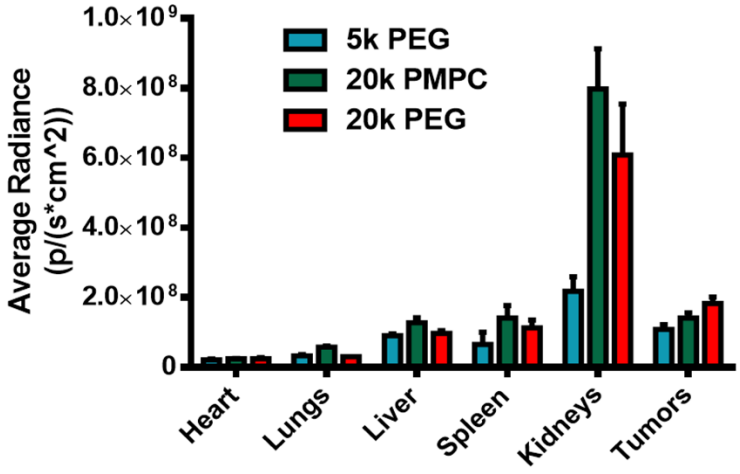

Supplemental Figure A.S13 Biodistribution of PEGylated vs zwitterated polyplexes at 24 hours in tumor-bearing mice (N^+:P^- 20). At 24 hours, although 20k PMPC DB and 20k PEG DB average fluorescence values in tumors were both higher than 5k PEG DB, there was no significant difference between the high molecular weight coronas.

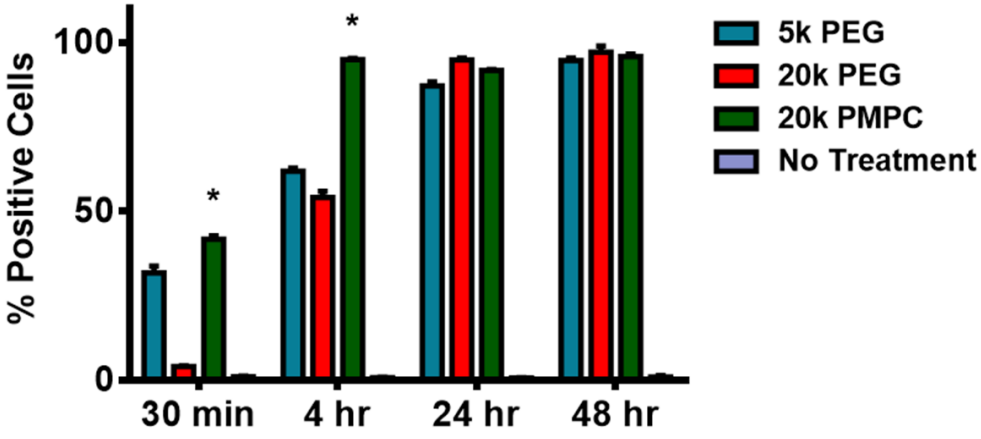

Supplemental Figure A.S14 Percent of cells taking up polyplexes *in vitro* over time. 20k PMPC polyplexes penetrated nearly 100% of cells *in vitro* after only 4 hours, significantly more than 5k PEG or 20k PEG polyplexes.

APPENDIX B

SUPPLEMENTARY MATERIAL FOR CHAPTER III

Supplementary Table 1 Sequences of Relevant Oligonucleotides

Oligonucleotide	Sequence (5' to 3')
Fluor- Sense	dGdTdCdAdGdAdAdAdTdAdGdAdAd AdCdTdGdGdTdCdAdTdC
Fluor- Sense Amine	[5AmMC6]dGdTdCdAdGdAdAdAdTd AdGdAdAdAdCdTdGdGdTdCdAdTdC
Fluor- Antisense	[Fluor]dGdAdTdGdAdCdCdAdGdTdT dTdCdTdAdTdTdTdCdTdGdAdC
Scrambled- Sense	rCrGrUrUrArArUrCrGrCrGrUrArUrArA rUrArCrGrCrGrUdAdT
Scrambled- Sense Amine	rCrGrUrUrArArUrCrGrCrGrUrArUrArA rUrArCrGrCrGrUdAdT[3AmMC6T]
Scrambled- Antisense	rArUrArCrGrCrGrUrArUmUrAmUrArC rGrCrGrArUmUrAmArCmGmAmC
Luciferase- Sense	rCrArArUrUrGrCrArCrUrGrArUrArArU rGrArArCrUrCrCdTdC
Luciferase- Sense Amine	rCrArArUrUrGrCrArCrUrGrArUrArArU rGrArArCrUrCrCdTdC[3AmMC6T]
Luciferase- Antisense	rGrArGrGrArGrUrUrCrAmUrUmArUrC rArGrUrGrCmArAmUrUmGmUmU

*Key: [Fluor]= [A488], [A546], or [Cy5]; d= DNA base; r= RNA base; m= backbone 2'O-methyl modification; [5AmMC6]= 5' amino modifier
*All oligonucleotides were sourced from Integrated DNA Technologies

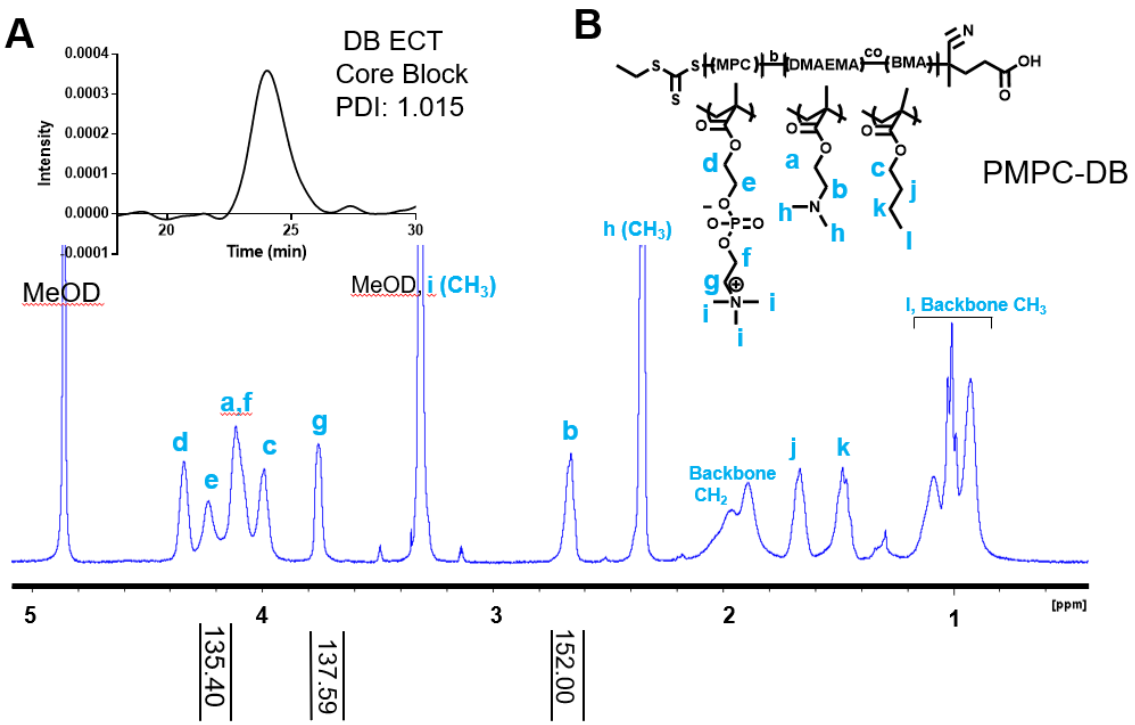

Supplemental Figure B.S1 PMPCDB Characterization (A) GPC of the monodisperse core DB ECT polymer block in DMF. (B) ^{1}H-NMR spectra of PMPC-DB polymers in MeOD. Each identified peak of interest corresponds to 2 H^{+} unless otherwise noted. PMPC peaks were quantified by comparison to known quantities of DMAEMA and BMA in the core polymer block (integrate peak b at δ2.66 and set at the number of repeating units of DMAEMA multiplied by 2 [152 in example shown]; integral of peaks e (δ4.24) and g (δ3.76) each indicate the number of repeating units of the MPC monomer times two [~138 in example shown]. The number of repeating units of DMAEMA and BMA were determined by ^{1}H-NMR as indicated in previously published work).

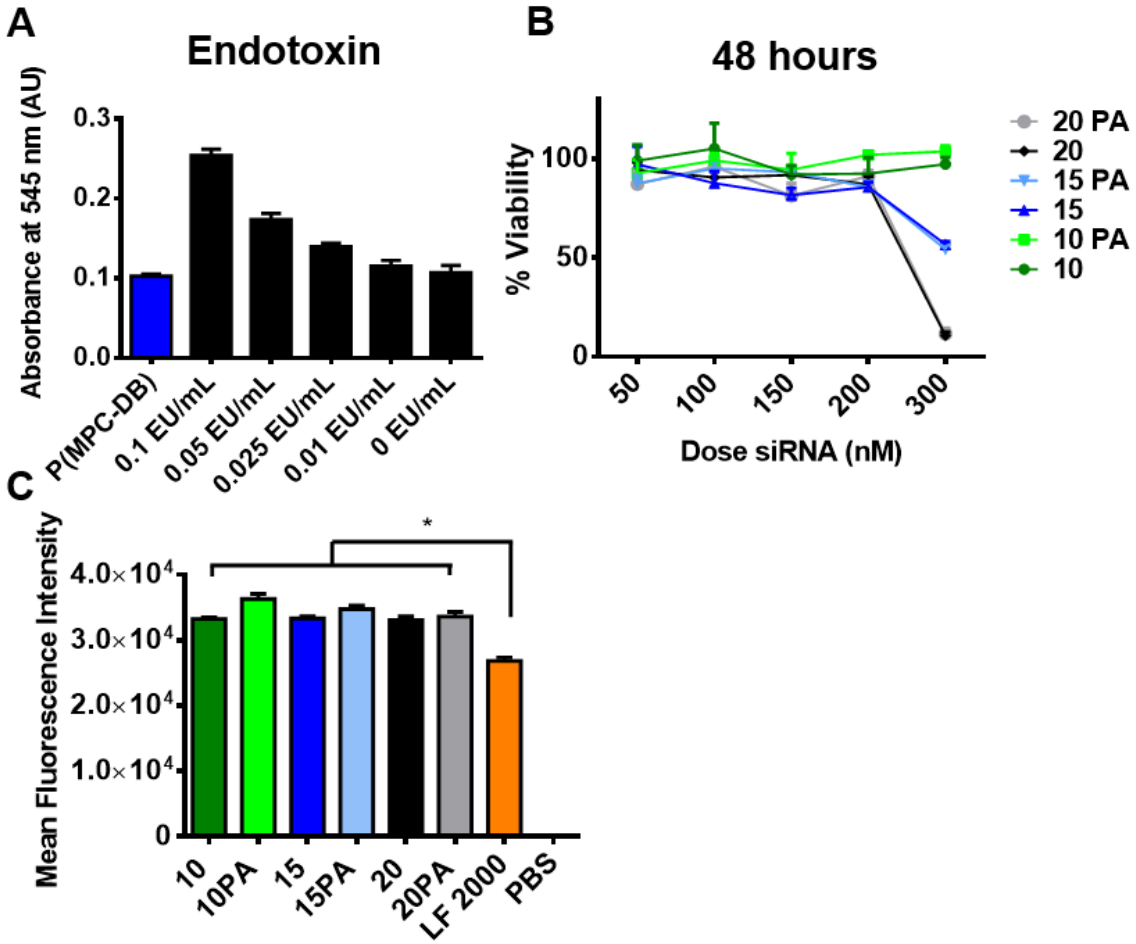

Supplemental Figure B.S2 Additional *in vitro* characterization. (A) P(MPC-*bl*-DMAEMA-*co*-BMA) polymers were free of endotoxin contamination. (B) At 48 hours after si-NP introduction and 24 hours after si-NP removal, cell viability was recovered at all doses except 300 nM, where N:P ratio-dependent toxicity persisted. (C) All si-NPs exhibited significantly increased cell uptake compared to equivalent doses of lipofectamine 2000 (n=3, $p<0.01$).

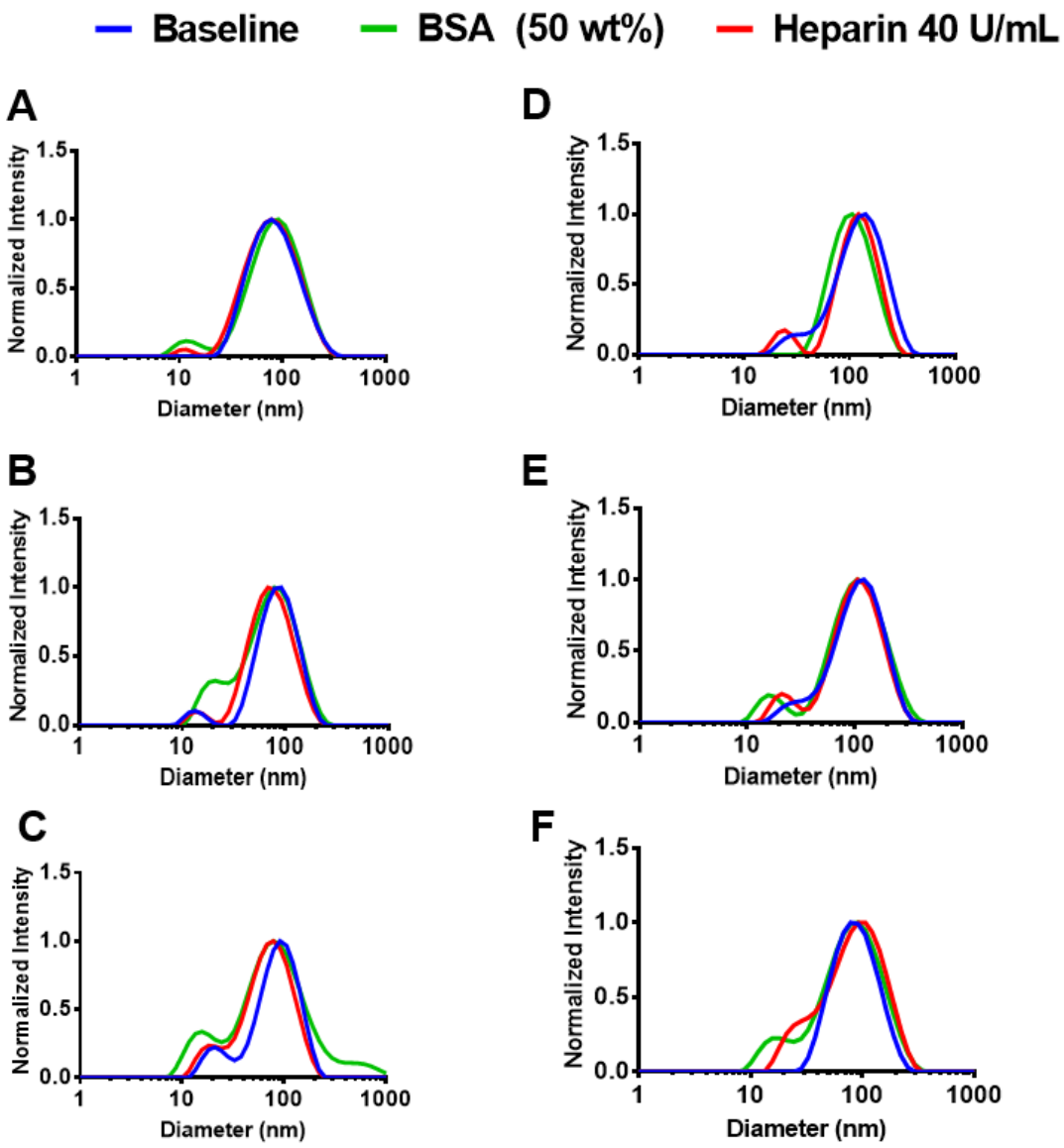

Supplemental Figure B.S3 Incubation of NPs in 40 U/mL heparin or 50 wt% bovine serum albumin (BSA) for 10 min did not significantly shift NP hydrodynamic size. NPs formulated at 10 (A), 15 (B), 20 (C), 10 PA (D), 15 PA (E), or 20 PA (F) retained size distribution in the presence of heparin or albumin challenge.

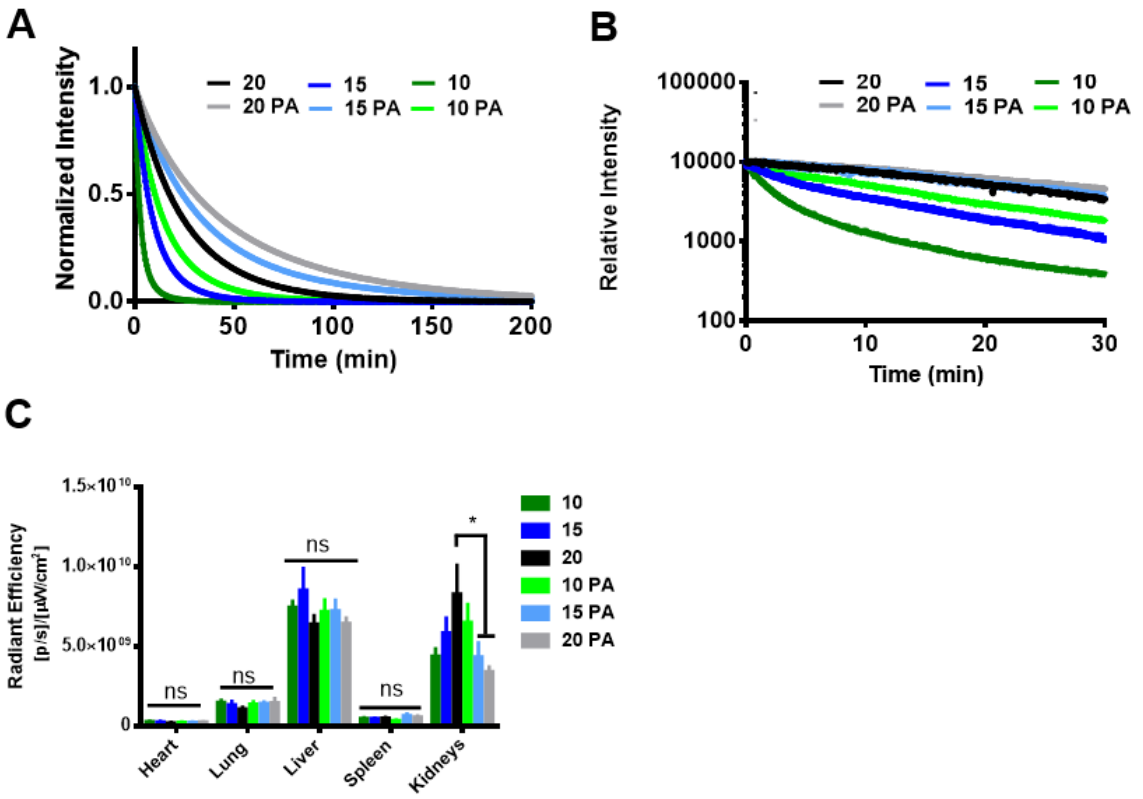

Supplemental Figure B.S4 Additional NP pharmacokinetic and biodistribution analysis. (A) Extended nonlinear regression curves for each siNP formulation. (B) Log-phase pharmacokinetic curves are linear, demonstrating single phase decay kinetics. (C)Total radiant efficiency values for each organ from mice injected with each siNP formulation reveals significantly lower kidney accumulation for 20PA and 15PA siNPs compared to siNPs at 20 (n=5, $p<0.05$).

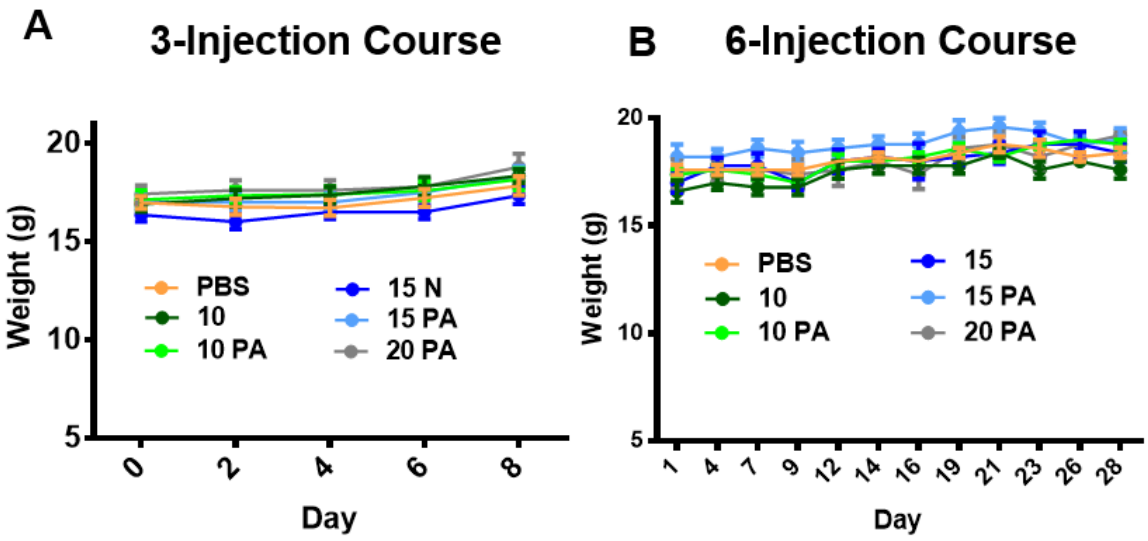

Supplemental Figure B.S5 Repeat NP treatments did not cause variation in body weight. Body weights of mice injected with (A) 3 doses of 1 mg/kg NPs over 1 week or (B) 6 doses of 1 mg/kg NPs over 1 month. No significant changes in body weight were detected for mice treated with any of the formulations.

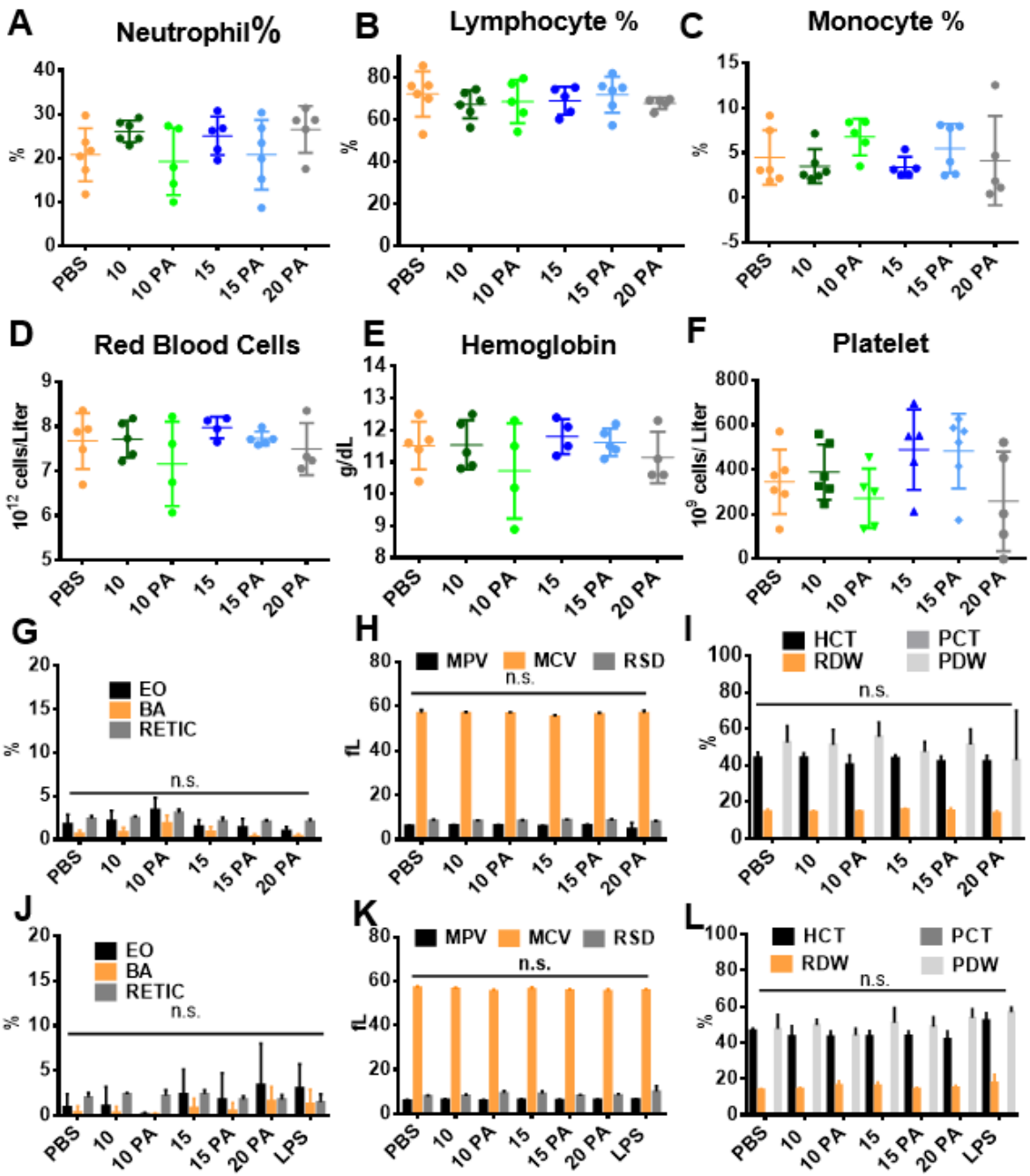

Supplemental Figure B.S6 No CBC differences were detected for any NPs tested in the repeated treatment protocol. (A-F) Complete blood count for mice subjected to 3-injection dosing course.(G-I) Additional complete blood count values, including (G, J) eosinophils (EO), basophils (BA), reticulocytes (RETIC); (H,K) mean corpuscular volume (MCV), mean platelet volume (MPV), and red cell standard deviation (RSD); (I,L) and hematocrit (HCT), platelet distribution width (PDW), red cell distribution width (RDW), and plateletcrit (PCT) for a 3-injection course (G-I) and a 6-injection course (J-L).

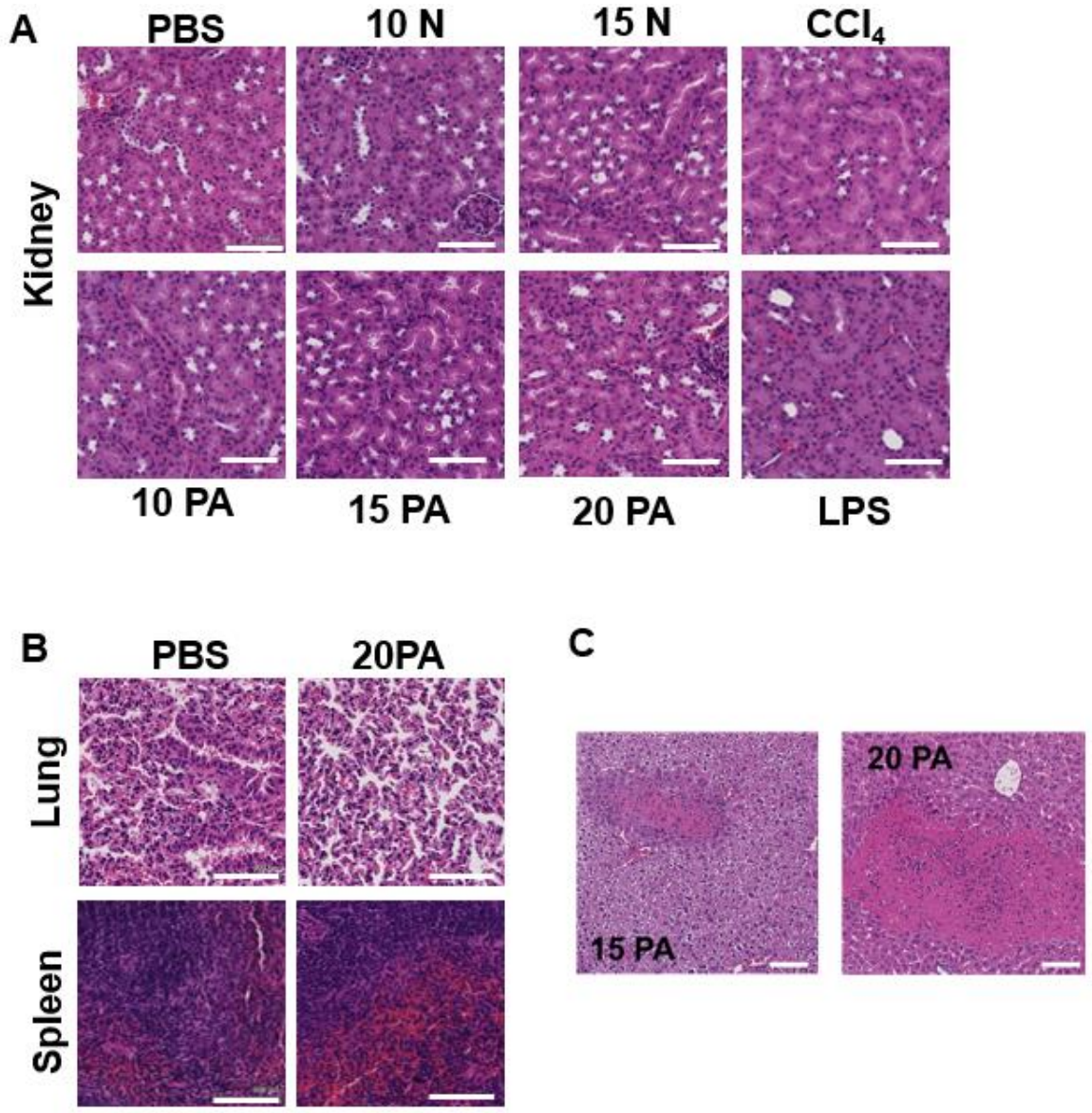

Supplemental Figure B.S7 Histopathology of mice from the 6-time treatment course. All scale bars represent 100 μm. (A) Kidneys from mice treated with all formulations of NPs were rated as normal. (B) Lung and spleens also showed no changes from saline-treated mice. Here only the saline and 20 PA –treated mouse organs are shown. (C) Of 5 mice treated with 15 PA formulations, only a single instance of focal necrosis was observed. In the 20 PA-treated group, areas of focal necrosis were larger and present in 2/5 mice.

A

siNP Group:	Number of Mice		
	Focal Necrosis	Single Cell Necrosis (3-6 foci)	Single Cell Necrosis (1-2 foci)
PBS	0	0	0
10	0	0	0
10 PA	0	0	0
15	0	0	2
15 PA	1	0	2
20 PA	2	1	3

B

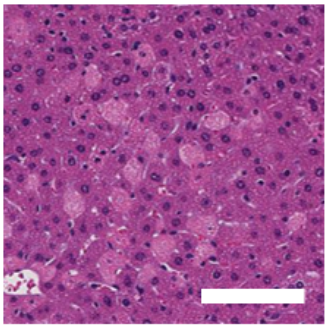

CCl_4

Supplemental Figure B.S8 Liver histology grading after 6-injection course. (A) Slides were graded by a blinded veterinary pathologist for focal necroses or single-cell necroses. (B) Livers from mice treated with CCl_4 were used as a positive control and displayed a high level of necrosis.

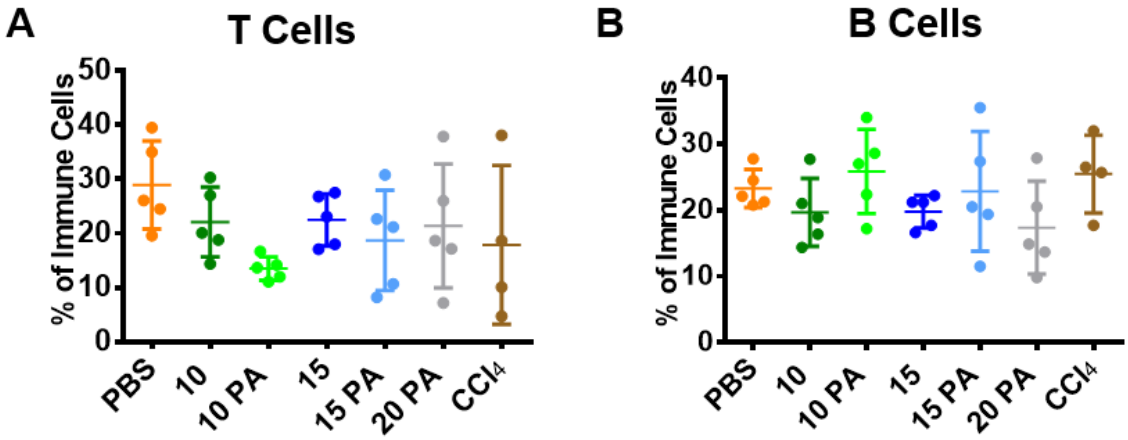

Supplemental Figure B.S9 T Cells and B Cells (A) T cell and (B) B cell percentages in the livers of mice treated with 6 injections of each siNP formulation indicate no significant change in the percentages of infiltrating adaptive immune cells.

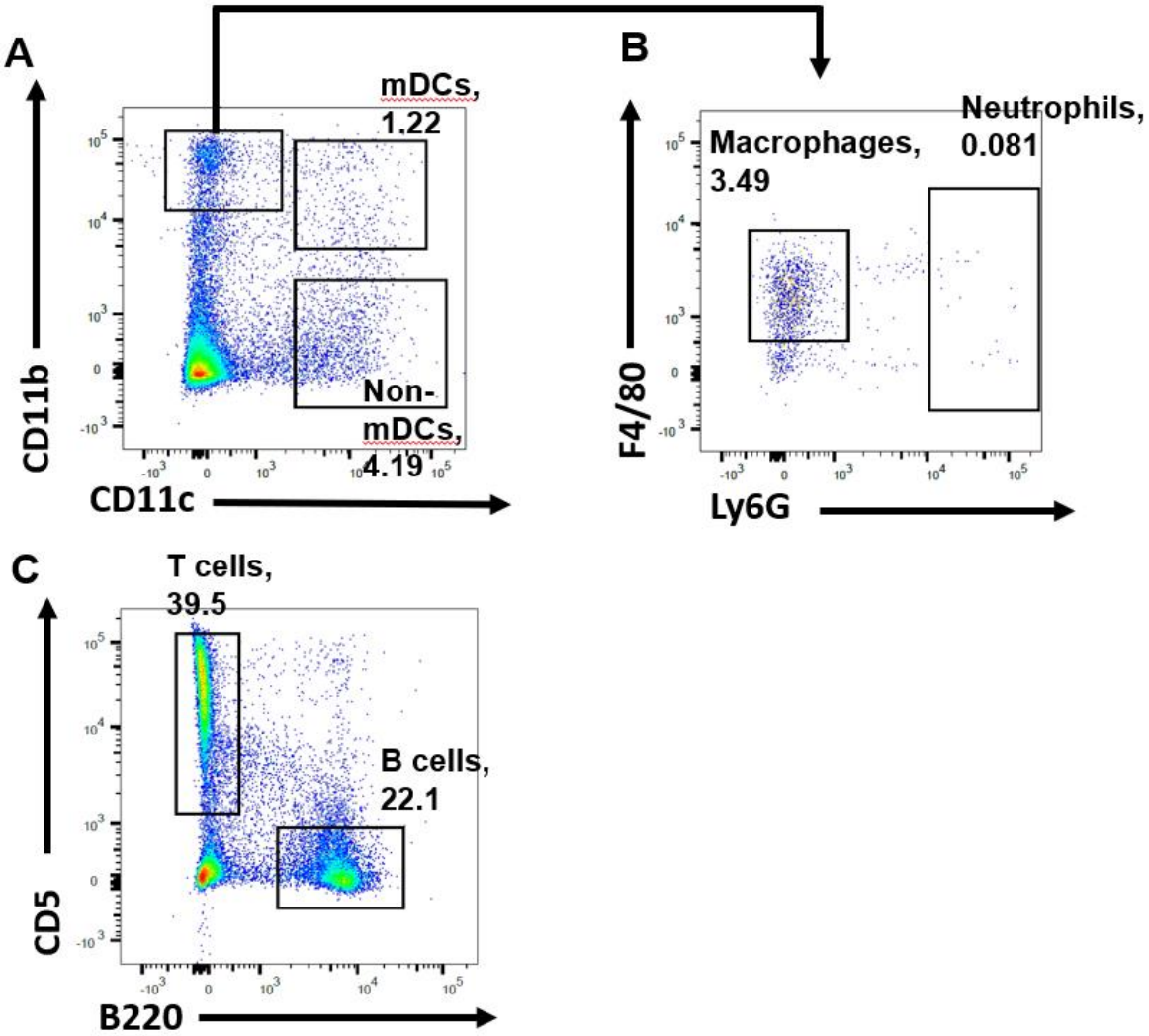

Supplemental Figure B.S10 Representative flow cytometry plots for gating and measurement of liver lymphocytes. Cells were pre-gated on live, single lymphocytes. (A) Myeloid dendritic cells were gated as CD11b+ CD11c+. Non-myeloid dendritic cells (n-mDCs) were CD11b-CD11c+. (B) Macrophages and neutrophils were pre-gated from CD11b+ CD11c - . Macrophages were then gated for F4/80+ Ly6G -, while neutrophils were Ly6G+. (C) T cells and B cells were gated as CD5+ B220- and CD5- B220+ , respectively. Cell populations were quantified as percent of live, single immune cells.

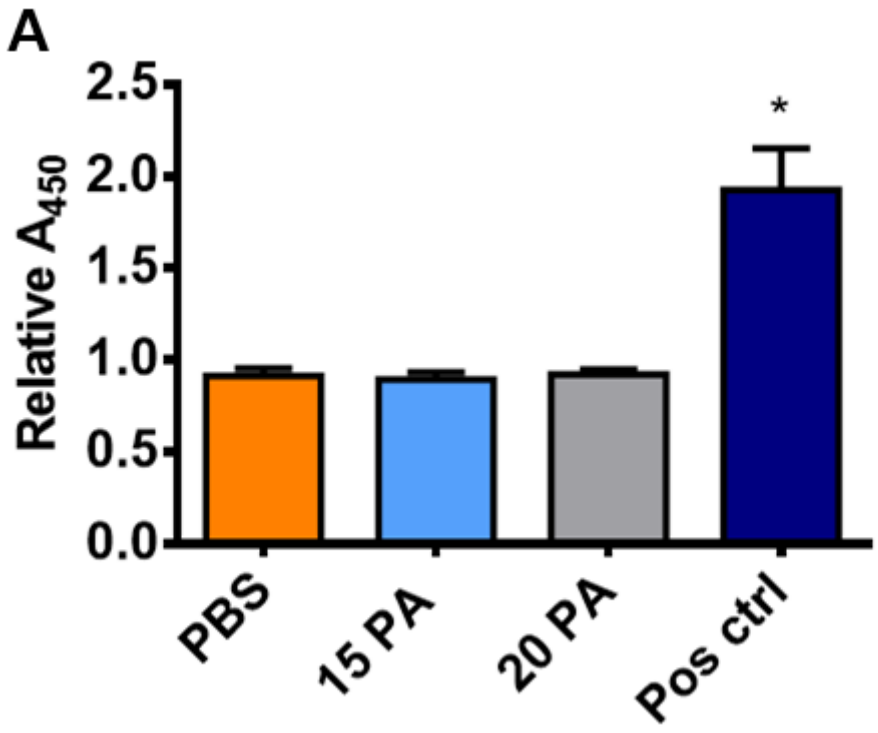

Supplemental Figure B.S11 Immunogenicity of PMPC-based NP formulations. Serum samples from mice treated with long-circulating 15 PA and 20 PA siPA-NP particles show no evidence of antibody production against phosphocholine (n=3, $p<0.01$)

APPENDIX C

SUPPLEMENTARY MATERIAL FOR CHAPTER IV

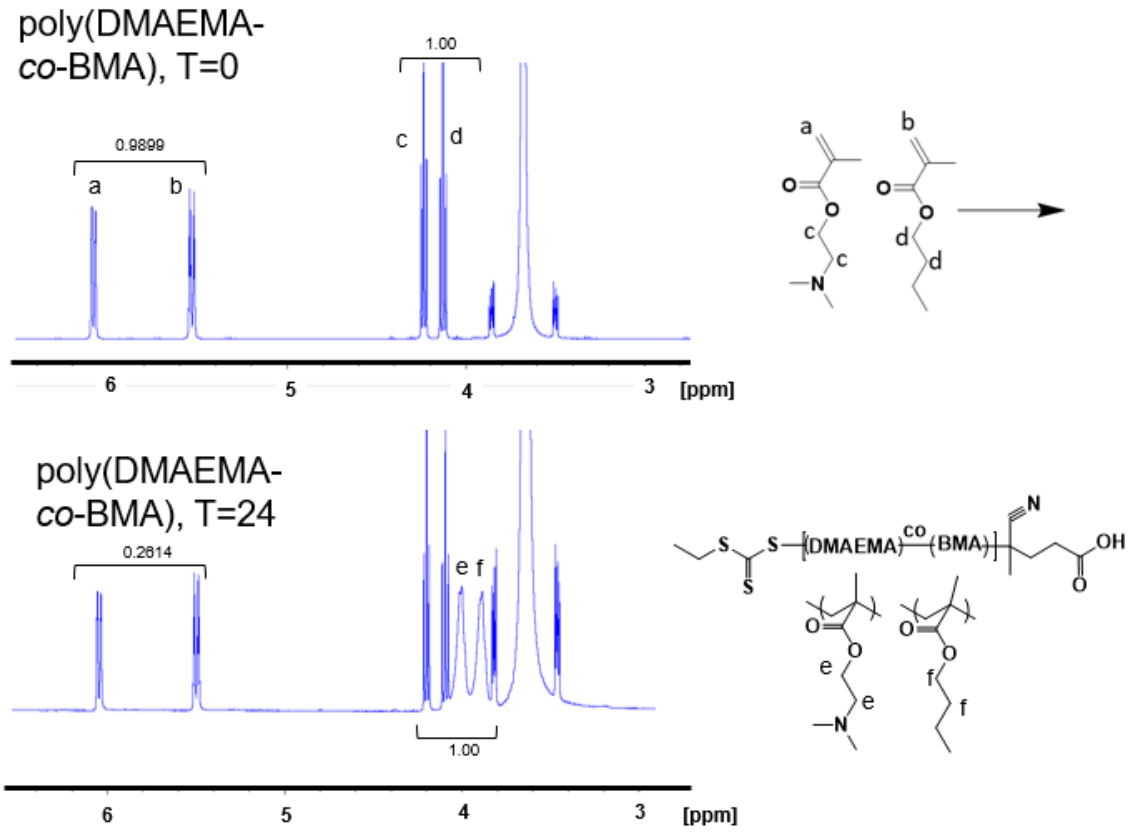

Supplemental Figure C.S1 ^{1}H-NMR of synthesis of poly(DMAEMA-co-BMA). Monomer conversion was calculated based on the disappearance of monomer peaks, as shown ((0.9899-0.2614)/0.9899). $CDCl_3$ solvent.

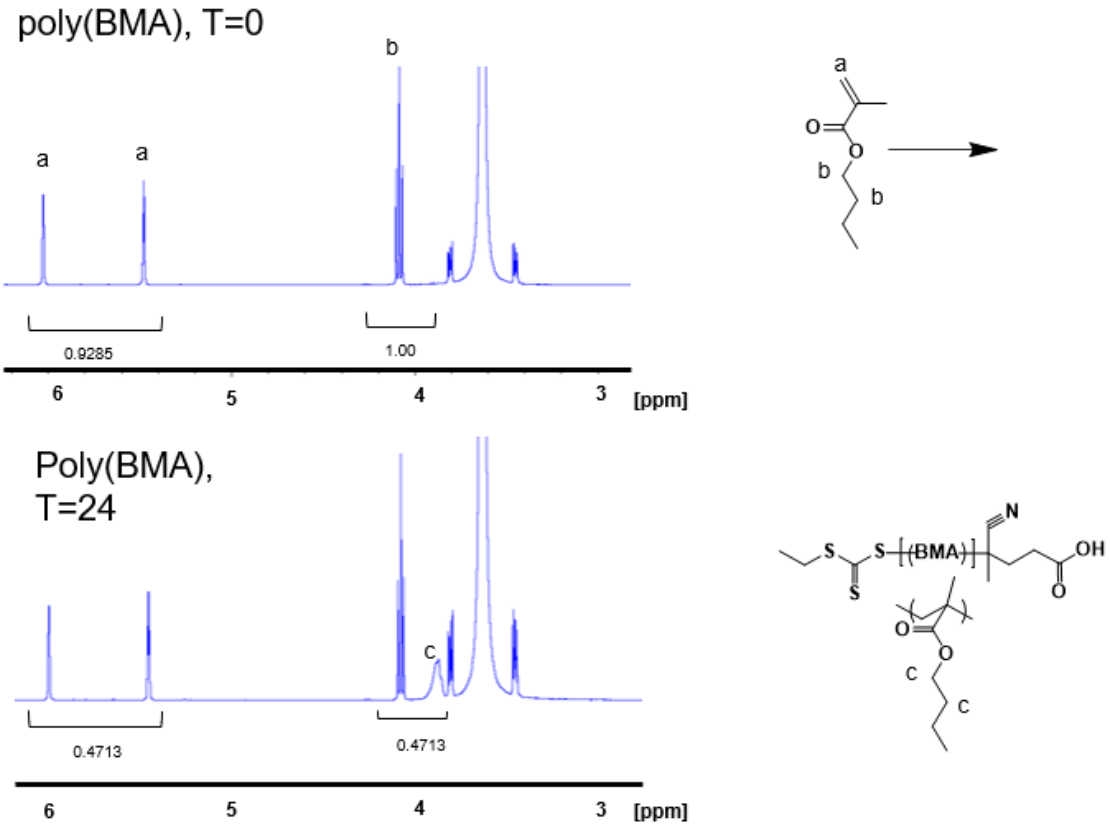

Supplemental Figure C.S2 ^{1}H-NMR demonstrating synthesis of poly(BMA). Monomer conversion was calculated based on the disappearance of monomer peaks, as shown. $CDCl_3$ solvent.

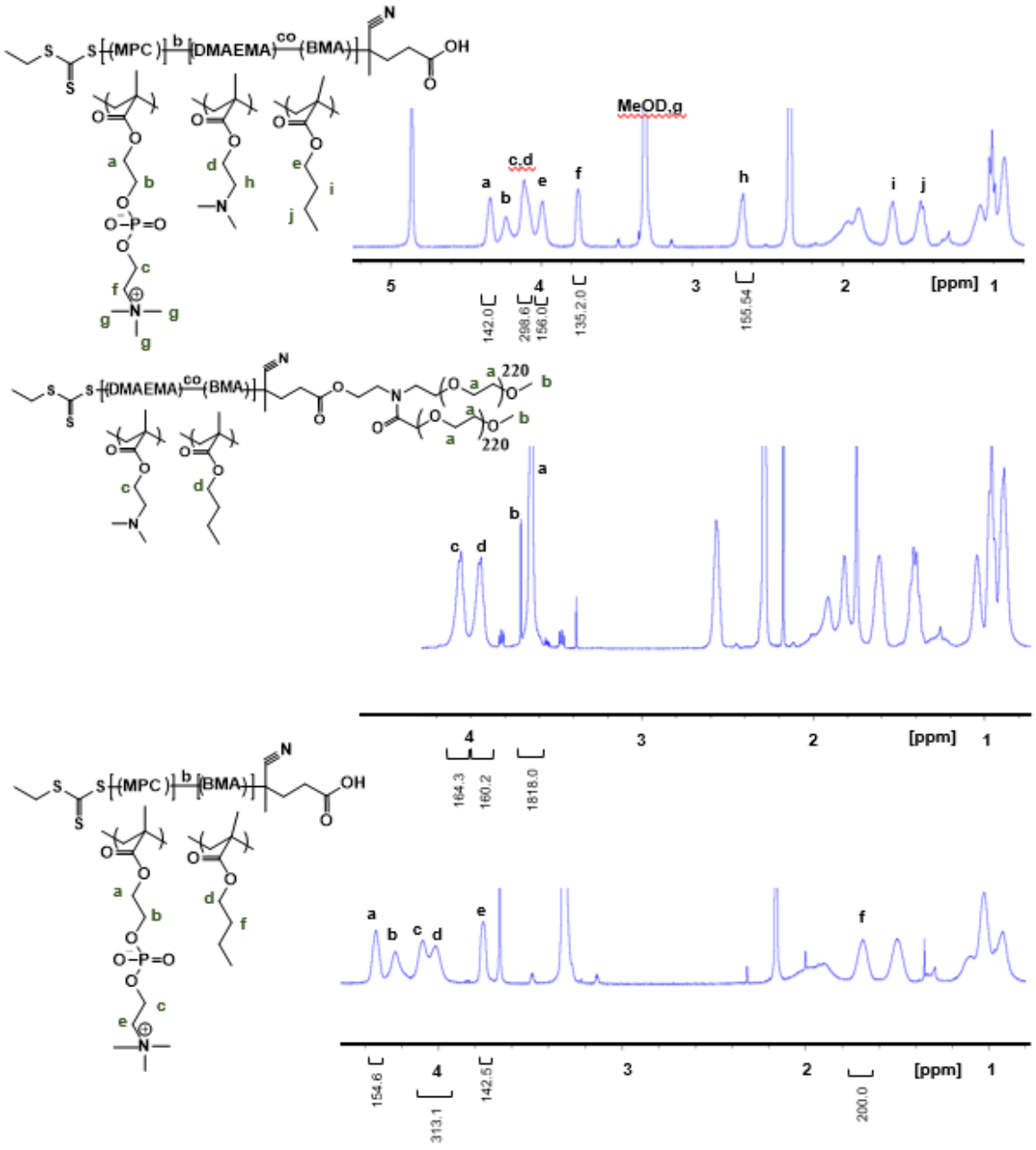

Supplemental Figure C.S3 ^{1}H-NMR characterizations for each RAFT polymer utilized in this work. Top-PMPC-DB, solvent MeOD. Middle panel- 20k PEG DB, solvent $CDCl_3$. Bottom panel- PMPC-BMA, solvent MeOD.

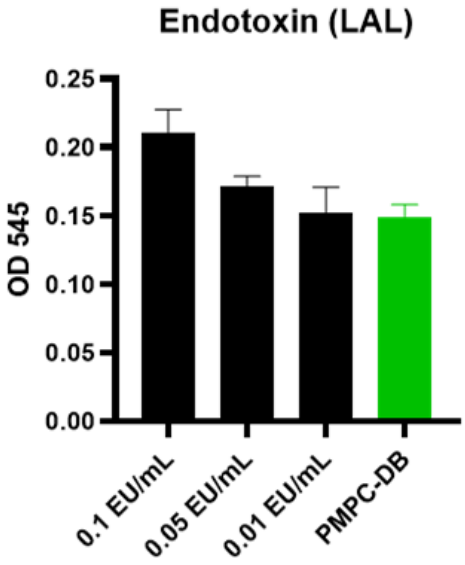

Supplemental Figure C.S4 PMPC-DB polymers were free of endotoxin contamination, as determined by the chromogenic LAL test (GenScript).

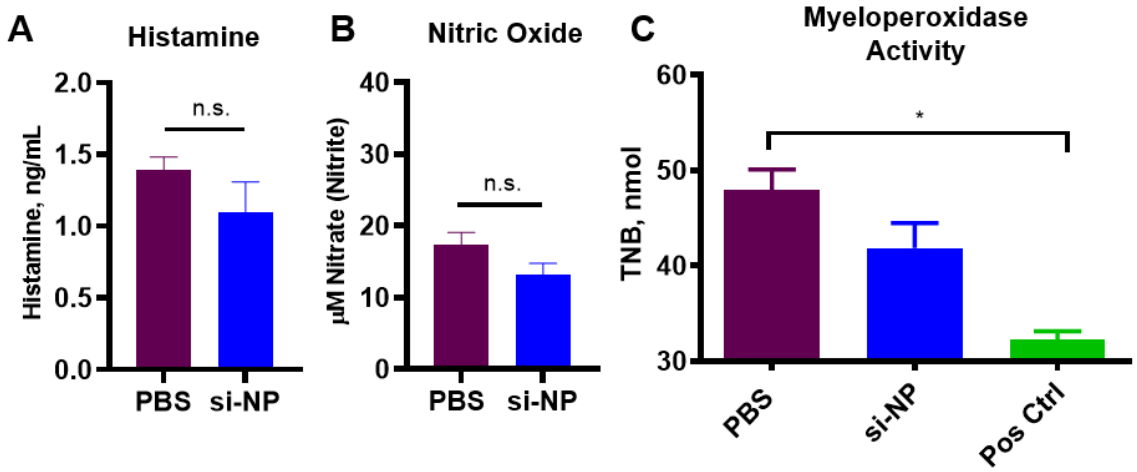

Supplemental Figure C.S5 Mice treated with si-NPs exhibited no signs of increased plasma histamine (A) or nitric oxide (B). Myeloperoxidase activity was slightly increased (indicated by reduction in TNB substrate) compared to saline-treated mice. (C)

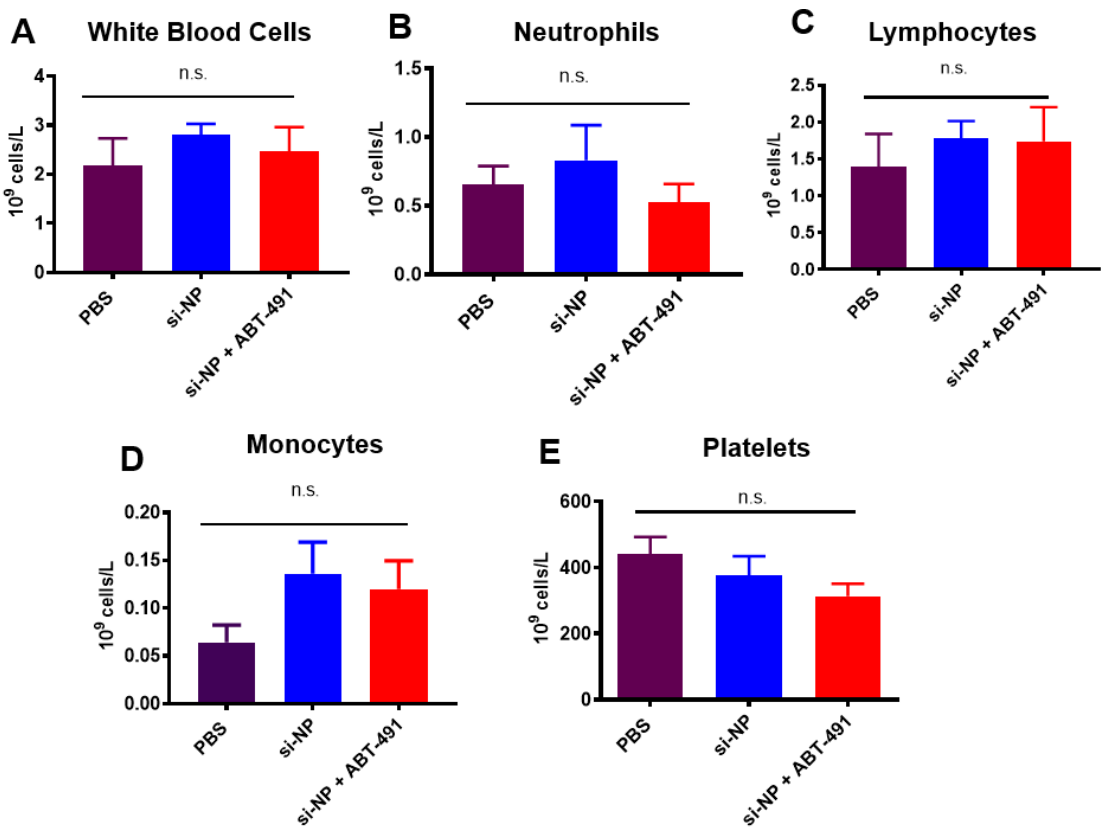

Supplemental Figure C.S6 Additional complete blood count information for si-NP-treated and ABT-491-pre-treated mice, including total white blood cells (A), neutrophils (B), lymphocytes (C), monocytes (D), and platelets (E).

A

Polymer	% DMAEMA:BMA in si-NP Core	Monomer DP	Total Mn (g/mol)
PMPC-DB	50:50	MPC:70 D:78 B:78	42961
PMPC-BMA	0:100	MPC: 70 D:0 B:100	35149
20k PEG DB	50:50	D:80 B:80	43592

B

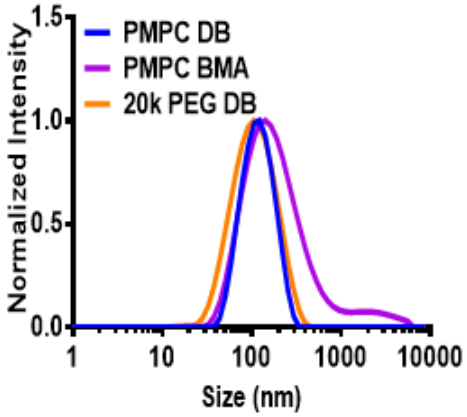

Supplemental Figure C.S7 Si-NP Characterization Data A) Table of polymer characteristics, including Mn and degree of polymerization (DP). B) DLS curves of each si-NP formulation

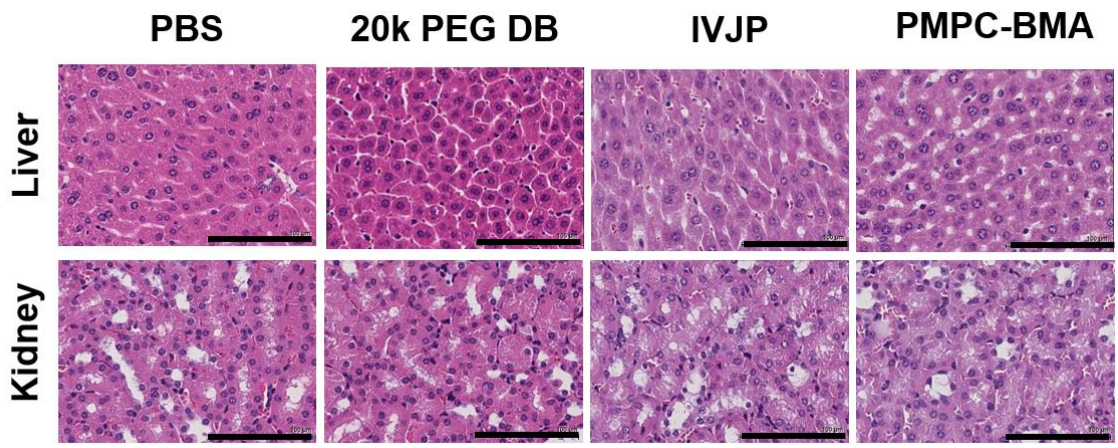

Supplemental Figure C.S8 Additional H&Es for BALB/c mice treated with each si-NP formulation. Scale bars= 100 µm

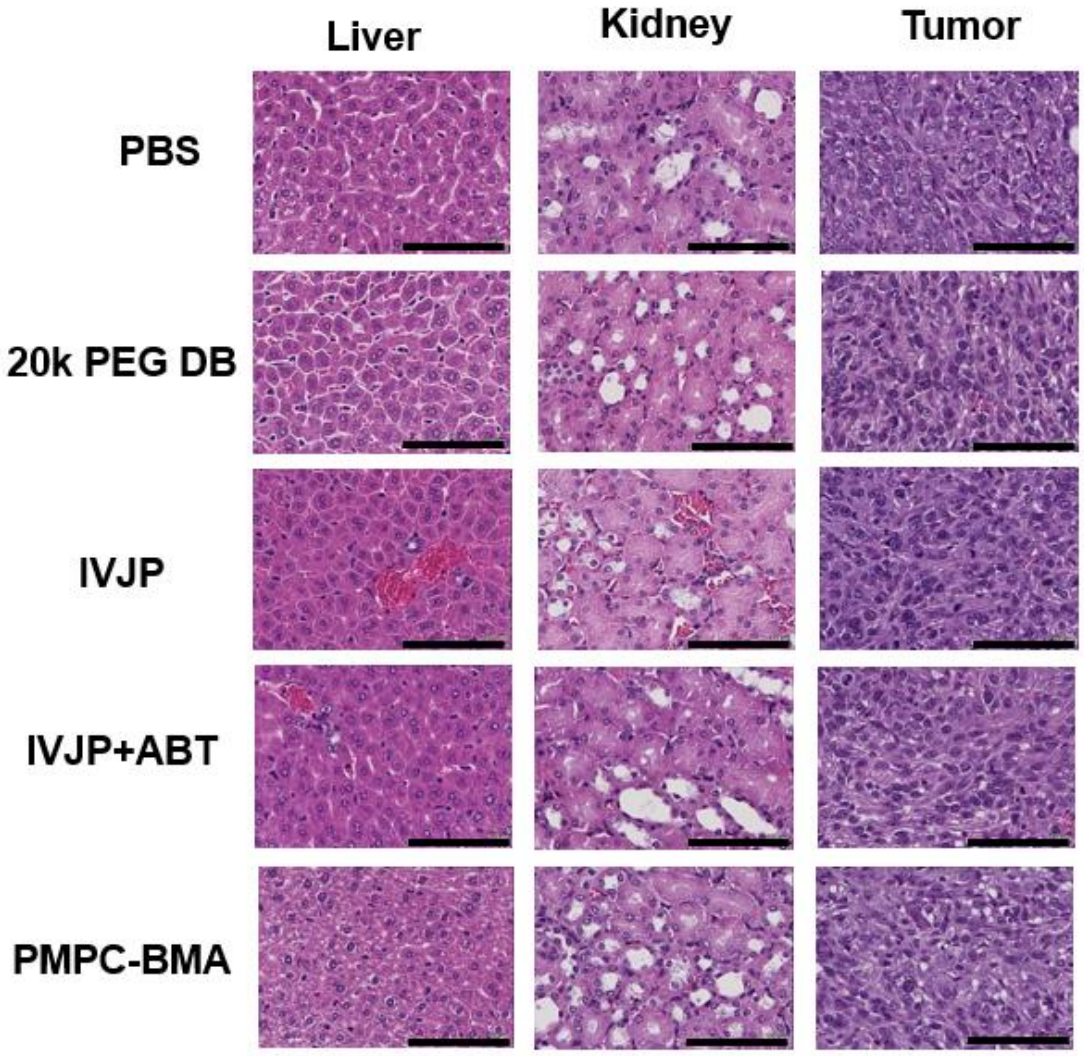

Supplemental Figure C.S9 Additional H&Es for BALB/c mice bearing 4T1 tumors and treated with each si-NP formulation. Scale bars= 100 µm

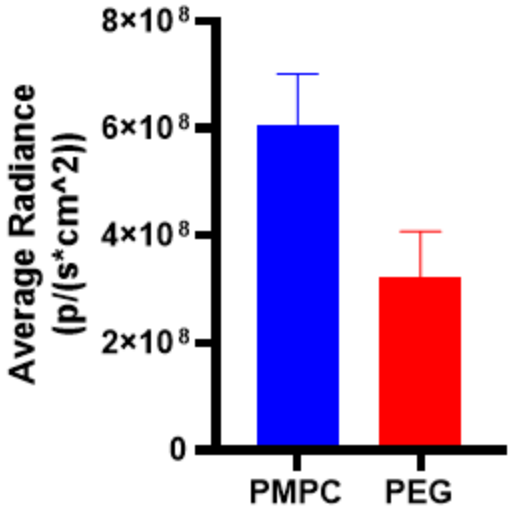

Supplemental Figure C.S10 IVIS quantification of liver fluorescence for particles containing PMPC vs. PEG coronas. Nude mice bearing MDA-MB-231 tumors were injected with 1 mg/kg of each formulation bearing Cy5-labeled nanoparticles. Fluorescence in livers was quantified at 2 hours post-injection.

BIBLIOGRAPHY

1. Setten, R. L.; Rossi, J. J.; Han, S. P. A.-O. h. o. o., The current state and future directions of RNAi-based therapeutics. LID - 10.1038/s41573-019-0017-4 [doi]. (1474-1784 (Electronic)).
2. Yang, J., Patisiran for the treatment of hereditary transthyretin-mediated amyloidosis. *Expert Rev Clin Pharmacol* **2019,** *12* (2), 95-99.
3. Levin, A. A., Treating Disease at the RNA Level with Oligonucleotides. *N Engl J Med* **2019,** *380* (1), 57-70.
4. Dang, C. V.; Reddy, E. P.; Shokat, K. M.; Soucek, L., Drugging the 'undruggable' cancer targets. *Nature Reviews Cancer* **2017,** *17*, 502.
5. Liao, D. J.; Dickson, R. B., c-Myc in breast cancer. *Endocr Relat Cancer* **2000,** *7* (3), 143-64.
6. Liedtke, C.; Mazouni, C.; Hess, K. R.; André, F.; Tordai, A.; Mejia, J. A.; Symmans, W. F.; Gonzalez-Angulo, A. M.; Hennessy, B.; Green, M.; Cristofanilli, M.; Hortobagyi, G. N.; Pusztai, L., Response to Neoadjuvant Therapy and Long-Term Survival in Patients With Triple-Negative Breast Cancer. *Journal of Clinical Oncology* **2008,** *26* (8), 1275-1281.
7. Werfel, T. A.; Wang, S.; Jackson, M. A.; Kavanaugh, T. E.; Morrison Joly, M.; Lee, L.; Hicks, D. J.; Sanchez, V.; Gonzalez-Ericsson, P. I.; Kilchrist, K. V.; Dimobi, S. C.; Sarett, S. M.; Brantley-Sieders, D. M.; Cook, R. S.; Duvall, C., Selective mTORC2 inhibitor therapeutically blocks breast cancer cell growth and survival. *Cancer Research* **2018**.
8. Viney, N. J.; van Capelleveen, J. C.; Geary, R. S.; Xia, S.; Tami, J. A.; Yu, R. Z.; Marcovina, S. M.; Hughes, S. G.; Graham, M. J.; Crooke, R. M.; Crooke, S. T.; Witztum, J. L.; Stroes, E. S.; Tsimikas, S., Antisense oligonucleotides targeting apolipoprotein(a) in people with raised lipoprotein(a): two randomised, double-blind, placebo-controlled, dose-ranging trials. *The Lancet* **2016,** *388* (10057), 2239-2253.
9. Huang, Y., Preclinical and Clinical Advances of GalNAc-Decorated Nucleic Acid Therapeutics. *Molecular Therapy - Nucleic Acids* **2017,** *6*, 116-132.
10. Wilhelm, S.; Tavares, A. J.; Dai, Q.; Ohta, S.; Audet, J.; Dvorak, H. F.; Chan, W. C. W., Analysis of nanoparticle delivery to tumours. **2016,** *1*, 16014.
11. Parhiz, H.; Khoshnejad, M.; Myerson, J. W.; Hood, E.; Patel, P. N.; Brenner, J. S.; Muzykantov, V. R., Unintended effects of drug carriers: Big issues of small particles. *Advanced Drug Delivery Reviews* **2018,** *130*, 90-112.
12. Whitehead, K. A.; Langer, R.; Anderson, D. G., Knocking down barriers: advances in siRNA delivery. *Nat Rev Drug Discov* **2009,** *8* (2), 129-138.
13. Kanasty, R.; Dorkin, J. R.; Vegas, A.; Anderson, D., Delivery materials for siRNA therapeutics. *Nat Mater* **2013,** *12* (11), 967-77.
14. Wang, J.; Lu, Z.; Wientjes, M. G.; Au, J. L., Delivery of siRNA therapeutics: barriers and carriers. *AAPS J* **2010,** *12* (4), 492-503.
15. Durymanov, M.; Reineke, J., Non-viral Delivery of Nucleic Acids: Insight Into Mechanisms of Overcoming Intracellular Barriers. *Front Pharmacol* **2018,** *9*, 971.
16. Schroeder, A.; Levins, C. G.; Cortez, C.; Langer, R.; Anderson, D. G., Lipid-based nanotherapeutics for siRNA delivery. *J Intern Med* **2010,** *267* (1), 9-21.
17. Nishiyama, N.; Kataoka, K., Current state, achievements, and future prospects of polymeric micelles as nanocarriers for drug and gene delivery. *Pharmacology & Therapeutics* **2006,** *112* (3), 630-648.

18. Behr, J.-P., *The Proton Sponge: a Trick to Enter Cells the Viruses Did Not Exploit*. 1997; Vol. 51, p 34-36.
19. Gref, R.; Lück, M.; Quellec, P.; Marchand, M.; Dellacherie, E.; Harnisch, S.; Blunk, T.; Müller, R. H., 'Stealth' corona-core nanoparticles surface modified by polyethylene glycol (PEG): influences of the corona (PEG chain length and surface density) and of the core composition on phagocytic uptake and plasma protein adsorption. *Colloids and Surfaces B: Biointerfaces* **2000,** *18* (3–4), 301-313.
20. Kunath, K.; von Harpe, A.; Petersen, H.; Fischer, D.; Voigt, K.; Kissel, T.; Bickel, U., The Structure of PEG-Modified Poly(Ethylene Imines) Influences Biodistribution and Pharmacokinetics of Their Complexes with NF-κB Decoy in Mice. *Pharmaceutical Research* **2002,** *19* (6), 810-817.
21. Nelson, C. E.; Kintzing, J. R.; Hanna, A.; Shannon, J. M.; Gupta, M. K.; Duvall, C. L., Balancing Cationic and Hydrophobic Content of PEGylated siRNA Polyplexes Enhances Endosome Escape, Stability, Blood Circulation Time, and Bioactivity in Vivo. *ACS Nano* **2013,** *7* (10), 8870-8880.
22. Jackson, M. A.; Bedingfield, S. K.; Yu, F.; Stokan, M. E.; Miles, R. E.; Curvino, E. J.; Hoogenboezem, E. N.; Bonami, R. H.; Patel, S. S.; Kendall, P. L.; Giorgio, T. D.; Duvall, C. L., Dual carrier-cargo hydrophobization and charge ratio optimization improve the systemic circulation and safety of zwitterionic nano-polyplexes. *Biomaterials* **2019,** *192*, 245-259.
23. Oe, Y.; Christie, R. J.; Naito, M.; Low, S. A.; Fukushima, S.; Toh, K.; Miura, Y.; Matsumoto, Y.; Nishiyama, N.; Miyata, K.; Kataoka, K., Actively-targeted polyion complex micelles stabilized by cholesterol and disulfide cross-linking for systemic delivery of siRNA to solid tumors. *Biomaterials* **2014,** *35* (27), 7887-7895.
24. Kim, H. J.; Ishii, T.; Zheng, M.; Watanabe, S.; Toh, K.; Matsumoto, Y.; Nishiyama, N.; Miyata, K.; Kataoka, K., Multifunctional polyion complex micelle featuring enhanced stability, targetability, and endosome escapability for systemic siRNA delivery to subcutaneous model of lung cancer. *Drug Delivery and Translational Research* **2014,** *4* (1), 50-60.
25. Zuckerman, J. E.; Choi, C. H.; Han, H.; Davis, M. E., Polycation-siRNA nanoparticles can disassemble at the kidney glomerular basement membrane. *Proc Natl Acad Sci U S A* **2012,** *109* (8), 3137-42.
26. Pelaz, B.; del Pino, P.; Maffre, P.; Hartmann, R.; Gallego, M.; Rivera-Fernández, S.; de la Fuente, J. M.; Nienhaus, G. U.; Parak, W. J., Surface Functionalization of Nanoparticles with Polyethylene Glycol: Effects on Protein Adsorption and Cellular Uptake. *ACS Nano* **2015,** *9* (7), 6996-7008.
27. Schöttler, S.; Becker, G.; Winzen, S.; Steinbach, T.; Mohr, K.; Landfester, K.; Mailänder, V.; Wurm, F. R., Protein adsorption is required for stealth effect of poly(ethylene glycol)- and poly(phosphoester)-coated nanocarriers. *Nat Nano* **2016,** *11* (4), 372-377.
28. Hatakeyama, H.; Akita, H.; Harashima, H., The Polyethyleneglycol Dilemma: Advantage and Disadvantage of PEGylation of Liposomes for Systemic Genes and Nucleic Acids Delivery to Tumors. *Biological and Pharmaceutical Bulletin* **2013,** *36* (6), 892-899.
29. Hansen, A. E.; Petersen, A. L.; Henriksen, J. R.; Boerresen, B.; Rasmussen, P.; Elema, D. R.; Rosenschöld, P. M. a.; Kristensen, A. T.; Kjær, A.; Andresen, T. L., Positron Emission Tomography Based Elucidation of the Enhanced Permeability and Retention Effect in Dogs with Cancer Using Copper-64 Liposomes. *ACS Nano* **2015,** *9* (7), 6985-6995.
30. Torchilin, V., Tumor delivery of macromolecular drugs based on the EPR effect. *Adv Drug Deliv Rev* **2011,** *63* (3), 131-5.

31. Prabhakar, U.; Maeda, H.; Jain, R. K.; Sevick-Muraca, E. M.; Zamboni, W.; Farokhzad, O. C.; Barry, S. T.; Gabizon, A.; Grodzinski, P.; Blakey, D. C., Challenges and key considerations of the enhanced permeability and retention (EPR) effect for nanomedicine drug delivery in oncology. *Cancer research* **2013,** *73* (8), 2412-2417.
32. Miller, M. A.; Gadde, S.; Pfirschke, C.; Engblom, C.; Sprachman, M. M.; Kohler, R. H.; Yang, K. S.; Laughney, A. M.; Wojtkiewicz, G.; Kamaly, N.; Bhonagiri, S.; Pittet, M. J.; Farokhzad, O. C.; Weissleder, R., Predicting therapeutic nanomedicine efficacy using a companion magnetic resonance imaging nanoparticle. *Science Translational Medicine* **2015,** *7* (314), 314ra183-314ra183.
33. Wang, A. Z., EPR or no EPR? The billion-dollar question. *Science Translational Medicine* **2015,** *7* (294), 294ec112.
34. Clark, A. J.; Wiley, D. T.; Zuckerman, J. E.; Webster, P.; Chao, J.; Lin, J.; Yen, Y.; Davis, M. E., CRLX101 nanoparticles localize in human tumors and not in adjacent, nonneoplastic tissue after intravenous dosing. *Proc Natl Acad Sci U S A* **2016,** *113* (14), 3850-4.
35. Lammers, T.; Kiessling, F.; Hennink, W. E.; Storm, G., Drug targeting to tumors: Principles, pitfalls and (pre-) clinical progress. *Journal of Controlled Release* **2012,** *161* (2), 175-187.
36. Barros, S. A.; Gollob, J. A., Safety profile of RNAi nanomedicines. *Advanced Drug Delivery Reviews* **2012,** *64* (15), 1730-1737.
37. Zuckerman, J. E.; Gritli, I.; Tolcher, A.; Heidel, J. D.; Lim, D.; Morgan, R.; Chmielowski, B.; Ribas, A.; Davis, M. E.; Yen, Y., Correlating animal and human phase Ia/Ib clinical data with CALAA-01, a targeted, polymer-based nanoparticle containing siRNA. *Proceedings of the National Academy of Sciences* **2014,** *111* (31), 11449-11454.
38. Wu, S. Y.; McMillan, N. A. J., Lipidic Systems for In Vivo siRNA Delivery. *The AAPS Journal* **2009,** *11* (4), 639-652.
39. Filion, M. C.; Phillips, N. C., Toxicity and immunomodulatory activity of liposomal vectors formulated with cationic lipids toward immune effector cells. *Biochimica et Biophysica Acta (BBA) - Biomembranes* **1997,** *1329* (2), 345-356.
40. Dass, C. R., Lipoplex-mediated delivery of nucleic acids: factors affecting in vivo transfection. *J Mol Med (Berl)* **2004,** *82* (9), 579-91.
41. Akhtar, S.; Benter, I., Toxicogenomics of non-viral drug delivery systems for RNAi: Potential impact on siRNA-mediated gene silencing activity and specificity. *Advanced Drug Delivery Reviews* **2007,** *59* (2), 164-182.
42. Lv, H.; Zhang, S.; Wang, B.; Cui, S.; Yan, J., Toxicity of cationic lipids and cationic polymers in gene delivery. *Journal of Controlled Release* **2006,** *114* (1), 100-109.
43. Jackson, M. A.; Werfel, T. A.; Curvino, E. J.; Yu, F.; Kavanaugh, T. E.; Sarett, S. M.; Dockery, M. D.; Kilchrist, K. V.; Jackson, A. N.; Giorgio, T. D.; Duvall, C. L., Zwitterionic Nanocarrier Surface Chemistry Improves siRNA Tumor Delivery and Silencing Activity Relative to Polyethylene Glycol. *ACS Nano* **2017**.
44. Schlenoff, J. B., Zwitteration: Coating Surfaces with Zwitterionic Functionality to Reduce Nonspecific Adsorption. *Langmuir* **2014,** *30* (32), 9625-9636.
45. Lewis, A. L.; Tolhurst, L. A.; Stratford, P. W., Analysis of a phosphorylcholine-based polymer coating on a coronary stent pre- and post-implantation. *Biomaterials* **2002,** *23* (7), 1697-1706.
46. Bakhai, A.; Booth, J.; Delahunty, N.; Nugara, F.; Clayton, T.; McNeill, J.; Davies, S. W.; Cumberland, D. C.; Stables, R. H., The SV stent study: a prospective, multicentre, angiographic

evaluation of the BiodivYsio phosphorylcholine coated small vessel stent in small coronary vessels. *International Journal of Cardiology* **2005,** *102* (1), 95-102.
47. Sarett, S. M.; Werfel, T. A.; Chandra, I.; Jackson, M. A.; Kavanaugh, T. E.; Hattaway, M. E.; Giorgio, T. D.; Duvall, C. L., Hydrophobic interactions between polymeric carrier and palmitic acid-conjugated siRNA improve PEGylated polyplex stability and enhance in vivo pharmacokinetics and tumor gene silencing. *Biomaterials* **2016,** *97*, 122-132.
48. Kim, H. J.; Ishii, A.; Miyata, K.; Lee, Y.; Wu, S.; Oba, M.; Nishiyama, N.; Kataoka, K., Introduction of stearoyl moieties into a biocompatible cationic polyaspartamide derivative, PAsp(DET), with endosomal escaping function for enhanced siRNA-mediated gene knockdown. *J Control Release* **2010,** *145* (2), 141-8.
49. Falamarzian, A.; Montazeri Aliabadi, H.; Molavi, O.; Seubert, J. M.; Lai, R.; Uludağ, H.; Lavasanifar, A., Effective down-regulation of signal transducer and activator of transcription 3 (STAT3) by polyplexes of siRNA and lipid-substituted polyethyleneimine for sensitization of breast tumor cells to conventional chemotherapy. *Journal of Biomedical Materials Research Part A* **2014,** *102* (9), 3216-3228.
50. Kubo, T.; Takei, Y.; Mihara, K.; Yanagihara, K.; Seyama, T., Amino-Modified and Lipid-Conjugated Dicer-Substrate siRNA Enhances RNAi Efficacy. *Bioconjugate Chemistry* **2012,** *23* (2), 164-173.
51. Resh, M. D., Myristylation and palmitylation of Src family members: The fats of the matter. *Cell 76* (3), 411-413.
52. Clements, B. A.; Incani, V.; Kucharski, C.; Lavasanifar, A.; Ritchie, B.; Uludağ, H., A comparative evaluation of poly-l-lysine-palmitic acid and Lipofectamine ™ 2000 for plasmid delivery to bone marrow stromal cells. *Biomaterials* **2007,** *28* (31), 4693-4704.
53. Nishina, K.; Unno, T.; Uno, Y.; Kubodera, T.; Kanouchi, T.; Mizusawa, H.; Yokota, T., Efficient In Vivo Delivery of siRNA to the Liver by Conjugation of α-Tocopherol. *Molecular Therapy* **2008,** *16* (4), 734-740.
54. Liu, H.; Li, Y.; Mozhi, A.; Zhang, L.; Liu, Y.; Xu, X.; Xing, J.; Liang, X.; Ma, G.; Yang, J.; Zhang, X., SiRNA-phospholipid conjugates for gene and drug delivery in cancer treatment. *Biomaterials* **2014,** *35* (24), 6519-6533.
55. Oba, M.; Miyata K Fau - Osada, K.; Osada K Fau - Christie, R. J.; Christie Rj Fau - Sanjoh, M.; Sanjoh M Fau - Li, W.; Li W Fau - Fukushima, S.; Fukushima S Fau - Ishii, T.; Ishii T Fau - Kano, M. R.; Kano Mr Fau - Nishiyama, N.; Nishiyama N Fau - Koyama, H.; Koyama H Fau - Kataoka, K.; Kataoka, K., Polyplex micelles prepared from omega-cholesteryl PEG-polycation block copolymers for systemic gene delivery. (1878-5905 (Electronic)).
56. Bishop, C. J.; Abubaker-Sharif, B.; Guiriba, T.; Tzeng, S. Y.; Green, J. J., Gene delivery polymer structure-function relationships elucidated via principal component analysis. *Chemical Communications* **2015,** *51* (60), 12134-12137.
57. Liu, Z.; Zhang, Z.; Zhou, C.; Jiao, Y., Hydrophobic modifications of cationic polymers for gene delivery. *Progress in Polymer Science* **2010,** *35* (9), 1144-1162.
58. Gary, D. J.; Min, J. B.; Kim, Y.; Park, K.; Won, Y.-Y., The Effect of N/P Ratio on the In Vitro and In Vivo Interaction Properties of PEGylated Poly(2-(dimethylamino)ethyl methacrylate)-Based siRNA Complexes. *Macromolecular bioscience* **2013,** *13* (8), 1059-1071.
59. Parhamifar, L.; Andersen, H.; Wu, L.; Hall, A.; Hudzech, D.; Moghimi, S. M., Chapter Twelve - Polycation-Mediated Integrated Cell Death Processes. In *Advances in Genetics*, Huang, L.; Liu, D.; Wagner, E., Eds. Academic Press: 2014; Vol. 88, pp 353-398.
60. Nayak, S.; Herzog, R. W., Progress and prospects: immune responses to viral vectors.

Gene Ther **2010,** *17* (3), 295-304.
61. Ozcan, G.; Ozpolat, B.; Coleman, R. L.; Sood, A. K.; Lopez-Berestein, G., Preclinical and clinical development of siRNA-based therapeutics. *Advanced Drug Delivery Reviews* **2015,** *87*, 108-119.
62. Zuckerman, J. E.; Davis, M. E., Clinical experiences with systemically administered siRNA-based therapeutics in cancer. *Nat Rev Drug Discov* **2015,** *14* (12), 843-856.
63. Ozpolat, B.; Sood, A. K.; Lopez-Berestein, G., Nanomedicine based approaches for the delivery of siRNA in cancer. *J Intern Med* **2010,** *267* (1), 44-53.
64. Nichols, J. W.; Bae, Y. H., Odyssey of a cancer nanoparticle: From injection site to site of action. *Nano Today* **2012,** *7* (6), 606-618.
65. Alexis, F.; Pridgen, E.; Molnar, L. K.; Farokhzad, O. C., Factors Affecting the Clearance and Biodistribution of Polymeric Nanoparticles. *Molecular Pharmaceutics* **2008,** *5* (4), 505-515.
66. Naeye, B.; Deschout, H.; Caveliers, V.; Descamps, B.; Braeckmans, K.; Vanhove, C.; Demeester, J.; Lahoutte, T.; De Smedt, S. C.; Raemdonck, K., In vivo disassembly of IV administered siRNA matrix nanoparticles at the renal filtration barrier. *Biomaterials* **2013,** *34* (9), 2350-2358.
67. Owens Iii, D. E.; Peppas, N. A., Opsonization, biodistribution, and pharmacokinetics of polymeric nanoparticles. *Int J Pharm* **2006,** *307* (1), 93-102.
68. Walkey, C. D.; Olsen, J. B.; Guo, H.; Emili, A.; Chan, W. C. W., Nanoparticle Size and Surface Chemistry Determine Serum Protein Adsorption and Macrophage Uptake. *Journal of the American Chemical Society* **2012,** *134* (4), 2139-2147.
69. Aggarwal, P.; Hall, J. B.; McLeland, C. B.; Dobrovolskaia, M. A.; McNeil, S. E., Nanoparticle interaction with plasma proteins as it relates to particle biodistribution, biocompatibility and therapeutic efficacy. *Advanced Drug Delivery Reviews* **2009,** *61* (6), 428-437.
70. Perry, J. L.; Reuter, K. G.; Kai, M. P.; Herlihy, K. P.; Jones, S. W.; Luft, J. C.; Napier, M.; Bear, J. E.; DeSimone, J. M., PEGylated PRINT Nanoparticles: The Impact of PEG Density on Protein Binding, Macrophage Association, Biodistribution, and Pharmacokinetics. *Nano Letters* **2012,** *12* (10), 5304-5310.
71. Miteva, M.; Kirkbride, K. C.; Kilchrist, K. V.; Werfel, T. A.; Li, H.; Nelson, C. E.; Gupta, M. K.; Giorgio, T. D.; Duvall, C. L., Tuning PEGylation of mixed micelles to overcome intracellular and systemic siRNA delivery barriers. *Biomaterials* **2015,** *38*, 97-107.
72. Zhang, Y.; Xiao, C.; Ding, J.; Li, M.; Chen, X.; Tang, Z.; Zhuang, X., A comparative study of linear, Y-shaped and linear-dendritic methoxy poly(ethylene glycol)-block-polyamidoamine-block-poly(l-glutamic acid) block copolymers for doxorubicin delivery in vitro and in vivo. *Acta Biomater* **2016,** *40*, 243-53.
73. Tockary, T. A.; Osada, K.; Chen, Q.; Machitani, K.; Dirisala, A.; Uchida, S.; Nomoto, T.; Toh, K.; Matsumoto, Y.; Itaka, K.; Nitta, K.; Nagayama, K.; Kataoka, K., Tethered PEG Crowdedness Determining Shape and Blood Circulation Profile of Polyplex Micelle Gene Carriers. *Macromolecules* **2013,** *46* (16), 6585-6592.
74. Moghimi, S. M.; Szebeni, J., Stealth liposomes and long circulating nanoparticles: critical issues in pharmacokinetics, opsonization and protein-binding properties. *Progress in Lipid Research* **2003,** *42* (6), 463-478.
75. Mishra, S.; Webster, P.; Davis, M. E., PEGylation significantly affects cellular uptake and intracellular trafficking of non-viral gene delivery particles. *Eur J Cell Biol* **2004,** *83* (3), 97-111.

76. Sin, M.-C.; Chen, S.-H.; Chang, Y., Hemocompatibility of zwitterionic interfaces and membranes. *Polym J* **2014,** *46* (8), 436-443.
77. Jin, Q.; Chen, Y.; Wang, Y.; Ji, J., Zwitterionic drug nanocarriers: A biomimetic strategy for drug delivery. *Colloids and Surfaces B: Biointerfaces* **2014,** *124*, 80-86.
78. Zou, H.; Wang, Z.; Feng, M., Nanocarriers with tunable surface properties to unblock bottlenecks in systemic drug and gene delivery. *Journal of Controlled Release* **2015,** *214*, 121-133.
79. Ukawa, M.; Akita, H.; Masuda, T.; Hayashi, Y.; Konno, T.; Ishihara, K.; Harashima, H., 2-Methacryloyloxyethyl phosphorylcholine polymer (MPC)-coating improves the transfection activity of GALA-modified lipid nanoparticles by assisting the cellular uptake and intracellular dissociation of plasmid DNA in primary hepatocytes. *Biomaterials* **2010,** *31* (24), 6355-62.
80. Yu, H.; Zou, Y.; Jiang, L.; Yin, Q.; He, X.; Chen, L.; Zhang, Z.; Gu, W.; Li, Y., Induction of apoptosis in non-small cell lung cancer by downregulation of MDM2 using pH-responsive PMPC-b-PDPA/siRNA complex nanoparticles. *Biomaterials* **2013,** *34* (11), 2738-2747.
81. Uddin, M. J.; Werfel, T. A.; Crews, B. C.; Gupta, M. K.; Kavanaugh, T. E.; Kingsley, P. J.; Boyd, K.; Marnett, L. J.; Duvall, C. L., Fluorocoxib A loaded nanoparticles enable targeted visualization of cyclooxygenase-2 in inflammation and cancer. *Biomaterials* **2016,** *92*, 71-80.
82. Roy, D.; Berguig, G. Y.; Ghosn, B.; Lane, D.; Braswell, S.; Stayton, P. S.; Convertine, A. J., Synthesis and characterization of transferrin-targeted chemotherapeutic delivery systems prepared via RAFT copolymerization of high molecular weight PEG macromonomers. *Polymer chemistry* **2014,** *5* (5), 1791-1799.
83. Crownover, E.; Duvall, C. L.; Convertine, A.; Hoffman, A. S.; Stayton, P. S., RAFT-synthesized graft copolymers that enhance pH-dependent membrane destabilization and protein circulation times. *J Control Release* **2011,** *155* (2), 167-74.
84. Swierczewska, M.; Lee, K. C.; Lee, S., What is the future of PEGylated therapies? *Expert Opinion on Emerging Drugs* **2015,** *20* (4), 531-536.
85. Colombo, C.; Gatti, S.; Ferrari, R.; Casalini, T.; Cuccato, D.; Morosi, L.; Zucchetti, M.; Moscatelli, D., Self-assembling amphiphilic PEGylated block copolymers obtained through RAFT polymerization for drug-delivery applications. *Journal of Applied Polymer Science* **2016,** *133* (11), n/a-n/a.
86. Liu, M.; Leroux, J.-C.; Gauthier, M. A., Conformation–function relationships for the comb-shaped polymer pOEGMA. *Progress in Polymer Science* **2015,** *48*, 111-121.
87. Evans, B. C.; Nelson, C. E.; Yu, S. S.; Beavers, K. R.; Kim, A. J.; Li, H.; Nelson, H. M.; Giorgio, T. D.; Duvall, C. L., Ex Vivo Red Blood Cell Hemolysis Assay for the Evaluation of pH-responsive Endosomolytic Agents for Cytosolic Delivery of Biomacromolecular Drugs. *Journal of Visualized Experiments : JoVE* **2013,** (73), 50166.
88. Albanese, A.; Tang, P. S.; Chan, W. C., The effect of nanoparticle size, shape, and surface chemistry on biological systems. *Annu Rev Biomed Eng* **2012,** *14*, 1-16.
89. Huang, R.; Lau, B. L., Biomolecule-nanoparticle interactions: Elucidation of the thermodynamics by isothermal titration calorimetry. (0006-3002 (Print)).
90. Sanchez-Moreno, P.; Buzon, P.; Boulaiz, H.; Peula-Garcia, J. M.; Ortega-Vinuesa, J. L.; Luque, I.; Salvati, A.; Marchal, J. A., Balancing the effect of corona on therapeutic efficacy and macrophage uptake of lipid nanocapsules. *Biomaterials* **2015,** *61*, 266-78.
91. Walkey, C. D.; Chan, W. C., Understanding and controlling the interaction of nanomaterials with proteins in a physiological environment. *Chem Soc Rev* **2012,** *41* (7), 2780-

99.
92. Loizou, E.; Triftaridou, A. I.; Georgiou, T. K.; Vamvakaki, M.; Patrickios, C. S., Cationic Double-Hydrophilic Model Networks: Synthesis, Characterization, Modeling and Protein Adsorption Studies. *Biomacromolecules* **2003,** *4* (5), 1150-1160.
93. Bartlett, D. W.; Davis, M. E., Physicochemical and biological characterization of targeted, nucleic acid-containing nanoparticles. *Bioconjugate chemistry* **2007,** *18* (2), 456-468.
94. Nomoto, T.; Matsumoto, Y.; Miyata, K.; Oba, M.; Fukushima, S.; Nishiyama, N.; Yamasoba, T.; Kataoka, K., In situ quantitative monitoring of polyplexes and polyplex micelles in the blood circulation using intravital real-time confocal laser scanning microscopy. *Journal of Controlled Release* **2011,** *151* (2), 104-109.
95. Jones, S. W.; Roberts, R. A.; Robbins, G. R.; Perry, J. L.; Kai, M. P.; Chen, K.; Bo, T.; Napier, M. E.; Ting, J. P. Y.; DeSimone, J. M.; Bear, J. E., Nanoparticle clearance is governed by Th1/Th2 immunity and strain background. *The Journal of Clinical Investigation 123* (7), 3061-3073.
96. Christie, R. J.; Matsumoto, Y.; Miyata, K.; Nomoto, T.; Fukushima, S.; Osada, K.; Halnaut, J.; Pittella, F.; Kim, H. J.; Nishiyama, N.; Kataoka, K., Targeted Polymeric Micelles for siRNA Treatment of Experimental Cancer by Intravenous Injection. *ACS Nano* **2012,** *6* (6), 5174-5189.
97. Bartlett, D. W.; Su, H.; Hildebrandt, I. J.; Weber, W. A.; Davis, M. E., Impact of tumor-specific targeting on the biodistribution and efficacy of siRNA nanoparticles measured by multimodality in vivo imaging. *Proc Natl Acad Sci U S A* **2007,** *104* (39), 15549-54.
98. Dahlman, J. E.; Barnes, C.; Khan, O. F.; Thiriot, A.; Jhunjunwala, S.; Shaw, T. E.; Xing, Y.; Sager, H. B.; Sahay, G.; Speciner, L.; Bader, A.; Bogorad, R. L.; Yin, H.; Racie, T.; Dong, Y.; Jiang, S.; Seedorf, D.; Dave, A.; Singh Sandhu, K.; Webber, M. J.; Novobrantseva, T.; Ruda, V. M.; Lytton-JeanAbigail, K. R.; Levins, C. G.; Kalish, B.; Mudge, D. K.; Perez, M.; Abezgauz, L.; Dutta, P.; Smith, L.; Charisse, K.; Kieran, M. W.; Fitzgerald, K.; Nahrendorf, M.; Danino, D.; Tuder, R. M.; von Andrian, U. H.; Akinc, A.; Panigrahy, D.; Schroeder, A.; Koteliansky, V.; Langer, R.; Anderson, D. G., In vivo endothelial siRNA delivery using polymeric nanoparticles with low molecular weight. *Nat Nano* **2014,** *9* (8), 648-655.
99. Huang, Y.; Lin, D.; Jiang, Q.; Zhang, W.; Guo, S.; Xiao, P.; Zheng, S.; Wang, X.; Chen, H.; Zhang, H. Y.; Deng, L.; Xing, J.; Du, Q.; Dong, A.; Liang, Z., Binary and ternary complexes based on polycaprolactone-graft-poly (N, N-dimethylaminoethyl methacrylate) for targeted siRNA delivery. *Biomaterials* **2012,** *33* (18), 4653-64.
100. Liu, X.; Chen, Y.; Li, H.; Huang, N.; Jin, Q.; Ren, K.; Ji, J., Enhanced Retention and Cellular Uptake of Nanoparticles in Tumors by Controlling Their Aggregation Behavior. *ACS Nano* **2013,** *7* (7), 6244-6257.
101. Liu, X.; Li, H.; Chen, Y.; Jin, Q.; Ren, K.; Ji, J., Mixed-charge nanoparticles for long circulation, low reticuloendothelial system clearance, and high tumor accumulation. *Adv Healthc Mater* **2014,** *3* (9), 1439-47.
102. Wang, J.; Yuan, S.; Zhang, Y.; Wu, W.; Hu, Y.; Jiang, X., The effects of poly(zwitterions)s versus poly(ethylene glycol) surface coatings on the biodistribution of protein nanoparticles. *Biomater Sci* **2016,** *4* (9), 1351-60.
103. Zhou, W.; Shao, J.; Jin, Q.; Wei, Q.; Tang, J.; Ji, J., Zwitterionic phosphorylcholine as a better ligand for gold nanorods cell uptake and selective photothermal ablation of cancer cells. *Chemical Communications* **2010,** *46* (9), 1479-1481.
104. Tu, S.; Chen, Y. W.; Qiu, Y. B.; Zhu, K.; Luo, X. L., Enhancement of cellular uptake and

antitumor efficiencies of micelles with phosphorylcholine. *Macromol Biosci* **2011,** *11* (10), 1416-25.
105. Chen, L.; Wang, H.; Zhang, Y.; Wang, Y.; Hu, Q.; Ji, J., Bioinspired phosphorylcholine-modified polyplexes as an effective strategy for selective uptake and transfection of cancer cells. *Colloids and Surfaces B: Biointerfaces* **2013,** *111*, 297-305.
106. Murdoch, C.; Reeves, K. J.; Hearnden, V.; Colley, H.; Massignani, M.; Canton, I.; Madsen, J.; Blanazs, A.; Armes, S. P.; Lewis, A. L.; MacNeil, S.; Brown, N. J.; Thornhill, M. H.; Battaglia, G., Internalization and biodistribution of polymersomes into oral squamous cell carcinoma cells in vitro and in vivo. *Nanomedicine* **2010,** *5* (7), 1025-1036.
107. Eliyahu, G.; Kreizman, T.; Degani, H., Phosphocholine as a biomarker of breast cancer: Molecular and biochemical studies. *International Journal of Cancer* **2007,** *120* (8), 1721-1730.
108. Chen, Q.; Osada, K.; Ge, Z.; Uchida, S.; Tockary, T. A.; Dirisala, A.; Matsui, A.; Toh, K.; Takeda, K. M.; Liu, X.; Nomoto, T.; Ishii, T.; Oba, M.; Matsumoto, Y.; Kataoka, K., Polyplex micelle installing intracellular self-processing functionalities without free catiomers for safe and efficient systemic gene therapy through tumor vasculature targeting. *Biomaterials* **2017,** *113*, 253-265.
109. Convertine, A. J.; Benoit, D. S.; Duvall, C. L.; Hoffman, A. S.; Stayton, P. S., Development of a novel endosomolytic diblock copolymer for siRNA delivery. *J Control Release* **2009,** *133* (3), 221-9.
110. Nelson, C. E.; Gupta, M. K.; Adolph, E. J.; Shannon, J. M.; Guelcher, S. A.; Duvall, C. L., Sustained local delivery of siRNA from an injectable scaffold. *Biomaterials* **2012,** *33* (4), 1154-1161.
111. Nelson, C. E.; Kim, A. J.; Adolph, E. J.; Gupta, M. K.; Yu, F.; Hocking, K. M.; Davidson, J. M.; Guelcher, S. A.; Duvall, C. L., Tunable Delivery of siRNA from a Biodegradable Scaffold to Promote Angiogenesis In Vivo. *Advanced Materials* **2014,** *26* (4), 607-614.
112. Adams, D.; Gonzalez-Duarte, A.; O'Riordan, W.; Yang, C.-C.; Yamashita, T.; Kristen, A.; Tournev, I.; Schmidt, H.; Coelho, T.; Berk, J. L.; Lin, K.-P.; Dyck, P. J.; Gandhi, P.; Sweetser, M.; Chen, J.; Goyal, S.; Gollob, J.; Suhr, O., Patisiran, an Investigational RNAi Therapeutic for Patients with Hereditary Transthyretin-Mediated (hATTR) Amyloidosis with Polyneuropathy: Results from the Phase 3 APOLLO study (CT.001). *Neurology* **2018,** *90* (15 Supplement).
113. Haussecker, D., Current issues of RNAi therapeutics delivery and development. *J Control Release* **2014,** *195*, 49-54.
114. Kaczmarek, J. C.; Kowalski, P. S.; Anderson, D. G., Advances in the delivery of RNA therapeutics: from concept to clinical reality. *Genome Medicine* **2017,** *9*, 60.
115. Li, H.; Nelson, C. E.; Evans, B. C.; Duvall, C. L., Delivery of intracellular-acting biologics in pro-apoptotic therapies. *Curr Pharm Des* **2011,** *17* (3), 293-319.
116. Wittrup, A.; Lieberman, J., Knocking down disease: a progress report on siRNA therapeutics. *Nat Rev Genet* **2015,** *16* (9), 543-552.
117. Papahadjopoulos, D.; Allen, T. M.; Gabizon, A.; Mayhew, E.; Matthay, K.; Huang, S. K.; Lee, K. D.; Woodle, M. C.; Lasic, D. D.; Redemann, C., Sterically stabilized liposomes: improvements in pharmacokinetics and antitumor therapeutic efficacy. *Proc Natl Acad Sci U S A* **1991,** *88* (24), 11460-4.
118. Werfel, T. A.; Jackson, M. A.; Kavanaugh, T. E.; Kirkbride, K. C.; Miteva, M.; Giorgio, T. D.; Duvall, C., Combinatorial optimization of PEG architecture and hydrophobic content

improves ternary siRNA polyplex stability, pharmacokinetics, and potency in vivo. *Journal of Controlled Release* **2017,** *255*, 12-26.
119. Sarett, S. M.; Werfel, T. A.; Lee, L.; Jackson, M. A.; Kilchrist, K. V.; Brantley-Sieders, D.; Duvall, C. L., Lipophilic siRNA targets albumin in situ and promotes bioavailability, tumor penetration, and carrier-free gene silencing. *Proceedings of the National Academy of Sciences* **2017**.
120. Gabizon, A.; Papahadjopoulos, D., Liposome formulations with prolonged circulation time in blood and enhanced uptake by tumors. *Proceedings of the National Academy of Sciences* **1988,** *85* (18), 6949.
121. Gabizon, A.; Catane, R.; Uziely, B.; Kaufman, B.; Safra, T.; Cohen, R.; Martin, F.; Huang, A.; Barenholz, Y., Prolonged Circulation Time and Enhanced Accumulation in Malignant Exudates of Doxorubicin Encapsulated in Polyethylene-glycol Coated Liposomes. *Cancer Research* **1994,** *54* (4), 987.
122. Blanco, E.; Shen, H.; Ferrari, M., Principles of nanoparticle design for overcoming biological barriers to drug delivery. *Nature Biotechnology* **2015,** *33*, 941.
123. Agarwal, S.; Zhang, Y.; Maji, S.; Greiner, A., PDMAEMA based gene delivery materials. *Materials Today* **2012,** *15* (9), 388-393.
124. Sato, A.; Choi, S. W.; Hirai, M.; Yamayoshi, A.; Moriyama, R.; Yamano, T.; Takagi, M.; Kano, A.; Shimamoto, A.; Maruyama, A., Polymer brush-stabilized polyplex for a siRNA carrier with long circulatory half-life. *Journal of Controlled Release* **2007,** *122* (3), 209-216.
125. Merkel, O. M.; Librizzi, D.; Pfestroff, A.; Schurrat, T.; Buyens, K.; Sanders, N. N.; De Smedt, S. C.; Béhé, M.; Kissel, T., Stability of siRNA polyplexes from poly(ethylenimine) and poly(ethylenimine)-g-poly(ethylene glycol) under in vivo conditions: Effects on pharmacokinetics and biodistribution measured by Fluorescence Fluctuation Spectroscopy and Single Photon Emission Computed Tomography (SPECT) imaging. *Journal of Controlled Release* **2009,** *138* (2), 148-159.
126. Naahidi, S.; Jafari, M.; Edalat, F.; Raymond, K.; Khademhosseini, A.; Chen, P., Biocompatibility of engineered nanoparticles for drug delivery. *Journal of Controlled Release* **2013,** *166* (2), 182-194.
127. Breunig, M.; Lungwitz, U.; Liebl, R.; Goepferich, A., Breaking up the correlation between efficacy and toxicity for nonviral gene delivery. *Proc Natl Acad Sci U S A* **2007,** *104* (36), 14454-9.
128. Kim, H. J.; Kim, A.; Miyata, K.; Kataoka, K., Recent progress in development of siRNA delivery vehicles for cancer therapy. *Adv Drug Deliv Rev* **2016,** *104*, 61-77.
129. Green, J. J.; Langer, R.; Anderson, D. G., A Combinatorial Polymer Library Approach Yields Insight into Nonviral Gene Delivery. *Accounts of Chemical Research* **2008,** *41* (6), 749-759.
130. Siegwart, D. J.; Whitehead, K. A.; Nuhn, L.; Sahay, G.; Cheng, H.; Jiang, S.; Ma, M.; Lytton-Jean, A.; Vegas, A.; Fenton, P.; Levins, C. G.; Love, K. T.; Lee, H.; Cortez, C.; Collins, S. P.; Li, Y. F.; Jang, J.; Querbes, W.; Zurenko, C.; Novobrantseva, T.; Langer, R.; Anderson, D. G., Combinatorial synthesis of chemically diverse core-shell nanoparticles for intracellular delivery. *Proceedings of the National Academy of Sciences* **2011,** *108* (32), 12996.
131. Cabral, H.; Miyata, K.; Osada, K.; Kataoka, K., Block Copolymer Micelles in Nanomedicine Applications. *Chemical Reviews* **2018**.
132. Fitzsimmons, R. E. B.; Uludağ, H., Specific effects of PEGylation on gene delivery efficacy of polyethylenimine: Interplay between PEG substitution and N/P ratio. *Acta*

Biomaterialia **2012,** *8* (11), 3941-3955.
133. Malek, A.; Merkel, O.; Fink, L.; Czubayko, F.; Kissel, T.; Aigner, A., In vivo pharmacokinetics, tissue distribution and underlying mechanisms of various PEI(–PEG)/siRNA complexes. *Toxicology and Applied Pharmacology* **2009,** *236* (1), 97-108.
134. Verbaan, F.; van Dam, I.; Takakura, Y.; Hashida, M.; Hennink, W.; Storm, G.; Oussoren, C., Intravenous fate of poly(2-(dimethylamino)ethyl methacrylate)-based polyplexes. *European Journal of Pharmaceutical Sciences* **2003,** *20* (4), 419-427.
135. Kawakami, S.; Ito, Y.; Charoensit, P.; Yamashita, F.; Hashida, M., Evaluation of Proinflammatory Cytokine Production Induced by Linear and Branched Polyethylenimine/Plasmid DNA Complexes in Mice. *Journal of Pharmacology and Experimental Therapeutics* **2006,** *317* (3), 1382.
136. Yue, Y.; Jin, F.; Deng, R.; Cai, J.; Chen, Y.; Lin, M. C. M.; Kung, H.-F.; Wu, C., Revisit complexation between DNA and polyethylenimine — Effect of uncomplexed chains free in the solution mixture on gene transfection. *Journal of Controlled Release* **2011,** *155* (1), 67-76.
137. Thibault, M.; Astolfi, M.; Tran-Khanh, N.; Lavertu, M.; Darras, V.; Merzouki, A.; Buschmann, M. D., Excess polycation mediates efficient chitosan-based gene transfer by promoting lysosomal release of the polyplexes. *Biomaterials* **2011,** *32* (20), 4639-4646.
138. Verbaan, F. J.; Klouwenberg, P. K.; Steenis, J. H. v.; Snel, C. J.; Boerman, O.; Hennink, W. E.; Storm, G., Application of poly(2-(dimethylamino)ethyl methacrylate)-based polyplexes for gene transfer into human ovarian carcinoma cells. *International Journal of Pharmaceutics* **2005,** *304* (1), 185-192.
139. Zhang, P.; Sun, F.; Tsao, C.; Liu, S.; Jain, P.; Sinclair, A.; Hung, H. C.; Bai, T.; Wu, K.; Jiang, S., Zwitterionic gel encapsulation promotes protein stability, enhances pharmacokinetics, and reduces immunogenicity. *Proc Natl Acad Sci U S A* **2015,** *112* (39), 12046-51.
140. Men, Y.; Peng, S.; Yang, P.; Jiang, Q.; Zhang, Y.; Shen, B.; Dong, P.; Pang, Z.; Yang, W., Biodegradable Zwitterionic Nanogels with Long Circulation for Antitumor Drug Delivery. *ACS Applied Materials & Interfaces* **2018,** *10* (28), 23509-23521.
141. Kim, H. J.; Miyata, K.; Nomoto, T.; Zheng, M.; Kim, A.; Liu, X.; Cabral, H.; Christie, R. J.; Nishiyama, N.; Kataoka, K., siRNA delivery from triblock copolymer micelles with spatially-ordered compartments of PEG shell, siRNA-loaded intermediate layer, and hydrophobic core. *Biomaterials* **2014,** *35* (15), 4548-56.
142. Ambardekar, V. V.; Han, H. Y.; Varney, M. L.; Vinogradov, S. V.; Singh, R. K.; Vetro, J. A., The modification of siRNA with 3' cholesterol to increase nuclease protection and suppression of native mRNA by select siRNA polyplexes. *Biomaterials* **2011,** *32* (5), 1404-11.
143. Betker, J. L.; Anchordoquy, T. J., Effect of charge ratio on lipoplex-mediated gene delivery and liver toxicity. *Therapeutic Delivery* **2015,** *6* (11), 1243-1253.
144. Maeda, H.; Nakamura, H.; Fang, J., The EPR effect for macromolecular drug delivery to solid tumors: Improvement of tumor uptake, lowering of systemic toxicity, and distinct tumor imaging in vivo. *Adv Drug Deliv Rev* **2013,** *65* (1), 71-9.
145. Zheng, M.; Librizzi, D.; Kılıç, A.; Liu, Y.; Renz, H.; Merkel, O. M.; Kissel, T., Enhancing in vivo circulation and siRNA delivery with biodegradable polyethylenimine-graft-polycaprolactone-block-poly(ethylene glycol) copolymers. *Biomaterials* **2012,** *33* (27), 6551-6558.
146. Christie, R. J.; Miyata, K.; Matsumoto, Y.; Nomoto, T.; Menasco, D.; Lai, T. C.; Pennisi, M.; Osada, K.; Fukushima, S.; Nishiyama, N.; Yamasaki, Y.; Kataoka, K., Effect of Polymer Structure on Micelles Formed between siRNA and Cationic Block Copolymer Comprising

Thiols and Amidines. *Biomacromolecules* **2011,** *12* (9), 3174-3185.
147. Rahman, A. H.; Aloman, C., Dendritic cells and liver fibrosis. *Biochimica et Biophysica Acta (BBA) - Molecular Basis of Disease* **2013,** *1832* (7), 998-1004.
148. Heymann, F.; Tacke, F., Immunology in the liver — from homeostasis to disease. *Nature Reviews Gastroenterology &Amp; Hepatology* **2016,** *13*, 88.
149. Lau, A. H.; Thomson, A. W., Dendritic cells and immune regulation in the liver. *Gut* **2003,** *52* (2), 307-314.
150. Robinson, M. W.; Harmon, C.; O'Farrelly, C., Liver immunology and its role in inflammation and homeostasis. *Cellular &Amp; Molecular Immunology* **2016,** *13*, 267.
151. Zhang, P.; Sun, F.; Liu, S.; Jiang, S., Anti-PEG antibodies in the clinic: Current issues and beyond PEGylation. *J Control Release* **2016,** *244* (Pt B), 184-193.
152. Hsieh, Y.-C.; Wang, H.-E.; Lin, W.-W.; Roffler, S. R.; Cheng, T.-C.; Su, Y.-C.; Li, J.-J.; Chen, C.-C.; Huang, C.-H.; Chen, B.-M.; Wang, J.-Y.; Cheng, T.-L.; Chen, F.-M., Pre-existing anti-polyethylene glycol antibody reduces the therapeutic efficacy and pharmacokinetics of PEGylated liposomes. *Theranostics* **2018,** *8* (11), 3164-3175.
153. Qi, Y.; Simakova, A.; Ganson, N. J.; Li, X.; Luginbuhl, K. M.; Ozer, I.; Liu, W.; Hershfield, M. S.; Matyjaszewski, K.; Chilkoti, A., A brush-polymer/exendin-4 conjugate reduces blood glucose levels for up to five days and eliminates poly(ethylene glycol) antigenicity. *Nature Biomedical Engineering* **2016,** *1*, 0002.
154. Ishihara, T.; Takeda, M.; Sakamoto, H.; Kimoto, A.; Kobayashi, C.; Takasaki, N.; Yuki, K.; Tanaka, K.; Takenaga, M.; Igarashi, R.; Maeda, T.; Yamakawa, N.; Okamoto, Y.; Otsuka, M.; Ishida, T.; Kiwada, H.; Mizushima, Y.; Mizushima, T., Accelerated blood clearance phenomenon upon repeated injection of PEG-modified PLA-nanoparticles. *Pharm Res* **2009,** *26* (10), 2270-9.
155. Ishihara, T.; Maeda, T.; Sakamoto, H.; Takasaki, N.; Shigyo, M.; Ishida, T.; Kiwada, H.; Mizushima, Y.; Mizushima, T., Evasion of the Accelerated Blood Clearance Phenomenon by Coating of Nanoparticles with Various Hydrophilic Polymers. *Biomacromolecules* **2010,** *11* (10), 2700-2706.
156. Leroueil, P. R.; Hong, S.; Mecke, A.; Baker, J. R.; Orr, B. G.; Banaszak Holl, M. M., Nanoparticle Interaction with Biological Membranes: Does Nanotechnology Present a Janus Face? *Accounts of Chemical Research* **2007,** *40* (5), 335-342.
157. Chen, J.; Hessler, J. A.; Putchakayala, K.; Panama, B. K.; Khan, D. P.; Hong, S.; Mullen, D. G.; DiMaggio, S. C.; Som, A.; Tew, G. N.; Lopatin, A. N.; Baker, J. R.; Holl, M. M. B.; Orr, B. G., Cationic Nanoparticles Induce Nanoscale Disruption in Living Cell Plasma Membranes. *The Journal of Physical Chemistry B* **2009,** *113* (32), 11179-11185.
158. Moghimi, S. M.; Symonds, P.; Murray, J. C.; Hunter, A. C.; Debska, G.; Szewczyk, A., A two-stage poly(ethylenimine)-mediated cytotoxicity: implications for gene transfer/therapy. *Mol Ther* **2005,** *11* (6), 990-5.
159. Grandinetti, G.; Smith, A. E.; Reineke, T. M., Membrane and nuclear permeabilization by polymeric pDNA vehicles: efficient method for gene delivery or mechanism of cytotoxicity? *Mol Pharm* **2012,** *9* (3), 523-38.
160. Ballarín-González, B.; Howard, K. A., Polycation-based nanoparticle delivery of RNAi therapeutics: Adverse effects and solutions. *Advanced Drug Delivery Reviews* **2012,** *64* (15), 1717-1729.
161. Rizk, M.; Tüzmen, Ş., Update on the clinical utility of an RNA interference-based treatment: focus on Patisiran. *Pharmacogenomics and personalized medicine* **2017,** *10*, 267-278.

162. Hall, A.; Lachelt, U.; Bartek, J.; Wagner, E.; Moghimi, S. M., Polyplex Evolution: Understanding Biology, Optimizing Performance. *Mol Ther* **2017,** *25* (7), 1476-1490.
163. Hwang, T.-L.; Aljuffali, I. A.; Lin, C.-F.; Chang, Y.-T.; Fang, J.-Y., Cationic additives in nanosystems activate cytotoxicity and inflammatory response of human neutrophils: lipid nanoparticles versus polymeric nanoparticles. *International journal of nanomedicine* **2015,** *10*, 371-385.
164. Merkel, O. M.; Urbanics, R.; Bedőcs, P.; Rozsnyay, Z.; Rosivall, L.; Toth, M.; Kissel, T.; Szebeni, J., In vitro and in vivo complement activation and related anaphylactic effects associated with polyethylenimine and polyethylenimine-graft-poly(ethylene glycol) block copolymers. *Biomaterials* **2011,** *32* (21), 4936-4942.
165. Chollet, P.; Favrot Mc Fau - Hurbin, A.; Hurbin A Fau - Coll, J.-L.; Coll, J. L., Side-effects of a systemic injection of linear polyethylenimine-DNA complexes. (1099-498X (Print)).
166. Ogris, M.; Brunner, S.; Schuller, S.; Kircheis, R.; Wagner, E., PEGylated DNA/transferrin-PEI complexes: reduced interaction with blood components, extended circulation in blood and potential for systemic gene delivery. *Gene Ther* **1999,** *6* (4), 595-605.
167. Merdan, T.; Kunath, K.; Petersen, H.; Bakowsky, U.; Voigt, K. H.; Kopecek, J.; Kissel, T., PEGylation of Poly(ethylene imine) Affects Stability of Complexes with Plasmid DNA under in Vivo Conditions in a Dose-Dependent Manner after Intravenous Injection into Mice. *Bioconjugate Chemistry* **2005,** *16* (4), 785-792.
168. Moghimi, S. M., Complement Propriety and Conspiracy in Nanomedicine: Perspective and a Hypothesis. *Nucleic Acid Ther* **2016,** *26* (2), 67-72.
169. Zuckerman, J. E.; Gritli, I.; Tolcher, A.; Heidel, J. D.; Lim, D.; Morgan, R.; Chmielowski, B.; Ribas, A.; Davis, M. E.; Yen, Y., Correlating animal and human phase Ia/Ib clinical data with CALAA-01, a targeted, polymer-based nanoparticle containing siRNA. *Proc Natl Acad Sci U S A* **2014,** *111* (31), 11449-54.
170. Xu, Z.; Smith, J. S.; Tian, J.; Byrnes, A. P., Induction of shock after intravenous injection of adenovirus vectors: a critical role for platelet-activating factor. *Mol Ther* **2010,** *18* (3), 609-16.
171. Schiedner, G.; Bloch, W.; Hertel, S.; Johnston, M.; Molojavyi, A.; Dries, V.; Varga, G.; Van Rooijen, N.; Kochanek, S., A hemodynamic response to intravenous adenovirus vector particles is caused by systemic Kupffer cell-mediated activation of endothelial cells. *Hum Gene Ther* **2003,** *14* (17), 1631-41.
172. Gill, P.; Jindal, N. L.; Jagdis, A.; Vadas, P., Platelets in the immune response: Revisiting platelet-activating factor in anaphylaxis. *Journal of Allergy and Clinical Immunology* **2015,** *135* (6), 1424-1432.
173. Upton, J.; Vadas, P., Potential Therapeutic Strategies for Severe Anaphylaxis Targeting Platelet-Activating Factor and PAF Acetylhydrolase. *Current Treatment Options in Allergy* **2014,** *1* (3), 232-246.
174. Weijer, S.; Rijneveld, A. W.; van der Poll, T.; Speelman, P.; Florquin, S.; Ishii, S.; Shimizu, T., Improved Host Defense against Pneumococcal Pneumonia in Platelet-Activating Factor Receptor-Deficient Mice. *The Journal of Infectious Diseases* **2004,** *189* (4), 711-716.
175. Iñarrea, P.; Alonso, F.; Sanchez-Crespo, M., Platelet-activating factor: An effector substance of the vasopermeability changes induced by the infusion of immune aggregates in the mouse. *Immunopharmacology* **1983,** *6* (1), 7-14.
176. Albert, D. H.; Magoc, T. J.; Tapang, P.; Luo, G.; Morgan, D. W.; Curtin, M.; Sheppard, G. S.; Xu, L.; Heyman, H. R.; Davidsen, S. K.; Summers, J. B.; Carter, G. W., Pharmacology of ABT-491, a highly potent platelet-activating factor receptor antagonist. *European Journal of*

Pharmacology **1997,** *325* (1), 69-80.
177. Yamamoto, Y.; Sugimura, R.; Watanabe, T.; Shigemori, S.; Okajima, T.; Nigar, S.; Namai, F.; Sato, T.; Ogita, T.; Shimosato, T., Class A CpG Oligonucleotide Priming Rescues Mice from Septic Shock via Activation of Platelet-Activating Factor Acetylhydrolase. *Front Immunol* **2017,** *8*, 1049.
178. Decker, K., Biologically active products of stimulated liver macrophages (Kupffer cells). *Eur J Biochem* **1990,** *192* (2), 245-61.
179. Ying, W.; Cheruku, P. S.; Bazer, F. W.; Safe, S. H.; Zhou, B., Investigation of macrophage polarization using bone marrow derived macrophages. *J Vis Exp* **2013,** (76).
180. Albert, D. H.; Malo, P. E.; Tapang, P.; Shaughnessy, T. K.; Morgan, D. W.; Wegner, C. D.; Curtin, M. L.; Sheppard, G. S.; Xu, L.; Davidsen, S. K.; Summers, J. B.; Carter, G. W., The Role of Platelet-Activating Factor (PAF) and the Efficacy of ABT-491, a Highly Potent and Selective PAF Antagonist, in Experimental Allergic Rhinitis. *Journal of Pharmacology and Experimental Therapeutics* **1998,** *284* (1), 83.
181. Kelefiotis, D.; Vakirtzi-Lemonias, C., In vivo responses of mouse blood cells to platelet-activating factor (PAF): role of the mediators of anaphylaxis. *Agents Actions* **1993,** *40* (3-4), 150-6.
182. Au - Wick, M. J.; Au - Harral, J. W.; Au - Loomis, Z. L.; Au - Dempsey, E. C., An Optimized Evans Blue Protocol to Assess Vascular Leak in the Mouse. *JoVE* **2018,** (139), e57037.
183. Ramírez, M. a. M.; Quardt, S. M.; Kim, D.; Oshiro, H.; Minnicozzi, M.; Durán, W. N., Platelet Activating Factor Modulates Microvascular Permeability through Nitric Oxide Synthesis. *Microvascular Research* **1995,** *50* (2), 223-234.
184. Montrucchio, G.; Alloatti, G.; Camussi, G., Role of platelet-activating factor in cardiovascular pathophysiology. *Physiol Rev* **2000,** *80* (4), 1669-99.
185. Hergott, C. B.; Roche, A. M.; Naidu, N. A.; Mesaros, C.; Blair, I. A.; Weiser, J. N., Bacterial exploitation of phosphorylcholine mimicry suppresses inflammation to promote airway infection. *The Journal of Clinical Investigation* **2015,** *125* (10), 3878-3890.
186. Tanaka, T.; Iimori, M.; Tsukatani, H.; Tokumura, A., Platelet-aggregating effects of platelet-activating factor-like phosphollpids formed by oxidation of phosphatidylcholines containing an sn-2-polyunsaturated fatty acyl group. *Biochimica et Biophysica Acta (BBA) - Lipids and Lipid Metabolism* **1994,** *1210* (2), 202-208.
187. van Rooijen, N.; Hendrikx, E., Liposomes for specific depletion of macrophages from organs and tissues. *Methods Mol Biol* **2010,** *605*, 189-203.
188. Mencia-Huerta, J. M.; Benveniste, J., Platelet-activating factor (PAF-acether) and macrophages: II. Phagocytosis-associated release of PAF-acether from rat peritoneal macrophages. *Cellular Immunology* **1981,** *57* (2), 281-292.
189. Yang, Y.; Harvey, S. A. K.; Gandhi, C. R., Kupffer cells are a major source of increased platelet activating factor in the CCl4-induced cirrhotic rat liver. *Journal of Hepatology* **2003,** *39* (2), 200-207.
190. Sakagami, Y.; Mizoguchi, Y.; Seki, S.; Kobayashi, K.; Morisawa, S.; Yamamoto, S., Release of peptide leukotrienes from rat kupffer cells. *Biochemical and Biophysical Research Communications* **1988,** *156* (1), 217-221.
191. Shindou, H.; Shiraishi, S.; Tokuoka, S. M.; Takahashi, Y.; Harayama, T.; Abe, T.; Bando, K.; Miyano, K.; Kita, Y.; Uezono, Y.; Shimizu, T., Relief from neuropathic pain by blocking of the platelet-activating factor-pain loop. (1530-6860 (Electronic)).

192. Li, Z.; Vance, D. E., Thematic Review Series: Glycerolipids. Phosphatidylcholine and choline homeostasis. *Journal of Lipid Research* **2008,** *49* (6), 1187-1194.
193. Smith, J. S.; Xu, Z.; Tian, J.; Palmer, D. J.; Ng, P.; Byrnes, A. P., The role of endosomal escape and mitogen-activated protein kinases in adenoviral activation of the innate immune response. *PloS one* **2011,** *6* (10), e26755-e26755.
194. Baljon, J. J.; Dandy, A.; Wang-Bishop, L.; Wehbe, M.; Jacobson, M. E.; Wilson, J. T., The efficiency of cytosolic drug delivery using pH-responsive endosomolytic polymers does not correlate with activation of the NLRP3 inflammasome. *Biomaterials Science* **2019**.
195. Vlasova, M. A.; Tarasova, O. S.; Riikonen, J.; Raula, J.; Lobach, A. S.; Borzykh, A. A.; Smirin, B. V.; Kauppinen, E. I.; Eletskii, A. V.; Herzig, K.-H.; Salonen, J.; Tavi, P.; Lehto, V.-P.; Järvinen, K., Injected nanoparticles: The combination of experimental systems to assess cardiovascular adverse effects. *European Journal of Pharmaceutics and Biopharmaceutics* **2014,** *87* (1), 64-72.
196. Yu, X.; Hong, F.; Zhang, Y.-Q., Bio-effect of nanoparticles in the cardiovascular system. *Journal of Biomedical Materials Research Part A* **2016,** *104* (11), 2881-2897.
197. Pande, K.; Ueda, R.; Machemer, T.; Sathe, M.; Tsai, V.; Brin, E.; Delano, M. J.; Van Rooijen, N.; McClanahan, T. K.; Talmadge, J. E.; Moldawer, L. L.; Phillips, J. H.; LaFace, D. M., Cancer-induced expansion and activation of CD11b+ Gr-1+ cells predispose mice to adenoviral-triggered anaphylactoid-type reactions. *Molecular therapy : the journal of the American Society of Gene Therapy* **2009,** *17* (3), 508-515.
198. Frohlich, E., Action of Nanoparticles on Platelet Activation and Plasmatic Coagulation. *Curr Med Chem* **2016,** *23* (5), 408-30.
199. Peng, F.; Setyawati, M. I.; Tee, J. K.; Ding, X.; Wang, J.; Nga, M. E.; Ho, H. K.; Leong, D. T., Nanoparticles promote in vivo breast cancer cell intravasation and extravasation by inducing endothelial leakiness. *Nature Nanotechnology* **2019,** *14* (3), 279-286.
200. Hume, D. A., The mononuclear phagocyte system. *Current Opinion in Immunology* **2006,** *18* (1), 49-53.
201. Chiefari, J.; Chong, Y. K.; Ercole, F.; Krstina, J.; Jeffery, J.; Le, T. P. T.; Mayadunne, R. T. A.; Meijs, G. F.; Moad, C. L.; Moad, G.; Rizzardo, E.; Thang, S. H., Living Free-Radical Polymerization by Reversible Addition−Fragmentation Chain Transfer: The RAFT Process. *Macromolecules* **1998,** *31* (16), 5559-5562.
202. Micic, N.; Young, A.; Rosselgong, J.; Hornung, C. H., Scale-up of the Reversible Addition-Fragmentation Chain Transfer (RAFT) Polymerization Using Continuous Flow Processing. *Processes* **2014,** *2* (1), 58-70.
203. Zhang, J.; Saltzman, M., Engineering biodegradable nanoparticles for drug and gene delivery. *Chem Eng Prog* **2013,** *109* (3), 25-30.
204. Belliveau, N. M.; Huft, J.; Lin, P. J. C.; Chen, S.; Leung, A. K. K.; Leaver, T. J.; Wild, A. W.; Lee, J. B.; Taylor, R. J.; Tam, Y. K.; Hansen, C. L.; Cullis, P. R., Microfluidic Synthesis of Highly Potent Limit-size Lipid Nanoparticles for In Vivo Delivery of siRNA. *Molecular Therapy - Nucleic Acids* **2012,** *1*.
205. Mukalel, A. J.; Evans, B. C.; Kilchrist, K. V.; Dailing, E. A.; Burdette, B.; Cheung-Flynn, J.; Brophy, C. M.; Duvall, C. L., Excipients for the lyoprotection of MAPKAP kinase 2 inhibitory peptide nano-polyplexes. *Journal of Controlled Release* **2018,** *282*, 110-119.
206. Perry, J. L.; Reuter, K. G.; Luft, J. C.; Pecot, C. V.; Zamboni, W.; DeSimone, J. M., Mediating Passive Tumor Accumulation through Particle Size, Tumor Type, and Location. *Nano Lett* **2017,** *17* (5), 2879-2886.

207. Yoo, J. W.; Chambers, E.; Mitragotri, S., Factors that control the circulation time of nanoparticles in blood: challenges, solutions and future prospects. *Curr Pharm Des* **2010,** *16* (21), 2298-307.
208. Salehi, P.; Makhoul, G.; Roy, R.; Malhotra, M.; Mood, Z. A.; Daniel, S. J., Curcumin loaded NIPAAM/VP/PEG-A nanoparticles: physicochemical and chemopreventive properties. *J Biomater Sci Polym Ed* **2013,** *24* (5), 574-88.
209. Hwang, S. J.; Bellocq, N. C.; Davis, M. E., Effects of structure of beta-cyclodextrin-containing polymers on gene delivery. *Bioconjug Chem* **2001,** *12* (2), 280-90.
210. Shae, D.; Becker, K. W.; Christov, P.; Yun, D. S.; Lytton-Jean, A. K. R.; Sevimli, S.; Ascano, M.; Kelley, M.; Johnson, D. B.; Balko, J. M.; Wilson, J. T., Endosomolytic polymersomes increase the activity of cyclic dinucleotide STING agonists to enhance cancer immunotherapy. *Nature Nanotechnology* **2019,** *14* (3), 269-278.
211. Knowles, B. R.; Wagner, P.; Maclaughlin, S.; Higgins, M. J.; Molino, P. J., Silica Nanoparticles Functionalized with Zwitterionic Sulfobetaine Siloxane for Application as a Versatile Antifouling Coating System. *ACS Appl Mater Interfaces* **2017,** *9* (22), 18584-18594.
212. Dai, F.; Liu, Y.; Wang, W.; Liu, W., Stable gene transfection mediated by polysulfobetaine/PDMAEMA diblock copolymer in salted medium. *J Biomater Sci Polym Ed* **2013,** *24* (3), 330-43.
213. Li, Y.; Liu, R.; Shi, Y.; Zhang, Z.; Zhang, X., Zwitterionic poly(carboxybetaine)-based cationic liposomes for effective delivery of small interfering RNA therapeutics without accelerated blood clearance phenomenon. *Theranostics* **2015,** *5* (6), 583-96.
214. Xiu, K.-M.; Zhao, N.-N.; Yang, W.-T.; Xu, F.-J., Versatile functionalization of gene vectors via different types of zwitterionic betaine species for serum-tolerant transfection. *Acta Biomaterialia* **2013,** *9* (7), 7439-7448.
215. Qie, Y.; Yuan, H.; von Roemeling, C. A.; Chen, Y.; Liu, X.; Shih, K. D.; Knight, J. A.; Tun, H. W.; Wharen, R. E.; Jiang, W.; Kim, B. Y., Surface modification of nanoparticles enables selective evasion of phagocytic clearance by distinct macrophage phenotypes. *Sci Rep* **2016,** *6*, 26269.
216. Rodriguez, P. L.; Harada, T.; Christian, D. A.; Pantano, D. A.; Tsai, R. K.; Discher, D. E., Minimal "Self" peptides that inhibit phagocytic clearance and enhance delivery of nanoparticles. *Science* **2013,** *339* (6122), 971-5.
217. Liu, H. L.; Hua, M. Y.; Yang, H. W.; Huang, C. Y.; Chu, P. C.; Wu, J. S.; Tseng, I. C.; Wang, J. J.; Yen, T. C.; Chen, P. Y.; Wei, K. C., Magnetic resonance monitoring of focused ultrasound/magnetic nanoparticle targeting delivery of therapeutic agents to the brain. *Proc Natl Acad Sci U S A* **2010,** *107* (34), 15205-10.
218. Gonzalez-Angulo, A. M.; Akcakanat, A.; Liu, S.; Green, M. C.; Murray, J. L.; Chen, H.; Palla, S. L.; Koenig, K. B.; Brewster, A. M.; Valero, V.; Ibrahim, N. K.; Moulder-Thompson, S.; Litton, J. K.; Tarco, E.; Moore, J.; Flores, P.; Crawford, D.; Dryden, M. J.; Symmans, W. F.; Sahin, A.; Giordano, S. H.; Pusztai, L.; Do, K. A.; Mills, G. B.; Hortobagyi, G. N.; Meric-Bernstam, F., Open-label randomized clinical trial of standard neoadjuvant chemotherapy with paclitaxel followed by FEC versus the combination of paclitaxel and everolimus followed by FEC in women with triple receptor-negative breast cancerdagger. *Ann Oncol* **2014,** *25* (6), 1122-7.
219. Bhola, N. E.; Jansen, V. M.; Koch, J. P.; Li, H.; Formisano, L.; Williams, J. A.; Grandis, J. R.; Arteaga, C. L., Treatment of Triple-Negative Breast Cancer with TORC1/2 Inhibitors Sustains a Drug-Resistant and Notch-Dependent Cancer Stem Cell Population. *Cancer Res* **2016,**

76 (2), 440-52.